

STAR 04 DEC 12 1985

Temp # 02928

NASA Contractor Report 171904

1983 NASA/ASEE Summer Faculty Fellowship Program

Research Reports

Lyndon B. Johnson Space Center

Texas A&M University

City of Houston
(NASA-CR-171904) THE 1983 NASA/ASEE SUMMER
FACULTY FELLOWSHIP RESEARCH PROGRAM RESEARCH
REPORTS Final Reports (NASA) 409 P
HC A18/MF A01

CSSL 05I

G3/85

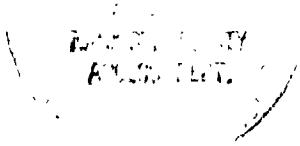
N86-14078
THRU
N86-14105
Unclass
02928

Editors:

Dr. Walter J. Horn
Professor of Aerospace Engineering
Texas A&M University
College Station, Texas

Dr. Michael B. Duke
Office of University Affairs
Lyndon B. Johnson Space Center
Houston, Texas

September 1983



Prepared for

NASA Lyndon B. Johnson Space Center
Houston, Texas 77058

PREFACE

The 1983 NASA/ASEE Summer Faculty Fellowship Research Program was conducted by Texas A&M University and the Lyndon B. Johnson Space Center (JSC). The 10-week program was operated under the auspices of the American Society for Engineering Education (ASEE). These programs, conducted by JSC and other NASA Centers, began in 1964. They are sponsored and funded by the Office of University Affairs, NASA Headquarters, Washington, D.C. The objectives of the programs are the following:

- a. To further the professional knowledge of qualified engineering and science faculty members
- b. To stimulate an exchange of ideas between participants and NASA
- c. To enrich and refresh the research and teaching activities of participants' institutions
- d. To contribute to the research objectives of the NASA Centers

The faculty fellows spent 10 weeks at JSC engaged in a research project commensurate with their interests and background. They worked in co collaboration with a NASA/JSC colleague. This document is a compilation of the final reports on their research during the summer of 1983. Texas A&M Research Foundation Report No. 4194-83 is the Co-Directors' report on the administrative operations of the Summer Faculty Fellowship Program.

CONTENTS

1. Anderson, Charles: Estimation of Finite Mixtures Using the Empirical Characteristic Function.
2. Barrett, Roy A.: The Scanning Electron Microscope as a Tool in Space Biology.
3. Blanford, George E.: Electron Microscopic Observations of Hydrogen Implantation in Ilmenites.
- 4. Bustin, Roberta: A Pyrolysis Technique for Determining Microamounts of Hydrogen in Lunar Soil Using the Helium Ionization Detector.
5. Durgun, Kanat: Finite Element or Galerkin Type Semidiscrete Schemes.
- 6. Ghorai, Susanta K.: Determination of Neutron Flux Distribution by Using Anisn, A One-Dimensional Discrete S_n Ordinates Transport Code with Anisotropic Scattering.
7. Hall, Minard L.: Paper Unavailable
8. Hanania, Jack I.: A Study of Some Features of AC and DC Electric Power Systems for a Space Station.
9. Ito, Takeru: Nutritional Characteristics of Moon Dust for Soil Microorganisms.
10. Jackson, A. A.: Some Applications of Lie Groups in Astrodynamics.
11. Johansson, Karl R.: Interaction Between Escherichia coli and Lunar Fines.
12. Kieseewetter, Carl H.: Spectral Reflectance of Surface Soils - Relationships with Some Soil Properties.
13. Lee, Kwang Y.: Control of Space Stations.
14. Marrero, Thomas R.: Solid Waste Treatment Processes for Space Station.
15. Measel, John W.: Paper Unavailable
- 16. Morgan, Thomas H.: Lunar Luminescence Measurements.
17. Palma, Russell L.: Development of a Mass Spectrometer System for the Measurement of Inert Gases in Meteorites.
- 18. Presley, Bobby Joe: Paper Unavailable
19. Rakow, Allen: An Analysis of Cryotrap Heat Exchanger Performance Test Data (400 area) and Recommendations for a System to Handle Apollo RCS Engines.
20. Ridley, Esther J.: Comparative Effect of Lunar Fines and Terrestrial Ash on the Growth of a Blue-Green Alga and Germinating Radish Seeds.

PRECEDING PAGE BLANK NOT FILMED

21. Runnels, Robert C.: Variability of Rainfall Over Small Areas.
22. Sartain, Robert L.: Transformation Matrices Between Non-Linear and Linear Differential Equations.
23. Schulze, Paul D.: Ion Bombardment and Adsorption Studies on Ilmenite (FeTiO_3) by X-Ray Photoelectron Spectroscopy.
24. Szebehely, Victor: Advanced Algorithm for Orbit Computation.
25. Thomas, Richard G.: Solar Concentrator Degradation in Low Earth Orbit (LEO).
26. Williams, Raymond: Fortran Plotting Subroutines for the Space Plasma Laboratory.
27. Wyzkoski, Joan: Computer Graphics Applications to Crew Displays.
28. Zimmermann, Wayne J.: Signal Processing of Anthropometric Data.

ESTIMATION OF FINITE MIXTURES USING THE
EMPIRICAL CHARACTERISTIC FUNCTION

By

N86-14079

Charles Anderson, Associate Professor
Thomas Boullion, Professor
Department of Mathematics and Statistics
University of Southwestern Louisiana
Lafayette, Louisiana 70504

ABSTRACT

A problem which occurs in analyzing Landsat scenes is the problem of separating the components of a finite mixture of several distinct probability distributions. A review of the literature indicates this is a problem which occurs in many disciplines, such as engineering, biology, physiology and economics. Many approaches to this problem have appeared in the literature; however, most are very restrictive in their assumptions or have met with only a limited degree of success when applied to realistic situations.

We have been investigating a procedure which combines the "k-L procedure" of [Feurverger and McDunnough, 1981] with the "MAICE" procedure of [Akaike, 1974]. The feasibility of this approach is being investigated numerically via the development of a computer software package enabling a simulation study and comparison with other procedures.

Center Research Advisor: M. C. Trichel

INTRODUCTION

A Problem which occurs in many disciplines is that of separating the components of a probability distribution which is a finite mixture of several distinct distributions. See, for instance, [Yakowitz, 1970], [Bhattacharya, 1976], and [Day, 1969]. This problem is encountered in the Remote Sensing Research Branch of NASA Johnson Space Center in analyzing Landsat data.

A number of different approaches have been taken to resolve this problem, each enjoying a rather limited degree of success or being too restrictive to be widely applicable. Since the likelihood function corresponding to finite mixtures of normal distributions is unbounded, maximum likelihood estimation frequently breaks down in practice. The estimator which minimizes the sum of squares of differences between the theoretical and sample moment generating functions, given by [Quandt and Ramsey, 1978], seems to suffer from inefficiency and some arbitrariness in the choice of weights given to the moments. Estimating the mixing proportions of a mixture of known distributions [Bryant and Paulson, 1983], using the distance between characteristic functions is too restrictive, since it assumes the parameters in the component distributions are completely known.

A recent approach by [Heydorn and Basu, 1983] makes use of a constructive proof of a theorem of Caratheodory on a trigonometric moment problem, as discussed in [Grenander and Szego, 1958], to determine identifiable mixtures for certain special cases of families of distributions. When only sample data is available, this approach does not seem to be immediately applicable.

PROCEDURE AND JUSTIFICATION

The "k-L procedure" introduced by [Feurverger and McDunnough, 1981], refers generally to approximate maximum likelihood estimation based on the asymptotic distribution at k points of the empirical characteristic function (e.c.f.). Since the e.c.f. contains all the information in the sample, and for other reasons given later, it seems to be a promising technique. See Figure 1.

Let ξ be a column vector composed of the real and imaginary parts of the e.c.f. at points $d, 2d, \dots, kd$. The probability distribution of ξ is approximately multivariate normal, even for fairly small sample sizes, because of the smoothness and boundedness of the trigonometric functions. The covariance matrix $\Omega = E(\xi - E(\xi)) (\xi - E(\xi))^T$ is determined by the values of the true characteristic function $\phi(t)$ at $t=d, 2d, \dots, 2kd$ and can be estimated from the values of the e.c.f. at these points. Since this estimate $\hat{\Omega}$ is consistent, the following estimation criteria are asymptotically equivalent: (1) maximize the likelihood given ξ , (2) minimize $(\xi - E(\xi))^T \Omega^{-1} (\xi - E(\xi))$, (3) minimize $(\xi - E(\xi))^T \hat{\Omega}^{-1} (\xi - E(\xi))$.

The hypothesis $H_0: \phi(t) = \sum_1^M P_i \phi_i(t) | \theta_{i1}, \dots$ with certain of the parameters P_i, θ_{i_j} specified, can be tested against an alternative hypothesis specifying the same form of the model but with parameters not all as specified by H_0 , using the approximate chi-square distribution of $L = n(\xi - E(\xi))^T \Omega^{-1} (\xi - E(\xi))$. The hypothesis H_0 is rejected if L is greater than the $(1-\alpha)$ point of its null distribution, which is approximately the chi-square with degrees of freedom equal to $2k$ minus the number of functionally independent unspecified parameters under H_0 .

When there are several competing models, the MAICE procedure, introduced by [Akaike, 1974], selects the model which gives the minimum value of

$$\text{AIC} = (-2) \log (\text{maximum likelihood}) + \\ 2(\text{number of independently adjusted} \\ \text{parameters within the model}).$$

This procedure has been investigated by [Redner, Kitagawa, and Coberly, 1981], working directly with the mixed distributions. Our procedure applies the MAICE method to data reduced to a few carefully selected points of the e.c.f. Also, maximum likelihood is computed approximately using the approximate normality of the e.c.f.

FURTHER INVESTIGATIONS

Although the above procedure is based on sound theoretical arguments, no numerical results have appeared indicating its efficiency of implementation on a computer or its accuracy in determining the best model and estimates of the parameters. Thus, a software package is being developed which will enable us to implement and test the procedure. This work has led to numerical and theoretical investigations on optimally selecting the points t_i where the e.c.f. is evaluated. Other numerical problems are being investigated to determine efficient computational procedures and to increase the accuracy of the computed values. The package is written in FORTRAN 77 and uses IMSL subroutines whenever possible. Basic components are (1) a very flexible subroutine (MIXSIM) to simulate data from any specified mixture of standard distributions, (2) an equally flexible subroutine (THEOCF) which computes the theoretical characteristic function for any specified mixture distribution, and (3) a subroutine (FITCF) which seeks parameter estimates, given a specified mixture model, to minimize the chi-square criterion L given above.

REFERENCES

1. Feurverger, A., and McDunnough, P., "On the Efficiency of Empirical Characteristic Function Procedures," J. R. Statist. Soc. B., 43:20-27, 1981.
2. Koutrouvelis, I. A., and Kellermeier, J., "A Goodness-of-Fit Test Based on the Empirical Characteristic Function when Parameters must be Estimated," J. R. Statist. Soc. B., 43:173-176, 1981.
3. Akaike, H., "A New Look at the Statistical Model Identification," IEEE Trans. Auto. Control, AC-19, No. 6, pp. 716-723, 1974.
4. Bhattacharya, C. G., "A Simple Method of Resolution of a Distribution into Gaussian Components," Biometrics, 23:115-135, 1967.
5. Day, N. E., "Estimating the Components of a Mixture of Normal Distributions," Biometrics, 56:463-474, 1969.
6. Yakowitz, S. J., "Unsupervised Learning and the Identification of Finite Mixtures," IEEE Transaction on Info. Theory, IT-16:330-338, 1970.
7. Quandt, R. E., and Ramsey, J. B., "Estimating Mixtures of Normal Distributions and Switching Regressions," JASA, 73# 364, 730-738. Comments 738-752, 1978.
8. Bryant, J. L., and Paulson, A. S., "Estimation of Mixing Proportions via Distance Between Characteristic Functions," Commun. Statist.-Theor. Meth., 12(9), pp. 1009-1029, 1983.

9. Feurverger, A., and Mureika, R. A., "The Empirical Characteristic Function and Its Applications," Ann. Statist., 5:86-97, 1977.
10. Redner, R. A., Kitagawa, G., and Coberly, W. A., "The Akaike Information Criterion and Its Application to Mixture Proportion Estimation," NASA-JSC Report SR-TI-04207, prepared for EOD under Contract NAS9-14689-95, 1981.
11. Heydorn, R. P., and Basu, R., "Estimating Location Parameters in a Mixture Model," NASA-JSC Internal Note, 1983.
12. Genander, U., and Szego, G., Toeplitz Forms and Their Applications, (Berkeley, University of California Press, 1958).

CHARACTERISTIC FUNCTIONS

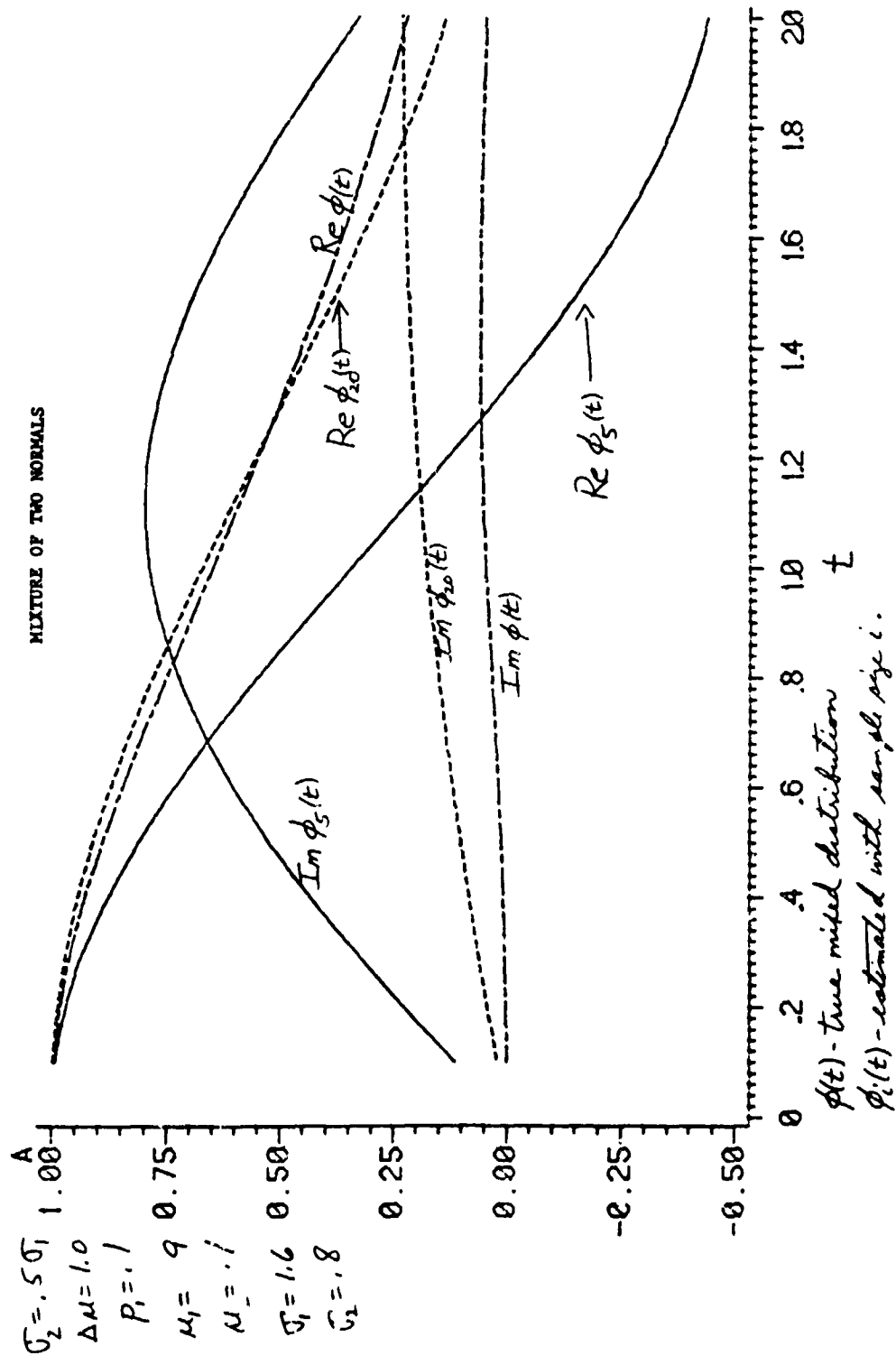


Figure 1

N86-14080

THE SCANNING ELECTRON MICROSCOPE AS A TOOL IN SPACE BIOLOGY

Roy A. Barrett
Associate Professor
Department of Biology
Fayetteville State University
Fayetteville North Carolina

ABSTRACT

Normal erythrocytes are disc-shaped and are referred to here descriptively as discocytes. Several morphologically variant forms occur normally but in rather small amounts, usually less than one percent of total. It has been shown though, that spiculed variant forms referred to as echinocytes are generated in significant amounts at zero g.

Normal red cells have been stressed in vitro in an effort to duplicate the observed discocyte-echinocyte transformation at zero g. The significance of this transformation to extended stay in space and some of the plausible reasons for this transformation are discussed.

Center Research Advisor: Duane Pierson

INTRODUCTION

Most departures from the biological norm are accompanied by structural and hence morphological changes at the molecular level or above.

The ability of the scanning electron microscope to resolve ultra-microscopic details is viewed as capable of facilitating the visualization of minute morphological changes in the ultrastructure of biological systems that might well permit the monitoring of biochemical events, and these may be used as indices in predicting functional changes. This could have significant applications both diagnostically and therapeutically. Also, conceivably, its predictive component could be invaluable in screening humans for stressful undertakings as in selecting candidates for missions in zero g and above one g environments.

This study looks at the morphological aberrations of erythrocytes brought about by zero g. stress and the consequences thereof.

MATERIALS AND METHODS

Blood samples (0.5 ml) were taken from the author. Some samples were collected in standard fixative of 0.5% gluteraldehyde - pH 7.4 and held for 5 hrs at room temperature. Other samples were collected in EDTA and held at room temperature for 48 hrs to subject the erythrocytes to energetic and osmotic stress.

Erythrocytes from all samples were sedimented by centrifugation and dehydrated by stepwise passage through a series of 20, 50, 75, 90 and 100 per cent ethyl alcohol. The cells were collected on SELAS Flotronics FM-25 silver membrane filters (0.8 micron pore size) and critical point dried using liquid CO₂ on a Denton critical point drying apparatus according to the method of Anderson (1). The membrane filters bearing the samples were cut to suitable sizes, mounted on standard aluminum specimen stubs with Scotch double stick tape and grounded to the stubs with conductive silver paint. The samples were then coated with ca. 100Å gold/palladium (60/40 per cent) in a Varian VE-10 vacuum evaporator and examined in an ETEC Autoscan scanning electron microscope at 20 kV.

RESULTS AND DISCUSSION

Data from the Gemini and Apollo space flight missions have suggested possible influences of the space environment on erythrocyte integrity and mean count — a consequence of the stress brought about by the 1-0 g or the 1-0-1 g shifts. Immunological changes have been observed also but this study is limited to hematological considerations only, and specifically to erythrocyte competence as measured by morphological variations — all this as an index to biochemical changes.

Echinocytes account for less than 1% of the erythrocytes at one g. However at zero g. the echinocyte population increases dramatically. For the Skylab missions, the average zero g. population reached some 7% or more than 700% increase. But the variation among crew members was significant with the pilot of Skylab 3 demonstrating a 16% echinocyte population or ca. 2000% increase (2).

Since echinocytes are aberrant forms of erythrocytes considered to represent lower efficiency and reduced competence, such significant increases might be cause for alarm. Furthermore, echinocytogenesis seemed to increase with length of time at zero g.

There are no data to indicate at what point (during an extended stay in space) echinocytogenesis would plateau or even if it would. If reduced hematological competence is attendant to echinocytogenesis, then an extrapolation of the existing data is quite disconcerting.

One very interesting observation however is the fact that discocyte—
echinocyte transformation as a function of zero g. is reversible and
dramatically so. All the data indicate a rapid reversal during the
time of re-entry. Since the zero g. induced echinocytes monitored
to date failed to attain the final stage of development, it is not
known if fully developed echinocytes (0g. induced) are reversible,
although it is generally recognized that extrinsically induced mor-
phological changes may be reversed.

Figure 1 show normal erythrocytes 5 hrs after collection (discocytes)
while figures 2 and 3 show cells from the same subject, collected at
the same time, but stressed in vitro for 48 hrs. Several echinocytes
can be seen in early (stage 1) middle (stage 2) and late (stage 3) stages
of development. Although the stage 1 cells are identical to those
developed by astronauts in flight, it is significant that no stage 2 nor
stage 3 cells were developed by those same astronauts even over an
84 day mission. It is unfortunate that in-flight lipid and ATP levels
were not ascertained as it has been shown (3) that these factors could
well be causative agents.

The simultaneous monitoring of erythrocytic morphological changes and
lipid/ATP levels would be of extreme importance in future missions and
is therefore recommended.

ACKNOWLEDGEMENT

The author wished to thank Joe Dardano of Northup Services for technical assistance.

REFERENCES

1. Anderson, T.F. 1966. Electron microscopy of microorganisms. In Physical Techniques in Biological Research pp 319-387, A.W. Pollister ed. Academic Press, New York.
2. Kimzey, S.L. 1977. Hematology and immunology studies. In Biomedical Results from Skylab pp 249-282. R.S. Johnston and L.F. Dietlein ed. NASA, Washington D.C.
3. Shohet, S.B. and J.E. Haley 1973. Red cell membrane shape and stability: relation to cell lipid renewal pathways and cell ATP. In Red Cell Shape pp 41-50. M. Bessis, R.I. Weed and P.F. LeBlond ed. Springer Verlag, New York.

ORIGINAL
OF POOR QUALITY



Figure 1 Normal erythrocytes (discocytes)
Magnification 3000X

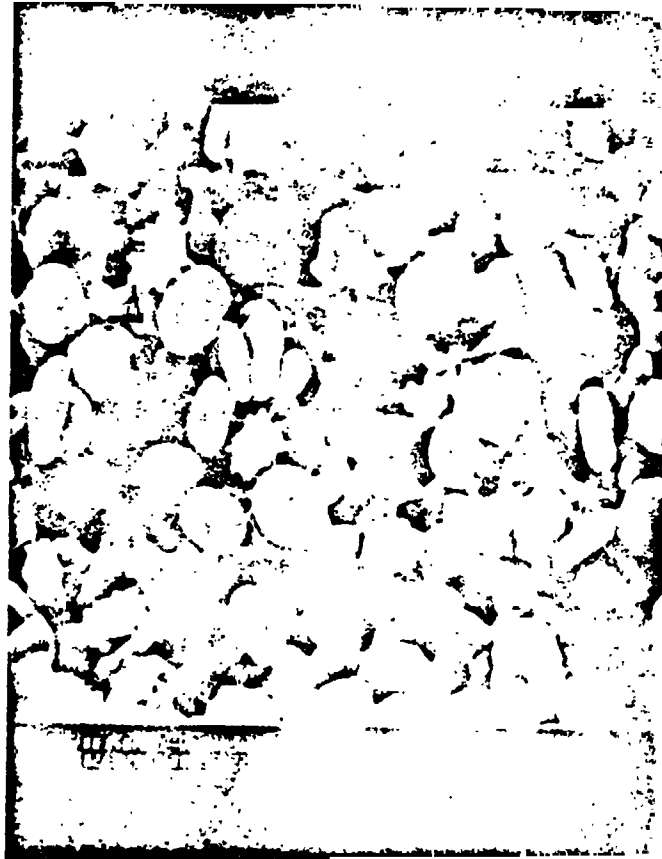


Figure 2 Stressed erythrocytes showing echinocytes
in various stages of development.
Magnification 2000X

ORIGINAL IMAGE IS
OF POOR QUALITY

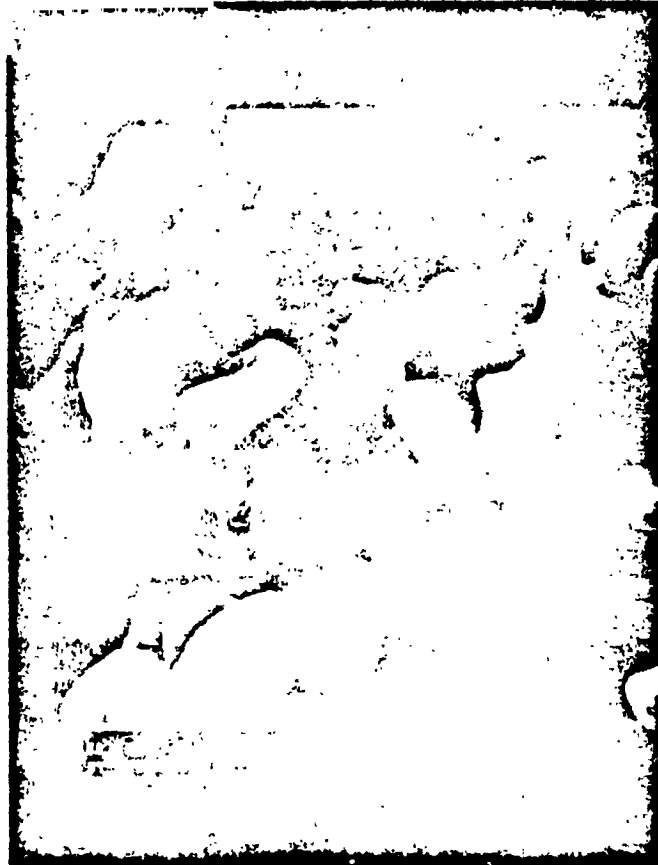


Figure 3. Stressed erythrocytes
Magnification 4000X

N86-14081

ELECTRON MICROSCOPIC OBSERVATIONS OF HYDROGEN
IMPLANTATION IN ILMENITES

George E. Blanford
Associate Professor
Programs in Science
University of Houston - Clear Lake
Houston, Texas

ABSTRACT

Hydrogen ion beams were found to form submicrometer, bumpy textures on the surface of ilmenite grains. From this effect we believe that similar bumpy textures seen on lunar ilmenite, pyroxene, and olivine grains are likely to be caused by solar wind irradiation. As a consequence, the concentration of bumpy textured grains may be a useful index of surface maturity for lunar soils. We believe it is worthwhile to search for grains with these bumpy textures in interplanetary dust and lunar and meteoritic regolith breccias in order to obtain information about the duration of their exposure to the solar wind

Center Research Advisor: David S. McKay

The interaction of solar wind and solar flare atomic particles with lunar minerals is known to cause several types of damage to the minerals including the formation of particle tracks (Croaz, et al., 1970; Fleischer, et al., 1970), sputter rounding, and the formation of amorphous rims on grain surfaces (Borg, et al., 1970; Dran, et al., 1970). Here I describe another effect which may involve not only structural damage but also chemical alteration.

Blanford, et al. (1981) reported observing bumpy surface texture on 0.5-1.0 μm grains from the lunar regolith from sample 15010,1130 (Fig. 1). Because these soil grains are very small, they most probably were exposed to the solar wind. Consequently Blanford, et al. (1981) inferred that the bumpy texture is some form of solar wind damage. This texture is confined to ironbearing minerals: ilmenite, olivine, and pyroxene. Of these, ilmenite grains have the best developed bumpy texture. Transmission electron micrographs (TEM) of the textured grains show some relatively opaque spots indicating a relatively high density. Precise correlation of these spots with the surface bumps was not always possible, although some of the bumps can be identified in TEM but are not always completely opaque. Energy dispersive X-ray (EDX) spot analyses indicate an enrichment in iron relative to that of the background mineral. For these

reasons Blanford, et al. (1981) hypothesized that iron in these minerals was reduced to metal by the solar-wind implanted hydrogen ions.

In order to test this hypothesis I have simulated solar wind irradiation on natural, terrestrial ilmenite. Hydrogen ion beams were directed at small grains and polished sections which were then examined by electron microscopy.

METHOD

Samples were prepared from ilmenite ground with an agate mortar and pestle, ultrasonically stirred in a fluorocarbon solvent, and precipitated onto a copper TEM grid covered with a holey, carbon substrate. Ilmenite grains were identified by EDX analysis. The sample was irradiated with a Denton model DB-1 ion-gun using hydrogen as the operating gas. This gun is a high voltage gas discharge ion source which has an inherently large energy spread, perhaps duplicating solar-wind velocity distributions better than a sharply defined ion source. Irradiations were made with the ion gun at an angle of 45° and the sample was continuously rotated. The sample was 2 cm from the cathode of the gun and the beam spread to an 1 cm^2 area. Ambient pressure was 10 - 30 mTorr. Our average dose rate was $4.3 \pm 0.3 \times 10^{14} \text{ cm}^{-2} \cdot \text{s}^{-1}$ or 10^6 times that of the solar wind on the Moon ($3.8 \times 10^8 \text{ cm}^{-2} \cdot \text{s}^{-1}$; Feldman, et al., 1977). The maximum accelerating potential for hydrogen was 4 kV resulting in a maximum ion velocity of 550 km/s which is typical of the solar wind (Feldman, et al., 1977).

RESULTS

Irradiation with $2 - 5 \times 10^7 \text{ cm}^{-2}$ hydrogen ions forms texturing on ilmenite grains (Fig. 2). Sputtering also occurs and, judging from rounding and erosion of small surface features, is estimated to be as much as 50% of the texturing effect (Carter and Colligon, 1968). Some sputtered droplets can be seen in our micrographs, but sputtered droplets are rare on lunar samples. Our analogue grains remain sharp with only some thin features sputtered away; lunar ilmenite grains are sharp and do not form amorphous coatings as do plagioclase grains (Borg, et al., 1980). The texturing effect is definitely not the deposition of sputtered droplets because irradiated grains of iron oxide do not have this texture (Fig. 2).

Identification of the bumpy features continues to be an analytical problem. Microelectron diffraction and EDX analysis have not been useful. Selected area (SA) electron diffraction has given inconsistent results. On lunar ilmenites one can find reflections from iron, but they seem to come from several, unidentified locations on the sample. Freshly irradiated terrestrial samples show ringed SA diffraction patterns typical of finely divided substances. These patterns appear to be those of FeTi which has a CsCl cubic structure with lattice spacing $a_0 = 2.976 \text{ \AA}$; the pattern is the same as for $\alpha\text{-Fe}$ which has a lattice spacing $a_0 = 2.8664 \text{ \AA}$. Although the difference of 0.1 \AA is twice the estimated resolving power, I hesitate to identify the bumps by this result. Samples are being prepared for Mössbauer

spectroscopy. Another NASA/ASEE summer faculty fellow, Paul Schulze, is using X-ray photoelectron spectroscopy to study ilmenites before and after hydrogen implantation. Hopefully, one of these techniques will produce a definitive identification of the irradiation effects.

In comparing irradiated samples to lunar samples we have found that the simulated samples have finer texturing (Figs. 1 and 2). There is a factor of 2 to 3 difference in the size of the bumps. This effect may relate either to differences in dose rate or to differences in total dose. However, experiments done at a 6 times lower dose rate showed the same effect, but seemed to require a greater total dose by about a factor of 2.

Even though there may be a textural size difference between the simulated samples and lunar samples, we propose that this texturing on lunar samples is caused by the solar wind. This effect has implications which concern lunar reworking rates and maturity indices and it may be useful in studying the space exposure of interplanetary dust grains and grains in meteoritic breccias. We do not have space in this report to discuss these implications.

In conclusion, we have found by simulating solar wind irradiations that pumpy-textures can be formed on ilmenite grains.

REFERENCES

- Blanford G.E., McKay D.S., Nace G., and Mackinnon I.D.R. 1981. Electron microscopic observations of micron-sized lunar soil. In Lunar and Planetary Science XII, p. 86-88.

- Lunar and Planetary Institute, Houston.
- Borg J., Dran J.C., Durrieu L., Jouret C., and Maurette M. 1970. High voltage electron microscope studies of fossil nuclear particle tracks in extraterrestrial matter. Earth Planet. Sci. Lett. 8, 379-386.
- Borg J., Chaumont J., Jouret C., Langevin Y., and Maurette M. 1980. Solar wind radiation damage in lunar dust grains and the characteristics of the ancient solar wind. In The Ancient Sun: Fossil Record in the Earth, Moon, and Meteorites (Pepin R.O., Eddy J.A., and Merrill R.B., eds.), p. 431-461. Pergamon, New York.
- Carter G. and Colligon J.S. 1968. Ion Bombardment of Solids. American Elsevier, New York. 446 pp.
- Crozaz G., Haack U., Hair M., Hoyt H., Kardos J., Maurette M., Miyajima M., Seitz M., Sun S., Walker R., Wittels M., and Woolum D. 1970. Solid state studies of the radiation history of lunar samples. Science 167, 563-566.
- Dran J.C., Durrieu L., Jouret C., and Maurette M. 1970. Habit and texture studies of lunar and meteoritic materials with a 1 MeV electron microscope. Earth Planet. Sci. Lett. 9, 391-400.
- Feldman W.C., Asbridge J.R., Bame S.J., and Gosling J.T. 1977. Plasma and magnetic fields from the Sun. In The Solar Output and Its Variation (White O.R., ed.), p. 351-381. Colorado Associated University Press, Boulder.
- Fleischer R.L., Haines E.L., Hanneman R.E., Hart H.R., Kasper

J.S., Lifshin E., Woods R.T., and Price P.B. 1970.
Particle track, X-ray, thermal, and mass spectrometric
studies of lunar material. Science 167, 568-570.

ORIGINAL PAGE IS
OF POOR QUALITY



Figure 1: Scanning electron micrographs taken with a JEOL 100CX microscope of a) an ilmenite, and b) an olivine grain showing bumpy texture from lunar soil (core) sample 15010,1130. The marker represents a length of 0.1 μm on all micrographs.

ORIGINAL PAGE IS
OF POOR QUALITY

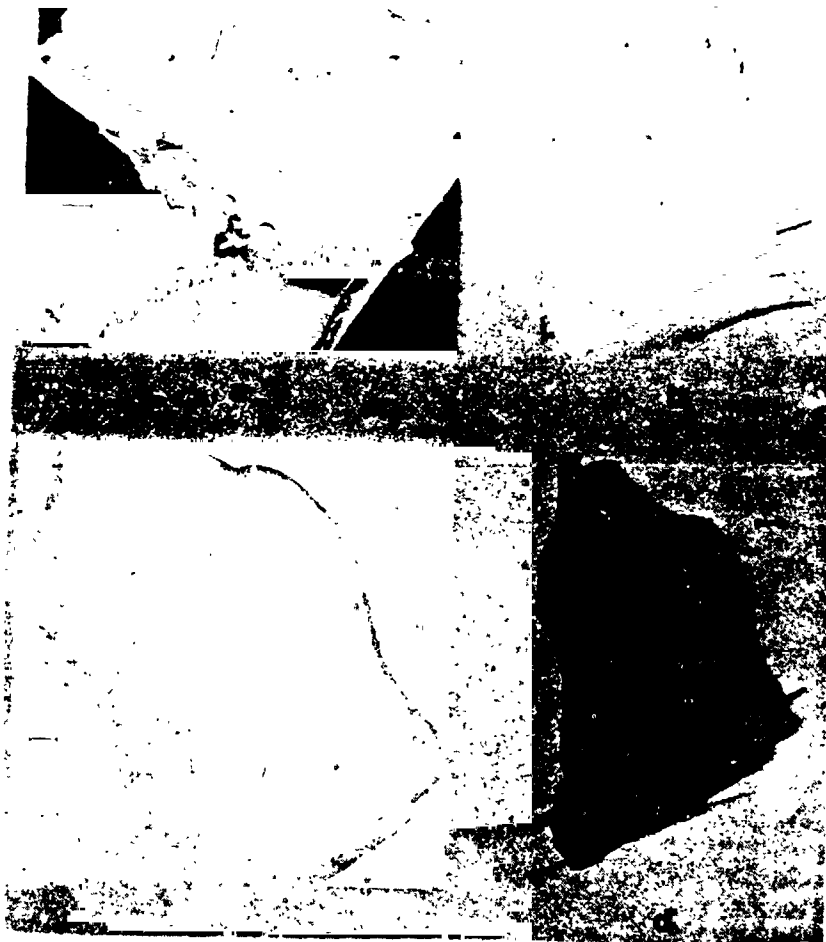


Figure 2: Scanning and transmission electron micrographs of an ilmenite-iron oxide grain before (a and b) and after (c and d) irradiation with 2.5×10^{17} cm^{-2} hydrogen ions. The bumpy-texturing uniquely forms on the ilmenite crystal.

N86-14082

A PYROLYSIS TECHNIQUE
FOR DETERMINING MICROAMOUNTS OF HYDROGEN IN LUNAR SOIL
USING THE HELIUM IONIZATION DETECTOR

Roberta Bustin
Professor of Chemistry
Arkansas College
Batesville, Arkansas

ABSTRACT

A method has been developed which will determine hydrogen in sub-milligram samples of lunar soil. It consists of heating the sample in a pyroprobe followed by the gas chromatographic determination of hydrogen using the helium ionization detector. Using a 7 foot, 1/8" OD stainless steel column packed with Carbosieve S, 120/140 mesh, hydrogen was well-separated from the other gases released from lunar soil.

Standards of hydrogen in helium were used for calibration. The limit of detection under the conditions used was about 2 ng. The method was linear from 2 ng to 270 ng.

The method was checked using some actual lunar samples. Results were typical of those obtained for lunar soils using other methods.

Center Research Advisor: Dr. Everett Gibson

INTRODUCTION

Many times chemical analyses must be run on samples which are limited in amount or which cannot be destroyed. In most instances, a few tenths of a milligram can be spared for analysis. With increasing information about a future lunar base, there is a renewed interest in the soils returned from the moon. Hydrogen is a solar wind species whose concentration in lunar soil is very small. In order to predict the potential usefulness of this lunar hydrogen for propellants and consumables, it is desirable to determine the hydrogen content not only of bulk soil but of various size fractions and of different particle types within a given size fraction. This necessarily limits the amount of sample available for analysis.

A method has been developed which will determine hydrogen in sub-milligram samples. It consists of heating the sample in a pyroprobe followed by the gas chromatographic determination of hydrogen using the helium ionization detector.

EXPERIMENTAL

An Antek 300 gas chromatograph fitted with a helium ionization detector was used in this study. The detector was operated at room temperature and at an applied potential of 150 volts. The column was a 7 foot, 1/8" OD stainless steel tube packed with Carbosieve S, 120/140 mesh. The column was conditioned at 220°C overnight with a helium

flow of 25 ml/min. A schematic diagram of the system is shown in Figure 1. Experimental conditions are given in Figure 2.

A Chemical Data System 122 Micro-extended Pyroprobe was used. The coil was heated to 900°C for 1 minute immediately prior to introducing the weighed sample. The sample was contained in a quartz tube sealed on one end. The tube was placed directly into the pyroprobe coil. The coil served as both the sample holder and the heating element. After reassembling the pyroprobe, the sample was heated to 150°C to eliminate any adsorbed surface moisture. When a steady base-line was obtained, valves were closed, isolating the pyroprobe. The sample was then heated for 1 minute, after which the released gases were introduced onto the column where hydrogen was separated from the other components. Prior to use, the quartz tubes were heated at 900°C for several hours and then stored in a desiccator. A blank was run on each quartz tube prior to sample determination. Blanks typically showed no hydrogen peak or a peak too small to be integrated by the central processor.

The carrier gas was helium which contained 104 ppm nitrogen. Standards of hydrogen in helium were used to calibrate the system. They were injected by means of a Valco gas sampling valve with a 100 µl sampling loop. Chromatographic signals were recorded on an OmniScribe recorder, using 0.001 Volt full scale, and were integrated on a Spectra-Physics 4000 central processor. The smallest peak which could be integrated corresponded to about 1 ppm of hydrogen.

RESULTS AND DISCUSSION

After preliminary evaluations were made of Carbosieve S, Carbosieve B, Molecular Sieve 5A, Molecular Sieve 13X, and Porapak Q; Carbosieve S was chosen for the column packing material because it gave the best separation of hydrogen from the other gases released from lunar soil. Figure 3 shows a chromatogram of a typical pyrolysis of a lunar soil sample. The helium ionization detector gives the best response when ultrapure helium is used as the carrier gas (Andrawes et al., 1981a). However, under these conditions, hydrogen sometimes gives a negative peak and sometimes a W-shaped peak. Andrawes et al. (1981b) discussed the relationship between purity of the carrier gas and peak shape. In order to always obtain hydrogen peaks with the same polarity which could be integrated by the data system, helium containing 104 ppm nitrogen was chosen as the carrier gas. To eliminate the detector instability problems caused primarily by water in the carrier gas line, a liquid nitrogen trap for condensibles was placed in the line.

Preliminary runs showed that hydrogen began to be evolved around 700°C. The amount of evolved hydrogen increased with temperature until around 900°C but showed a marked decrease at 1000°C. Thus, the temperature for pyrolysis was chosen as 900°C.

The valves in the carrier gas line served a two-fold purpose. Closing the by-pass valves made it possible to isolate the pyroprobe during sample change so that a minimum amount of air entered the carrier gas line. This

effected a considerable time savings because the helium ionization detector is very sensitive to air and requires a long time to stabilize after a significant amount of air hits the detector. Isolating the pyroprobe from the rest of the system also made it possible to heat the sample and subsequently to introduce the released volatiles onto the column as a plug when the valves were opened. The pyroprobe controller is a versatile one, allowing heating intervals from 20 milliseconds to 4 hours. A pyrolysis time of 1 minute was found to be optimum for this study because 1) most of the hydrogen was released during the first minute of pyrolysis, and 2) not enough air diffused into the pyroprobe in 1 minute to result in interference. Longer heating times showed this interference. One-minute pyrolyses were continued on the same sample until no more hydrogen was released. This usually required from 2 to 4 pyrolyses.

When standards are introduced onto the column by a gas sampling valve, the retention time for a particular species is different from that obtained by using a pyroprobe to release the species into the carrier gas line. Pyrolysis of an actual sample usually releases many more components than the standards contain; thus, the peak for the species in question may not be obvious. To establish retention times using the pyroprobe system, individual pyrolyses were run using calcium hydride, potassium chlorate, and ammonium dichromate to get retention times of hydrogen, oxygen, and nitrogen, respectively. This method was not used for standardization of the hydrogen because reagent grade calcium hydride was not available for this study.

Standards of hydrogen in helium were used for calibration. The limit of detection under the conditions used was about 2 ng. The method was linear from 2 ng to 270 ng.

The method was checked using some actual lunar samples. Results are shown in Table 1 for 12 bulk lunar soils. Values are typical of those obtained for lunar soils (Chang et al., 1974; DesMarais et al., 1974; Epstein and Taylor, 1970, 1973, 1975; Friedman et al., 1970; and Merlivat et al., 1974). Hydrogen was determined in different particle size fractions for two lunar soils. Figures 4 and 5 show that hydrogen concentration decreases with increasing particle size. This is predictable because more solar wind hydrogen could be implanted in the large surface area provided by small particles. DesMarais et al. (1974) obtained similar trends for other lunar soils.

The pyrolysis technique is simple, fairly rapid, and very sensitive. It can be adapted for the determination of volatiles in a variety of materials.

REFERENCES

Andrawes, F. F.; Byers, T. B.; and Gibson, E. K.; Anal. Chem. 1981a, 53, 1544-1545.

Andrawes, F. F.; Byers, T. B.; and Gibson, E. K.; J. Chromatogr. 1981b, 205, 419-424.

Chang, S.; Lennon, K.; and Gibson, E. K.; Proc. Fifth Lunar Sci. Conf., Geochim. Cosmochim. Acta 1974, 2, 1785-1800.

DesMarais, D. J.; Hayes, J. M.; and Meinschein, W. G.; Proc. Fifth Lunar Sci. Conf.; Geochim. Cosmochim. Acta 1974, 2, 1811-1822.

Epstein, S. and Taylor, H. P., Jr.; Proc. Apollo 11 Lunar Sci. Conf., Geochim. Cosmochim. Acta 1970, 2, 1085-1096.

Epstein, S. and Taylor, H. P., Jr.; Proc. Fourth Lunar Sci. Conf., Geochim. Cosmochim. Acta 1973, 2, 1559-1575.

Epstein, S. and Taylor, H. P., Jr.; Proc. Sixth Lunar Sci. Conf., Geochim. Cosmochim. Acta 1975, 2, 1771-1798.

Friedman, I.; Gleason, J. D.; and Hardcastle, K. G.; Proc. Apollo 11 Lunar Sci. Conf., Geochim. Cosmochim. Acta 1970, 2, 1103-1109.

Merlivat, L.; Lelu, M.; Nief, G; and Roth, E; Proc. Fifth Lunar Sci. Conf. Geochim. Cosmochim. Acta 1974, 2, 1885-1895.

SCHEMATIC OF EQUIPMENT

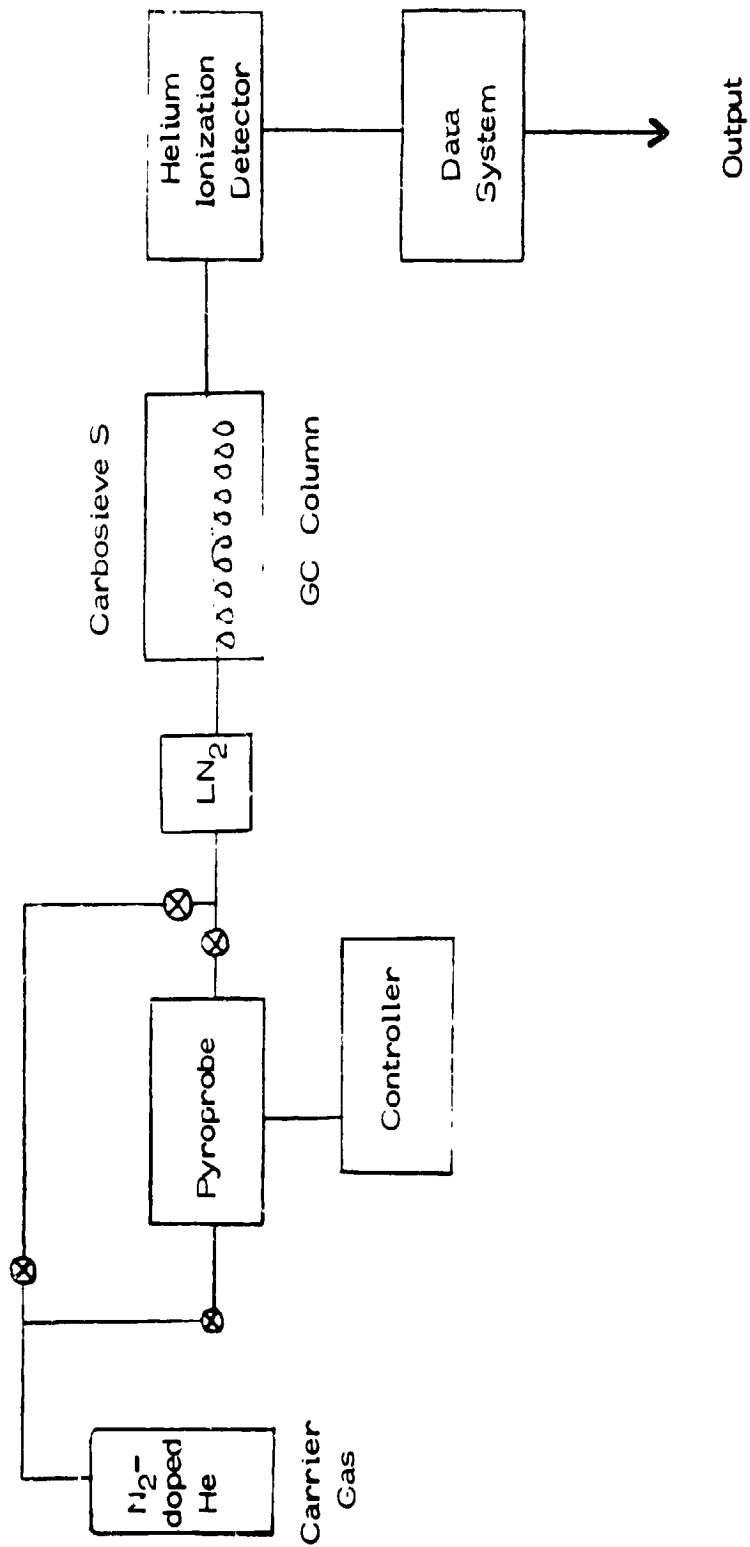


Figure 1

EXPERIMENTAL CONDITIONS

Column 7 ft. Carbosieve S, 120/140 mesh

Column Temperature 60°C

Detector Helium Ionization Detector

Carrier Gas Helium doped with 104 ppm nitrogen

Flow Rate 20 ml/min

Pyrolysis Temperature 900°C

Pyrolysis Time 1 minute

Trap for Condensibles Liquid nitrogen

Figure 2

CHROMATOGRAM OF A TYPICAL LUNAR SOIL PYROLYSIS

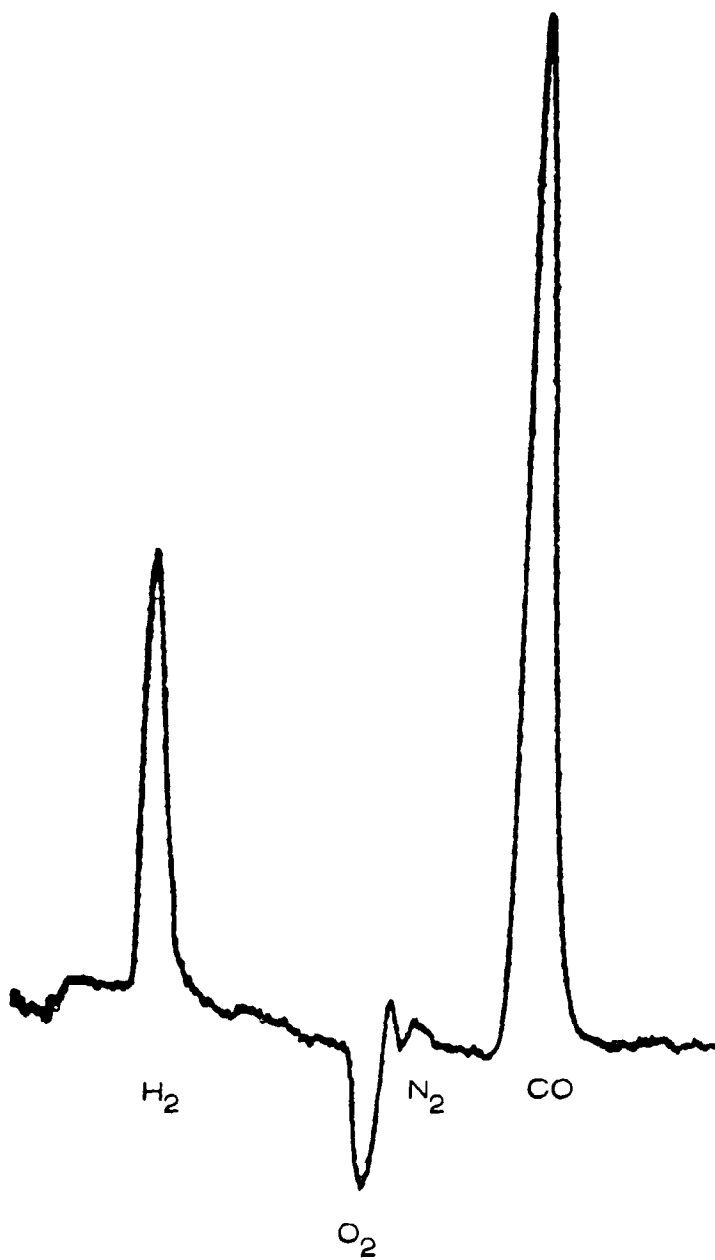
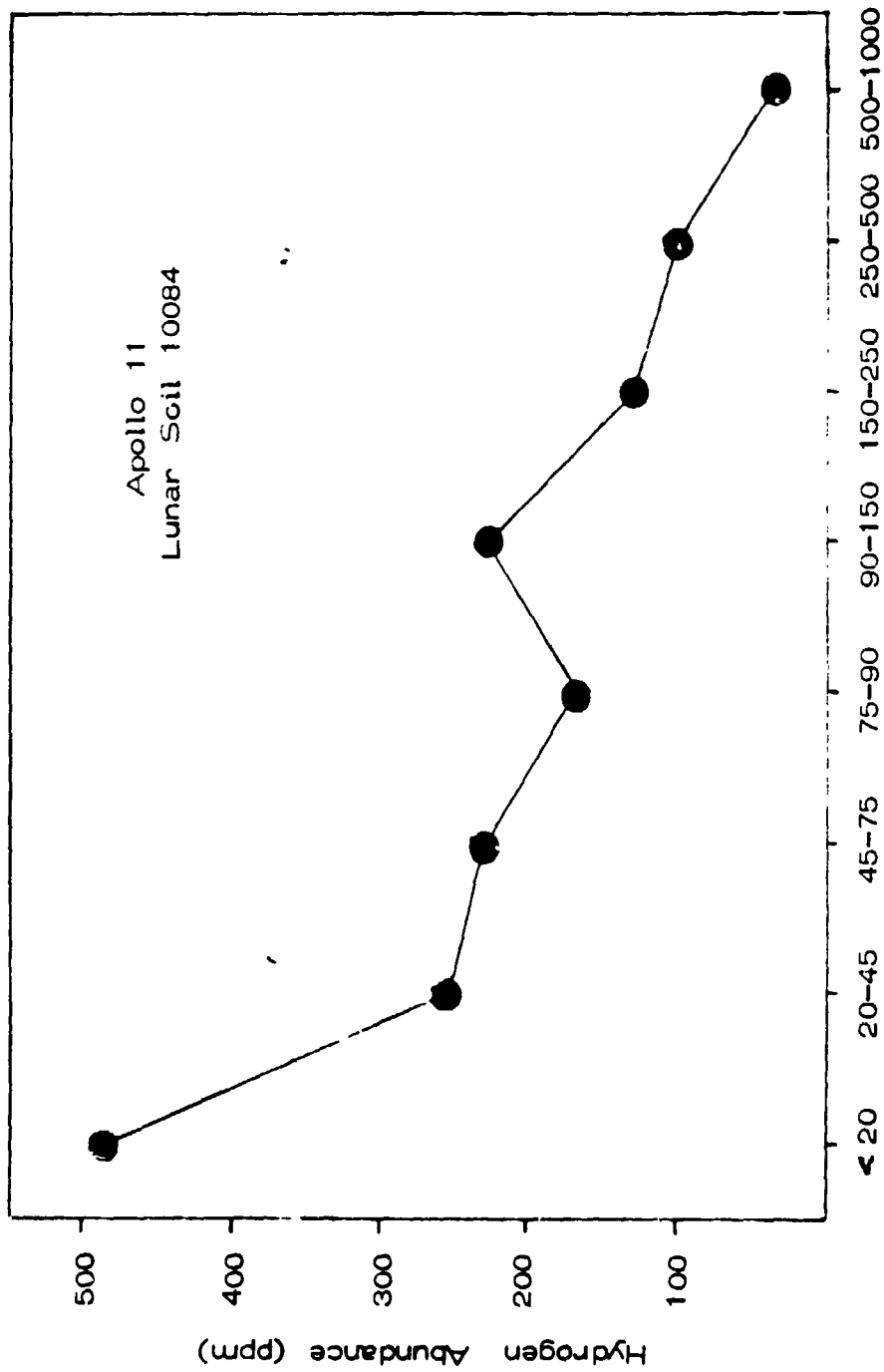


Figure 3

DISTRIBUTION OF HYDROGEN
WITH RESPECT TO PARTICLE SIZE

Apollo 11
Lunar Soil 10084



Particle Size (µm)

Figure 4

DISTRIBUTION OF HYDROGEN
WITH RESPECT TO PARTICLE SIZE.

Apollo 17
Lunar Soil 71501

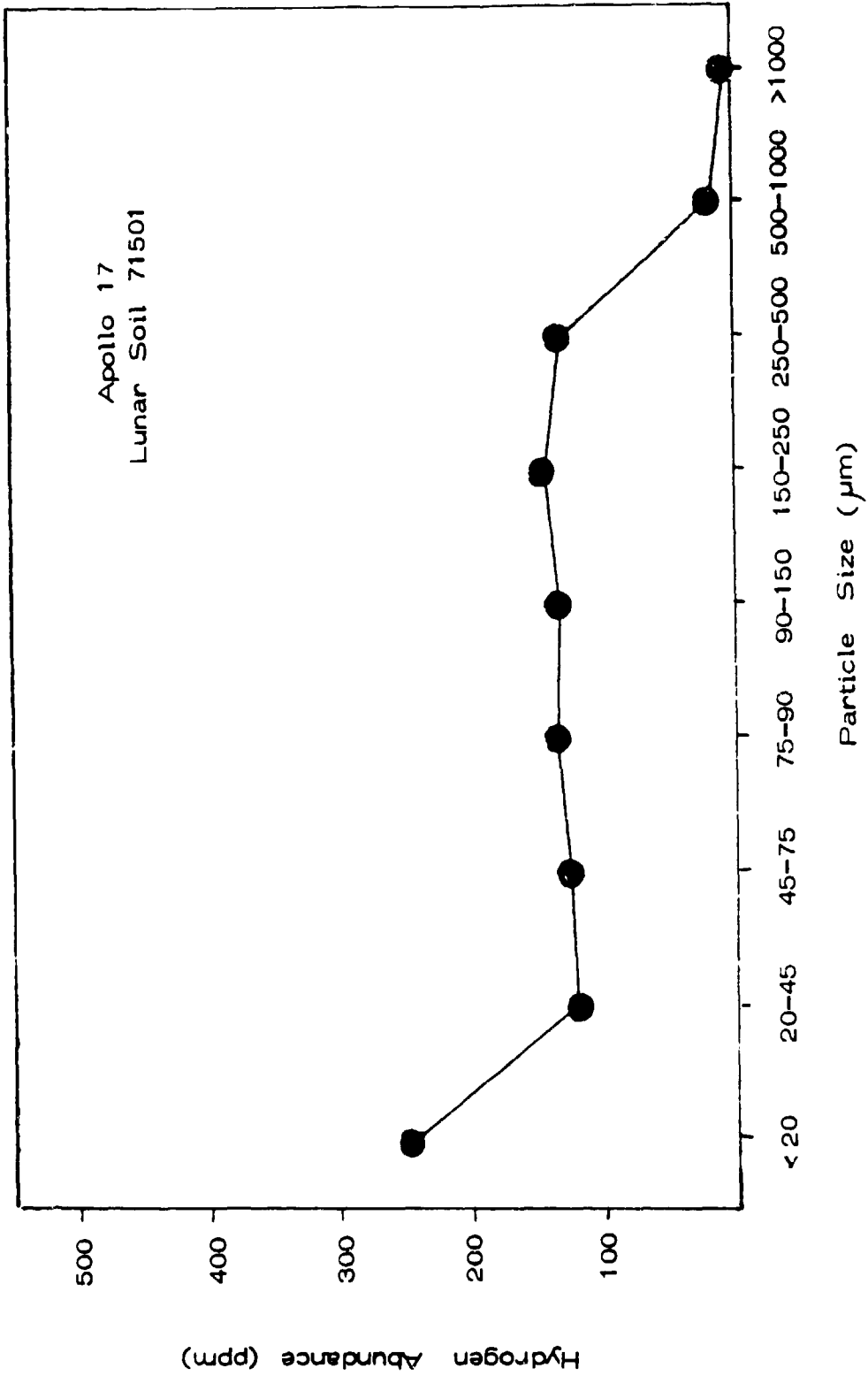


Figure 5

Table 1. CONCENTRATIONS OF HYDROGEN IN LUNAR SOILS

Sample Number	Hydrogen Concentration ppm
10084	59
14003	106
14163	67
14259	61
15021	70
15271	38
15601	54
61221	19
64421	60
66041	76
73141	50
75111	47

FINITE ELEMENT OR GALERKIN TYPE SEMIDISCRETE SCHEMES †

Kanat Durgun *

ABSTRACT

A finite element or Galerkin type semidiscrete method is proposed for numerical solution of a linear hyperbolic partial differential equation. The question of stability is reduced to the stability of a system of ordinary differential equations for which Dahlquist theory applies.

We also present some results of separating the part of numerical solution which causes the spurious oscillation near shock-like response of semidiscrete scheme to a step function initial condition. In general all methods produce such oscillatory overshoots on either side of shocks. This overshoot pathology, which displays a behaviour similar to Gibb's phenomena of Fourier series, is explained on the basis of dispersion of separated Fourier components which relies on linearized theory to be satisfactory. We present expository results, polished formal proofs will appear elsewhere.

INTRODUCTION

Our model of one and two dimensional linear hyperbolic equations are

$$(1) \quad \frac{\partial U}{\partial t} + c \frac{\partial U}{\partial x} = 0$$

$$(2) \quad \frac{\partial U}{\partial t} + a \frac{\partial U}{\partial x} + b \frac{\partial U}{\partial y} = 0$$

† NASA Summer Faculty Fellow

* Associate Professor of Mathematics, University of Arkansas at Little Rock.

Introducing $c = \sqrt{a^2 + b^2}$, $c_x = c \cos \alpha$ and $c_y = c \sin \alpha$ equation (2) can be written as

$$(2') \quad \frac{\partial U}{\partial t} + c \cos \alpha \frac{\partial U}{\partial x} + c \sin \alpha \frac{\partial U}{\partial y} = 0$$

Galerkin or finite element semidiscretization [1], [2], [3], [4], seeks an approximate solution for equation (2') in the form

$$(3) \quad u(x, y, t) = \sum_{m,n} \varphi_{mn}(x, y) u_{mn}(t)$$

where

$$(4) \quad \varphi_{mn}(x, y) = \begin{cases} 1 & x = x_m, y = y_n \\ 0 & \text{Otherwise.} \end{cases}$$

We obtain a system of ordinary differential equations by requiring that the residual $R = \frac{\partial u}{\partial t} + c \cos \alpha \frac{\partial u}{\partial x} + c \sin \alpha \frac{\partial u}{\partial y}$ be orthogonal to the basis functions φ_{mn} i.e. $\langle \varphi_{mn}, R \rangle = 0$. Candidates for φ_{mn} are too many producing algorithms with increasing complexity proportional with their smoothness. We only present bilinear finite elements on squares. The orthogonality requirement yields, say in one dimensional case

$$(5) \quad \frac{d}{dt} K_h u_n(t) = L_h u_n(t)$$

where K_h and L_h are discrete Toeplitz operators with eigenvectors $\{e^{i\omega x_n}\}$. If K_h is an identity operator then scheme is explicit, otherwise implicit. If the real part of the corresponding eigenvalue $\lambda(\omega)$ is zero then the scheme is conservative [6], [7]. The quantity

$$(6) \quad \tilde{c}(\omega) = -\frac{\text{Im} \lambda(\omega)}{\omega}$$

is the velocity of propagation of numerical solutions in comparison with exact propagation velocity C in (1). The quotient $\tilde{c}(\omega)/C$ or difference $\tilde{c}(\omega) - C$ in an appropriate norm is the measure of spurious oscillations and dispersions in numerical solutions. Purely mathematical treatment without the effects of discretization i.e. nonnumerical can be found in [8].

In the next sections, to study the response of semidiscrete scheme to sharp

gradient changes we simulate a shock by a step function initial condition in (1), here we present an heuristic argument for the cause of parasitic oscillations around a point of discontinuity.

Consider the weighted Galerkin semidiscretization

$$(7) \quad \frac{\alpha}{2} \frac{du_{n+1}}{dt} + (1-\alpha) \frac{du_n}{dt} + \frac{\alpha}{2} \frac{du_{n-1}}{dt} = -\frac{c}{2h} (u_{n+1} - u_{n-1})$$

of our model equation (1), where $\alpha \in [0,1]$ is a parameter. Note that $\alpha=0$ corresponds to the equation

$$(8) \quad \frac{du_n}{dt} = \text{centered difference approximation to } \left(-c \frac{\partial u}{\partial x}\right)$$

Since for any n , in equation (7), indices take three successive integer values we may relabel them for n even as u_n and for n odd as v_n we then obtain respectively the following systems

$$(9) \quad \begin{aligned} \frac{du_n}{dt} &= -\frac{c}{2h} (v_{n+1} - v_{n-1}) \\ \frac{dv_n}{dt} &= -\frac{c}{2h} (u_{n+1} - u_{n-1}) \end{aligned}$$

for $\alpha=0$, and

$$(10) \quad \begin{aligned} \frac{\alpha}{2} \left(\frac{dv_n}{dt} + \frac{dv_{n-1}}{dt} \right) + (1-\alpha) \frac{du_n}{dt} &= -\frac{c}{2h} (v_{n+1} - v_{n-1}) \\ (1-\alpha) \frac{dv_n}{dt} + \frac{\alpha}{2} \left(\frac{du_{n+1}}{dt} + \frac{du_{n-1}}{dt} \right) &= -\frac{c}{2h} (u_{n+1} - u_{n-1}) \end{aligned}$$

These equations are consistent approximations for the following systems

$$(11) \quad \begin{aligned} \frac{\partial u}{\partial t} &= -c \frac{\partial v}{\partial x} \\ \frac{\partial v}{\partial t} &= -c \frac{\partial u}{\partial x} \end{aligned}$$

$$(12) \quad \begin{aligned} \alpha \frac{\partial v}{\partial t} + (1-\alpha) \frac{\partial u}{\partial t} &= -c \frac{\partial v}{\partial x} \\ (1-\alpha) \frac{\partial v}{\partial t} + \alpha \frac{\partial u}{\partial t} &= -c \frac{\partial u}{\partial x} \end{aligned}$$

Eliminating u or v in (11) we obtain respectively

$$(13) \quad \begin{aligned} \frac{\partial^2 u}{\partial t^2} &= c^2 \frac{\partial^2 u}{\partial x^2} \\ \frac{\partial^2 v}{\partial t^2} &= c^2 \frac{\partial^2 v}{\partial x^2} \end{aligned}$$

Showing that in a doubly spaced grid wave equation is satisfied. This indicates that finite differencing is consistent with (13) rather than (1). Also adding the equations in (11)

$$(14) \quad \frac{\partial}{\partial t} \left(\frac{u+v}{2} \right) = -c \frac{\partial}{\partial x} \left(\frac{u+v}{2} \right)$$

we see that discretization is consistent for the average of the solutions at two successive grid points. However subtracting equations in (11) we obtain

$$(15) \quad \frac{\partial}{\partial t} (u-v) = c \frac{\partial}{\partial x} (u-v)$$

This shows that due to discretization difference, however small, of two successive solutions propagates as an error wave in the discrete medium in the opposite direction.

For (12), adding we obtain

$$(16) \quad \frac{\partial}{\partial t} \left(\frac{u+v}{2} \right) = -c \frac{\partial}{\partial x} \left(\frac{u+v}{2} \right)$$

and subtracting we find

$$(17) \quad \frac{\partial}{\partial t} (v-u) = \frac{-c}{1-2\alpha} \frac{\partial}{\partial x} (v-u) \quad \alpha \neq \frac{1}{2},$$

which is the cause of oscillations in general.

GALERKIN SEMIDISCRETIZATION FOR EQUATION (2')

On the square with vertices (x_{m-1}, y_{n+1}) , (x_{m+1}, y_{n+1}) , (x_{m+1}, y_{n-1}) and (x_{m-1}, y_{n-1}) we take basis functions to be

$$(18) \quad \psi_{mn}(x,y) = \begin{cases} 1 + \frac{x-x_m}{h} & \text{for } \begin{array}{l} x_{m-1} \leq x \leq x_m \\ y_n - (x-x_m) \leq y \leq y_n + (x-x_m) \end{array} \\ 1 - \frac{y-y_n}{h} & \text{for } \begin{array}{l} y_n \leq y \leq y_{n+1} \\ x_m - (y-y_n) \leq x \leq x_m + (y-y_n) \end{array} \\ 1 - \frac{x-x_m}{h} & \text{for } \begin{array}{l} x_m \leq x \leq x_{m+1} \\ y_n - (x-x_m) \leq y \leq y_n + (x-x_m) \end{array} \\ 1 + \frac{y-y_n}{h} & \text{for } \begin{array}{l} y_{n-1} \leq y \leq y_n \\ x_m + (y-y_n) \leq x \leq x_m - (y-y_n) \end{array} \\ 0 & \text{otherwise} \end{cases}$$

These are pyramids whose base is a square with vertices are given above, centered at (x_m, y_n) with unit height. Forming the inner products with the residual we obtain

$$(19) \quad \langle \varphi_{m,n}, \sum_{k,l} [\varphi_{kl} \frac{du_{kl}}{dt} + c_x u_{kl} \frac{\partial \varphi_{kl}}{\partial x} + c_y u_{kl} \frac{\partial \varphi_{kl}}{\partial y}] \rangle = 0 \quad \forall m,n.$$

Only nonvanishing terms come for the values of indices $k = m-1, m, m+1$ and $l = n-1, n, n+1$.

Thus equation (19) reduces to

$$(20) \quad \sum_{k=1}^1 \sum_{l=1}^1 \langle \varphi_{m,n}, \varphi_{m-k, n-l} \frac{du_{m-k, n-l}}{dt} + c_x u_{m-k, n-l} \frac{\partial \varphi_{m-k, n-l}}{\partial x} + c_y u_{m-k, n-l} \frac{\partial \varphi_{m-k, n-l}}{\partial y} \rangle = 0$$

Computation of inner products as double integrals are straightforward but

tedious. Replacing the values of various integrals in equation (20), we obtain

$$(21) \quad \frac{1}{36} \frac{d}{dt} [u_{m-1, n-1} + 4u_{m, n-1} + u_{m+1, n-1} + 4u_{m-1, n} + 16u_{m, n} + 4u_{m+1, n} + u_{m-1, n+1} + 4u_{m, n+1} + u_{m+1, n+1}] \\ = -\frac{1}{2h} [-\theta u_{m-1, n-1} - \alpha_y u_{m, n-1} + \mu u_{m+1, n-1} - \alpha_x u_{m-1, n} + \alpha_x u_{m+1, n} - (\mu u_{m-1, n+1} + \alpha_y u_{m, n+1} + \theta u_{m+1, n+1})]$$

where $\theta = \frac{c_x + c_y}{6}$, $\mu = \frac{c_x - c_y}{6}$, $\alpha_x = \frac{2c_x}{3}$ and $\alpha_y = \frac{2c_y}{3}$.

system of equations (21) can be written in matrix notation on a rectangle $[0, (M+1)h]$

$\times [0, (N+1)h]$ in various ways. Let $U_k = [u_{k1}, u_{k2}, \dots, u_{kN}]^T$, $k=1, 2, \dots, N$, I_N be the

$N \times N$ identity matrix, and $L_N = [l_{ij}]_{N \times N}$ where

$$l_{ij} = \begin{cases} 1 & j = i-1 \\ 0 & \text{otherwise,} \end{cases}$$

superscript T indicates transposition. Then

$$\frac{1}{36} \frac{d}{dt} [4(L_N + 4I_N + L_N^T)U_1 + (L_N + 4I_N + L_N^T)U_2] = -\frac{1}{2h} [\alpha_y (-L_N + L_N^T)U_1 + (\mu L_N + \alpha_x I_N + \theta L_N^T)U_2] - \frac{1}{2h} [v_0 + w_1 + x_2 - (\theta L_N + \alpha_x I_N + \mu L_N^T)U_0] - \frac{1}{36} \frac{d}{dt} [(L_N + 4I_N + L_N^T)U_0 + y_0 + 4y_1 + y_2]$$

$$(22) \quad \frac{1}{36} \frac{d}{dt} [(L_N + 4I_N + L_N^T)U_{m-1} + 4(L_N + 4I_N + L_N^T)U_m + (L_N + 4I_N + L_N^T)U_{m+1}] = -\frac{1}{2h} [-(\theta L_N + \alpha_x I_N + \mu L_N^T)U_{m-1} + \alpha_y (-L_N + L_N^T)U_m + (\mu L_N + \alpha_x I_N + \theta L_N^T)U_{m+1}]$$

Then the system (22) in vector and block tridiagonal matrix notation becomes

$$(23) \quad \frac{1}{36} \frac{d}{dt} \begin{bmatrix} 4T_N & T_N & & & \\ T_N & 4T_N & & & \\ & & \circ & & \\ & & & T_N & \\ & & & T_N & 4T_N \end{bmatrix} \begin{bmatrix} U_1 \\ U_2 \\ \vdots \\ U_M \end{bmatrix} = -\frac{1}{2h} \begin{bmatrix} \alpha_N & \beta_N & & & \\ -\beta_N^T & \alpha_N & & & \\ & & \circ & & \\ & & & \beta_N & \\ & & & -\beta_N^T & \alpha_N \end{bmatrix} \begin{bmatrix} U_1 \\ U_2 \\ \vdots \\ U_M \end{bmatrix}$$

$$-\frac{1}{2h} \left\{ \begin{bmatrix} -\beta_N^T & & & & \\ & \circ & & & \\ & & \circ & & \\ & & & \circ & \\ & & & & \beta_N \end{bmatrix} \begin{bmatrix} U_0 \\ 0 \\ \vdots \\ 0 \\ U_{M+1} \end{bmatrix} + \begin{bmatrix} v_0 + w_1 + x_2 \\ v_1 + w_2 + x_3 \\ \vdots \\ v_{M-1} + w_M + x_{M+1} \end{bmatrix} \right\} - \frac{1}{36} \frac{d}{dt} \left\{ \begin{bmatrix} T_N & & & & \\ & \circ & & & \\ & & \circ & & \\ & & & \circ & \\ & & & & T_N \end{bmatrix} \begin{bmatrix} U_0 \\ 0 \\ \vdots \\ 0 \\ U_{M+1} \end{bmatrix} + y \right\}$$

where

$$y = [y_0 + y_1 + y_2, y_1 + y_2 + y_3, \dots, y_{M-1} + y_M + y_{M+1}]^T$$

Here entries of matrices are $N \times N$ matrices and entries of vectors are N vectors.

Note that for time independent boundary conditions the last term in this equation vanishes. Further simplification is obtained by introducing NM dimensional vectors or M dimensional compound vectors i.e vectors whose components are N dimensional vectors,

$$U = \begin{bmatrix} U_1 \\ U_2 \\ \vdots \\ U_M \end{bmatrix}, \quad V = \begin{bmatrix} v_0 \\ v_1 \\ \vdots \\ v_{M+1} \end{bmatrix}, \quad W = \begin{bmatrix} w_1 \\ w_2 \\ \vdots \\ w_M \end{bmatrix}, \quad X = \begin{bmatrix} x_2 \\ x_3 \\ \vdots \\ x_{M+1} \end{bmatrix}, \quad Z = \begin{bmatrix} -\beta_N^T U_0 \\ 0 \\ \vdots \\ \beta_N U_{M+1} \end{bmatrix}, \quad C = -\frac{1}{2h} [Z + V + W + X]$$

and the square matrices of order NM , A for the matrix on the left and B for the matrix on the right hand side of equation (23).

The linear system (22) or equivalently (23) can be written as

$$(24) \quad \frac{1}{36} \frac{d}{dt} A U = -\frac{1}{2h} B U + C$$

corrector), once a starting procedure is realized by a one step method, are available, and their stability theory is well understood and detailed treatment can be found in [10], [11].

To show that the finite differencing scheme is conservative, we must show that the eigenvalues $\lambda(\omega, \alpha)$ of Galerkin difference operators in (21) belonging to eigenvectors $\exp i[\omega_x x_m + \omega_y y_n]$, are purely imaginary where $\omega_x = \omega \cos \alpha$ and $\omega_y = \omega \sin \alpha$. Substituting $u_{mn}(t) = a_w(t) \exp i[\omega_x x_m + \omega_y y_n]$ in (21) after some manipulation yields for the left hand side

$$\text{L.H.S} = \frac{1}{36} a_w'(t) e^{i[\omega_x x_m + \omega_y y_n]} \left[e^{-ih(\omega_x + \omega_y)} + 4e^{-ih\omega_y} + e^{ih(\omega_x - \omega_y)} + 4e^{-ih\omega_x} + 16 + 4e^{ih\omega_x} + e^{-ih(\omega_x - \omega_y)} + 4e^{ih\omega_y} + e^{ih(\omega_x + \omega_y)} \right] = \frac{1}{9} a_w'(t) e^{i[\omega_x x_m + \omega_y y_n]} [2 + \cos \omega_x h][2 + \cos \omega_y h],$$

and for the right hand side

$$\text{R.H.S} = -\frac{1}{2h} a_w(t) e^{i[\omega_x x_m + \omega_y y_n]} \left[\theta (e^{ih(\omega_x + \omega_y)} - e^{-ih(\omega_x + \omega_y)}) + \alpha_y (e^{ih\omega_y} - e^{-ih\omega_y}) + \alpha_x (e^{ih\omega_x} - e^{-ih\omega_x}) + \mu (e^{ih(\omega_x - \omega_y)} - e^{-ih(\omega_x - \omega_y)}) \right] = -\frac{i}{3h} a_w(t) e^{i[\omega_x x_m + \omega_y y_n]} [C_x \sin \omega_x h (2 + \cos \omega_y h) + C_y \sin \omega_y h (2 + \cos \omega_x h)]$$

Hence

$$a_w'(t) = a_w(t) \lambda(\omega, \alpha)$$

where

$$(26) \lambda(\omega, \alpha) = -i \mu \left[\cos^2 \alpha \frac{\sin \omega_x h}{\omega_x h} \frac{1}{\frac{2}{3} + \frac{1}{3} \cos \omega_x h} + \sin^2 \alpha \frac{\sin \omega_y h}{\omega_y h} \frac{1}{\frac{2}{3} + \frac{1}{3} \cos \omega_y h} \right]$$

which is imaginary. Setting $\omega \tilde{C}(\omega, \alpha) = -\text{Im} \lambda(\omega, \alpha)$ we find the numerical solution

$$u_{mn}(t) = a_w(0) \exp i[\omega_x x_m + \omega_y y_n - \omega \tilde{C}(\omega, \alpha) t].$$

The discrepancy between $\tilde{C}(\omega, \alpha)$ and C or more precisely the order of zero of $\tilde{C}(\omega, \alpha) - C$ about $\omega h = 0$ is the the order of accuracy of the semidiscrete method.

To show that this method is of order four, we expand $\tilde{C}(\omega, \alpha)$ in a Taylor series

and a straightforward computation shows that

$$(27) \tilde{C}(\omega, \alpha) - C = -\frac{C(\cos^6 \alpha + \sin^6 \alpha)}{180} (\omega h)^4 + O((\omega_x h)^6 + (\omega_y h)^6).$$

ERROR ESTIMATES FOR PRE AND POST OSCILLATIONS ABOUT DISCONTINUITIES

To justify the heuristic argument presented earlier we may assume that this spurious oscillations are represented by small perturbations in ω , and replace ω by $\omega + \epsilon$ in trial solutions

$$(28) \quad u(x,t) = a_\epsilon e^{i(\omega + \epsilon)[x - \tilde{c}(\omega + \epsilon)t]}$$

Expanding $\tilde{c}(\omega + \epsilon)$ in a Taylor series about $\epsilon = 0$ and retaining only the linear terms we obtain

$$\tilde{c}(\omega + \epsilon) \approx \tilde{c}(\omega) + \epsilon \tilde{c}'(\omega)$$

Since $\omega \gg \epsilon$, terms of order ϵ^2 can be neglected and introducing group velocity

$$(29) \quad g(\omega) = \frac{d}{d\omega} (\omega \tilde{c}(\omega))$$

(28) can be written as

$$(30) \quad u(x,t) = a_\epsilon e^{i\omega(x - \tilde{c}(\omega)t)} e^{i\epsilon(x - g(\omega)t)}$$

Straightforward computation shows that eigenvalues of (7) corresponding to eigenvectors $\{e^{i\omega x_n}\}$, are

$$\lambda(\omega) = \frac{-ic}{1 - \alpha + \alpha \cos \omega h} \frac{\sin \omega h}{h}$$

and therefore

$$\tilde{c}(\omega) = \frac{c}{1 - \alpha + \alpha \cos \omega h} \frac{\sin \omega h}{\omega h}$$

Using (29), $g(\omega)$ is easily computed as

$$(31) \quad g(\omega) = c \frac{\alpha + (1 - \alpha) \cos \omega h}{(1 - \alpha + \alpha \cos \omega h)^2}$$

Due to the discretization of the domain of the equation, the group velocity corresponding to $2h$ wavelength, from equation (31) is

$$(32) \quad g\left(\frac{\pi}{h}\right) = -\frac{c}{1 - 2\alpha}$$

which is the same as depicted in (17) and for $\alpha = c$ in (15).

To obtain estimates on local and global error of numerical solution we recall the definitions. [5] p.43, [13]. We say an infinite series $\sum u_k$ is (C,1)

summable if $\lim_{n \rightarrow \infty} \sigma_n = \lim_{n \rightarrow \infty} \frac{S_0 + S_1 + \dots + S_n}{n+1} = S$ exists where $S_k = \sum_{l=0}^k u_l$, in this case we write $\sum u_k = S$ (C,1) sense.

An infinite series $\sum u_k$ is said to be summable by Abel's method (some say Poisson's) or simply A-summable to s , if $\sum u_k r^k$ is convergent for $|r| < 1$ and $\lim_{r \rightarrow 1} \sum u_k r^k = \lim_{r \rightarrow 1} (1-r) \sum S_k r^k = S$ where S_k is defined above.

We need two results, the first is that the series

$$(33) \quad \frac{1}{2} + \sum_{n=1}^{\infty} \cos nx$$

is (C,1) and also A-summable to zero.

It is known that, [5] p.20

$$S_n = \frac{1}{2} + \sum_{k=1}^n \cos kx = \frac{1}{2} \frac{\sin(n+\frac{1}{2})x}{\sin \frac{x}{2}} \quad x \neq 2l\pi$$

and from the trigonometric identity

$$2 \sin \frac{x}{2} \sin(k+\frac{1}{2})x = \cos kx - \cos(k+1)x.$$

It follows that

$$\sum_{k=0}^{n-1} \sin(k+\frac{1}{2})x = \frac{\sin^2 \frac{nx}{2}}{\sin \frac{x}{2}}$$

Thus

$$\sigma_n = \frac{1}{n+1} \sum_{k=0}^n S_k = \frac{1}{n+1} \frac{1}{2 \sin \frac{x}{2}} \sum_{k=0}^n \sin(k+\frac{1}{2})x = \frac{1}{n+1} \frac{\sin^2 \frac{n+1}{2} x}{\sin^2 \frac{x}{2}} \quad x \neq 2l\pi$$

and $\lim_{n \rightarrow \infty} \sigma_n = 0$. To show A-summability, recall the Poisson's formula [5], p.61;

$$\frac{1}{2} + \sum_{n=1}^{\infty} r^n \cos nx = \frac{1-r^2}{2(1-2r \cos x + r^2)} \quad |r| < 1$$

Letting $r \rightarrow 1$ we see that the assertion is true.

The second result is that

$$(34) \quad \sum_{n=1}^{\infty} \sin nx$$

is (C,1) and also A-summable to $\frac{1}{2} \cot \frac{x}{2}$

It is known that [5], p.21;

$$S_n = \sum_{k=1}^n \sin kx = \frac{1}{2} \cot \frac{x}{2} - \frac{1}{2} \frac{\cos(n+\frac{1}{2})x}{\sin \frac{x}{2}}$$

Using the trigonometric identity

$$2 \sin \frac{x}{2} [\cos \frac{3x}{2} + \cos \frac{5x}{2} + \dots + \cos(n+\frac{1}{2})x] = \sin(n+1)x - \sin x$$

we find

$$\sigma_n = \frac{S_1 + S_2 + \dots + S_n}{n+1} = \frac{n}{n+1} \frac{1}{2} \cot \frac{x}{2} - \frac{1}{4 \sin^2 \frac{x}{2}} \frac{\sin(n+1)x - \sin x}{n+1}$$

and the result follows by letting $n \rightarrow \infty$

To show A-summability we use Poisson's formula

$$\sum_{n=1}^{\infty} r^n \sin nx = \frac{r \sin x}{1 - 2r \cos x + r^2}$$

and let $r \rightarrow 1$.

We now estimate the \mathcal{L}_2 norm of the global error. As a direct consequence of Parseval's identity, it is known that Fourier transform is an isometric isomorphism between the Hilbert spaces involved [16] p.51-52, [15] p.25. Therefore it suffices to compute the \mathcal{L}_2 norm of the Fourier transform of the error. To simulate the shock, we let the initial condition to be the step function

$$(35) \quad U(x, 0) = \begin{cases} 1 & x \geq 0 \\ 0 & x < 0 \end{cases}$$

Without loss of generality we may assume that the discrete Fourier transform of the net initial condition $u_n(0)$ is equal to the Fourier transform of (35), and we obtain

$$(36) \quad \hat{U}(\omega, 0) = \hat{u}_n(\omega, 0) = h \sum_{-\infty}^{\infty} u_n(0) e^{-i\omega x_n} = h \sum_{n=0}^{\infty} e^{-i\omega n h} = h \left[1 + \sum_1^{\infty} \cos \omega n h - i \sum_1^{\infty} \sin \omega n h \right]$$

It follows from the proofs of statements concerning equations (33) and (34) that series on the right of equation (36) is (C,1) and hence A-summable to

$$(37) \quad \hat{U}(\omega, 0) = \hat{u}_n(\omega, 0) = \frac{h e^{\frac{i\omega h}{2}}}{2i \sin \frac{\omega h}{2}}$$

From equation (1), Fourier transform of the exact solution is easily computed

$$\hat{U}(\omega, t) = \hat{U}(\omega, 0) e^{-i\omega t}$$

$u_n(t)$ is the solution of semidiscrete equation, for simplicity we assume K_h to be the identity operator, taking the discrete Fourier transform of the semidiscrete equation and solving the resulting differential equation one obtains

$$\hat{u}(\omega, t) = \hat{u}(\omega, 0) e^{\lambda(\omega)t}$$

For conservative schemes $\lambda(\omega) = -i\omega \tilde{c}(\omega)$, therefore the \mathcal{L}_2 norm of the global error is

$$\|E\|_2^2 = \frac{1}{2\pi} \int_{-\frac{\pi}{h}}^{\frac{\pi}{h}} |\hat{u}(\omega, 0)|^2 |e^{-i\omega \tilde{c}(\omega)t} - e^{-i\omega t}|^2 d\omega$$

Introducing dimensionless variables $\tau = \frac{tc}{h}$ and $y = \omega h$, a straightforward computation shows that

$$\|E\|_2^2 = \frac{h}{\pi} \int_0^\pi \frac{\sin^2 \frac{y\tau}{c} (\tilde{c}(\frac{y}{\pi}) - c)}{\sin^2 \frac{y}{2}} dy.$$

CONCLUSION

The semidiscrete method proposed here has a reasonable Courant number and a fourth order accuracy. Results are theoretically conclusive. Computational evidence for detailed comparison of this method with conventional methods will await our numerical experiments.

The measure of oscillations in the numerical solution, in a neighborhood of sharp changes is the pointwise error. We were able to show with a lengthy argument, although there are some gaps in details of proofs, that maxima of the difference between the exact and the numerical solutions continually diminish and minima continually increase in an interval of length $4h$ on each side of the sharp gradient change. Numerical solution is approximately $0.28h$ larger in the upstream direction.

ACKNOWLEDGEMENT

I wish to express my sincere appreciation to Dr. W. Goodrich for providing me the encouragement and this gratifying experience. I would also like to acknowledge the pleasant working environment provided for NASA at Johnson Space Center.

REFERENCES

1. Babuska, I. and Aziz, A. K.: Survey Lectures on the Mathematical Foundations of the Finite Elements Method with Applications to Partial Differential Equations Academic Press, NY 1972.
2. Mitchell, A. R. and Wait, R.: The Finite Element Method in Partial Differential Equations, Wiley, 1977.
3. Thomee, V.: Convergence Estimates for Semidiscrete Galerkin Methods for Variable Coefficient Initial Value Problems. Lecture notes in Math., 333, Springer, Berlin, 1973, pp. 243-262.
4. Layton, W. J.: Stable Galerkin Methods for Hyperbolic Systems. SIAM J. Numerical Analysis, Vol. 20, April 1983, pp. 221-233.
5. Zygmund, A.: Trigonometrical Series. Dover, 1955.
6. Hyman, J. M.: A Method of Lines Approach to the Numerical Solution of Conservation Laws. Advances in Computer Methods for Partial Differential Equations. IMACS, New Brunswick, NJ, 1979.
7. Lax, P. D.: Hyperbolic Systems of Conservation Laws II. Comm. on Pure and Applied Math., Vol. 7, 1959, pp. 159-193.
8. Morawetz, C. S.: Notes on Time Decay and Scattering for Some Hypersolic Problems. SIAM Regional Conference Series in Applied Mathematics.
9. Varga, R. S.: Matrix Iterative Analysis, Prentice-Hall, Englewood Cliffs, NJ, 1962.
10. Dahlquist, G.: Stability and Error Bounds in the Numerical Integration of Ordinary Differential Equations. Inaugural Dissertation. Appala, Sweden, 1958.
11. Henrici, P.: Error Propagation for Difference Methods. SIAM Series in Applied Mathematics. John Wiley, 1963.
12. Vichnevetsky, R. and Bowles, J. B.: Fouries Analysis of Numerical Approximations of Hyperbolic Equations. SIAM Studies in Applied Mathematics. 1982.
13. Hardy, G. H. and Rogosinski, W. W.: Fourier Series. Cambridge. 1968.
14. Whitham, G. D.: Linear and Nonlinear Waves, Wiley. 1974.
15. Sneddon, I. N.: Fourier Transforms. McGraw Hill. 1951.
16. Richtmyer, R. D.: Difference Methods for Initial Value Problems. Interscience. 1962.

N86-14084

DETERMINATION OF NEUTRON FLUX DISTRIBUTION BY USING ANISN, A ONE-DIMENSIONAL DISCRETE S_n ORDINATES TRANSPORT CODE WITH ANISOTROPIC SCATTERING

by

Susanta K. Ghorai

Associate Professor of Physics

Alabama State University

Montgomery, Alabama 36195

ABSTRACT

The purpose of this project was to use a one-dimensional discrete ordinates transport code called ANISN in order to determine the energy-angle-spatial distribution of neutrons in a 6-foot cube rock box which houses a D-T neutron generator at its center. The project was two-fold. The first phase of the project involved adaptation of the ANISN code written for an IBM 360/75/91 computer to the UNIVAC system at JSC. The second phase of the project was to use the code with proper geometry, source function and rock material composition in order to determine the neutron flux distribution around the rock box when a 14.1 MeV neutron generator placed at its center is activated.

Advisor: Dr. James E. Keith

INTRODUCTION

Accurate determination of neutron flux distribution as a function of energy, angle and space is highly important in situations such as neutron dosimetry work, shielding problems, and in situations which involve neutron exposure. Analytical method of determining energy-angle-spatial distribution of neutrons or photons involves solving the conservation equation known as the Boltzmann transport equation. Much of the stimulus for the development of transport theory came from problems connected with the design and operation of nuclear reactors. However, actual problems are usually highly complex which can be best handled through high speed computing machines by using approximate numerical solution of the transport equation. The method of discrete ordinates has become a powerful tool for the numerical solution of the Boltzmann transport equation. Oak Ridge National Laboratory transport program called ANISN-ORNL (1) is a one dimensional discrete ordinates S_n transport code with general anisotropic scattering. In this project ANISN has been successfully adapted to the UNIVAC system of JSC and some progress has been made in analyzing the rock box problem.

ANISN AND ITS ADAPTATION

ANISN is a FORTRAN IV, version 13 program which uses the discrete ordinates or S_n method in solving one dimensional Boltzmann transport equation for slab, cylinder and spherical geometry. As a secondary calculation, the detailed flux generated as the solution may be used to perform group reduction of the cross sections. The discrete ordinates method has been reviewed by Carlson (2), Lee (3), Mynatt (4) and Lathrop (5). It is not the purpose of this report to discuss the discrete ordinates method or to describe the ANISN code. However, for facilitating the process of running the ANISN program,

some observations will be made here regarding the approximation features used in ANISN. Although the discrete ordinates method should solve the transport equation exactly in the limit of infinite computation time and infinitesimally fine mesh in all variables, in practice a number of approximations are essential. These include the approximation of continuous functions by discontinuous sets of approximations in energy, spatial and angular meshes and representation of the angular dependence of scattering by a small set of truncated Legendre polynomials.

a. Selection of Groups and P_ℓ

ANISN allows general anisotropic scattering through an ℓ -th order (P_ℓ) Legendre polynomial expansion of the scattering cross section. There are really two types of anisotropic scattering, first is the heavy nuclide elastic scattering of neutrons which at high energies is extremely anisotropic but the angle-energy correlation is unimportant; second is the elastic scattering of neutrons by hydrogen or the Compton scattering of gammas which has an important angle-energy correlation which becomes an angle-group correlation. The method used for anisotropic scattering in the discrete ordinates equations appears to work very well for both types of scattering (4). Low order approximations such as P_2 or P_3 are adequate for most practical problems (4).

The multigroup Legendre polynomial expansion method is used to prepare cross sections. A typical discrete ordinates transport calculation may use from 30 to 100 groups and a P_3 expansion (6). One group-to-group transfer table is required for each Legendre term, hence 4 for P_3 (P_0, P_1, P_2, P_3). Computer storage increases rapidly with the number of energy groups and tables. Bugle-80 which has been used in this project to provide cross sections for ANISN, provides 47 neutron and 20 gamma, P_3 cross sections for ANISN. An example of neutron group cross section is given in Table 1. This

table gives the P_0 through P_3 cross section tables for the first three neutron groups in iron. The format corresponds to the positions used in ANISN. Position 1 contains the absorption cross section. Position 2 contains $\nu\sigma_f$ (it is 0 in case of iron since there is no fission in iron). The total cross section appears in position 3. Position 4 contains the within-group scattering cross section $\sigma_{g \rightarrow g}$ where g is the group number. Position 5 contains the cross section for scattering from group $(g-1)$ into group g . Position 6 contains the cross section for scattering from group $(g-2)$ into group g , and so forth.

b. Selection of Angular Quadrature

The flux is anisotropic, and a reasonably large order of angular quadrature set (quadrature direction μ_m and quadrature weights w_m) is necessary (7). The most accurate quadrature set for integrating the Legendre polynomials for a given n is the Gauss-Legendre quadratures (μ_m at zeros of Legendre polynomials, $m = 1, 2, 3, \dots, n+1$). A relatively low-order quadrature, such as S_8 for P_3 cross sections, would be sufficient as far as inscattering source is concerned (6). However, in radiation transport, the angular flux density is usually very anisotropic and a high-order set may be needed to properly represent the angular distribution in the output (6).

TABLE 1
IRON NEUTRON GROUP CROSS SECTION FOR FIRST THREE NEUTRON GROUPS (BARNs)

	Position		Group 1	Group 2	Group 3
P_0	1	σ_a	2.022-1	1.608-1	1.121-1
	2	$\nu\sigma_f$	0.0	0.0	0.0



	3	σ_{tot}	2.620		2.939		3.259
	4	$\sigma_{1 \rightarrow 1}$	1.267	$\sigma_{2 \rightarrow 2}$	1.546	$\sigma_{3 \rightarrow 3}$	1.784
	5		0.0	$\sigma_{1 \rightarrow 2}$	1.097-1	$\sigma_{2 \rightarrow 3}$	1.155-1
	6		0.0		0.0	$\sigma_{1 \rightarrow 3}$	2.100-2
P_1	1		0.0		0.0		0.0
	2		0.0		0.0		0.0
	3		0.0		0.0		0.0
	4	$\sigma_{1 \rightarrow 1}$	3.002	$\sigma_{2 \rightarrow 2}$	3.881	$\sigma_{3 \rightarrow 3}$	4.522
	5		0.0	$\sigma_{1 \rightarrow 2}$	1.356-2	$\sigma_{2 \rightarrow 3}$	2.748-2
	6		0.0		0.0	$\sigma_{1 \rightarrow 3}$	0.0
P_2	1		0.0		0.0		0.0
	2		0.0		0.0		0.0
	3		0.0		0.0		0.0
	4		4.250		5.550		6.531
	5		0.0		4.013		7.055-2
	6		0.0		0.0		0.0
P_3	1		0.0		0.0		0.0
	2		0.0		0.0		0.0
	3		0.0		0.0		0.0
	4		4.968		6.252		6.858
	5		0.0		3.535-2		3.979-2
	6		0.0		0.0		0.0

c. Selection of Spatial Mesh

Nested spherical shells or layers of different materials can be handled



by specifying a radius at the interface, and specifying the material in each layer or zone. The spacing Δr should be small in regions of large attenuation or curvature, such as near the origin in spherical and cylindrical geometry (6). On the other hand, small Δr implies very many space points in a thick shield, and some compromise may be necessary. Typical shielding problem in one dimension may use 100 to 300 radii. One rule of thumb is $\Delta r \leq 2\mu_{\min}/\Sigma_{t\max}$ where μ_{\min} is the smallest discrete cosine and $\Sigma_{t\max}$ is the largest total cross section in the multigroup set (6). Near the origin in curved geometry the angular flux density changes rapidly even without collisions, and a smaller Δr may be required.

Following comments in addition to the use of ANISN manual would be helpful in running ANISN code.

1. A better definition of some of the parameters and terms used in ANISN can be found in reference 8. However, one must be careful in using this reference, since it does not use the same array number as ANISN.

2. The ANISN manual (1) does not include an output. Reference 9 includes a sample output for a three-group ANISN problem.

3. Before using any cross section file from Bugle-80 tape, it is necessary to convert this file to binary form. Four Bugle files (nos. 4-7) are needed for this conversion. File 4 contains the IBM JCL cards for conversion, and file 6 contains the IBM DD cards. File 7 contains an input data card for the conversion program contained in file 5. Before a cross section file is converted to binary form, it must first be converted to field data, and all "&" signs must be changed to "+" signs. The conversion program can now be applied to make a binary cross section tape which can be used with ANISN.

4. The output should always be examined for possible lack of convergence

and for negative or oscillatory angular flux densities (6). The total flux should not contain any negative value. If there are any at all, they must be very few in numbers.

5. There are four ID numbers for cross section of each element or physical material in bugle-80. The first ID number refers to P_0 cross section set, the second one to P_1 set, the third one to P_2 set, and the fourth one to P_3 set. Each of these sets is counted as one material in the parameters MTP, MCR or MT in the 15\$ array. However, in the 9\$ array (material number by zone) only the P_0 material ID number of each element or physical material in a given zone is required.

ROCK BOX PROBLEM

The second phase of the project was to determine the neutron flux distribution around a 6-ft cube solid rock box which houses a D-T neutron generator at its center. This experimental arrangement was designed to conduct a combined pulsed neutron experiment and to study its application to nuclear waste disposal testing. When the generator is activated, it produces 5 microsecond pulses (1 to 10 pulses/s) of 14.1 MeV neutrons. The strength of the neutron source is less than 10^9 n/s. The rock has a bulk density of about 2 g/cm^3 and the composition shown in Table 2.

In order to use ANISN code to determine the energy-angle-spatial flux distribution around the rock box, the neutron source can be treated as a point source which can be approximated for ANISN by a small shell source at the center of a sphere of radius 90 cm. The problem of selecting a suitable set of approximation parameters to be used in ANISN code is acute in the calculation of fast neutron penetration to large depths (7). Following parameters have been worked out in the rock box analysis.

1. The finite-difference equations are solved subject to boundary conditions. The vacuum condition is usually specified at the outer boundary. The reflective condition is required at the "left" boundary ($r = 0$) in the sphere (6). Hence $IBR = 0$ and $IBL = 1$.

2. As discussed earlier, near the origin in spherical geometry, the angular flux changes rapidly even without collisions, and hence a smaller Δr is required. The intervals used in this problem for 4* array input are given as follows:

4**310.00410.0010410.010410.108410.10391050.0090.0

There are 144 intervals, and Δr is very small near the origin and it increases outwards.

3. An S_8-P_3 analysis is being applied. The neutrons are generated in the energy group 2. Because of the discretization of ANISN code in angle and space, with an isotropic source in spherical geometry, the source has to be placed in the last angle which, in this case, is the 9th angle. The shell source used in this analysis is given below in ANISN format.

```
col 1
  ↓
  18*
    9Rb0.0   col16
    8Rb0.0   ↓
              1.5734+07
    Fb0.0
    T
```

The total shell source given in 18* array was derived as follows.

$$\text{Total shell source} = \sum_{i=1}^{\text{all intervals}} \sum_{j=1}^{\text{all angles}} \sum_{k=1}^{\text{all energy groups}} (\phi_{ijk} \cdot \omega_j |\mu_j| A_{i+1})$$

Total shell source must be 1 neutron/s.

Since the source is in the first interval, 9th angle and group 2,

$$i = 1, j = 9 \text{ and } k = 2$$

$$\text{Hence total shell source} = \phi_{192} \cdot \omega_9 |\mu_9| \cdot A_2 = 1 \text{ n/s}$$

From the output using the above 144 intervals we find that

$$A_2 = 7.85398 \times 10^{-7} \text{ cm}^2$$

Also from the output we find from the Angular quadrature constants

$$\omega_9 |\mu_9| = 8.09256 \times 10^{-2}$$

Hence

$$\phi_{192} = \frac{1 \text{ n/s}}{\omega_9 |\mu_9| A_2} = 1.57335 \times 10^7 \text{ n/cm}^2/\text{s}$$

If the shell source = $1.57335 \times 10^7 \text{ n/cm}^2/\text{s}$ is used, it will give a total source strength of 1 n/s.

4. The composition of the rock box and the number densities (12*) in cross section mixing table are given in table 2. Note that the number densities are in units of $10^{24} \text{ atoms/cm}^3$.

TABLE 2
 ROCK COMPOSITION AND NUMBER DENSITIES (12*)
 (in 10^{24} atoms/cm³)

Bugle-80 ID	Element	% by wt.	Number density (12*)
1-4	H	0.63	0.0075884
9-12	O	48.39	0.0364286
13-16	Cr	0.000003	0.069477×10^{-8}
21-24	Fe	2.46	0.0005305
45-48	Si	28.01	0.0120107
53-56	Na	1.35	0.0007073
57-60	Mg	0.54	0.0002674
61-64	A	5.08	0.0022673
69-72	K	2.62	0.0008071
73-76	Ca	10.87	0.0032667
129-132	Ti	0.11	0.0000277
137-140	Co	0.00000059	0.0120573
153-156	Ba	0.000282	2.4728378×10^{-8}

The first ten elements (H through Ca) are in bugle file 1 and the last three elements (Ti, Co and Ba) are in bugle file 2.

5. Cross section mixing table (10\$, 11\$, 12*) for the rock box composition with thirteen elements has been prepared as shown in table 3. In this table the first 10 elements are in Bugle file 1 and the last three are in

Bugle file 2. Table 3 shows how the cross sections of the thirteen elements could be combined to form those of the mixture (the rock). When the cross sections are read from Bugle binary tape, the materials are identified by integers 1,2,3,....,52 (52 materials read in 15\$ array) according to the order in which they were read from the tape. Positions 1 through 4 in table 3 cause the block of locations reserved for materials 1,2,3 and 4 to be replaced by zeros. Position 5 through 52 cause materials 5 through 52 to be multiplied by their respective number densities in column 12* and combined to form four new macroscopic materials, material numbers 1 through 4.

TABLE 3
CROSS SECTION MIXING TABLE FOR ROCK BOX

Position	Element ID	10\$	11\$	12*
1		1	0	0.0075884
2	H-1	2	0	"
3	1-4	3	0	"
4		4	0	"
5		1	5	0.0364286
6	0-16	2	6	"
7	9-12	3	7	"

8		4	8	"
9		1	9	6.9477-10
10	Cr	2	10	"
11	13-16	3	11	"
12		4	12	"
13		1	13	0.0005305
14	Fe	2	14	"
15	21-24	3	15	"
16		4	16	"
17		1	17	0.0120107
18	Si	2	18	"
19	45-48	3	19	"
20		4	20	"
21	Na	1	21	0.0007073
22	53-56	2	22	"
23		3	23	"
24		4	24	"
25		1	25	0.0002674

26	MG	2	26	"
27	57-60	3	27	"
28		4	28	"
<hr/>				
29		1	29	0.0022673
30	Al	2	30	"
31	61-64	3	31	"
32		4	32	"
<hr/>				
33		1	33	0.0008071
34	K	2	34	"
35	69-72	3	35	"
36		4	36	"
<hr/>				
37		1	37	0.0032667
38	Ca	2	38	"
39	73-76	3	39	"
40		4	40	"
<hr/>				
41		1	41	0.0000277
42	Ti	2	42	"
43	129-132	3	43	"
44		4	44	"

45		1	45	1.2057-10
46	Co	2	46	
47	137-140	3	47	
48		4	48	

49		1	49	2.4728-8
50	Ba	2	50	"
51	153-156	3	51	"
52		4	52	"

In this case

MS = 52

MCR = 0

MTP = 52

MT = 52

and material number 1 is entered into 9\$ array.

There are different possible ways a mixing table can be prepared. Some are more efficient than others. For example, reference 8 gives an illustration of a mixing table which is composed differently than table 3.

CONCLUSIONS

At the time of writing, all the input data for the rock box problem have

been worked out, and the binary tapes for Bugle files 1 and 2 have been prepared. Computer runs have been made with all the input data as discussed above, except that in spherical geometry the concrete problem has been executed instead of the mixture. A stepwise approach will be taken to use the mixture. At first, runs will be made with first two elements of the mixture, next with five elements, next with ten elements, and lastly with all the thirteen elements. In this approach it will be easier to apply corrections, if needed, to the program input. There is also a possibility of reaching the storage limit of the computer.

Before using all the thirteen elements, some "runstream" cards need to be changed and some added in order that ANISN can read the binary tapes of Bugle files 1 and 2 in one run. Another approach would be to combine these two binary tapes into one.

FUTURE PROJECT

Experience in other places working with ANISN has shown that when as few as 2 or 3 elements are used in a mixture, it is possible that the resulting input cross-section matrix will exceed the storage capacity of the computer (10). When this occurs, two approaches may be attempted (10).

1. First, attempt may be made to increase the dimension in the statement COMMON/BULKBU/I, J. A(45000) in the main routine from 45000 to the maximum permissible number. It will also be necessary to change the statement J = 45000 in the main routine (10).

2. Secondly, use can be made of the routine LIM1 (given in ANISN manual) to prepare a group independent cross section tape for ANISN. When this tape is used, rather than storing the entire matrix for the mixture, only the cross-section data for a single group are stored in the memory while the calculations for this group is performed. Data for the next group are then read from the group independent tape replacing the data of the previous group, and the calculations for this group are performed. The process continues for all groups.

Acknowledgement:

The author wishes to express sincere appreciation to Dr. P.K. Ray, Professor of Nuclear Engineering at Tuskegee Institute, Tuskegee, Alabama for his help throughout the project.

LIST OF TAPES

ANISN X08628 (6-22-83)

Bugle X23300 (7-21-83, created from a new tape from Oak Ridge)

Binary Tapes Created

Bugle file 1....X19289 (7-26-83)

Bugle file 2....X20761 (7-29-83)

Bugle file 3....X07033 (7-29-83)

Bugle files 1, 2, & 3....X21958 (7-29-83)

References

1. Ward W. Engle, Jr. "ANISN-ORNL: A Multigroup One Dimensional Discrete Ordinates Transport Code with Anisotropic Scattering", Oak Ridge National Laboratory Report CCC-254 (October 1975).
2. Bengt G. Carlson, "The Numerical Theory of Neutron Transport," in B. Adler, S. Fernback and M. Rotenberg, Eds., Methods in Computational Physics, vol. 1, Academic Press, New York, 1963, pp. 1-42.
3. Clarence E. Lee, "The Discrete Sn Approximation to Transport Theory", Los Alamos Scientific Lab. Report LA-2595, Los Alamos, N. Mexico (1962).
4. F. R. Mynatt, "The Discrete Ordinates Method in Problems involving Deep Penetration", in "A Review of the Discrete Ordinates Sn Method for Radiation Transport Calculations", Oak Ridge National Labs Report ORNL-RSIC-19, Oak Ridge, Tenn. (1968) pp 25-51.
5. K. D. Lathrop, "Discrete Ordinates Quadratures", ORNL-RSIC-19, pp. 53-63.
6. A. E. Profio, "Radiation Shielding and Dosimetry", John-Wiley and Sons, Inc., New York., Chapter 4 (1979).
7. A. E. Profio, "Comparison of discrete Ordinates Calculations with Measured Neutron Spectra in Standard Solid Geometries", ORNL-RSIC-19 (March 1968).
8. W. W. Engle, M.A. Boling and B.W. Colston, DTF-II, "A One-Dimensional, multigroup Neutron Transport Problem", NAA-SR-10951 (March 1966).
9. Ward W. Engle, Jr., "A Users Manual for ANISN: A one Dimensional Discrete Ordinates Transport Code with Anisotropic Scattering". K-1693 (March 1967).
10. R.W. Roussin, Oak Ridge National Laboratory (private communication).

ADDENDUM

After the report was completed, a successful ANISN run was made with a two-components mixture using the first two elements, H and O of the mixing table 3. But when the third element, Cr of table 3 was added, ANISN would not run because the resulting cross section matrix for a three-elements mixture exceeded the allowed computer storage space.

MINARD L. HALL

PAPER UNAVAILABLE

N86-14085

A STUDY OF SOME FEATURES OF AC AND DC
ELECTRIC POWER SYSTEMS FOR A SPACE STATION

by

Jack I. Hanania, Ph.D.
Professor of Electrical Engineering
American University of Beirut
Beirut, Lebanon

A B S T R A C T

This study analyzes certain selected topics in rival DC and high frequency AC electric power systems for a Space Station. The topics are chosen either because they are potential problem areas or because there seems to be the need for further study and development work.

The interaction between the Space Station and the plasma environment is analyzed, leading to a limit on the voltage of the solar array and a potential problem with resonance coupling at high frequencies. Certain problems are pointed out in the concept of a rotary transformer, and further development work is indicated in connection with DC circuit switching, special design of a transmission conductor for the AC system, and electric motors. The question of electric shock hazards, particularly at high frequency, is also explored, and a problem with reduced skin resistance and therefore increased hazard with high frequency AC is pointed out.

The study concludes with a comparison of the main advantages and disadvantages of the two rival systems, and it is suggested that the choice between the two should be made after further studies and development work are completed.

Center Research Advisor: William A. Chandler

INTRODUCTION

The design of the electric power system for a Space Station in low earth orbit has received considerable attention over many years. A number of studies⁽¹⁻⁶⁾ have been carried out based upon different alternative systems, some primarily DC, some primarily AC, and some a hybrid of the two, but it was clear from the start that the old 28 volt DC system used in previous space missions would no longer be adequate for the Space Station powers envisaged, while the familiar 60 Hz and 400 Hz AC systems would lead to excessive weight of electromagnetic equipment.

The choice of system therefore essentially rests between a relatively high voltage DC and a relatively high voltage, high frequency AC, with some variations based upon these two. The voltages are referred to as relatively high since there are factors that tend to limit these voltages to a few hundred volts, as will be shown below. Too low a voltage, however, would lead to excessive transmission conductor size and losses. The optimum voltage level, as well as optimum frequency if AC, will have to be determined subject to some constraints, in view of the effect that these factors have on the overall station weight and cost.

A study of the two rival systems shows that they are both essentially feasible, subject to some constraints and problems which are discussed below. There are strengths and weaknesses in both systems, and a good case can be made for one or the other. No attempt will be made to choose between the two systems. However, certain specific topics are selected for study, either because they seem to be potential problem areas in one system or the other, or because there may be inadequate data or insufficient past development work.

THEORY AND RESULTS

Plasma Interactions

The voltage of the solar array is limited by the level of discharge from the array to the surrounding plasma and the resulting power loss^(7,8). This discharge is a function of the plasma density, which depends upon the altitude of the Space Station. The optimum station altitude, taking into account correction for aerodynamic drag and the launching of resupply missions from earth, is in the region of 400 km (215 Nmi). Unfortunately, this is an altitude at which plasma density is close to a peak⁽⁸⁾, Figure 1. At 400 km, the plasma density is of the order of $1 \times 10^6 / \text{cm}^3$, and the voltage breakdown threshold, Figure 2, is roughly 400 volts. The positive/negative solar array potentials are not symmetrical with respect to the surrounding plasma because of the ease of collection of electrons, resulting in approximately +20V/-380V potential distribution for a 400-volt array. Other factors to be considered are: the additional ionized material introduced through the action of the ion thrusters, the sharp rise in array voltage as the array emerges at the end of the eclipse period into sunlight, and the apparent ineffectiveness of attempting to insulate exposed areas of the array in order to operate at higher voltages. Pending additional plasma data in low earth orbit, it would be prudent to limit the solar array voltage to between 250V and 275V or below.

There is a possibility of resonance between the AC transmission system frequency, if an AC system is used, and some natural plasma frequencies⁽⁹⁾, particularly the ion plasma frequency ω_i and the lower hybrid frequency ω_{LH} . These are given by:

$$\omega_i = Q \left(\frac{N_i}{M_i \epsilon_0} \right)^{\frac{1}{2}} \qquad \omega_{LH} = \left(\frac{Q_e B^2}{M_e M_i} \right)^{\frac{1}{2}}$$

where Q is ion charge, M_i ion mass, N_i ion density, e electron charge, M_e electron mass and B the earth's magnetic field. Estimates of ω_i and ω_{UH} have been made by General Dynamics⁽³⁾ for a range of altitudes around low earth orbit, giving ω_i as varying from 23 to 74 kHz at 300 km, and from 7 to 43 kHz at 600 km, and ω_{UH} varying from 5 to 10 kHz over the range 300 to 600 km. If resonance coupling were to take place unchecked, large power losses would result. This points to the need for avoiding parallel conductors with an AC system and for proper shielding of electromagnetic equipment. Meanwhile, more work should be done to verify the plasma density data presently available and then to recompute the plasma frequencies.

Rotary Transformer

As part of an AC system, a rotary transformer has been proposed to provide power transfer electromagnetically from the solar array side to the rest of the Space Station, thus avoiding the need for sliding contacts. A General Electric^(10,11) design uses four 25-kW modules with a ferrite core and a 0.01" airgap, with a frequency of 20 kHz and a flux density of 0.25 T. The airgap leads to questions about leakage inductance, and the compactness of the transformer achieved through the use of high frequency makes heat dissipation more difficult. Unless proper dissipation is achieved, winding failures could occur leading to a total shut down of power to the Space Station, unless redundancy is introduced by using more than one transformer. Because of the need for an electrical link between the solar array and energy storage equipment (fuel cells or batteries), the use of the rotary transformer gives two options: either energy storage is on the station side of the rotary joint which needs additional conversion equipment, or it is on the array side, adding to the mass of the array and preventing a decentralized storage and conversion system.

Circuit Switching

Although AC circuit interruption has always been easier to achieve than DC because of the availability of current zeros, recent developments^(12,13,14) with solid state devices are making DC circuit interruption easier than it has been. The following techniques can be used:

(i) GTOs (gate turn-off thyristors) can switch a circuit very rapidly, from 2 to 10 microseconds. Units have been developed and tested up to 65A, 800V, and GTOs with substantially higher ratings are presently available.

(ii) Power MOSFETs have been tested in units up to 100A, 150V. Because of current rating limits, parallel operation of MOSFETs is needed, unlike the GTOs.

(iii) GTO/SCR systems are used with the GTO driving an SCR bridge circuit, either by controlling the on/off function of the SCRs or by diverting current away from the SCRs. This eliminates bulky commutation circuits from the usual SCR system.

Although there is an obvious need for further development work and there are some problems to be resolved, it is expected that MOSFETs will replace SCR systems up to 30 to 40 kW, and GTOs or hybrid GTO systems will take over at higher power levels.

Transmission Line Parameters

With a DC system, designing a transmission line conductor and computing line parameters present no problem. With an AC system at high frequency, several points should be considered. Skin effect is prominent, leading to a thin hollow tube construction. Reactive voltage drop can be very high unless a coaxial conductor design is used. This can be seen in Figure 3 and Figure 4 which are taken from the work of Renz⁽⁸⁾ and his associates. The computation of line parameters at high frequency and with unsymmetrical conductor sections

needs further study and experimental verification.

Electric Motors

The traditional DC motor with commutator and brushgear cannot be used because of the plasma environment, and the "brushless DC motor" is in fact an AC motor supplied through a DC/AC converter. With a high frequency AC system, frequency conversion will be needed to avoid excessively high motor speeds. The choice is between the 3-phase synchronous samarium cobalt permanent magnet motor and the 3-phase squirrel-cage induction motor. The latter has the advantages of simplicity, ruggedness and greater long-term reliability. The compactness of the high frequency motor results in the need for proper heat dissipation, since core losses rise substantially with frequency. Additional rotor losses arise with non-uniform rotating magnetic fields⁽¹⁵⁾

Electric Shock Hazards

In view of the widely varying body resistance, current rather than voltage is used as a measure of electric shock hazard. The let-go current, which is the level at which a person just fails to release an electrode, is a danger threshold. With such a current, prolonged contact with the electrode can lead to respiratory difficulties and to skin changes that greatly reduce skin resistance thereby allowing larger currents to flow. With these higher currents, ventricular fibrillation can set in. Table 1⁽¹⁶⁾ gives typical figures for DC, 60 Hz and 10 kHz AC, and the median let-go currents at 60 Hz are seen to be about one-fifth those with DC. That is why 60 Hz AC is sometimes said to be five times as dangerous as DC⁽¹⁷⁾. Since skin resistance is by far the largest component of the overall body resistance, skin condition greatly affects the severity of shocks. Voltage also affects skin resistance, high voltage causing a sudden drop of resistance.

Table 1 also shows the let-go currents at 10 kHz to be about equal to

those with DC. This is confirmed by the work of Daziel^(18,19), and is shown in Figure 5, although the curves of Figure 5 go as far as 7 kHz only. But the skin resistance at high frequency may present a problem. The curves of Figure 6 were taken from the work of Stacy⁽²⁰⁾ and Burns⁽²¹⁾, and show dry skin resistance at 10 to 20 kHz to be about one-hundredth that with DC. If this is confirmed by other studies, it would mean that high frequency AC voltages would have to be much lower than DC voltages for the same degree of safety. Other factors that add to the uncertainties⁽²²⁾ are the effect of the varying time element, the wide range of let-go currents for the different percentiles, and the extrapolation, for obvious reasons, of the ventricular fibrillation threshold currents from the results of animal studies to humans.

Comparison of AC and DC Systems

The main advantages of the AC system are:

1. The system is inherently flexible because of ease of voltage transformations.
2. Circuit switching and fault interruption are inherently easier because of current zeros.
3. With a rotary transformer, sliding contact across the rotary joint is eliminated.

The main disadvantages of the AC system are:

1. More development work is needed for the rotary transformer and other components for high frequency operation.
2. More work is needed in the study and design of a suitable transmission line.
3. There is the possibility of resonance coupling with plasma natural frequencies.
4. There is a possibility of high electric shock hazard through reduced skin

resistance.

5. There are potential problems with synchronizing separate AC buses if needed.
6. There is a need to balance single-phase loads in the 3-phase system in order to minimize the neutral current.

The main advantages of the DC system are:

1. The system is basically simpler and therefore potentially more reliable.
2. With the exception of circuit interruption, system design and components are generally at a higher stage of development than with high frequency AC.
3. The DC system is inherently free of potential problems peculiar to all polyphase AC systems, such as reactive voltage drop, load balancing across phases, synchronization.

The main disadvantages of the DC system are:

1. Absence of current zeros makes circuit interruption more difficult.
2. Circuit switching techniques using GTOs or MOSFETs are still in an early stage of development.
3. DC systems are inflexible in matching a suitable voltage to the load.
4. A sliding contact, as in a slip ring, will be needed for the rotary joint, or the roll-ring if that proves to be reliable.

CONCLUSIONS

Some special features of AC and DC system designs have been studied, and certain potential problems have been pointed out, leading to a comparison between the principal strengths and weaknesses of the two systems.

Interaction of the solar array with the surrounding plasma sets an upper

limit to the array voltage at between 250 and 275V or below. The use of a 10 to 20 kHz AC system could lead to resonance coupling with plasma frequencies under certain conditions.

Specific problems with the rotary transformer, DC circuit switching, AC transmission line design and electric motors have been pointed out. The possibility of a higher electric shock hazard at high frequency was referred to.

The comparison between the AC and DC systems shows problem areas on both sides, and it would be advisable to defer making a choice between the two until further development work is done and some of those problems are resolved.

REFERENCES

1. Feiste, V. K., "Conceptual Design of Space Base Electrical Power System", NASA JSC, August 1969.
2. "Space Vehicle Electrical Power Processing Distribution and Control Study", TRW Report, NASA-CR-123907, June 1972.
3. "Study of Power Management Technology for Orbital Multi-100 kWe Applications", General Dynamics report, GDC-ASP80-015, NASA-CR-159834, July 1980.
4. "Study of Multi-Megawatt Technology Needs for Photovoltaic Space Power Systems", General Dynamics report, GDC-ASP81-019, NASA-CR-165323, May 1981.
5. "Solar Array Switching Power Management Technology for Space Power Systems", TRW Report 37243, NASA-CR-167890, September 1982.
6. "Space Power Distribution System Technology", TRW Report 34579-6001, NASA Control NAS8-3198, March 1983.
7. Stevens, N. J., Berkopoc, F. D., Purvis, C. K., Grier, N. T., and Staskus, J. V., "Investigation of High Voltage Spacecraft System Interactions with Plasma Environments", AIAA Paper 78-672, April 1978.
8. Renz, D. D., Finke, R. C., Stevens, N. J., Triner, J. E., and Hansen, I. G., "Design Considerations for Large Space Electric Power Systems", NASA Technical Memorandum 83064, April 1983.
9. Chen, F. C., Introduction to Plasma Physics, Plenum Publications, 1974.
10. "Preliminary Design Development of 100 kW Rotary Power Transfer Device", General Electric Report GE-81SDS4215, NASA-CR-1654, March 1981.
11. "Design Study of a High Power Rotary Transformer", General Electric Report GE-82SDS4222, NASA-CR-168012, July 1982.
12. Billings, W. W. and Sundberg, G. R., "Solid State Remote Power Controllers for High Voltage DC Distribution Systems", National Aerospace and Electronics Conference, Dayton, Ohio, May 1977.
13. "High Voltage DC Switchgear Development for Multi-kW Space Power Systems", Westinghouse Electric Corporation Report, WAED-81-05E, NASA-CR-165413.
14. "Kilovolt DC Solid State Remote Power Controller Development", Westinghouse Electric Corporation Report, WESDL-82-07E, NASA-CR-168041.
15. Nagarkatti, A. A., Mohammed, O. A., Demerdash, N. A., "Special Losses in Rotors of Electronically Commutated Brushless DC Motors Induced by Non-Uniformly Rotating Armature MMFs", Transactions, Power Apparatus & Systems, 101, no. 12, December 1982. pages 4502-7.

16. "Handbook of Laboratory Safety", edited by N. V. Steere, Chemical Rubber Company.
17. "Compendium of Human Response to the Aerospace Environment", NASA-CR-1205, Volume I, Section 1-6.
18. Dalziel, C. F., Ogden, E., and Abbot, C. E., "Effect of Frequency on Let-Go Currents", AIEE Transactions, 62, 1943, pages 745-50.
19. Dalziel, C. F., "Electric Shock Hazard", IEEE Spectrum, February 1972, pages 41-50.
20. Stacy, R. W., Williams, D. T., Worden, R. E., et al, Essentials of Biological and Medical Physics, McGraw Hill, 1955.
21. Burns, R. C., "Study of Skin Impedance", Electronics, 23, April 1950, pages 190-200.
22. Bridges, J., "Investigation on Low-Impedance Low-Voltage Shocks", IEEE Transactions, Power Apparatus & Systems, 100, No. 4, April 1981, pages 1529-37.

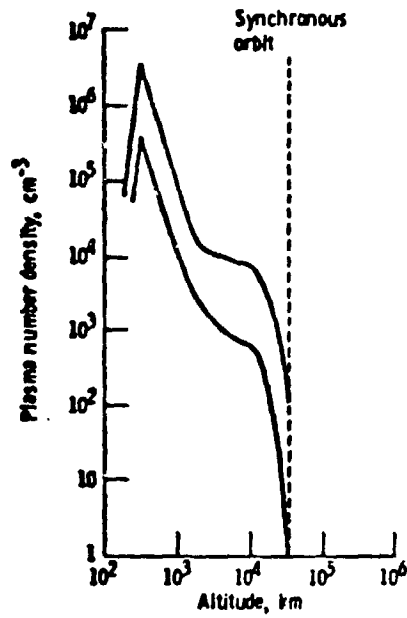


Figure 1. Plasma Number Density as a Function of Altitude in Equatorial Orbit (After Sevens, Reference 8)

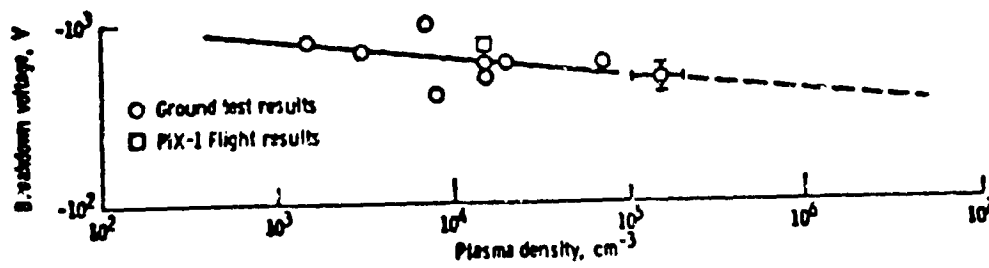
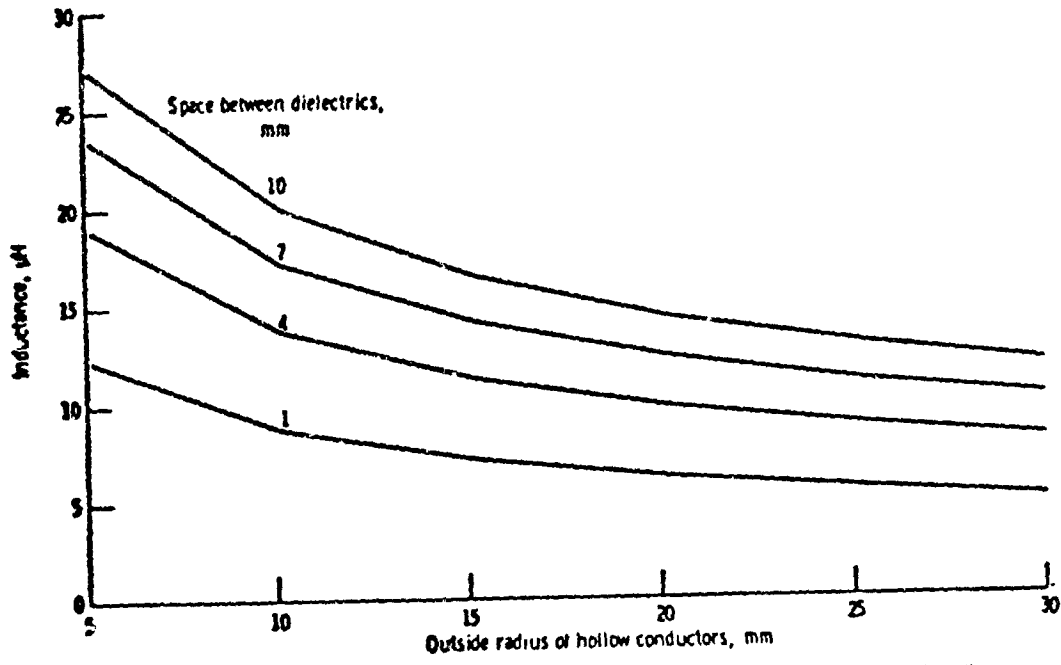
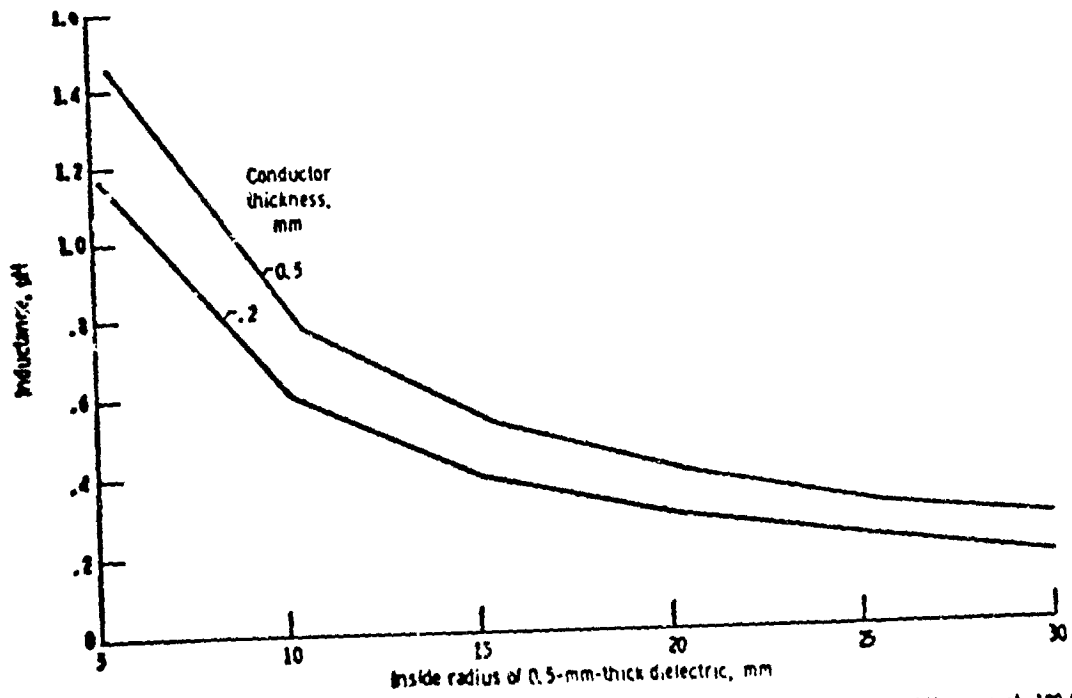


Figure 2. Voltage Threshold for Discharges (After Stevens, Reference 8)



Inductance of 50 m of unshielded parallel conductors as a function of conductor outside radius. Voltage, 1000 V; current, 100 A.

Figure 3. (After Renz, Reference 8)



Inductance as a function of inside radius for 50-m-long coaxial cable. Voltage, 1000 V; current, 100 A.

Figure 4. (After Renz, Reference 8)

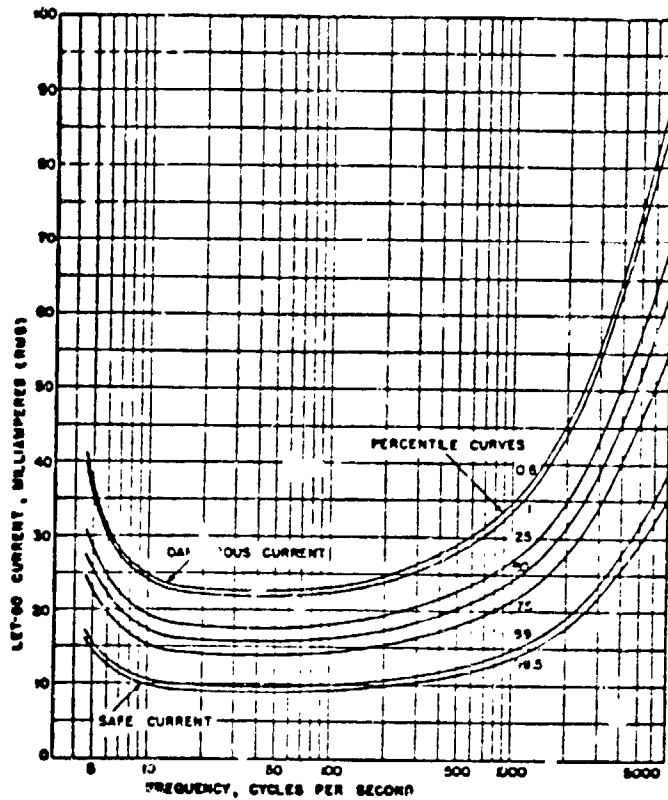
ORIGINAL PAGE IS
OF POOR QUALITY

Table 1
Quantitative effects of electric current on man.

Effect	Milliamperes					
	Direct Current		Alternating Current			
			60-Hertz		100,000 Hertz	
	Men	Women	Men	Women	Men	Women
Slight sensation on hand	1	0.6	0.4	0.3	7	5
Perception threshold, median	5.2	3.5	1.1	0.7	12	8
Shock — not painful and muscular control not lost	9	6	1.8	1.2	17	11
Painful shock — muscular control lost by 1/2%	62	41	9	6	35	37
Painful shock — let-go threshold, median	76	51	16	10.5	75	50
Painful and severe shock — breathing difficult, muscular control lost by 99 1/2%	90	60	23	15	94	63
Possible ventricular fibrillation						
Three-second shocks	500	500	675	675		
Short shocks (T in seconds)			$116/\sqrt{T}$	$116/\sqrt{T}$		
Capacitor discharges	50*	50*				

*Energy in watt-seconds

(Taken from Reference 16)



ORIGINAL FIGURE IS
OF POOR QUALITY

Figure 5. Sine Wave Let-Go Current for Men Versus Frequency (After Dalziel, Reference 18)

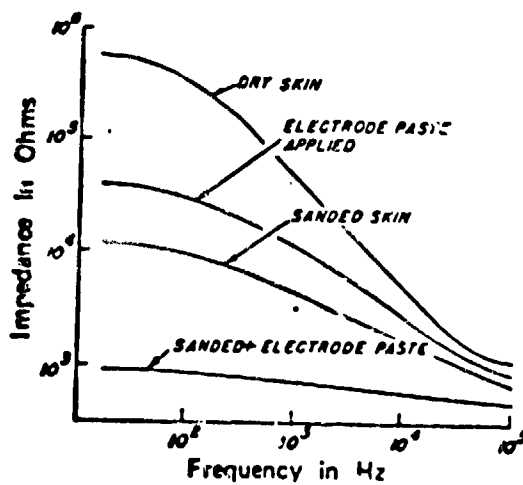


Figure 6. An Example of the Variation of Skin Impedance with Frequency and Condition of Electrode-Skin Contact (After Stacy and Burrs, Reference 17)

N86-14086

NUTRITIONAL CHARACTERISTICS OF MOON DUST FOR SOIL MICROORGANISMS

By

Takeru Ito, Ph. D.
Professor of Biology
East Carolina University
Greenville, North Carolina 27834

ABSTRACT

Approximately 46% of the lunar sample (10084,151), 125.42 mg, was solubilized in 680 ml 0.01 M salicylic acid. Atomic absorption spectroscopic analysis of the solubilized lunar sample showed the following amount of metal ions: Ca, 3.1; Mg, 4.0; K, 0.09; Na, 0.67; Fe, 7.3; Mn, 1.6; Cu, Ni, Cr, less than 0.1 each. All are in ppm.

Salicylic acid used to solubilize the lunar sample was highly inhibitory to the growth of mixed soil microbes. However, the mineral part of the lunar extract stimulated the growth. For optimal growth of the soil microbes the following nutrients must be added to the moon extract: sources of carbon, nitrogen, sulfur, phosphorus, and magnesium in addition to water.

Center Research Advisors: Wendell Mendell, Michael Duke

*

C-2

INTRODUCTION

Although there are many studies on chemical composition of lunar rocks and dust (Laul and Papike, 1980; Morris et al., 1983; Abelson, 1970), relatively little work has been reported on effects of the lunar dust on growth of living organisms. Taylor et al. (1971) observed a toxic effect of an Apollo 11 lunar core sample on growth of *Pseudomonas aeruginosa* (ATCC 15442). Later, Taylor and his associates (1973) described failure to observe toxicity under a somewhat different condition. Silverman et al. (1971) found no inhibition of the growth of any of the organisms tested in growth media containing Apollo 11 samples.

Examination of available chemical data on the moon dust makes it clear that the moon dust is nutritionally deficient in C, H, O, N, P, S, and perhaps Mg as well for the normal growth of living organisms. Other micronutrients required for the organisms, such as Fe, Cu, Zn, Co, Mn, Mo, are probably sufficient in the moon dust provided they become available for the microorganisms during an extraction process of the moon dust. The purpose of the present study is to find what nutrients are available (and unavailable) and whether toxins are present in the moon dust for the optimal growth of soil microorganisms.

MATERIALS AND METHODS

Moon Extract in 0.01 M Salicylic Acid

The lunar sample (10084,151) weighing 0.12542 g was stirred in 680 ml of 0.01 M salicylic acid at near boiling temperature for about five hours. The mixture was filtered through Whatman No. 42 filter paper (ashless). The final

volume of the filtrate was adjusted to 680 ml with 0.01 M salicylic acid. A portion of this extract was neutralized with a sodium hydroxide solution to pH near 7.0, and used as needed.

Composition of Growth Media

Growth medium I consisted of 4.5 ml moon extract, 0.1 ml 0.8 M sodium glutamate, 0.1 ml 0.04 M magnesium sulfate, and 0.1 ml 0.4 M sodium potassium phosphate buffer pH 7.0.

Growth medium II consisted of 4.5 ml moon extract, 0.1 ml 0.6 M sodium nitrate, 0.1 ml 0.1 M magnesium chloride, 0.1 ml 0.07 M sodium sulfate, 0.1 ml 0.4 M sodium potassium phosphate buffer pH 7.0, and 0.1 ml 0.56 M D-glucose.

Other growth media included those in which one or more of the constituents of the above media was omitted and replaced by water and those in which the moon extract was replaced by 4.5 ml 0.01 M salicylate in distilled water pH 7.0, or replaced by 4.5 ml 0.01 M salicylate in tap water pH 7.0. Nutrient broth was used as a positive control to test whether an inoculum contained any living cells. In some experiments, nutrient broth was prepared in 0.01 M salicylate pH 7.0 instead of in water.

The growth media were dispensed to culture tubes (12x100mm) with screw caps and not sterilized since the inoculum was a mixed population of soil microorganisms. Since they were not sterilized, they were inoculated immediately after the preparation.

Inoculum

The inoculum was prepared by filtering a mixture of 10 g wet garden soil and 50 ml 0.85 percent sodium chloride (isotonic saline), centrifuging the filtrate at full speed (2500 RPM) with a HN-S International centrifuge for 15 minutes,

washing twice with isotonic saline, and suspending the sediment in a 50 ml isotonic saline. One drop of the inoculum was added to each culture tube containing a culture medium.

Determination of Growth

The culture tubes to which the growth media were dispensed were directly used as cuvettes to determine the absorbance at 700 nm. The selection of this particular wavelength was based on a finding that the moon extract especially at pH near 7 was highly colored (wine color) with an absorption peak at 470 nm. At 700 nm absorption was negligible.

Determination of Extracted Matters from the Lunar Sample

A 100 ml of the moon extract (unneutralized) was evaporated to dryness in a platinum crucible on a hotplate and placed in a 600°C oven for three days, and the weight of the dry matter was determined.

Determination of Undissolved Matters from the Lunar Sample after Extraction in the Salicylic Acid Solution

The undissolved materials filtered on the filter paper in the process of the moon extract preparation were added in a platinum crucible and placed in a 600°C oven for three days, and the weight of the residue was determined.

Analysis of the Moon Extract

The following metal ions in the moon extract (unneutralized) were analyzed by atomic absorption spectroscopy: Ca, Mg, K, Na, Fe, Mn, Cu, Ni, Cr.

RESULTS

Extent of Extraction of the Lunar Sample by Salicylic Acid

The treatment of 125.42 mg of the lunar sample (10084,151) in 680 ml aqueous salicylic acid solution resulted in 58.14 mg into the solution and 59.96 mg undissolved. The correction due to the oxygen addition to the minerals during the combustion at 600°C was not made.

Chemical Analysis of the Moon Extract

The moon extract in 0.01 M salicylic acid contained the following amount of metal ions: Ca, 3.1; Mg, 4.0; K, 0.09; Na, 0.67; Fe, 7.3; Mn, 1.6; Cu, Ni, Cr, less than 0.1 each. All are in ppm (part per million).

Effect of the Moon Extract on the Growth of Soil Microorganisms

Removal of either phosphate or magnesium sulfate from the complete growth medium that contained the moon extract, glutamate, magnesium sulfate, and phosphate buffer decreased the growth of the soil microbes. The removal of the moon extract greatly increased the growth. The replacement of the moon extract with unboiled tap water completely inhibited the growth (Fig. 1).

- In order to determine whether the inhibitory effect of the moon extract was due to a possible toxic effect of the moon minerals or to an effect of the salicylic acid, 0.01 M salicylate in distilled water pH 7.0 was used in place of the moon extract in a growth medium. The salicylate decreased the microbial growth considerably, and the moon minerals stimulated the growth (Fig. 2). The replacement of the distilled water with boiled tap water slightly inhibited the growth (Fig. 2), although not as much as found in the previous experiment (Fig. 1).

In order to determine what nutrients must be added to the moon extract for optimal growth of the soil microbes, various growth media were tested. As can be seen in Fig. 3, the removal of the moon extract (i.e., salicylate) again showed a dramatic increase in growth. The considerable inhibition of the microbial growth by salicylate was quite evident. The addition of salicylate in the nutrient broth (Fig. 3) increased the lag period considerably over the nutrient broth alone (Fig. 1).

Although not shown in the graph, in the absence of any one of the nutrients sulfate, magnesium, nitrate, and phosphate buffer, the highest absorbance reading of the triplicate samples of each growth medium lacking one of these nutrients was lower than the lowest absorbance reading of the triplicate samples of the complete growth medium (i.e., growth medium II). The average growth of the triplicate samples containing no glucose as a carbon source was lower than the one containing the complete medium. However, two of the absorbance readings were higher than the lowest reading of the triplicate samples of the complete medium.

CONCLUSIONS AND DISCUSSION

One can conclude that the moon would form excellent trace mineral nutrients for soil microbes, since nearly one-half of the lunar sample used went into the salicylic acid solution and since the moon extract prepared in this study was probably even a saturated solution of the lunar sample according to Keller and Huang (1971), whose data on an Apollo 12 sample indicated that twice as much solids could go into the salicylic acid solution. Another reason for this conclusion is that the moon minerals did stimulate the growth of the soil microbes (Figs. 2, 3).

The weights of the soluble and the insoluble materials, 58.14 mg and 59.96 mg respectively from the total of the 125.42 mg lunar sample, were obviously a little overestimated since the combustion at 600°C would oxidize some mineral components of the lunar materials, particularly ferrous oxide. Assuming that all ferrous oxide was converted to ferric oxide during the combustion and that 16 percent of the total lunar sample used was ferrous oxide (Laul and Papike, 1980), the correction would be approximately 0.9 mg. From the atomic absorption data given in Results, it can be calculated that the moon extract in the salicylic acid solution contained 11 percent (16.2 percent) ferrous oxide, 9.8 percent (9.2 percent) magnesium oxide, 6.4 percent (12.4 percent) calcium oxide, and 1.8 percent (0.38 percent) sodium oxide in the total solid dissolved. The percentage in the parentheses was from the data of Laul and Papike (1980), indicating the content in this particular lunar sample. Compared with their data, one can see that magnesium oxide and ferrous oxide but not calcium oxide went proportionately into the salicylic acid solution. The high concentration of sodium may have been due to a possible presence of sodium in the salicylic acid used. This could not be ascertained, since the salicylic acid control was not

analyzed.

The complete inhibition of the microbial growth (Fig. 1) in the medium containing unboiled tap water in the place of the moon extract was probably in major part due to the chlorine in the tap water. However, even when boiled tap water containing salicylate replaced the moon extract, there was a slight inhibition of growth compared with a similar growth medium in which distilled water instead of the tap water was used. It is possible that some minerals in the tap water were inhibitory to the growth of some microbes but perhaps not of others in the mixed population of soil organisms. This was probably why the absorbance readings of the triplicate samples were widely different. (Individual readings were not shown.) It can be speculated that calcium ions, a component of hard water, in the tap water may be inhibitory to the growth of some microbes since it is not required for microorganisms in as large a quantity as vertebrates.

The considerable inhibition of the growth of the soil microbes by salicylate was quite evident in this study (Figs. 1, 2, 3). The use of pure culture of a salicylate-utilizing soil Pseudomonad instead of the mixed soil microbes as an inoculum would remove the complication created by the inhibition of the microbial growth by salicylate.

The finding that even without glucose two of the three culture tubes gave higher absorbance readings than with glucose needs explanation. Without glucose, there was still salicylate as a carbon source in the growth medium and perhaps the rate of the growth of salicylate-utilizing bacteria, which were obviously expected in the inoculum, in these two tubes was high. This result was another example of the complications created by the use of the mixed soil microbes as an inoculum in this study. In any case, a carbon source must be added to a growth medium for optimal growth of the microbes because available

chemical data show that very little carbon is present in the lunar sample (Laul and Papike).

It appeared that sulfate, nitrate, magnesium, and phosphate, in addition to a source of carbon, were required for the growth of the soil microbes.

The finding that without the moon minerals there was an optimal growth (Figs. 1, 2, 3) of the soil microbes indicated that the lunar sample was a poor source of nutrients and that the mineral requirements for the optimal growth were evidently met by contaminants coming from the chemicals and the laboratory wares used in the experiments. The lunar dust, however, did obviously supply the trace nutrients required for the growth, for the growth was stimulated by the presence of the moon extract (Fig. 2).

In conclusion, the lunar dust was a poor source of nutrients for the soil microbes to grow, although it appeared that it contained enough trace mineral nutrients and could be solubilized to support the growth of the soil microbes provided other macronutrients, including sources of carbon, nitrogen, sulfur, magnesium, and phosphate in addition to water, were available to them. It showed no toxicity for the microbial growth. The ready solubilization into the salcylic acid solution, which is a normal component of humus in earth soil, the growth stimulation by the solubilized moon minerals, and the lack of toxicity obviously mean that the lunar dust (although it is a poor source of nutrients) will certainly become a productive soil to support growth of microbes and higher plants if supplemented with organic, inorganic macronutrients and an atmosphere similar to air.

ACKNOWLEDGEMENT

The atomic absorption analysis conducted by Bobby Joe Presley of Texas A&M University and the access to the equipment and supplies in the Solar System Exploration Division and the Life Sciences Directorate at NASA during this study are gratefully acknowledged.

REFERENCES

Abelson, P. H. (editor), 1970. "The Moon Issue," *Science*, 167, 447-784.

Keller, W. D. and W. H. Huang, 1971. "Response of Apollo 12 lunar dust to reagents simulative of those in the weathering environment of Earth," *Proceedings of 2nd Lunar Science Conference, Vol. 1*, pp. 973-981.

Laul, J. C. and J. J. Papike, 1980. "The lunar regolith: Comparative chemistry of the Apollo sites," *Proceedings of the 11th Lunar and Planetary Science Conference, Vol. 2*, pp. 1307-1340.

Morris, R. V., R. Score, C. Dardano and G. Heiken, 1983. "Handbook of Lunar Soils, Part I: Apollo 11-15," *Planetary Materials Branch Publication 67*, pp. 1-422. Johnson Space Center, Houston.

Silverman, M. P., E. F. Munoz and V. I. Oyama, 1971. "Effect of Apollo 11 lunar samples on terrestrial microorganisms," *Nature*, 230, 168-169.

Taylor, G. R., W. Ellis, P. H. Johnson, K. Kropp and T. Groves, 1971. "Microbial assay of lunar samples," *Proceedings of the 2nd Lunar Science Conference, Vol. 2*, pp. 1939-1948, MIT Press.

Taylor, G. R. and B. C. Wooley, 1973. "Evaluation of lunar samples for the presence of viable organisms," *Proceedings of the 4th Lunar Science Conference, Vol. 2*, pp. 2267-2274 (Supplement 4, *Geochimica et Cosmochimica Acta*), MIT Press.

Fig. 1 Effects of Moon Extract and Other Nutrients on Growth of Soil Microbes.

- : Growth medium I minus moon extract.
- : Growth medium I.
- : Growth medium I minus phosphate buffer.
- △ : Growth medium I minus magnesium sulfate.
- : Nutrient broth.

See the text for the composition of the growth medium I.
Each point represents the average of three absorbance readings.

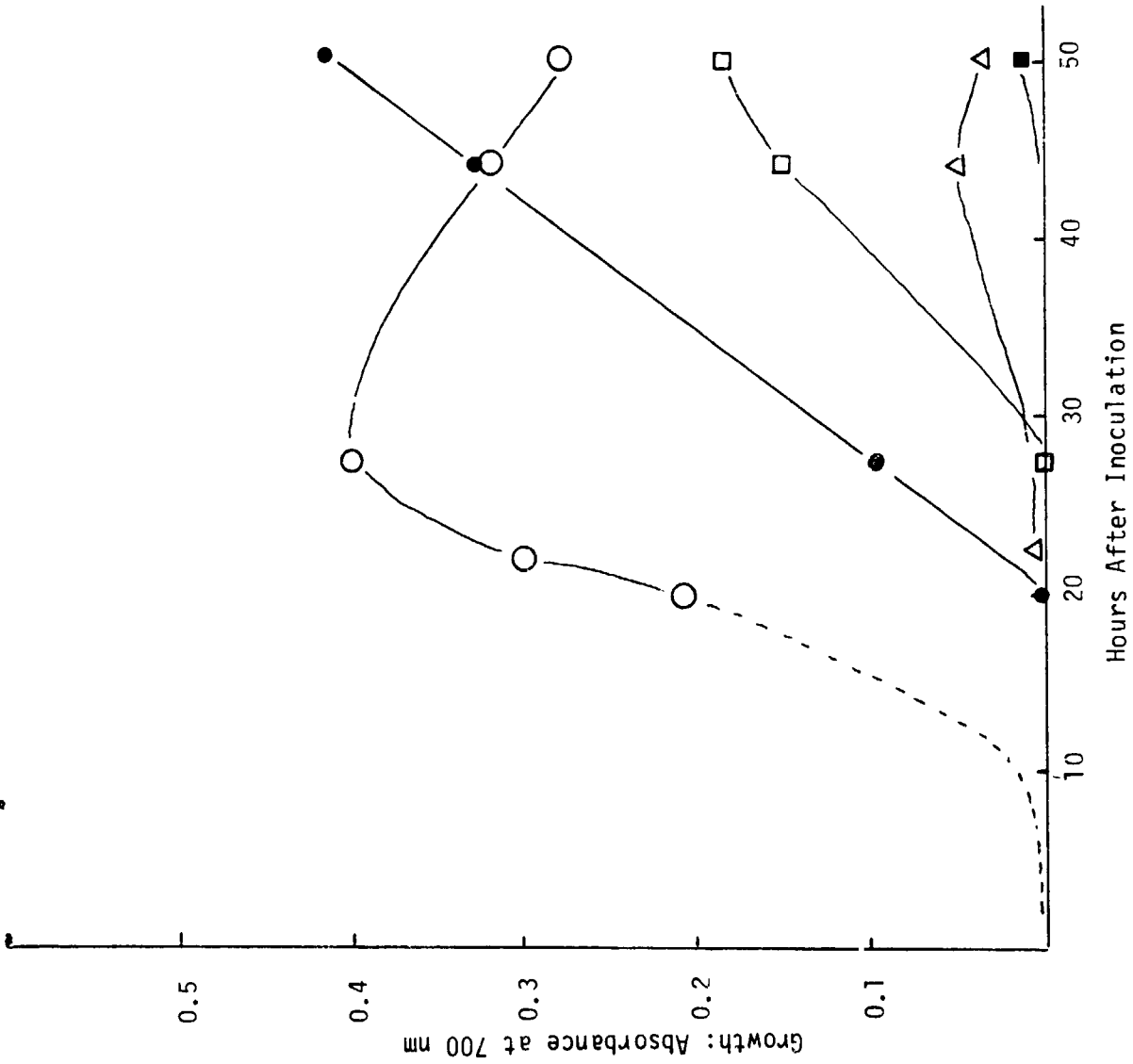


(Fig. 1)

Fig. 2 Effects of Salicylate and Moon Minerals on Growth of Soil Microbes.

- : Growth medium I minus moon extract.
- : Growth medium I.
- : Growth medium I minus moon extract plus salicylate in distilled water pH 7.0.
- △ : Growth medium I minus moon extract plus salicylate in tap water pH 7.0.

See the text for the composition of the growth medium I.
Each point represents the average of three absorbance readings.

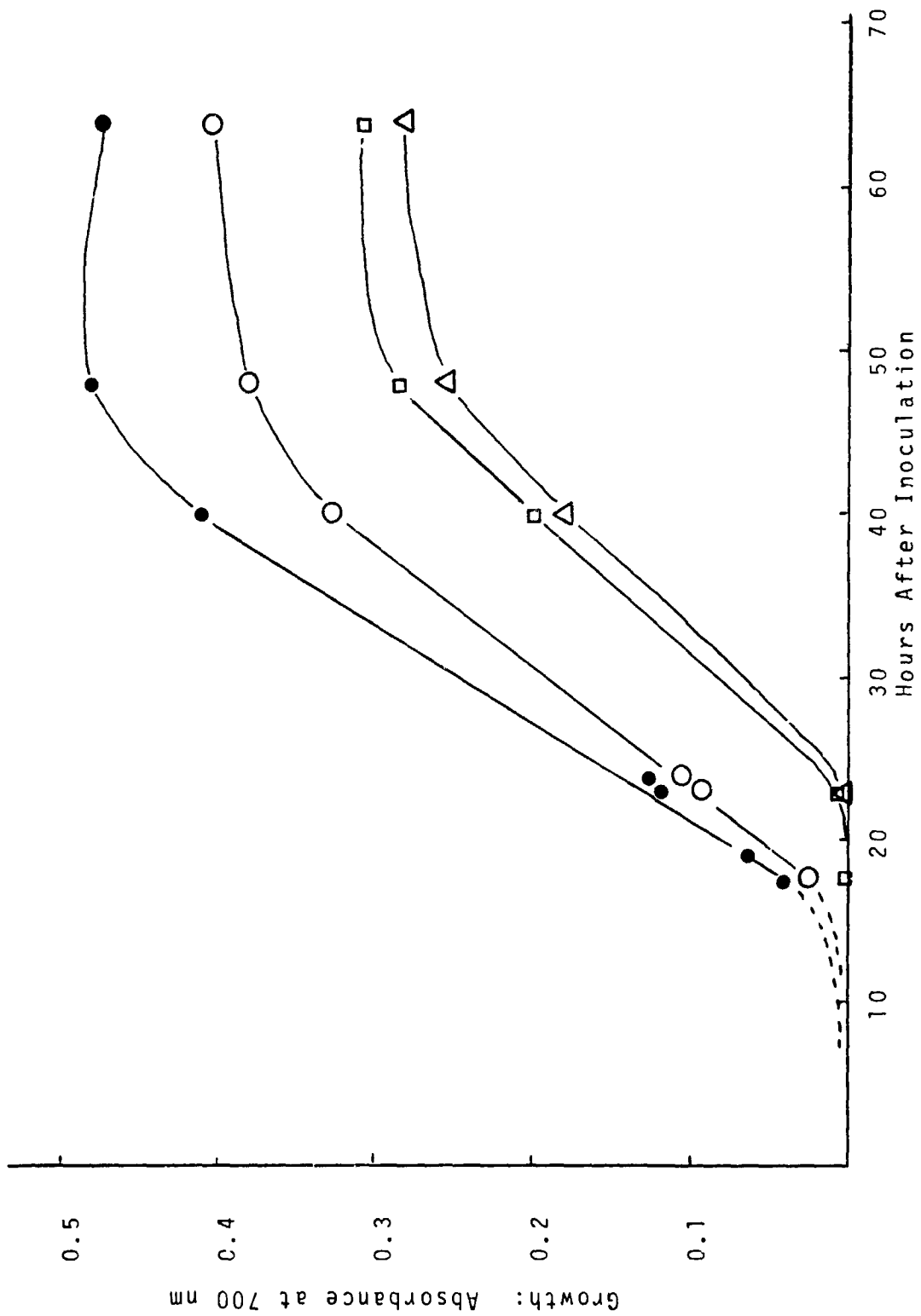


(Fig. 2)

Fig. 3 Effects of Salicylate, Moon Minerals, and Other Nutrients on Growth of Soil Microbes.

- : Growth medium II.
- : Growth medium II minus moon extract.
- △ : Growth medium II minus glucose.
- : Growth medium II minus sodium sulfate.
- : Growth medium II minus magnesium chloride.
- : Growth medium II minus sodium nitrate.
- ▽ : Growth medium II minus phosphate buffer.
- X : Growth medium II minus moon extract plus 0.01 M salicylate pH 7.0.
- N : Nutrient broth in 0.01 M salicylate pH 7.0.

See the text for the composition of growth medium II.
Each point represents the average of three absorbance readings.

N86-14087

SOME APPLICATIONS OF LIE GROUPS IN ASTRODYNAMICS

A.A.JACKSON
ASSISTANT PROFESSOR
DEPARTMENT OF PHYSICS
UNIVERSITY OF ST THOMAS
HOUSTON, TEXAS 77006

ABSTRACT

Differential equations that arise in astrodynamics are examined from the standpoint of Lie group theory. A summary of the Lie method is given for first degree differential equations. The Kepler problem in Hamiltonian form is treated by this method. Extension of the Lie method to optimal trajectories is outlined.

Introduction

The study of problems in astrodynamics, as well as applied mathematics in general, leads to differential equations. When the dynamic of a problem leads to non-linear differential equations there is usually no systematic method of attack for their solution. The use of continuous transformation groups, in particular Lie groups, provides a general method to approach to global integration.

A study was made of some elementary problems in astrodynamics : the one and three dimensional Kepler problems. These problems are important because they have a formulation by the variational methods of mechanics and the resulting invariants of the Lie groups are constants of the motion. It is thus tempting to use Lie theory to study optimal control theory in astrodynamics since the this variational theory may be cast into a form that is an analog of Hamiltonian theory in particle dynamics.

Theory: The Lie method of extended groups

The practical application of Lie groups to the solution of differential equations (Bluman and Cole, 1974) stems from the fact that if the differential equation

$$\frac{dy}{dx} = F(x, y) \quad \text{or} \quad \Omega(x, y, y') = 0$$

remains invariant under certain transformations, given by

$$x_1 = f(x, y) \qquad y_1 = g(x, y)$$

then the equations can be arranged in such a way that the independent variables do not occur explicitly. The re-arrangement involves a change of variable which are well defined by the invariance property. That is the invariance implies a change of variable

$$u = u(x, y) ; \quad v = v(x, u)$$

such that the differential equation becomes

$$\frac{du}{dv} = \bar{\Phi}(u)$$

The kind of transformation required defines a continuous one-parameter group. That is a mathematical entity with the properties: (1) the the product of two elements is uniquely defined and is an element of the group, (2) the associative law holds for elements of the group, (3) there is a unit element, (4) and there is an inverse element.

The basic procedure for solving ordinary differential equations starts from the infinitesimal parametric transformation

$$x_1 = x + \epsilon \xi(x, y)$$

and

$$y_1 = y + \epsilon \eta(x, y)$$

where ϵ is a parameter and ξ and η are the generators of the transformation. Demanding invariance of the differential equation and the integral invariants (that is constants of motion) u and v leads to the operational equations

$$\mathcal{L}^{(1)} \Omega = 0 \quad (1)$$

$$\mathcal{L} u = 0 \quad (2)$$

$$\mathcal{L} v = 1 \quad (3)$$

where \mathcal{L} is the Lie operator defined by

$$\mathcal{L} = \xi \partial_x + \eta \partial_y$$

and $\mathcal{L}^{(1)}$ is its extension

$$\mathcal{L}^{(1)} = \xi \partial_x + \eta \partial_y + \eta^{(1)}(\xi, \eta) \partial_y'$$

The generators are determined from (1) and the invariants u and v (in dynamics called canonical coordinates are calculated from the first order partial differential equations given by (2) and (3).

The calculation process can be summarized as, given the differential equation Ω apply the Lie operators $\mathcal{L}^{(1)}$ and \mathcal{L} to get

$$\mathcal{L}^{(1)} \Omega = 0$$

linear partial differential equations in the generators. Use

$$\mathcal{L} u = 0 \quad \mathcal{L} v = 1$$

and solve the resulting characteristic equations to get the invariants u and v . Form the equation

$$\frac{du}{dv} = \underline{\Phi}(u)$$

gaining a reduction in order and a final quadrature if possible.

Kepler Motion

- In the dynamics problems that follow focus is on the Hamiltonian formulation of the equations of motion (Leach, 1981), that is consider the first order system

$$\frac{dq}{dt} = \frac{\partial H}{\partial p} \quad \frac{dp}{dt} = - \frac{\partial H}{\partial q}$$

where p and q are the canonical momenta and coordinates and H is

the Hamiltonian.

As an example of a Lie group solution to a differential equation consider the one dimensional Hamiltonian defined by

$$H = \frac{p^2}{2m} - \mu/x$$

where p is the momentum, x the position of a particle and μ the gravitational constant. The equations of motion are given by

$$\Omega_1 = \dot{x} - p = 0$$

and

$$\Omega_2 = \dot{p} + \frac{\mu}{x^2} = 0.$$

Impose invariance under one-parameter group transformations, that is under the extended Lie operator

$$\mathcal{L}^{(1)} \Omega_1 = 0 \quad \mathcal{L}^{(2)} \Omega_2 = 0$$

The only surviving derivatives are

$$\frac{\partial \Omega_1}{\partial p} = -1$$

$$\frac{\partial H}{\partial x} = \mu x^{-2}$$

$$\frac{\partial \Omega_2}{\partial x} = -2\mu x^{-3}$$

$$\frac{\partial H}{\partial p} = p$$

$$\frac{\partial \Omega_1}{\partial \dot{x}} = 1$$

$$\frac{\partial \Omega_2}{\partial \dot{p}} = +1$$

These values lead to the equations for the generators

$$\eta - \partial_t \gamma + p \partial_x \gamma - p (\partial_t \xi + p \partial_x \xi) = 0 \quad (4)$$

$$-\frac{2\mu}{x^3} \eta + \partial_t \xi + p \partial_x \xi - \mu/x^2 \frac{\partial \eta}{\partial p} + \frac{\mu}{x^2} (\partial_t \xi + p \partial_x \xi) = 0 \quad (5)$$

Solving equation(4) for η and putting into(5) leads to solutions for the generators given by

$$\xi = \text{constant}$$

$$\gamma = 0$$

$$\eta = 0$$

The integral surfaces of the partial differential implied by are generated by the integral curves of the equations

$$\frac{dt}{1} = \frac{dx}{0} = \frac{dp}{0} = \frac{d\eta}{0} = \frac{d\nu}{0} = \frac{dw}{1}$$

there are the solutions

$$u = x \quad v = p \quad t = w$$

use of these coordinates and the equations of motion gives a relationship between u and v

$$\frac{du}{dt} = \bar{\Phi}(u, v) = -v u^2 / \mu$$

which integrates to

$$\mu u^{-1} = v^2/2 + \text{const.}$$

or that

$$\frac{p^2}{2} - \mu/x = E,$$

which means that E the energy is an invariant under translations in time.

From

$$\frac{du}{dw} = v$$

there results

$$\frac{\mu du}{[2\mu u - cu^2]^{1/2}} = dt$$

which can be integrated to

$$t - t_0 = (\mu/cx_0) \sin^{-1} \left[\frac{2\mu - cx}{2\mu} \right] - \frac{\sqrt{2\mu x - cx^2}}{c}$$

a known result for one-dimensional Kepler motion.

It is also possible to outline the three dimensional Kepler problem. The Hamiltonian will have the form

$$H = \frac{P \cdot P}{2} - \frac{\mu}{|Q|}$$

where P and Q are vectors. The extended Lie operator

$$J^{(1)} = \xi \partial_t + \gamma \cdot \nabla_Q + \mathcal{J} \cdot \nabla_P + \gamma' \cdot \nabla_{\xi} + \mathcal{J}' \cdot \nabla_{\mathcal{P}}$$

acting on the equations of motion

$$\Omega_1 = Q - \nabla_P H = 0 \quad \Omega_2 = P - \nabla_Q H$$

gives the vector partial differential equations

$$-\mathcal{J} + (P \cdot \nabla_Q) \gamma + \partial_t \gamma - P (P \cdot \nabla_Q \mathcal{J} + \partial_t \mathcal{J}) = 0 \quad (6)$$

and

$$\gamma \cdot \nabla_Q \left(\frac{\mu Q}{|Q|^3} \right) + P \cdot \nabla_Q \gamma - \frac{\mu Q}{|Q|^3} P \cdot \nabla_P \mathcal{J} + \partial_t \mathcal{J} + \frac{\mu Q}{|Q|^3} [P \cdot \nabla_Q \mathcal{J} + \partial_t \mathcal{J}] = 0 \quad (7)$$

Put γ from (6) into (7) and solve for ξ and γ . The process leads to 3 groups: translations in time, rotations in space, and affine translations in space and time. In turn these supply the 3 invariants of motion, energy, vector angular momentum and the Laplace vector.

Optimal Trajectories

Consider the problem of extremizing a scalar performance index

$$J[x_{\text{final}}, t_{\text{final}}]$$

subject to the constraints

$$\dot{x} = f(x, u, t)$$

where u is a vector of control variables. This state equation combined with boundary conditions defines the problem. For an

extremal the Hamiltonian defined by

$$H = \sum_i \lambda_i f_i$$

must satisfy the necessary conditions

$$\dot{x}_i = \frac{\partial H}{\partial \lambda_i}, \quad \dot{\lambda}_i = -\frac{\partial H}{\partial x_i} \quad (8)$$

The Lie approach to (8) for the Kepler coasting flight can be outlined as follows: from the Hamiltonian

$$H = \dot{R} \cdot \dot{\Lambda} + \frac{\mu \Lambda \cdot R}{R^3}$$

Writing the vector R, Λ as

$$Q_1 = \Lambda, \quad Q_2 = R, \quad P_1 = \dot{R}, \quad P_2 = \dot{\Lambda}$$

consider point transformations in R and Λ space

$$R_1 = R + \epsilon \gamma, \quad \Lambda_1 = \Lambda + \epsilon \xi \quad \text{and} \quad t_1 = t + \epsilon \zeta$$

where γ, ξ are vectors. Apply the Lie and extended Lie Operators to find the generators and the invariants.

Conclusion

It has been shown that the use of the method of the Lie theory of extended groups in the context of Hamilton's equations of motion yield the constants of motion. A method had been presented for use of Lie groups in optimal control theory, where hopefully with further work the non-linear equations will lead to invariants of the problem.

References

Bluman, G. and Cole J., Similarity Methods for Differential Equations, Springer, 1974.

Leach, P., Applications of the Lie Theory of Extended Groups in Hamiltonian Mechanics: The Oscillator and the Kepler Problem, J. Austral Math. Soc. (1981), 173-186.

N86-14088

INTERACTION BETWEEN ESCHERICHIA COLI AND LUNAR FINES

Karl R. Johanson
Professor of Microbiology
Department of Biological Sciences
North Texas State University
Denton, Texas 76203

ABSTRACT

A sample of mature lunar fines (10084.151) was solubilized to a high degree (about 17 percent) by the chelating agent salicylic acid (0.01 M). The neutralized (pH adjusted to 7.0) leachate was found to inhibit the growth of Escherichia coli (ATCC 25922) in a minimal mineral salts glucose medium; however, the inhibition was somewhat less than that caused by neutralized salicylic acid alone. The presence of lunar fines in the minimal medium was highly stimulatory to growth of E. coli following an early inhibitory response. The bacterium survived less well in the lunar leachate than in distilled water, no doubt because of the salicylate. It was concluded that the sample of lunar soil tested has nutritional value to E. coli and that certain products of fermentation helped to solubilize the lunar soil.

INTRODUCTION

The notion of a manned lunar base has been considered exhaustively by engineers, geochemists, biochemists, psychologists, and other experts, by and large through conferences, workshops, and contracts sponsored by NASA (5,10,18-20). Starting in 1960 with the first one entitled "Moonlab" (8). The ultimate goal would appear to be CELSS, an acronym coined by NASA meaning a "controlled ecological life support system" (18-20). To establish a self-sufficient, regenerative closed environment fit for human habitation for long periods will require a careful selection of desired species of living forms, from microbes to crop plants to man. At the microbial level, there are almost countless candidate species representing various physiologic types, e.g., photosynthetic, chemosynthetic, autotrophic, heterotrophic, anaerobic, fermentative, oxidative, sulfur oxidizers, denitrifiers, nitrifiers, iron oxidizers, etc., etc. (1). Those microbial types known to play key roles in the cycles of the "major elements" (C, H, O, N, S, P) are certainly prime candidates for a CELSS.

The moon is an inhospitable environment for all Earth's creatures, from bacteria to all higher forms of life. It has no atmosphere, is virtually devoid of water, contains in the regolith ppm/ppb levels of nitrogen, hydrogen, and carbon (CO , CO_2 , CH_4) and contains no free oxygen, although there is an abundance of combined oxygen, largely metal oxides in the lower oxidation state--ferrous, not ferric, for example (9,14,17). Temperature extremes from approximately 120°C to -180°C , intense radiation, a diurnal cycle of two earth weeks each of night and day, and a force of gravity one-sixth that of earth impose further complications in establishing a CELSS on the moon (9,14).

While exceedingly small amounts of amino acids have been detected in lunar soil, unquestionably the moon is sterile, i.e., without life (9,10,14). No life could possibly thrive on the moon without a supply of free oxygen and without additional water, nitrogen, and carbon dioxide and without protection from radiation and temperature fluctuations. All of these inadequacies or deficiencies would be compensated by the CELSS. The engineering and technology required to achieve a self-perpetuating (or nearly so) controlled ecological life support system seems feasible. To establish a dynamically stable (homeostatic) ecosystem is central to the concept of CELSS and no doubt will be the most stubborn, if not tantalizing, obstacle to an ultimately successful CELSS on the moon.

THEORY

It is important to ascertain whether lunar soil (i) is toxic to some species of life; (ii) can be a source of nutrients; and (iii) can be leached and biochemically modified by living systems.

Inevitably, there will be introduced into a lunar man-made, regenerative environment a variety of microbial species which are normal members of the body's microflora. A prime example is Escherichia coli, long used as an indicator of fecal pollution and probably the bacterium most widely investigated by molecular biologists and geneticists. Indeed, its entire genome has been essentially mapped (2). Although some strains of E. coli are capable of causing disease in man and animal, its introduction into a CELSS would be unavoidable once the recycling system were operative, and thus its influence on lunar soil and vice versa should be assessed.

Escherichia coli is a Gram-negative heterotroph which can derive all of its nutritional needs from simple inorganic compounds, except for carbon. It can utilize a variety of low molecular weight organic compounds as sources of carbon and energy. It will grow well in the absence of molecular oxygen, but also can utilize O_2 as an electron receptor; thus, it is a facultative aerobe. In the presence of fermentable carbohydrate, e.g., glucose, E. coli produces lactic, succinic, acetic, and formic acids plus ethanol. Most of the formate ends up as CO_2 and H_2 through catalysis by the formic hydrogenlyase enzyme complex. However, in the presence of an abundant oxygen supply, E. coli will grow most vigorously and few fermentative end products will accumulate; most of the glucose will thus be metabolized stoichiometrically into carbon dioxide and water. Under ideal conditions, E. coli is one of the most rapidly growing microbes known. E. coli is moderately tolerant of environmental change, although it does not produce spores. It will grow in a temperature range of approximately 10 to 42°C and in a pH range of approximately 5 to 8.

This study was designed principally to measure the effects of lunar leachates and of lunar soil on the growth and survival of E. coli. While chemical analyses of the leachate and of the spent culture medium containing lunar fines were intended, and would have provided some helpful information, they will have to await subsequent experiments that may emerge from this one.

METHODS

I. Bacterium and Culture Medium

A well-characterized strain of Escherichia coli (ATCC 25922) was obtained from the Microbiology Laboratory, Division of Life Sciences, NASA. It was grown on a brain heart infusion agar slant. The growth on the slant was suspended in 1 ml sterile distilled water and constituted the inoculum for 75 ml of a mineral salts glucose (MSG) medium contained in a 125-ml Erlenmeyer flask. The composition of the medium is listed in Table 1.

The inoculated MSG broth was incubated at 35°C and the cells were recovered 18 hours later by centrifugation and washing in sterile distilled water. Growth was not abundant in this minimal MSG medium, so the final cell suspension was concentrated 15-fold by resuspending the cells in 5 ml distilled water. One drop from a sterile 1-ml serologic pipette constituted the inoculum for each tube in the experiment.

II. Lunar Soil Leachate

Based upon the success of Keller and Huang (7) in partially solubilizing an Apollo 12 lunar dust (12070.128), salicylic acid was selected as the solvent. To 50 ml of .01 M salicylic acid in a small polypropylene container was added 0.11476 g of lunar soil (10084.151).

A plastic-coated stirring bar was placed in the vessel, a cap inserted and the contents heated in a boiling water bath on a hot plate-magnetic stirrer for eight hours. After cooling overnight, the vessel was stirred and heated for a second eight-hour period. For two more successive days, the lunar material was stirred at room temperature on the stirrer.

The leachate with the undissolved fines was filtered through a sterile membrane filter (0.45 μ m) and aseptically transferred to a sterile 50-ml flask. A portion of the leachate was adjusted to pH 7.01 with 1 N NaOH for incorporation into the culture medium.

Chemical analysis (2,9) of lunar soil 10084 has revealed its principal constituents to be SiO_2 (41.0%), FeO (16.2%), Al_2O_3 (12.8%), CaO (12.4%), MgO (9.2%), TiO_2 (7.3%); lesser amounts of MnO (0.22%), Na_2O (0.38%) and K_2O (0.15%) were found with ppm amounts of Ba, Co, Ni, Sc, Ce, and some ten other trace elements. There is no information on its content of sulfur or phosphorus. It is a "mature" soil (Is/FeO ratio of 78.0) (9), meaning that it had been long exposed to solar winds and micrometeorites.

In order to determine the amount of fines solubilized by the chelating solution, a measured volume was pipetted onto a tared watch glass. The sample was dried at 110°C overnight and weighed, thereby obtaining the weight of dissolved solids, including the salicylic acid. An alternative method consisted of heating a measured volume of leachate in a porcelain crucible placed in a muffle furnace at 700°C for a couple of hours, weighing before and after. The latter method would combust completely the salicylic acid and required a small correction resulting from the oxidation of FeO to Fe_2O_3 .

The leachate possessed an intense red-brown color, probably because of the iron complexed with the organic acid. Its absorption spectrum was measured over the range of 400 to 700 nm. Upon addition of the leachate to the culture medium, the color disappeared.

III. Effects of Lunar Leachate on E. coli

A. In mineral salts glucose broth

The neutralized sterile leachate was diluted serially 1:2 in sterile distilled water to yield a dilution series starting with 1:2 and ending with 1:128. Sterile screw-cap 10 x 100 mm test tubes were employed. An equal volume (2.5 ml) of sterile double-strength MSG medium was aseptically added to each tube resulting in a total volume in each tube of 5 ml.

Each tube, except for the MSG control tube, was inoculated with one drop of the freshly-washed suspension of E. coli and incubated at room temperature (about 22°C). At intervals the amount of growth was recorded by means of spectrophotometric (Bausch and Lomb, Spectronic 170) absorbance readings at 500 nm wavelength.

As a control, neutralized, sterilized 0.1 M salicylic acid was serially diluted and double-strength MSG broth was pipetted into each tube which also received one drop of the E. coli suspension.

B. In aqueous dilutions

The leachate was serially diluted in sterile distilled water as described in Part A above. After inoculation with a drop of E. coli suspension, a loopful was streaked periodically on nutrient agar Petri plates to check for viability. The control was a tube containing sterile distilled water.

IV. Effects of Lunar Fines on E. coli

A. In mineral salts glucose broth

Five ml single strength MSG broth was pipetted into each of three 10 x 100 mm screw-cap test tubes containing measured quantities of fines (50.94 mg, 20.42 mg, and 11.48 mg). The tubes were autoclaved at 121°C for 15 minutes. Upon cooling to room temperature, spectrophotometric readings were made and each tube was inoculated with one drop of the freshly-washed suspension of E. coli. Periodically thereafter, growth was measured in the spectrophotometer.

B. On agar plates

A suspension of E. coli from a recently seeded brain heart infusion slant was diluted in sterile distilled water. One drop of this suspension was spread evenly over the surface of a plate of nutrient agar by means of a sterile glass spreader.

Three small clumps of moon fines were placed upon the inoculated plate and the plate was incubated at room temperature for two days. The plate was examined intermittently for any signs of stimulation or inhibition of growth around the fines.

RESULTS

I. Leachate

It was not possible to achieve a constant dry weight value employing the low temperature oven (110°C), probably because of the tendency for salicylic acid to sublime slowly. The results from ashing revealed the 50 ml of solution to contain .0198 g solids. Thus, of the 0.14476 g suspended in the salicylic acid solution, 17.25% was solubilized.

The absorption spectrum revealed a peak at or near 475 nm (Figure 1).

II. Effects of Lunar Leachate on the Growth of E. coli

Tables 2 and 3 and Figure 2 clearly reveal the inhibitory effect of the solvent 0.01 M salicylate on growth of the test bacterium. A dilution of 1:128 of the leachate solution (equivalent to 7.8×10^{-5} M salicylic acid) was slightly inhibitory. Note that E. coli grew better in dilutions of the leachate than in comparable dilutions of the neutralized salicylate. The increase in growth after 180 hours is probably a response, in part, to autolytic products from the cells serving as nutrients.

III. Effects of Lunar Fines on the Growth of E. coli

Table 4 and Figure 3 show that while the presence of fines (not leachate) in the culture medium was inhibitory to growth of E. coli early in the incubation period (< 20 hours), the maximal growth achieved was greater in the presence of each of the three levels of fines than in the control culture. In fact, the stimulus was bimodal, with peaks at 24 hours and again at 216 hours of incubation, the latter being substantially greater than the former. Another interesting feature of these data is that the highest amount of fines (50.9 mg)

resulted in growth greater than the control all the way past the first peak at 24 hours; the lesser amounts of fines became inhibitory after the initial peak but later became stimulatory (216 hours).

IV. Toxicity of Leachate to E. coli

Undiluted leachate and its dilutions up to 1:64 were demonstrably toxic to E. coli. At approximately the eighth day, there were few if any viable bacteria present in either the undiluted or 1:2 dilution of leachate. In retrospect, a parallel study should have been made with neutralized salicylic acid.

V. Effects of Leachate and Lunar Fines Sprinkled on Agar Seeded with E. coli

Amounts of 20.9, 14.2, and 5.6 mg of lunar fines placed upon freshly-seeded nutrient agar failed to produce a noticeable effect upon the subsequent growth of E. coli.

One drop of leachate produced a circle within which there was no growth of the bacterium. The leachate preparation in which the pH was adjusted to 7.0, however, definitely stimulated growth as indicated by a circular area within which the agar medium was more opaque than the background.

CONCLUSIONS

It can be concluded that the lunar soil sample tested stimulates the growth of E. coli in a minimal mineral salts glucose culture medium. The chelator, salicylic acid, was toxic to E. coli; the leachate partially reversed this effect, however. The growth enhancement from the lunar fines is probably a nutritional response to unidentified trace elements or possibly to one or more major elements in the specimen.

REFERENCES

1. Brock, T. D. Biology of Microorganisms, 3rd ed., Prentice-Hall, Inc., Englewood, Cliffs, N.J., 1979.
2. Engel, A. E. J., Engel, C. G., Sutton, A. L., and Myers, A. F. Composition of fine Apollo 11 and Apollo 12 rocks and one Apollo 11 soil and some petrogenic considerations. In: Proceedings of the Second Lunar Science Conference, A. A. Levinson, ed. Houston, TX, January 11-14, 1971, MIT Press, 1971.
3. Fox, S. W. Looking forward to the present—abiogenesis theory illuminated by lunar amino acids. Biosystems 6:165-175, 1975.
4. Gibson, E. K. Distribution, movement, and evolution of the volatile elements in the lunar regolith. The Moon 13:321-326, 1975.
5. Glaser, P. E. and Mabel, J. A. Nutrition and food technology for a controlled ecological life support system (CELSS). Report to NASA, Contract No. NAS9-15652, 1981.
6. Johnson, P. H., Walkinshaw, C. H., Martin, J.R., Nance, W. B., Bennett, A. D., and Carranza, E. P. Elemental analysis of Apollo 15 surface fines used in biological studies in the lunar receiving laboratory. Bioscience 22:96-99.
7. Keller, W. D. and Huang, W. H. Response of Apollo 12 lunar dust to reagents simulative of those in the weathering environment of Earth. In: Proc. 2nd Lunar Science Conf., Vol. 1, p. 973-981. MIT Press, Cambridge, MA, 1971.
8. LaPatra, J. W. and Wilson, R. E. eds. Moonlab: a study by the Stanford-Ames summer faculty workshop in engineering systems design. NASA contract No. NSR 15-020-151, 1968.
9. Morris, R. V., Score, R., Dardano, C., and Heiken, G. Handbook of Lunar Soils.
10. Ponnampetuma, C., ed. NASA Conference (untitled). Space Life Sciences 3:309-561, 1972.
11. Silverman, M. P., Munoz, E. F., and Oyama, V. I. Effect of Apollo 11 lunar samples on terrestrial microorganisms. Nature 230:169-170, 1971.
12. Taylor, G. R., Ellis, W., Johnson, P. H., Kropp, K., and Groves, T. Microbial assay of lunar samples. In: Proc. 2nd Lunar Science Conf., Vol. 2, p. 1939-1948, 1971.
13. Taylor, G. R. and Wooley, B. C. Evaluations of lunar samples for the presence of viable microorganisms. In: Proc. 4th Lunar Science Conf., Vol. 2, p. 2267-2274.

14. Taylor, S. R. Lunar Science: A Post-Apollo View. Pergamon Press, Inc., New York, 372 pp. 1975.
15. Urey, L. C. The moon and its nature. In: Foundations of Space Biology and Medicine (3 vols.), pp. 115-132. NASA, Washington, D.C., 1975.
16. Walkinshaw, C. H. and Johnson, P. H. Analysis of vegetable seedlings grown in contact with Apollo 14 lunar surface fines. Hort. Science 6:532-535, 1971.
17. Williams, R. J. and Jadwick, J. J. Handbook of Lunar Materials. NASA Ref. Publ. 1057, Sci. and Tech. Info. Office, 120 pp., 1980.
18. Amer. Soc. Mech. Engineers. Intersociety Conf. on Environmental Systems. NASA-supported. 1981.
19. Amer. Soc. Mech. Engineers. Intersociety Conf. on Environmental Systems. NASA-supported. 1979.
20. Amer. Inst. Aeronautics and Astronautics Inst. Space Manufacturing III: Proceedings of the 4th Conf. NASA-supported. 1979.

INGREDIENT (wt./liter)	(g)	CONCENTRATION (ppm)
Glucose	2.0 g	2,000
$(\text{NH}_4)_2 \text{SO}_4$	1.0 g	1,000
K_2HPO_4	1.0 g	1,000
KH_2PO_4	0.5 g	500
NaCl	0.5 g	500
$\text{MgSO}_4 \cdot 7\text{H}_2\text{O}$	0.1 g	100
CaCl_2	1.0 mg	1
$\text{FeSO}_4 \cdot 7\text{H}_2\text{O}$	0.5 mg	0.5
$\text{MnSO}_4 \cdot 4\text{H}_2\text{O}$	0.25 mg	0.25
$\text{ZnSO}_4 \cdot 7\text{H}_2\text{O}$	0.1 mg	0.1
$\text{Co}(\text{NO}_3)_2 \cdot 6\text{H}_2\text{O}$	0.1 mg	0.1
EDTA*	50.0 mg	50

*Ethylene diamine tetraacetic acid (a chelator) was included in the trace element solution (Ca, Fe, Mn, Zn, Co) which was filter-sterilized as a concentrate. Glucose was sterilized by filtration as were the remaining salts.

Table 1. Mineral Salts Glucose Broth for Escherichia coli.

Diln. of Leachate 17	HOURS OF INCUBATION						
	24	41	48	70	185	209	
1:2	.062	.086	.076	.076'	.062	.066	.077
1:4	.076	.094	.054	.087	.076	.077	.085
1:8	.105	.115	.099	.096	.090	.091	.102
1:16	.143	.147	.128	.122	.115		.113
1:32*	.081	.144	.135	.111	.091	.099	.109
1:64	.198	.191	.173	.172	.151	.144	.179
1:128	.209	.207	.175	.177	.169	.168	.191
Control	.219	.229	.203	.189	.204	.181	.223

Incubation was at room temperature (22°C). The data are spectrophotometric readings which have been adjusted by deducting the zero time readings.

*This tube may be invalid since it was misplaced while taking the 17-hour readings and shortly found in another test tube rack with several similar tubes.

Table 2. Growth of Escherichia coli in a Mineral Salts Glucose Medium Containing Dilutions of Moon Leachate.

Diln. of .01 M Salicylic Acid	HOURS OF INCUBATION						
	17	24	41	48	70	185	209
1:2	.028	.060	.055	.055	.045	.033	.040
1:4	.057	.079	.073	.069	.069	.63	.066
1:8	.073	.096	.086	.080	.080	.69	.085
1:16	.099	.138	.112	.108	.103	.091	.101
1:32	.125	.147	.136	.135	.158		.119
1:64	.152	.180	.168	.166	.132	.159	.175
Control	.219	.229	.203	.189	.204	.181	.223

See note under Table 2

Table 3. Growth of Escherichia coli in a Mineral Salts Glucose Medium Containing Dilutions of Salicylic Acid.

Amount Moon Fines	HOURS OF INCUBATION						
	17	24	41	48	70	185	216
50.94 mg	.160	.260	.238	—	.208	.308	.345
20.42 mg	.144	.246	.181	—	.142	.186	.255
11.48 mg	.157	.237	.192	—	.152	.162	.277
0	.219	.229	.203	.189	.204	.181	.230

See note under Table 2.

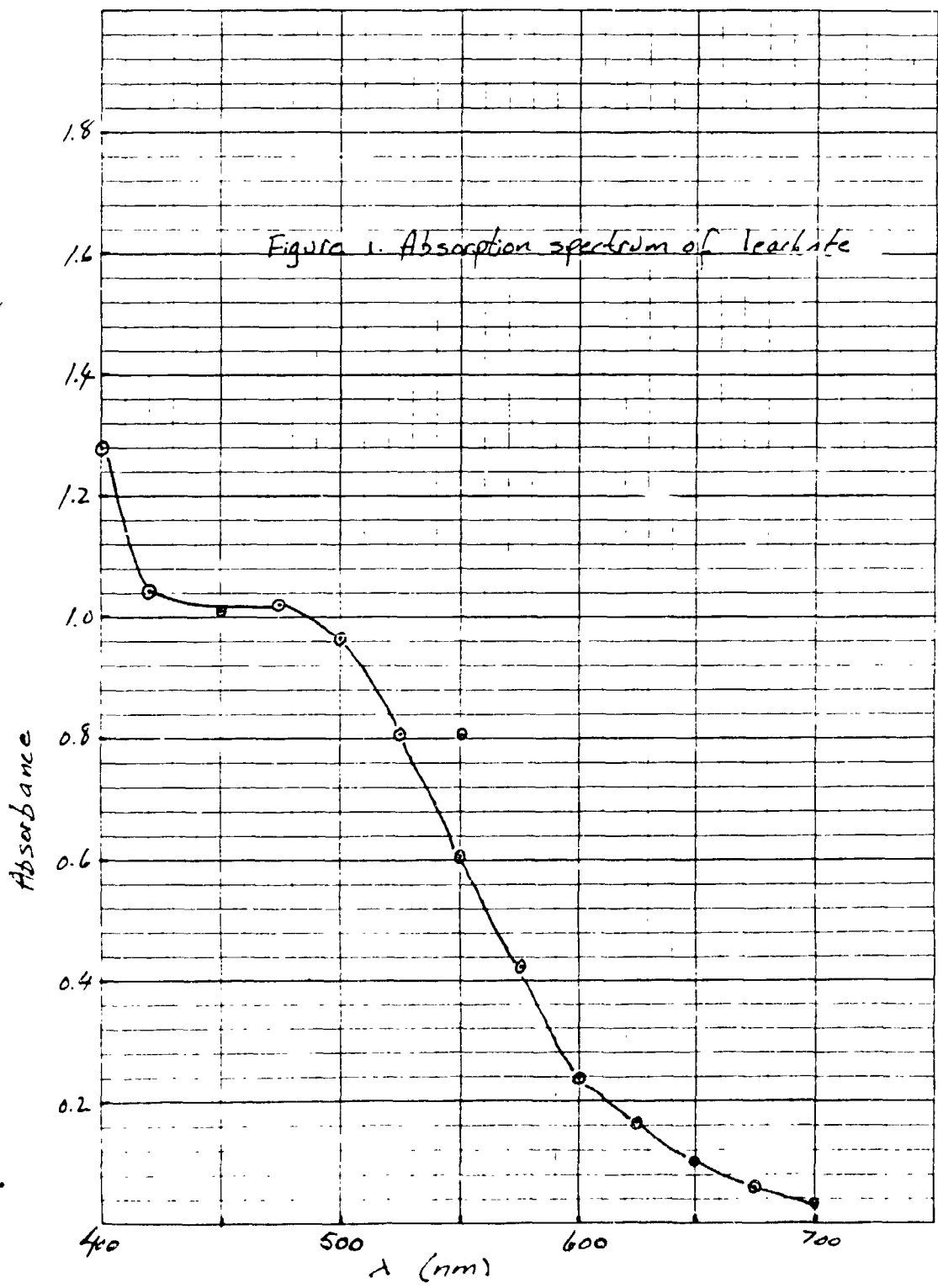
Table 4. Growth of Escherichia coli in a Mineral Salts Glucose Medium Containing Moon Fines (10084).

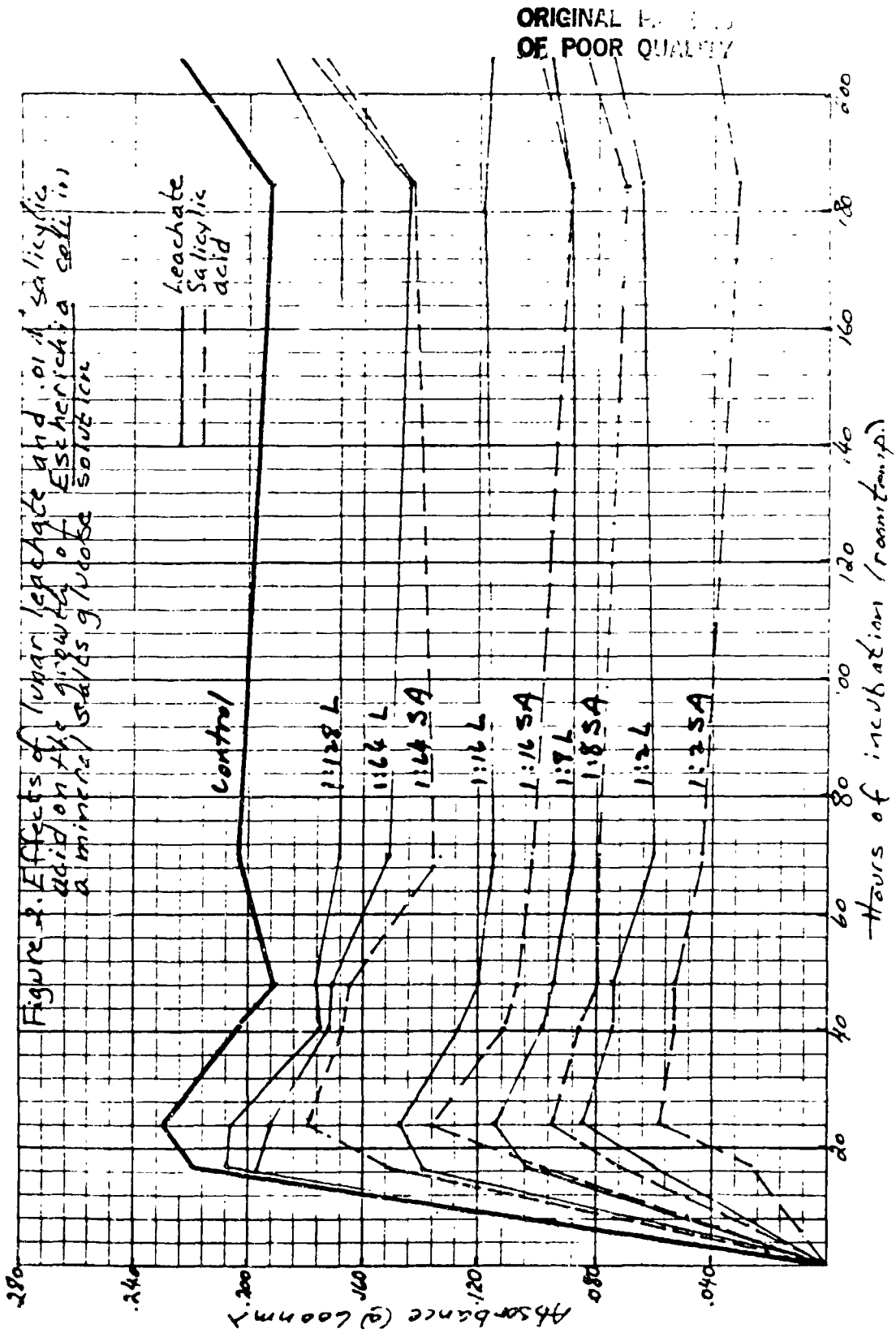
Hours of Incub.	Dist. Water	Undil.	1:2	1:4	1:8	1:16	1:32	1:64
24	++++	++	++	++	+++	+++	+++	++++
42	++++	+	++	++	++	+++	+++	+++
85	++++	-	-	+	+	+	++	++

++++ = dense growth (innumerable colonies).

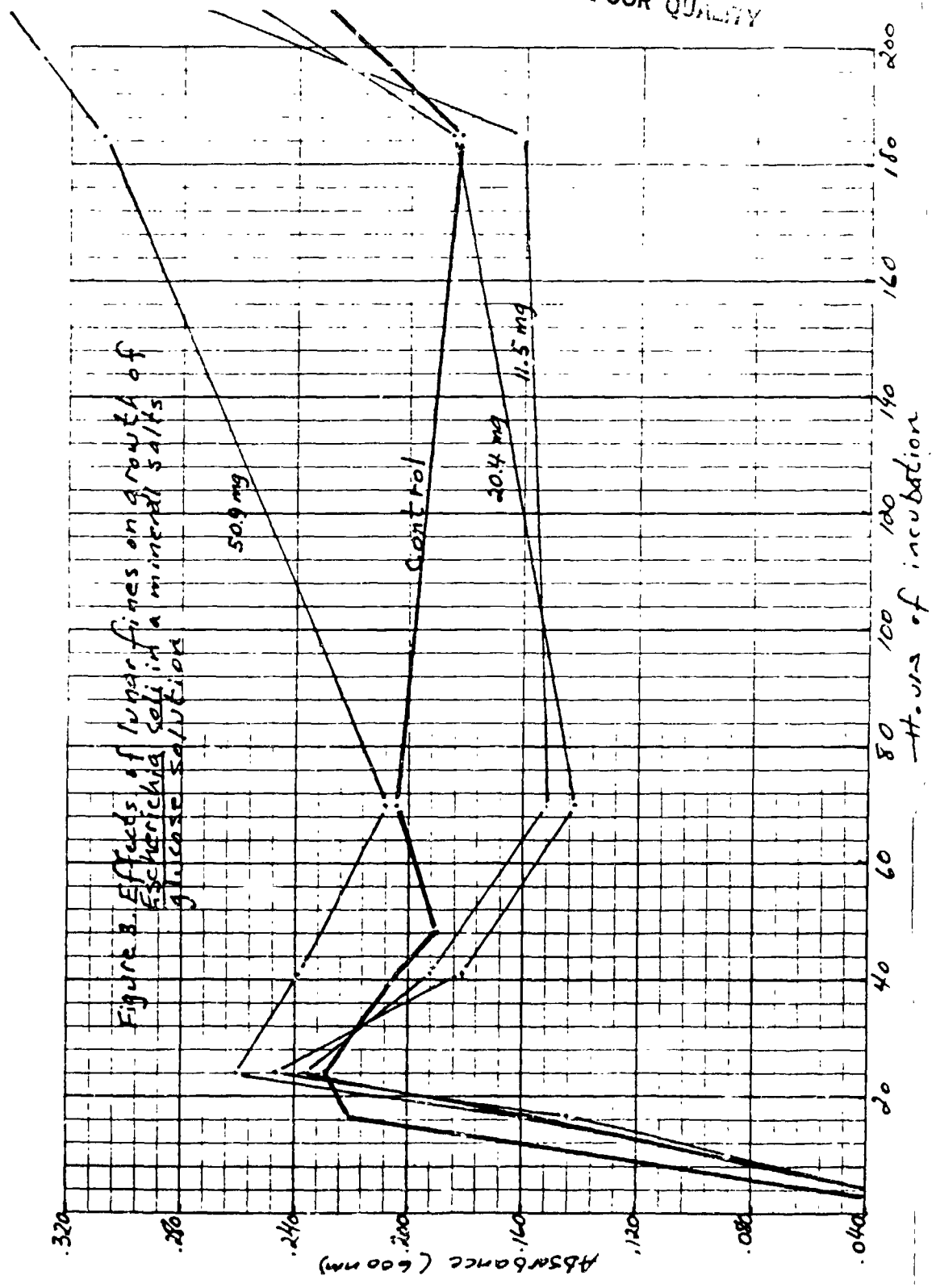
+ = light growth (a few colonies).

Table 5. Survival of E. coli in Aqueous Dilutions of Neutralized Leachate.





ORIGINAL P. ...
OF POOR QUALITY



N86-14089

SPECTRAL REFLECTANCE OF SURFACE SOILS - RELATIONSHIPS
WITH SOME SOIL PROPERTIES

By

Carl H. Kieseewetter*
Mech/Civil Technology Dept.
Middlesex County College, New Jersey

ABSTRACT

Using a published atlas of reflectance curves and physicochemical properties of soils, a statistical analysis was carried out. Reflectance bands which correspond to five of the wavebands used by NASA's Thematic Mapper were examined for relationships to specific soil properties. The properties considered in this study include: Sand Content, Silt Content, Clay Content, Organic Matter Content, Cation Exchange Capacity, Iron Oxide Content and Moisture Content. Regression of these seven properties on the mean values of five TM bands produced results that indicate that the predictability of the properties can be increased by stratifying the data. The data was stratified by parent material, taxonomic order, temperature zone, moisture zone and climate (combined temperature and moisture). The best results were obtained when the sample was examined by climatic classes. The middle Infra-red bands, 5 and 7, as well as the visible bands, 2 and 3, are significant in the model. The near Infra-red band, band 4, is almost as useful and should be included in any studies. General linear modeling procedures examined relationships of the seven properties with certain wavebands in the stratified samples. These results reinforced the hypothesis that the TM bands can be utilized to predict certain soil properties. Some relationships between curve shape and soil properties were also investigated and produced positive results.

Dr. Donald L. Henninger, SC4, was the Center Research Colleague.
*Instructor, Civil Engineering Technology

INTRODUCTION

Spectral reflectance of soil is influenced by the physical and chemical properties of that soil. Some of these physiochemical properties are more influential than others. These properties can be measured in the laboratory using standard tests. Recent works [Stoner and Baumgardner, 1980], [Crouse, et al., 1983], [Kiesewetter, 1982], have suggested relationships of several properties to the spectral signature of the respective soils, particularly in certain wavebands. The objective of these studies has been to utilize the Landsat Satellite data in identifying and classifying soils of the earth. Stoner (1979) measured the spectral reflectance of 485 soils of the United States along with physical, chemical and engineering properties of those soils. The result of that investigation has been published as the "Atlas of Soil Reflectance Properties," [Stoner, et al., 1979]. This data was used by Kiesewetter (1982) and Crouse, et al. (1983), to statistically establish relationships between the soil properties and reflectance at certain wavelengths. Crouse has selected six wavebands which correspond to those of the Thematic Mapper (TM) aboard NASA's Landsat 4 Satellite. That study suggested that four, and possibly 5, of the six TM wavebands may be important in the identification of certain properties. Figure shows a typical soil presentation from Stoner's work. The properties which showed the best results in regression studies were, in order of their relevance, as follow: Organic Carbon Content, Water Content, Clay Content, Cation Exchange Capacity (C.E.C.), Calcium, Magnesium, Fine Sand, Base Saturation, Sand Content, Extractable Acidity, and Iron Oxide Content. In addition, ten other properties were included in the original regression analysis but were later dropped from consideration because they showed little potential of being predicted from TM data. These properties include: Potassium, Medium

Sand Content, .pa Coarse Sand Content, Silt Content, Aluminum,, Coarse Silt, Fine silt, Very Coarse Silt, Sodium, and Very Fine Sand.

This current work looks at several properties and five of the six TM wavebands which are in the range of spectral reflectance measured by Stoner (1979) and attempts to stratify the soils on the basis of Climate, Taxonomy and Parent Material. The objective of this investigation is to determine which soil properties show an ability to be predicted from T.M., spectral measurements, knowing some information about the temperature and moisture zones (climate) and the underlying parent material. This information could conceivably be available for an unknown soil from sources such as a geographic atlas or geologic maps and reports.

THEORY

The physical and chemical properties of the soil, in combination, produce the spectral reflectance. Some of these properties exert more influence than others. Previous work, (Stoner and Baumgardner, 1980) suggests that moisture content, organic matter, iron oxide content, texture, cation exchange capacity are more influential than other properties. Kieseletter (1982) demonstrated that strong negative correlations exist when organic matter, iron oxide, and moisture content are compared with reflectance values. As the percentage of each of these increases the reflectance decreases. The strongest negative correlation seems to be with moisture content. Crouse et. al., (1983) have found, through regression analysis, that eleven properties seem to be dominant in determining reflectance.

Since reflectance is dependent upon the physical and chemical makeup of the soil, it is logical to try to ascertain how these properties are acquired. Parent material should be a place to begin since the soil will inherit certain characteristics from this source material. We know, however, that soils from similar parent materials can vary greatly in physical and chemical composition so other factors must be in play at the same time. Climate (temperature and moisture) is a contributing factor since temperature and moisture influence biological and chemical processes at work in a soil. Parent material is significant in determining the soil texture and chemical composition. Parent material may be residual (weathered from underlying rock or sediments) or it may be transported by means of wind, water or ice and deposited on the bedrock. Other factors at work in the formation of soils are topography, living organisms and time. Time is an important factor since it changes the characteristics of weathered material from those which are inherited from the parent material to those which are acquired in

the aging process. The presence of organisms, both plant and animal, is a strong contributor to the overall reflectance of the soil.

Another consideration was to examine the taxonomic order of the soil. This is done, primarily, to investigate the possibility that soils classified in a particular order will have similar reflective characteristics. Taxonomic order, as defined by the USDA in 1972, is a classification system based on properties of soils as found in the field. Earlier classification systems were based on soil genesis rather than field properties. Utilizing the information developed by Stoner et. al. (1979), which includes reflectance of various soil samples from around the continental United States as well as numerous physical and chemical properties, a statistical analysis was carried out to determine which properties affect which wavebands. The chosen wavebands for this study were those which match the bands of the Thematic Mapper. The thematic mapper operates on six narrow bands: Band 1 (0.45-0.52 μ m), Band 2 (0.52-0.60 μ m), Band 3 (0.63-0.69 μ m), Band 4 (0.76-0.90 μ m), Band 5 (1.55-1.75 μ m), Band 7 (2.08-2.35 μ m), and a broad thermal band (10.4-12.5 μ m). Since the laboratory reflectance values cover only the wavelengths 0.4 to 2.4 μ m, this study does not consider the thermal band.

The work of Crouse, et. al. (1983) has shown that bands 5 and 7, which are in the middle Infra-red portion of the spectrum, are significant in the study of soils using satellite information. The near Infra-red band, Band 4, also shows promise for these studies. The two visible bands, Band 2 and Band 3, will sometimes provide additional information. Band 1 does not appear to be useful for these purposes, because the laboratory data is sketchy in these wavelengths. For that reason Band 1 was not considered in the present study.

The statistical work in this study was carried out using the Statistical Analysis System package developed by SAS Institute, Cary, North Carolina. The procedure R-SQUARE was used to carry out the initial regression work. The GLM procedure was used to regress each soil property on the five TM bands and gave F values to indicate the significance of each TM band in the model.

RESULTS

Utilization of the published (Stoner, et. al., 1979) values limited this study to the following properties: Sand, Silt, Clay, Organic Matter, Cation Exchange Capacity, Iron Oxide content and Moisture content. By regressing these properties on the mean value of each of the five TM bands chosen for this study (Bands 2, 3, 4, 5, and 7) it was determined that prediction of certain properties was possible just by knowing these five wavebands. The results of this regression study, on the 467 soils in the data set, are presented in Table 1. The R-SQUARE values can be read as percentages of the various properties which can be accounted for by the five wavebands. For instance, from Table 1 we can say that we can account for 44.4% of the organic matter in the soil by knowing the reflectance values of the five bands.

The next step in the study was to stratify the total sample by Parent Material, Temperature Zone, Moisture Zone, Taxonomic Order and Climate (combined temperature and moisture). The results of those regressions are shown in Table 7 under the appropriate column headings. The values shown on Table 7 are mean values of the various classes within each group. Parent material was broken down into the following classes: Igneous Residuum, Sedimentary Residuum, Eolian (air transported) origin, Unconsolidated Terrigenous Deposits (alluvial and lacustrine), Marine Deposits, and Glacial

origins. Table 2 shows the various R-SQUARE values for these classes. The soils were then reclassified by temperature zones and analyzed. The results of that stratification and regression are shown in Table 3. Other classifications based on Moisture Zone, Taxonomic Order and Climate are tabulated in Tables 4, 5, and 6 respectively. The summary shown in Table 7 indicates that prediction values increase with stratification. Looking at the values in Table 7 it is apparent that a stratification based on Climate (temperature and moisture) would be beneficial. It is also intuitively apparent that these two factors are the only ones of which we could have prior knowledge for an unknown earth area. It would be easier to assign a climatic parameter to an unmapped area than to use Parent Material or Taxonomic Order, since these parameters imply a prior study of the soil. In simpler terms, if we knew these parameters we would no longer have an unmapped area. A known Taxonomic Order for a soil on the earth could, however, be used to verify or "fine tune" our TM data. We can assign a climatic parameter to an unknown earth area without any prior knowledge of the soil type.

The next phase of the study involved regressing the soil properties on the five TM wavebands in order to determine which bands are significant in predicting the soil properties. Table 8 shows the results of this procedure for the entire sample population of 467 soils. A high F value and a low (less than 0.0050) $PR > F$ value indicates significance. It can be seen from Table 8 that bands 2 and 7 are significant in predicting six of the seven properties. Band 3 is significant for five properties while Band 5 and Bands 4 are significant to a lesser degree. The F value tests how well the model as a whole accounts for the dependent variable's behavior. The value labeled " $PR > F$ " is the significance probability - if this value is small it indicates significance.

Again, the soil sample population was stratified and the results of the regression analyses were tabulated. Tables 9 and 10 show the values for each property in relation to the five TM bands, when stratified by temperature (Table 9) and moisture (Table 10). These results show only the greatest F values, where the significance probability is less than .0050 for the various properties on the five wavebands. Table 11 shows the results of combining temperature zones and moisture zones for a stratification based on climate. The importance of certain wavebands to the model are obvious from a perusal of Table 11. Based on all stratifications, it can be seen that Band 2, Band 7 and Band 3 are most significant in the prediction of soil properties. Bands 4 and 5 are slightly less important overall; but they should be considered in all models.

A preliminary approach to prediction of certain properties was attempted based on correlations which were evident when the angle of the tangent to the rising limb of the reflection curve was compared with the soil properties. This angle was designated "Angle X" and is referred to as such in this paper. The unstratified data indicated that correlations exist in Sand Content, Clay Content, Organic Matter, Cation Exchange Capacity and Moisture Content. When the data is stratified by climate, strong correlations were found for C.E.C., Organic Matter, Clay Content, Sand Content and Iron Oxide Content for certain temperature and moisture combinations.

Similar correlations were observed when looking at the declination angle of the tangent to the curve at the higher wavelengths of the data. This angle was designated "Angle Y" for this study. Correlations in the unstratified sample were strongest in Organic Matter, C.E.C., and Moisture

TABLE 1

R-SQUARE VALUES

OBTAINED BY REGRESSING SOIL PROPERTIES
ON THE FIVE T.M. BANDS

ALL SAMPLES (467) NON STRATIFIED

<u>PROPERTY</u>	<u>R-SQUARE</u>
SAND	.182
SILT	.049
CLAY	.362
ORGANIC MATTER	.444
CATION EXCHANGE CAPACITY	.340
IRON OXIDE	.119
MOISTURE CONTENT.	.347

TABLE 2
 R-SQUARE VALUES - REGRESSING SOIL PROPERTIES
 ON FIVE T.M. BANDS.
 STRATIFIED BY PARENT MATERIAL.

	IGNEOUS RESIDUUM	SEDIMENTARY RESIDUUM	EOLIAN ORIGIN	UNCONSOL. TERRIG. SO.	MARINE DEPOSITS	GLACIAL ORIGINS
SAND	.683	.399	.187	.226	.345	.197
SILT	.564	.274	.121	.074	.187	.052
CLAY	.715	.640	.484	.425	.525	.310
ORG. MATTER	.569	.430	.498	.526	.460	.651
C.E.C.	.742	.682	.504	.284	.490	.574
Fe ₂ O ₃	.711	.176	.124	.198	.304	.303
MOISTURE	.582	.654	.336	.376	.309	.462

TABLE 3
R-SQUARE VALUES
 MAST = MEAN ANNUAL SOIL TEMPERATURE

FRIED ZONE ($MAST < 8^{\circ}C$)

SAND	.255
SILT	.068
CLAY	.341
ORG.M	.378
CEC	.542
Fe ₂ O ₃	.339
MOISTURE	.443

MESIC ZONE ($8^{\circ}C \leq MAST < 15^{\circ}C$)

SAND	.143
SILT	.067
CLAY	.405
ORG.M.	.468
C.E.C.	.370
Fe ₂ O ₃	.140
MOISTURE	.270

THERMIC ZONE ($15^{\circ}C \leq MAST < 22^{\circ}C$)

SAND	.212
SILT	.071
CLAY	.432
ORG.M.	.363
CEC.	.268
Fe ₂ O ₃	.146
MOISTURE	.365

HYPERTHERMIC ZONE ($22^{\circ}C \leq MAST$)

SAND	.656
SILT	.602
CLAY	.644
ORG.M.	.583
CEC	.652
Fe ₂ O ₃	.331
MOISTURE	.560

TABLE 4

R-SQUARE VALUES - REGRESSING SOIL PROPERTIES
ON FIVE T. M. BANDS

STRATIFIED BY MOISTURE ZONE

-60 to -40 = MOISTURE INDEX (STONER & BAUMGARDNER)

PROPERTIES.	ARID -60 to -40	SEMI- ARID -40 to -20	SUB- HUMID -20 to 20	HUMID 20 to 100	PERHUMID 100 AND +
SAND	.508	.304	.368	.182	.944
SILT	.184	.187	.147	.113	.226
CLAY	.670	.415	.537	.222	.886
ORGANIC MATTER	.606	.416	.548	.442	.805
C.E.C.	.389	.415	.560	.426	.752
Fe ₂ O ₃	.343	.409	.076	.289	.735
MOISTURE	.626	.251	.604	.281	.842

TABLE 5
 R-SQUARE VALUES - REGRESSING SOIL PROPERTIES
 ON FIVE T.M. BANDS
 STRATIFIED BY TAXONOMIC ORDER

PROPERTY.	ALFISOLS	ENTISOLS	INCEPTISOLS	VERTISOLS	MOLLISOLS	SPodosOLS	ARIDISOLS	ULTISOLS
SAND	.175	.232	.126	.825	.250	.488	.363	.190
SILT	.120	.160	.121	.985	.088	.467	.296	.164
CLAY	.287	.366	.166	.938	.431	.398	.311	.394
O.M.	.474	.393	.733	.981	.497	.623	.514	.429
CEC	.442	.234	.319	.945	.481	.598	.262	.490
Fe ₂ O ₃	.348	.114	.386	.999	.082	.770	.480	.416
HORST	.221	.255	.460	.869	.403	.539	.285	.172

TABLE 6
R-SQUARE VALUES - REGRESSING SOIL PROPERTIES ON FIVE
T.M. BANDS - STRATIFIED BY CLIMATE

CLIMATE CLASS	SAND	SILT	CLAY	ORG. MATTER	CEC.	Fe ₂ O ₃	Moisture
FRIGID-SEMIARID	.489	.513	.502	.413	.317	.332	.469
FRIGID-SUBHUMID	.429	.337	.424	.605	.750	.231	.588
FRIGID-HUMID	.622	.296	.666	.664	.599	.516	.613
MESIC-ARID	.488	.207	.833	.702	.770	.305	.704
MESIC-SEMIARID	.433	.276	.494	.441	.565	.309	.420
MESIC-SUBHUMID	.489	.369	.595	.687	.555	.412	.408
MESIC-HUMID	.362	.349	.346	.457	.540	.095	.149
MESIC-PERHUMID	.944	.226	.886	.805	.752	.735	.842
THERMIC-ARID	.634	.665	.471	.592	.341	.659	.587
THERMIC-SEMIARID	.623	.583	.704	.722	.610	.841	.587
THERMIC-SUBHUMID	.626	.419	.662	.402	.629	.282	.748
THERMIC-HUMID	.148	.076	.393	.174	.395	.375	.205
HYPERHUMIC SEMIARID	.925	.866	.936	.814	.883	.269	.950
HYPERHUMIC HUMID	.791	.542	.623	.676	.593	0.000	.445

TABLE 7
 R-SQUARE VALUES FOR TOTAL SAMPLE
 AND FOR VARIOUS STRATIFICATIONS

PROP.	TOTAL SAMPLE	PARENT MATERIAL	TEMP. ZONE	TAXONOMIC ORDER	MOIST. ZONE	CLIMATE (TEMP & MOIST)
SKIND	.182	.3395	.3165	.3240	.4612	.5716
SILT	.049	.2120	.2020	.3001	.1714	.4089
CLAY	.362	.5222	.4555	.4114	.5460	.6096
ORG. MATTER	.444	.5223	.4480	.5805	.5634	.5824
C.E.C.	.340	.5460	.4580	.4715	.5084	.5928
Fe ₂ O ₃	.119	.3027	.2390	.4500	.3704	.4124
MOISTURE	.347	.4532	.4095	.3971	.5208	.5511

TABLE 8

F
PR>F } FROM REGRESSIONS OF SOIL PROPERTIES
ON T.M. BANDS

TOTAL SAMPLE POPULATION - NON STRATIFIED

SOIL PROP.	T.M. BANDS				
	2	3	4	5	7
SAND	21.17 0.0001	5.05 0.0251	2.79 0.0953	3.01 0.0833	70.54 0.0001
SILT	4.87 0.0279	1.69 0.1969	0.18 0.6696	8.58 0.0036	8.36 0.0040
CLAY	39.42 0.0001	7.96 0.0050	23.33 0.0001	3.02 0.0830	188.10 0.0001
ORG. MATTER	303.22 0.0001	69.50 0.0001	0.28 0.5956	5.69 0.0174	0.15 0.7024
C.E.C.	54.98 0.0001	9.41 0.0023	52.68 0.0001	2.35 0.1256	117.70 0.0001
Fe ₂ O ₃	9.23 0.0025	13.80 0.0002	0.37 0.5456	27.79 0.0001	10.79 0.0011
MOISTURE	108.24 0.0001	14.56 0.0002	7.77 0.0055	22.69 0.0001	92.03 0.0001

TABLE 9

F VALUES WHERE PROBABILITY SIGNIFICANCE (P>F) IS
LESS THAN .0050

SAMPLE STRATIFIED BY TEMPERATURE ZONE

SOIL PROP.	T.M. BANDS					TEMP. ZONE
	2	3	4	5	7	
SAND	13.46 14.06				25.73 27.30 10.89 19.87	FRIGID MESIC THERMIC HY-THER
SILT		12.86			12.25	F M T H
CLAY	28.46 11.47	9.66 14.70	18.80 9.12	26.71	29.97 71.80 56.51 22.17	F M T H
ORG. MATTER	44.82 170.04 32.42 10.23	40.57 16.10				F M T H
C.E.C.	54.63 23.20 12.25	12.89	27.78 17.73		37.80 52.39 24.95 22.36	F M T H
Fe ₂ O ₃	8.40	21.72 10.34			8.43	F M T H
MOISTURE	24.78 29.85 19.43 14.49	13.28		9.12	35.66 34.83 34.77	F M T H

TABLE 10

F VALUES - WHERE PROBABILITY SIGNIFICANCE (P) IS
LESS THAN .0050

SAMPLE STRATIFIED BY MOISTURE ZONE

SOIL PROP.	T.M. BANDS					MOISTURE ZONE
	2	3	4	5	7	
SAND	22.80	14.29		11.95		ARID SEMIARID SUBHUMID HUMID PERHUMID
	13.40	9.80	9.63	14.83	15.58	
		12.76			26.88	
		14.04	23.94		20.66	
SILT	8.61			12.96		A S H P
					11.80	
CLAY	36.56	17.12		37.81	23.60	A S H P
	21.76	24.51	8.32		47.23	
		21.63			79.51	
					20.92	
ORG. MATTER	68.44	15.51				A S H P
	9.13	42.53				
	115.92	15.35	9.00			
	106.39			19.16		
C.E.C.	20.23					A S H P
	10.30	10.63		10.52	12.04	
	52.73	25.77	16.77		32.57	
Fe ₂ O ₃	100.27				51.32	A S H P
	15.55	13.94	18.10	24.80	15.03	
		35.72				
					20.58	
MOISTURE	57.94	13.15		12.48	14.92	A S H P
	65.98	24.29	15.00	24.09	21.83	
	22.00			27.00	50.95	
					16.49	
					23.61	

TABLE II

ALL STRATIFICATIONS P > F IS LESS THAN .0050
SIGNIFICANCE OF VARIOUS BANDS TO PROPERTIES.

P = PARENT MATERIAL (3) C = CLIMATE CLASS (14)
T = TEMPERATURE ZONE (4)
M = MOISTURE ZONE (5) SUBSCRIPT = NO. TIMES BAND IS SIGNIFICANT

	T.M. BANDS				
	2	3	4	5	7
SAND	P ₂ T ₂ M ₂ C ₅ 10	P ₃ M ₄ C ₂ 9	P ₂ M ₁ C ₁ 4	M ₂ C ₂ 4	P ₂ T ₄ M ₄ C ₄ 14
SILT	T ₁ M ₁ C ₄ 6	P ₁ 1		M ₁ C ₁ 2	T ₁ M ₁ C ₁ 3
CLAY	P ₂ T ₂ M ₂ C ₈ 11	P ₂ T ₂ M ₃ C ₂ 13	P ₁ T ₁ M ₁ C ₁ 4	P ₂ T ₁ M ₁ C ₂ 6	P ₂ T ₂ M ₄ C ₄ 16
ORGANIC MATTER	P ₆ T ₃ M ₅ C ₈ 22	P ₃ T ₂ M ₃ C ₁ 9	P ₁ M ₁ 2	M ₁ C ₂ 3	
C.E.C.	P ₂ T ₃ M ₃ C ₇ 17	P ₃ T ₁ M ₂ C ₂ 8	P ₃ T ₂ M ₁ C ₃ 9	M ₂ C ₁ 3	P ₅ T ₄ M ₄ C ₆ 19
FE ₂ O ₃	P ₂ T ₁ M ₁ C ₂ 6	P ₁ T ₂ M ₂ C ₂ 7	M ₁ C ₁ 2	P ₂ M ₁ C ₁ 4	P ₁ T ₁ M ₁ 3
MOISTURE	P ₅ T ₄ M ₃ C ₇ 19	P ₂ T ₁ M ₂ C ₃ 10	P ₁ M ₁ C ₁ 3	P ₁ M ₃ C ₂ 6	P ₃ T ₃ M ₄ C ₄ 14

TYPICAL SOIL ENTRY IN ATLAS
(T.M BANDS ADDED FOR THIS STUDY)

DRUMMER (IL)

Typic Haplaquoll
fine-silty, mixed, mesic
humid zone
thick loess over outwash and drift
Champaign Co.

—
Ap horizon
A slope
poorly drained
silty clay loam
13%S 56%Si 32%C
10YR 2/1 (moist)
10YR 3/2 (dry)
5.61% O.M.
40.3 meq/100g CEC
0.76% Fe₂O₃

Ap horizon
A slope
poorly drained
silty clay loam
8%S 60%Si 32%C
10YR 2/1 (moist)
10YR 3/2 (dry)
6.09% O.M.
41.7 meq/100g CEC
0.92% Fe₂O₃

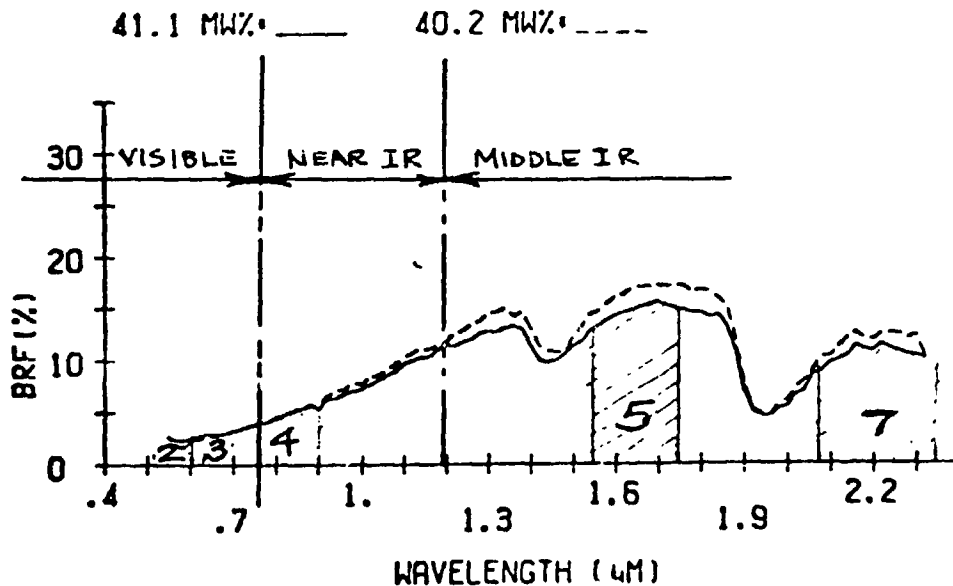
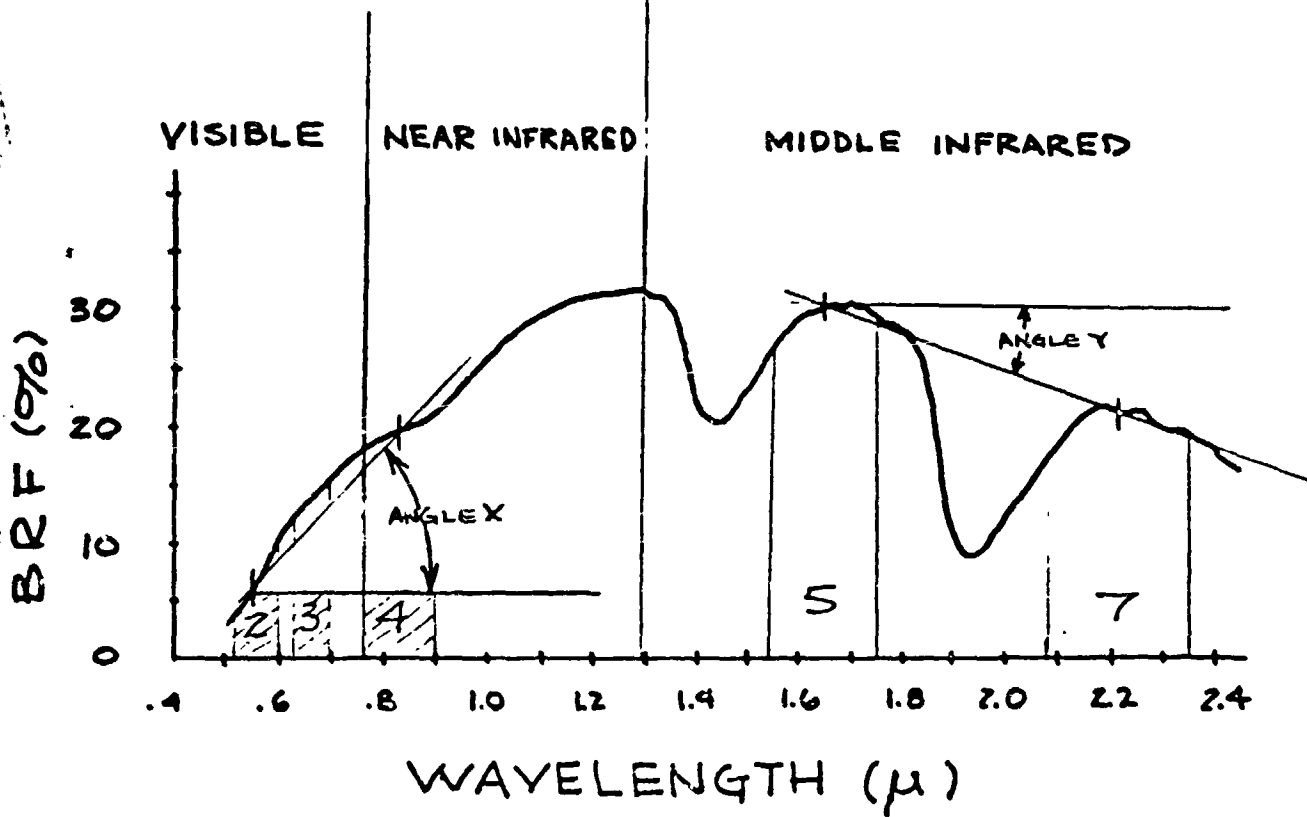


Figure 1

PLOT OF BR F (%) VS. WAVELENGTH (μ)
SHOWING ANGLE X AND ANGLE Y



CORRELATIONS

ANGLE X:

PROPERTIES

ORG. M, C.E.C.
ORG. M,
ORG. M, CLAY, C.E.C.
ORG. M, SILT.
FE,
ORG. M., SAND, CLAY, C.E.C., M.W.

CLIMATE CLASS

FRIGID-SUBHUMID
FRIGID-ARID
MESIC SUBHUMID
MESIC HUMID
THERMIC-SEMIARID
THERMIC-SUBHUMID

ANGLE Y:

ORG. M., C.E.C., M.W.
ORG. M.
ORG. M., M.W.
ORG. M.
FE
FE
M.W.

FRIGID-SUBHUMID
FRIGID-HUMID
MESIC-ARID
MESIC SUBHUMID
THERMIC ARID
THERMIC SEMIARID
THERMIC SUBHUMID

Figure 2

Content. The correlations were all negative-indicating that lower quantities of these properties produce a steeper angle of descent at the trailing end of the reflectance curve. When the data is stratified by climate, the correlations are strongest in certain climate classes for the three soil properties mentioned as well as a very strong relationship of iron oxide in the Thermic-Arid and Thermic-Semiarid sample set. Figure 2 shows these relationships in a summarized format.

CONCLUSIONS

The results of this work will aid in the utilization of TM data for soils investigations. We can define the wavebands which will supply the most significant data regarding soil properties. The study has indicated that bands 2 and 7 are very significant in the study of soil properties and their influence on TM responses. Band 2 is in the visible spectrum, while Band 7 is one of the middle IR bands. Bands 3 and 5 are somewhat less significant overall but become more important when stratification by climate is undertaken. Band 4, the near IR band, is individually important to some of the properties. Bands 2 and 4 were used to determine "Angle X", the slope of the tangent to the ascending limb of the reflectance curve. Bands 5 and 7 were used to obtain "Angle Y", the slope of the tangent to the trailing end of the curve.

Sand Content appears to be associated with responses in the visible range (Bands 2 and 3) and in the middle IR bands (Bands 5 and 7). In both cases a high sand content produces a strong reflectance response.

Silt content has shown consistantly poor potential for prediction. Only when stratified by climate does Band 2 come into play in several classes to produce positive correlations.

Clay content appears to be related negatively to responses in Bands 7, 2, and 3.

Organic Matter Content, under various stratifications, figures dominantly in the Band 2 and Band 3 responses. These are negative correlations indicating that high organic content tends to depress the responses in the visible bands. This reduced response in the visible area produces a flattened curve. This was used by Stoner (1981) to classify the curves by shape.

Cation Exchange Capacity shows excellent results in Bands 2 and 7, while several stratification classes show strong responses in Bands 3 and 4. These responses all show negative correlations, indicating that an inverse relationship exists between C.E.C. and waveband response.

Iron Oxide Content showed somewhat erratic results in the studied wavebands. This was not totally unexpected since Stoner pointed out iron absorption wavelengths in his study which lie outside the bands covered by the TM; however, two climatic zones (Thermic-Arid and Thermic-Semiarid), showed strong negative correlations of Iron Oxide content with the Y Angle.

Moisture Content produced strong negative correlations with Bands 2 and 7 with somewhat lesser results in Bands 3 and 5. Again, the negative correlations indicate that increasing moisture content tends to depress responses in these wavebands.

Clay content may be one key to the response prediction problem. Higher clay contents in soils tend to be associated with higher organic matter, increased Cation Exchange Capacity and increased moisture contents. The amount of clay present is not nearly as important as the type of clay minerals present. Soil scientists are quite aware of the role that climate plays in clay formation. All other things being equal, an increase in temperature and precipitation causes an increase and enhancement of the weathering reaction. High average temperatures tend to foster rapid weathering and clay formation. A minimum degree of weathering is produced by climates that are: warm and dry, cold and dry, or cold and moist. This is borne out in the climate-stratified sample population when the mean clay contents are examined for the various climate classes - the frigid dry, frigid moist and thermic dry classes all show reduced clay contents. This indicates that it may be practical to develop a model which takes into account the climatic zone of an unknown earth area and then makes an assumption of clay content before checking the various wavebands for reflectance responses.

REFERENCES

1. Brewer, R. "Fabric and Mineral Analysis of Soil," John Wiley & Sons, Inc., N.Y., 1964.
2. Condit, H. R., "The Spectral Reflectance of American Soils," Photogrammetric Engineering, Vol. 36, pp. 955-966, 1970.
3. Crouse, K. R., D. L. Henninger, D. R. Thompson, "Spectral Reflectance of Surface Soils - A Statistical Analysis," Internal Report, Remote Sensing Research Branch, NASA-JSC, Houston, Texas, 1983.
4. Heilman J. L., V. I. Myers, D. G. Moore, t. J. Schmugge, D. B. Friedman, "Soil Moisture Workshop," NASA Conference Publication 2073, NASA, 1978.
5. Hoffer, R. M., and C. J. Johannsen, "Ecological Potentials in Spectral Signature Analysis," pp. 1-29 In P. L. Johnson (ed.). Remote Sensing in Ecology, University of Georgia Press, Athens, 1969.
6. Hunt, c. B. "Geology of Soils," W. H. Freeman and Co., San Francisco, 1972.
7. Imhoff, M. L. and g. W. Petersen, "The Role of Landsat Data Products in Soil Surveys," Interim Report, Institute for Research on Land and Water Resources, the Pennsylvania State University, 1980.
8. Kieseletter, C. H., "Some Relationships Between Soil Properties and Soil Reflectances," Research Reports, NASA-ASEE Summer Faculty Fellowship Program, JSC, Houston, Texas, 1982.
9. Lillesand, T. M. and R. W. Diefer, Remote Sensing and Image Interpretation," John Wiley and Song, Inc., N.Y., 1979.

10. Lindberg, J. D. and D. G. Snyder, "Diffuse Reflectance Spectra of Several Clay Minerals," American Mineralogist, Vol. 57, pp. 485-493, 1972.
11. Miller, R. L. and J. S. Kahn, "Statistical Analysis in the Geological Sciences," John Wiley and Sons, Inc., N.Y., 1965.
12. Pouquet, J., "Geopedological Features Derived from Satellite Measurements in the 3.4-4.2 and 0.7-1.3 Spectral Regions," Proc. 6th International Symposium on Remote Sensing of Environment, Vols. II, pp. 967-988, 1969.
13. Silva, L. F., R. M. Hoffer, J. E. Cipra, "Extended Wavelength Field Spectroradiometry," Proc. 7th International Symposium on Remote Sensing of Environment, Vol. II, pp. 1509-1518, 1971.
14. Stoner, E. R., M. F. Baumgardner, L. L. Biehl, B. F. Robinson, "Atlas of Soil Reflectance Properties," LARS Technical Report 111579, Purdue University, West Lafayette, Ind., 1979.
15. Stoner, E. R., M. F. Baumgardner, "Physicochemical Site, and Bidirectional Reflectance Factor Characteristics of Uniformly Moist Soils," AgRISTARS Technical Report, LARS 111679, Purdue University, West Lafayette, Ind., 1980.
16. Stoner, E. R., M. F. Baumgardner, "Characteristic Variations in Reflectance of Surface Soils," Soil Science Soc. Am. Journal, Vol 45, pp. 1161-1165, 1981.
17. Tanquay, M. G., R. M. Hoffer, R. D. Miles, "Multispectral Imagery and Automatic Clasification of Spectral Response for Detailed Engineering

Soils Mapping," Proc. 6th International Symposium on Remote Sensing of Environment, Vol. I, pp. 33-64, 1969.

18. Thompson, D. R., D. E. Pitts, K. E. Henderson, "Simulation of LANDSAT MSS Spectral Response of Soils Using Laboratory Reflectance Measurements," Soil Science Society of America Journal, in Press, 1983.
19. Thompson, D. R., K. E. Henderson, A. G. Houston, D. E. Pitts, "Evaluation of LANDSAT Thematic Mapper for Vegetated Alluvium Soils Information," International Geoscience and Remote Sensing Symposium, San Francisco, CA., 1983.
20. Wendroth, S., E. Yost, R. Kalia, R. Anderson, "Multispectral Photography for Earth Resources," Science and Engineering Research Group, Long Island University, Greenvale, New York, 1972.

N86-14090

CONTROL OF SPACE STATIONS

By

Kwang Y. Lee
Associate Professor
Department of Electrical Engineering
University of Houston-University Park
Houston, Texas 77004

ABSTRACT

A study is made to develop controllers for the NASA-JSC Triangular Space Station and evaluate their performances to make recommendations for structural design and/or control alternatives. The control system design assumes the rigid body of the Space Station and develops the lumped parameter control system by using the Inverse Optimal Control Theory. In order to evaluate the performance of the control system, a Parameter Estimation algorithm is being developed which will be used in modeling an equivalent but simpler Space Station model. Finally, a scaled version of the Space Station is being built for the purpose of physical experiments to evaluate the control system performance.

Center Research Advisor: R. Berka

INTRODUCTION

For the case of advanced spacecraft such as the proposed Space Station, attitude control has typically been a major problem. The source of previous control difficulty has been centered on the requirement to control a highly flexible vehicle. Spacecrafts with cantilevered solar panels cause particular problems because of the low frequencies of the flex modes. If a classical control strategy is used, the flex modes are filtered out of the sensed vehicle response. This technique, unfortunately, has an adverse effect on the attitude control performance of the vehicle. In addition, the closed loop stability of the flex modes is not guaranteed for highly flexible appendages. For highly flexible structures the control system must not only account for attitude control, but also must exhibit vibration control features.

The Preliminary Space Station Design Team of the Structures Division of NASA-JSC has developed an alternative triangular configuration [Schneider,1982] for future Space Station in order to minimize the attitude control problem which is inherent in many proposed Space Station configurations. The flex mode of this configuration are relatively high (>5.4 Hz) and therefore can be filtered out of the sensed vehicle response. This allows rigid body control below the flex frequency bandwidth with acceptable vehicle rate and attitude performance. Furthermore, the behavior of the vehicle can be accurately predicted due to the simplicity of the structural configuration leading to a reduction of control model errors. The control system also benefits from this concept since most activity is centralized at the system center of mass.

The purpose of this study is to develop controllers for the proposed

Space Station and evaluate their performances to make recommendations for structural design and/or control alternatives.

ATTITUDE CONTROL

The problems of control for the Space Station have expensive solutions in cost and performance. As a preliminary guideline for the development of the Space Station proposed, the minimization of these control problems was a goal of high priority. To accomplish this objective, the flex frequency spectrum must be raised significantly to achieve desired separation between the flex and controller passband. Further, a configuration was sought that was relatively insensitive to operational activities. The configuration that resulted from these design guidelines is the triangular design studied here [Schneider,1982]. For the proposed station the flex spectrum begins at approximately 5.4 Hz. The controller passband, therefore, is sought to be placed below this frequency in order not to excite the flex modes of the structure.

To achieve this objective, the study is divided into the following three parts:

- (1) Control system design
- (2) Performance evaluation
- (3) Experiments

The control system design assumes the rigidity of the Space Station and develops the lumped parameter controller for the rigid body model. The performance of this controller will be evaluated with the real system (represented by more complex model with the flexibility of structure incorporated). The designed controller will also be tested through the experiments using a physical model.

1. Control System Design

The flexible structures are so called distributed parameter systems and, accordingly, the distributed controls are required to maintain a desired profile of the structure. Since these controls are additional controls beside the controls for attitude and maneuvering, it is attempted to minimize the flexibility of the Space Station as much as possible and use only the lumped parameter controls for the presumed rigid body.

Two basic methods can be used to design control systems; each with their respective emphasis. The time-domain, state-space method used in modern optimal control theory emphasizes the performance of the vehicle. The frequency domain approach is used when stability issues are a concern of high priority. For the operational Space Station, performance requirements are low compared to other space vehicles while system stability is an important control objective. The frequency domain approach, however, is limited in general to simple systems and not readily applicable to multivariable control systems. On the other hand, the time-domain optimal control theory is well developed for multivariable control systems.

In this study, an attempt is being made to utilize the advantages of both approaches. For stability considerations, specifications are made in the frequency domain, and then the time-domain optimal control theory is applied to design the optimal controller gains. This hybrid method is so called the Inverse Problem [Park and Lee, 1975] and it promises a bright future in the control system design of the Space Stations.

The Space Station model used to derive the control system design is the coupled three-axis Euler's equation, which is given by equating torques with inertia times acceleration as follows:

$$\begin{bmatrix} I_{xx} & I_{yx} & I_{xz} \\ I_{xy} & I_{yy} & I_{yz} \\ I_{xz} & I_{yz} & I_{zz} \end{bmatrix} \begin{bmatrix} \dot{p} \\ \dot{q} \\ \dot{r} \end{bmatrix} = \begin{bmatrix} T_{g_x} \\ T_{g_y} \\ T_{g_z} \end{bmatrix} + \begin{bmatrix} T_{\omega_1} \\ T_{\omega_2} \\ T_{\omega_3} \end{bmatrix} + \begin{bmatrix} T_{m_1} \\ T_{m_2} \\ T_{m_3} \end{bmatrix} + \begin{bmatrix} 0 & H_{T_3} & -H_{T_2} \\ H_{T_3} & 0 & -H_{T_1} \\ -H_{T_2} & H_{T_1} & 0 \end{bmatrix} \begin{bmatrix} p \\ q \\ r \end{bmatrix} + \begin{bmatrix} T_{d_x} \\ T_{d_y} \\ T_{d_z} \end{bmatrix} + \begin{bmatrix} T_{R_1} \\ T_{R_2} \\ T_{R_3} \end{bmatrix} \quad (1)$$

where:

- I_{xx}, I_{yy}, I_{zz} - Principle axis inertias
- I_{xy}, I_{xz}, I_{yz} - Cross axis inertias
- $T_{g_x}, T_{g_y}, T_{g_z}$ - Gravity gradient torques
- $T_{\omega_1}, T_{\omega_2}, T_{\omega_3}$ - Torques due to angular momentum changes
- $T_{m_1}, T_{m_2}, T_{m_3}$ - Torques due to magnetics
- $H_{T_1}, H_{T_2}, H_{T_3}$ - Angular momenta about the 3 axes
- p, q, r - Body axis rates (roll, pitch, and yaw, respectively)
- $T_{d_x}, T_{d_y}, T_{d_z}$ - "Disturbance" torques
- $T_{R_1}, T_{R_2}, T_{R_3}$ - RCS firing torques

A model of the vehicle disturbance environment was determined to quantify the cyclic and non-cyclic torques. Also, for the proposed Station, solar inertial pointing is a necessary maneuvering requirement (approximately 0.06°/sec). Because of the predominant cyclic nature of the disturbance torques a momentum management scheme was devised using CMG's (control moment gyro's) and RCS (reaction control system). Additional control capability is also being sought by means of the Magnetic Torques [Gran and Proise, 1981; Liegeois, 1970].

The three-axis model defined by Eq. 1 can be linearized and represented in the following matrix form:

$$\dot{x} = Ax + Bu + Cv \quad (2)$$

where x is the state vector of body axis rates and additional state

variables representing the dynamics of CMG and Magnetic Torquers; u is the control vector of CMG commands, Magnetic Torquer voltage controls, and RCS commands; and v is the vector of disturbances which may include the gravity gradient torques and the aerodynamic torques.

The time-domain optimal control problem is defined to minimize the following performance functional

$$J = \int_0^{\infty} (x^T Q x + u^T R u) dt \quad (3)$$

Solution of this optimal control problem gives the following optimal feedback control:

$$u = Kx \quad (4)$$

Note that the optimal feedback control gain matrix K will depend upon the choice of the weighting matrices Q and R of the performance equation (Eq. 3). This choice is arbitrary and subjective based upon engineering judgements. Here is where the Inverse Problem comes into the scene. The Inverse Problem is to make an optimal choice of the weighting matrices based upon the specifications in the frequency-domain which reflect the stability requirements.

2. Performance Evaluation

The control system design is based upon the rigid body assumption of the Space Station. Therefore, its performance requires evaluations when the controller is implemented in the real model of the Space Station. A Finite Element computer model for the Space Station was developed by using NASTRAN [Schneider,1982]. However, the model is complex and is not suitable for the evaluation purpose of the controller performance. It is necessary to develop a much simpler model which exhibit the same modal

characteristics as the original NASTRAN model.

To meet this objective, a Parameter Estimation method is being developed. Using the data generated by the NASTRAN model of the Space Station, the Parameter Estimation algorithm will estimate parameters representing an equivalent but much simplified version of the Station model. The Parameter Estimation method is based upon the least squares method [Meyer and Lee,1982] and the modified Newton-Raphson method [Taylor and Iliff,1972]. It gives an iterative algorithm of the parameters in the direction of reducing the modeling error of a simplified model as compared to the NASTRAN model.

It is expected that an equivalent model will be represented by three plate equations coupled with rigid modules located at each corner of the triangle. Once this is completed, then other operational experiments can also be performed by attaching Remote Manipulator System, or by docking the Space Shuttle. The overall performance of the Space Station will then be evaluated by implementing the attitude controllers designed.

Additional use of the Parameter Estimation algorithm is its application on real data telemetered after the Space Station is put into operation. This feature will be very useful in estimating parameters of vehicle in orbit, especially the damping coefficients.

3. Experiments

In parallel with the analytical study, a scaled version of the Space Station is being built in NASA-JSC. This physical model will be hung and evaluated when the control system is implemented. It is hoped that the physical experiments give a new insight in control system design, structure characteristics, and instrumentations.

CONCLUSIONS

The purpose of this study was to develop controllers for the proposed Triangular Space Station and evaluate their performances to make recommendations for structural design and/or control alternatives. The control system design assumes the rigidity of the Space Station and develops the lumped parameter controller by using the Inverse Problem in optimal control theory. In order to evaluate the performance of the control system, a Parameter ESTimation algorithm is being developed which will be used in modeling an equivalent Space Station model. Finally, a scaled version of the Space Station is being built for the purpose of physical experiments to evaluate the control system performance. Much of the work is still remains to be done continually.

REFERENCES

1. Gran, R. and Proise, M., "Magnetic Control System for Satellites in Synchronous Orbit", Annual Rocky Mountain Guidance and Control Conference, AAS 81-006, January, 1981.
2. Liegeois, A., "Controls for the Stabilization of a Satellite by Means of Magnetic Torquers", IFAC Symposium on Space Systems Control, pp. 515-523, 1970.
3. Meyer, F.J. and Lee, K.Y., "Improved Dynamic Load Model for Power System Stability Studies", IEEE Transactions on Power Apparatus and Systems, Vol. PAS-101, No. 9, pp. 3303-3309, September, 1982.
4. Park, J. and Lee, K.Y., "An Inverse Optimal Control Problem and Its Application to the Choice of Performance Index for Economic Stabilization Policy", IEEE Transactions on Systems, Man, and Cybernetics, Vol. SMC-5, No. 1, pp. 64-76, January, 1975.
5. Schneider, W.C., Space Station: Preliminary Design Report, NASA-JSC, September, 1982.
6. Taylor, L.W., Jr. and Iliff, K.W., Systems Identification Using a Modified Newton-Raphson Method-A Fortran Program, NASA TN D-6734, May, 1972.

SOLID WASTE TREATMENT PROCESSES FOR SPACE STATION

By

N86-14091

Thomas R. Marrero, Ph.D.

Associate Professor

Department of Chemical Engineering

University of Missouri-Columbia

Columbia, Missouri 65211

ABSTRACT

The purpose of this study was to evaluate the state-of-the-art of solid waste(s) treatment processes applicable to a Space Station. Previous studies, since the earlier 1960's, were collected to establish a project library and interviews were conducted of numerous personnel with NASA, from industry, and other researchers. From the review of available information a source term model for solid wastes was determined. An overall system is proposed to treat solid wastes under constraints of zero-gravity and zero-leakage. This study contains discussion of more promising potential treatment processes, including super-critical water oxidation, wet air (oxygen) oxidation, and chemical oxidation. A low pressure, batch-type treatment process is recommended. Processes needed for pretreatment and post-treatment are hardware already developed for space operations. The overall solid waste management system should minimize transfer of wastes from their collection point to treatment vessel.

Center Research Advisor: Chin H. Lin

INTRODUCTION

In this report potential processes are investigated for the treatment of solid wastes from the crew and tasks performed in a Space Station. A Space Station has been proposed by NASA as its next major program with an operational Station before the turn of the century. The Space Station would continuously orbit the earth for years, be operated (initially) by a six-man crew, and be resupplied by a Shuttle on about a ninety-day frequency. Resupply of the Station precludes the need for a closed environmental life support system, but the Station will have to treat wastes in order to at least reduce their volume prior to their return to Earth in the Shuttle. It is here assumed that wastes cannot be jettisoned to space from the Station; this is an important constraint to this evaluation of possible treatment systems. The Space Station treatment system will also need to function under zero-gravity conditions. In general, the Station environment will compare to a community with a high population density, limited available utilities (water, electricity, fuel, and air), and operate in a spacecraft with constraints on system size, weight, etc. There is no convenient place for waste disposal and no established recycle options for the waste materials.

The Space Station solid wastes are: feces, urine, paper trash, food wastes including food containers (plastics), and other

solid wastes from routine maintenance operations and special biological, physical and engineering tasks. These materials might somehow be converted to substances needed on the Station. For example, wastes containing carbon could be oxidized to carbon dioxide that could be reduced to oxygen needed for life support. Water in wastes could be separated, filtered, and recycled. Food wastes and metabolic wastes contain nitrogen compounds that could be a source of nitrogen gas needed to maintain cabin atmosphere. These examples do not exhaust the possible uses for solid wastes, but are indicative of more likely practical uses for wastes. Furthermore, solid wastes will need to be treated in order to maintain the habitability of the Space Station.

The primary purpose of this study was to evaluate the feasibility and potential of supercritical water oxidation and other waste incineration processes for use on a Space Station.

THEORY

In order to achieve the project objectives information was retrieved by means of a literature search and by direct discussions with knowledgeable personnel. At the start of the project only a few reports on supercritical water oxidation were in-hand. A computerized literature search was immediately initiated through the Technical Library of the Johnson Space Center. This search used the NASA/RECON data file. The useful reports were retrieved either in hard copy or microfiche form and

organized into an information file. References cited in the reports were checked and copies of applicable documents were added to the file. A limited "hand" search of current Chemical Abstracts and Science Citations was also done. By these means the solid waste treatment information file was developed as listed in table Footnotes and in References. References were classified into four main topics: Process Reviews, Supercritical Water Oxidation, Zimpro Process, and Treatment Processes.

In addition to the library search, many discussions were held with both NASA and non-NASA personnel. A list of people contacted is at the end of this report, after References. These discussions were very helpful towards the rapid establishment of major problems likely to be encountered and the state-of-the-art of solid waste treatment processes.

The scope of this study did not include experimental measurements.

On the basis of the in-hand documents and interview data, the available information was evaluated and organized into two major areas; namely, Source-Term (solid waste(s) mass rates and composition) and Treatment Processes.

RESULTS

The results of this evaluation of Space Station solid wastes and treatment processes are presented below. Results for the Source Term are presented first, then Treatment Processes.

A. Source Term

Metabolic solid wastes from the crew include feces and urine, primarily. Wastes, hair, skin tissue, and nails are relatively small contributions. Toilet tissue paper and wipes are generated along with metabolic wastes but these items are discussed later.

FECES

The rate, solids contents, and elemental composition of feces are listed in Tables 1 to 3. The reported total fecal rates range from 0.060 to 0.50 kg/man-day. This factor of eight difference can be due to many reasons. Variations in diet, particularly fiber content, is an important parameter. Another important factor is the duration of fecal rates, that is whether over 1-day or 1-month, etc. There are many other factors to be considered. In Table 2 results are listed from reports of fecal measurements, not second-hand sources which were included in Table 1. The data in Table 2 indicates a range of 0.1 to 0.4 or a factor of four. The results for Skylab (1974) and the McDonnell-Douglas (1971) have the largest experimental basis. This author would weigh the data towards the Skylab results which were made in a zero-gravity

TABLE 1
FECAL MASS RATE

YEAR	AUTHOR	MASS RATE, KG/MAN-DAY			COMMENT
		SOLIDS	WATER (0.060)	TOTAL 0.104	
1983	Hydeven	0.044	-	0.104	MASA/AMES for CELSS model; Bioastronautics Data Book
1983	Rapp	-	-	0.25 to 0.30	MASA/JSC, estimated for astronauts
1982	Guston and Vinopal	0.11	0.09	0.20	Boeing Aerospace Design Study; Bioastronautics Data Book
1981	Brose	0.032	-	-	Hamilton Standard Design Study
1976	Jagow	-	-	0.125	Lockheed Design Study
1975	Jones	-	-	0.168	USSR 1-year Test (ground) begun in 1967
1975	Bioenvironmental Systems	0.0338	-	-	Review Study
1974	Sauer, R.	0.0413	0.116	0.157	SkyLab Summary Data
1972	Nelson and Cody	-	0.12	-	Space Station Design Study - 6 man crew
1971	McDonnell-Douglas Astron.	0.133	0.260	0.393	Operational 90 Day Manned Test (ground), average of 319 uses.
1970	Schaedle and Laubach	0.036	0.113	0.150	Rockwell; Space Station Waste Model
1969	Hamilton Standard	0.050	0.113	0.163	Design Study
1965	Rich, Ingram and Berger	(0.025 to 0.037)	(0.075 to 0.113)	0.100 to 0.150	Review for U.S. PHS. Basis 1956 Study (Ingram) of cabin cruiser wastes.
1964	Dodson and Wallman	(0.0375)	(0.1125)	0.150	General Dynamics; Ignition ASH @ 1/16 total Mass.
1964	Webb	0.020 to 0.075	-	0.060 to 0.370	Various diets, compilation of results from 9 sources.
		0.0235 to 0.035	-	0.35 to 0.50	General Range. Feces solids contents 15 to 35 %
		0.061	-	0.150	Mixed diet - Wright - Patterson AFB study (1961)
		0.020	-	0.120	Unspecified diet - Wright - Patterson AFB study (1962)

NOTE: Numbers in parenthesis calculated in this work.

TABLE 1
REFERENCES

Dodson L. and Wallman, H., "Research on a Waste System for Aerospace Stations," Technical Documentary Report No. AMRL-TDR-64-33, 1964.

Webb, P., Ed., Bioastronautics Data Book, National Aeronautics and Space Administration, NASA-SP-3006, section 13 pp. 213-239, 1964.

Rich, L.H., Ingram, W.M., and Berger, B.B., "Waste Disposal on Space Craft and Its Bearing on Terrestrial Problems," U.S. Department Health, and Welfare, Public Health Service, PB 168787, 1965.

Hamilton Standard, "Alternate Mission Studies (AILSS)," NASA Contractor Report-66876, 1969.

Fairchild Hiller-Republic Aviation Division, "Housekeeping Concepts for Manned Space Systems," Document No. MS 124 Y0002, Vol. II Prepared for NASA, 1970.

Schaedle G.C. and Laubach G.E. "An Introduction to the Waste Management Problem for Large Space Stations," American Society of Mechanical Engineers., Proceedings Space Systems and Thermal Technology for the 70's Part 1, Los Angeles, CA June, Paper 70-Av/SpT-24, 1970.

McDonnell-Douglas Astronautics "Test Results, Operational Ninety-day Manned Test of a Regenerative Life Support System," NASA Contractor Report 111881 , 1971.

Nelson, W.G. and Cody J. "Life Support System Definition for a Low Cost Shuttle Launched Space Station," American Society of Mechanical Engineers, Publication 72-ENAv-17, 1972.

Bioenvironmental Systems Study Group of the Society of Automotive Engineers, "Evaluation and Comparison of Alternative Designs for Water/Solid-Waste Processing Systems for Spacecraft," Final Report, NASA-CR-162492, 1975.

Jones, W.L., "Life-Support Systems for Interplanetary Spacecraft and Space Stations for Long-Term Use," in Foundations of Space Biology and Medicine, Calvin, M. and Gzenko, O.G., Eds., National Aeronautics and Space Administration, Vol. III p.270, 1975.

Brose, H.F., "A Regenerative Life Support System for Space Operations Center (SOC) - A Probable First Flight Application," American Society of Mechanical Engineers, Paper 81-ENAs-12, 1981.

Guston, E. and Vinopal T., "Controlled Ecological Life Support System Transportation Analysis," NASA Contractor Report - 166420, pp. 48-51, 1982.

Rapp, R., Personal Communication, 1983.

Wydeven, T., "Composition and Analysis of a Model Waste for a CELSS," Preprint, to be published as a NASA Technical Memorandum, 1983.

Reference Added in Proof

Sauer R.L., "Summary Sky Lab Intake-Output Data Sheet, Personal Communication 1983.

TABLE 2. FECAL MASS RATE - EXPERIMENTAL VALUES

YEAR	AUTHOR	RATE, KG/MAN DAY		
		TOTAL	SOLIDS	SGLIDS %
1983	Rapp	0.25 to 0.30	-	-
1981	Onisko and Wydeven ^a	-	-	20
1971	McDonnell-Douglas (90 day ground study)	0.40	0.13	33.8
1975	Jones (USSR data of 1967)	0.17	-	-
1974	Sauer	0.16	0.041	26
1964	Webb	0.35 to 0.50	-	15 to 35
	Webb (Wright-Patterson AFB, 1961)	0.15	0.061	40.7
	Webb (Wright-Patterson AFB, 1962)	0.12	0.020	16.7
1965	Rich, et al. (Ingram, 1956)	0.10 to 0.15	0.025 to 0.037	25

a. Onisko, B. L. and Wydeven, T., "Wet Oxidation as a Waste Treatment Method in Closed Systems," NASA Conference Publication 2247, pp. 51-53, 1981.

TABLE 3. FECAL SOLIDS ELEMENTAL AND ASH COMPOSITION
REFERENCE

ELEMENT	A	B	C	D	E
C	41.92	41.92	26.3	67.73	-
O	-	-	34.6	11.71	11.71
N	8.26	8.26	3.92	4.00	6.0
H	6.59	6.59	6.98	11.71	-
K	2.8	2.8	-	-	0.88
Ca	2.5	2.5	-	-	3.5
CL ⁻	2.1	2.1	-	-	-
Na	1.8	1.8	-	-	0.34
P	1.4	-	0.99	-	-
Mg	0.66	0.66	-	-	0.77
S	-	-	0.39	0.28	-
Fe	0.043	0.043	-	-	0.087
Si	0.040	0.040	0.20	-	-
Zn	0.027	0.027	-	-	-
Mn	0.017	0.017	-	-	0.010
Cu	0.0040	0.0040	-	-	0.0032
B	0.0015	0.0015	-	-	-
V	0.0006	0.0006	-	-	-
ASH	-	-	9.34 (DRY)	4.53 (DRY)	3.1

A. Wydeven, T. 1983, op. cit.

B. Carden, J.L. and Browner, R., "Preparation and Analysis of Standardized Waste Samples for Controlled Ecological Life Support Systems (CELSS), "NASA Contractor Report 166392, 1982.

C. Onisko, B. L. and Wydeven, T., 1981, op. cit.

D. Bioenvironmental Space Systems Study Group, 1975, op. cit.

E. Goldblith, S. A. and Wick, E.L., "Analysis of Human Fecal Components and Study of Methods for Their Recovery in Space Systems, Aerospace Medical Laboratory, Wright-Patterson Air Force Base, 1961.

C-3

environment for about 120 days by nine different astronauts. The McDonnell-Douglas study was in a 1-g-gravity environment for 90 days by four men. The average of these two programs is 0.28 kg/man-day and for a weighted average take 0.25 kg feces per man per day. This average agrees well with Rapp's (1983) estimate of 0.25 to 0.30 kg/man-day.

The total solids content of feces varies from about 15 to 40 percent. This author takes an average value of 25% which is above the Ames data, below the McDonnell-Douglas results, and in agreement with results by Ingram (1956) and Skylab (Sauer). Data for the elemental composition of feces was not readily available, see Table 3. Rough estimates of the carbon, hydrogen, oxygen, and nitrogen levels are 26%, 7%, 35%, and 4%, respectively. These concentrations are basically values reported by NASA/Ames (Onisko and Wydeven, 1981).

On the basis of the above average fecal mass rates and composition, the elemental and water mass rates can be calculated. The results are as follows:

	Rate, kg/man-day
Carbon	0.016
Hydrogen	0.0044
Oxygen	0.022
Nitrogen	0.0025
Water	0.19

The total energy available from the burning of feces, assuming a heat of combustion of 7700 Btu/lb (18,000 kJ/kg) and a fecal rate of 0.25 kg/man-day, was calculated to be 5×10^{-5} kilowatts per man-day. Thus, feces is not a practical energy source by any incineration or oxidation process.

URINE

The urine mass rate and elemental composition data are presented in Tables 4 and 5, respectively. Variations in the urine rates are not as great as the fecal data. This author takes an average value of 1.6 kg per man per day. The Skylab average equals 1.58 kg/man day. During the Mercury-Apollo flights (6, 7 and 9) the urine rates varied considerably from 0.7 to 3.5 kg/man day, but the average value of these 3 flights is 1.8 kg/man day which is reasonable agreement with Skylab data. The solids content of urine is 5% based on the experimental data. Thus, from urine 1.52 kg of water per man day are available for recycle. The elemental composition of solids in urine is taken as follows:

TABLE 4. URINE MASS RATE^a

<u>YEAR</u>	<u>AUTHOR</u>	<u>MASS RATE, KG/MAN-DAY</u>		
		<u>SOLIDS</u>	<u>WATER</u>	<u>TOTAL</u>
1981	Brose	0.059	1.50	1.56
1976	Jagow	-	-	2.18
1975	Jones	-	-	1.28
1975	Bioenvironmental Systems Study	0.064	-	-
1974	Sauer	-	-	1.58
1972	Nelson and Cody	-	-	1.64
1971	McDonnell-Douglas Astronautics	-	-	1.5
1970	Schaedle and Laubach	0.059	1.57	1.63
1969	Hamilton Standard	0.70	0.70	1.4
1969	Shook and Thomas	not available		
1965	Rich, Ingram and Berger	0.06	-	1.2
1964	Webb	Avg.	-	1.2
		Mercury-Apollo Flt. 6	-	1.3
		Mercury-Apollo Flt. 7	-	3.5
		Mercury-Apollo Flt. 9	-	0.7
1964	Dodson and Wallman	0.075	-	1.5
1962	Mattoni and Sullivan	0.070	1.33	1.40

a. Footnotes are listed in Table 1 plus the following:

Mattoni, R.H. and Sullivan, G.H., "Sanitation and Personal Hygiene During Aerospace Missions," Wright-Patterson Air Force Base, Ohio, Technical Documentary Report No. MRL-TDR-62-68, 1962.

Dodson, J. and Wallman, H., "Research on a Waste System for Aerospace Stations," Wright-Patterson Air Force Base, AMRL-TDR-64-33, 1964.

Shook, R.E. and Thomas, E.C., "Urine Output Parameters for Space Cabin Environments," McDonnell-Douglas Astronautics Company, Paper 10069, April 1969.

TABLE 5. URINE ELEMENTAL COMPOSITION AND DRY WEIGHT ^A

<u>SUBSTANCE</u>	<u>B</u>	<u>C</u>	<u>D</u>	<u>E</u>	<u>F</u>	<u>G</u>
	WEIGHT, %					
N	21.69	21.69	20.1/20.7	20.69	21.91	21.92
C	17.58	17.58	19.9	17.62	18.29	18.55
H	4.93	4.93	4.62	3.83	4.06	4.08
O	-	-	25.9	21.10	17.21	22.28
S	1.80	1.80	0.97	1.76	0.36	0.362
Na	6.8	6.8	-	8.05	-	-
Cl	1.6	1.6	-	14.38	-	-
P	1.40	-	1.87	0.13	-	-
Si	0.015	0.015	0.046	-	-	-
K	4.2	4.2	-	6.21	-	-
Ca	0.45	0.45	-	5.72	-	-
Mg	0.21	0.21	-	0.51	-	-
Dry weight	-	-	3.12	-	-	-
ASH (dry)	-	-	30.6	-	38.18	-

Footnotes:

- A. Tabulation excludes extensive data compiled by Webb, 1964; these data are rates (mg/24 hr) of numerous compounds as well as their range.
- B. Wydeven, T., 1983; op. cit.
- C. Carden, J. L. and Browner, R., 1982, op. cit.
- D. Onisko, B. L. and Wydeven, T., 1981, op. cit.
- E. Hoshizaki, T. and Hansen, B.D., "Generic Waste Management Requirements for a Controlled Ecological Life Support System (CELSS), American Society of Mechanical Engineers, Paper 81-ENAs-23, 1981.
- F. Bioenvironmental Systems Study Group, 1975, op. cit.
- G. Putnam, D.F., "Composition and Concentrative Properties of Human Urine," NASA Contractor Report 1802, 1971.

carbon - 18%, hydrogen 4.9%, oxygen 25%, nitrogen 21%. Other elements are not included here, for additional details see Table 5. The elemental and water release rates from urine are calculated to be as follows:

	kg/man-day
Carbon	0.014
Hydrogen	0.0039
Oxygen	0.020
Nitrogen	0.017
Water	1.52

FOOD

The wastes generated from food include uneaten foods and used food containers. On the basis of Shuttle data 3.6 pounds (1.64 kg) of food (dry food, water in food, and packaging) are provided per person per day. This includes 0.73 kg of dry food per person per day and 0.46 kg of water. Not all the food is eaten. Assume 10% of the food is wasted; then 0.046 kg of water per person per day are available for recovery. If food is assumed to approximate sugar $C_6H_{12}O_6$, which is a crude assumption, but useful for the determination of elemental release rates. The carbon, hydrogen and oxygen available from wasted food are estimated to be as follows:

	kg/man-day
Carbon	0.03
Hydrogen	0.005
Oxygen	0.04

The amount of carbon, etc. from wasted food containers is discussed under plastics.

PAPER

Paper wastes would be generated on a Space Station due to personal hygiene requirements, used paper towels, wipes, gauze, Q-tips and miscellaneous other paper products. These wastes exclude washcloths, fecal-emesis collection bag, and a trash container liner spare. The total amount of cellulosic materials is estimated to be 1 kg per man-day. The empirical formula for cellulose is $C_6H_{10}O_5$, or 44% is carbon, 6% is hydrogen and 50% is oxygen. This estimate neglects the presence of water. The elemental release rates are calculated:

	kg/man-day
Carbon	0.44
Hydrogen	0.06
Oxygen	0.50

PLASTICS

Wastes composed primarily of polyethylene are generated from food containers, packing materials, medical supplies, and from experimental work. Food containers are used at a rate of about 0.45 kg per man-day. Packing materials and other plastics could be triple this amount, or 1.4 kg per man-day. This author assumes that the plastic wastes consist mostly of polyethylene. From plastics the elemental release rates are:

	kg/man-day
Carbon	1.6
Hydrogen	0.26

The total wastes generated are summarized in Table 6, and a summary of the elemental release rates and water are presented in Table 7. The total solid waste feed rate is 5.4 kg per man day, plastics will constitute the largest amount followed by food and urine. The weight of paper wastes is less than these latter three wastes, but its bulk volume will be the largest. Feces amounts to about five percent of the total mass. These results indicate that water is available in wastes (1.8 kg per man-day) to provide the drinking needs for 2 astronauts per day. Carbon oxidation would require 7.5 kg of oxygen per man-day because the amount of

TABLE 6

SOLID WASTE(S) TREATMENT SYSTEM FEED WASTES

<u>WASTE</u>	<u>RATE</u> kg/man-day
FECES	0.25
URINE	1.6
FOOD	1.6
PAPER	1.0
PLASTICS	1.9
TOTAL	<u>5.4</u>

TABLE 7

SUMMARY OF ELEMENTAL AND WATER WASTE RATES

<u>Element/ Waste</u>	<u>Carbon</u>	<u>Hydrogen</u>	<u>Oxygen</u>	<u>Nitrogen</u>	<u>Water</u>
	rate, kg per person per day				
Feces	0.016	0.0044	0.022	0.0025	0.19
Urine	0.014	0.0039	0.020	0.017	1.52
Food	0.03	0.005	0.04	-	0.046
Paper	0.44	0.06	0.50	-	-
Plastics	<u>1.6</u>	<u>0.26</u>	<u>-</u>	<u>-</u>	<u>-</u>
TOTAL	2.1	0.33	0.58	0.020	1.8

oxygen in the wastes is insufficient for complete combustion. Relatively small amounts of nitrogen are available for utilization on a Space Station.

Table 8 presents the heat of combustion of waste materials.

B. TREATMENT PROCESSES

There are many possible treatment processes for Space Station solid wastes. Some are conventional technology, for example, incineration and others are high technology processes, like electric discharge plasma and supercritical water oxidation. This report will discuss only a few of the processes. Information about others can be obtained from references cited in this report.

SUPERCRITICAL WATER OXIDATION

In 1975 Modell discovered that supercritical water would oxidize specific organic compounds. Supercritical water is water at temperature and pressure levels above water's critical point, 374 degrees C and 218 atm, see Figure 1. In 1979, supercritical water oxidation (SCWO) was applied to mixtures of organic wastes. Tests were conducted to show its effectiveness in destroying organic halides which are now commonly known as hazardous wastes. The exploitation of the SCWO process was commercialized in 1980 by Modell who formed Modar, Inc.

TABLE 8.

HEATS OF COMBUSTION

	$\frac{\text{Btu}}{\text{Lb}}$	$\frac{\text{kJ}}{\text{kg}}$
Cellulose	7500	17,000
Feces (dry)	7700	18,000
Polystyrene	17,200	40,000
Polyethylene	19,000	44,000

In the SCWO both organic material and oxygen dissolve in supercritical water and then oxidation is carried out in supercritical water medium. Organic substances and gases are completely soluble in supercritical water but inorganic salts exhibit greatly reduced solubilities. This is just the opposite effects of solubilities at normal conditions. Thus oxidation may be carried out in a homogenous system and salts separated. Figure 2 is a schematic of the SCWO process. The supercritical water reactor is described in Figure 3.

The SCWO process can be described in five steps:

(1) The solid waste is slurried with make-up water to provide a mixture of about 5 to 10 weight percent organics. The slurry is pressurized and heated to supercritical conditions. Heating is attained by mixing the feed with superheated SCW, which is generated in a subsequent step. During the period outside the oxidizer, organic materials in the feed are converted to combustible gases, low to intermediate molecular weight compounds (alcohols, aldehydes, furans) and inorganic salts.

(2) Oxygen or air is pressurized and mixed with the feed. In the adiabatic reactor organics are oxidized at residence times of less than one minute. The heat released by combustion is sufficient to raise the fluid phase to temperatures where all organics are rapidly oxidized, temperatures are about 550 degrees C.

(3) Effluent from the reactor/oxidizer is fed to a salt separator where inorganics originally present in the feed precipitate.

(4) A portion of the superheated SCW is recycled to an eductor upstream of the oxidizer. This recycle stream provides sufficient thermal energy to heat the feed to the oxidizer to supercritical conditions.

(5) The remainder of the superheated SCW (with some CO_2 and N_2) is available for power generation or use as high-pressure steam.

The available data from SCWO is presented in Tables 9 to 15.

For urea destruction, Figure 4 shows the pertinent reactions, including heats of reaction and temperatures. At certain temperatures all the nitrogen in urea ($(\text{NH}_2)_2\text{CO}$) is not produced as N_2 , but can be in the form of ammonia NH_3 or nitrous oxide N_2O . Figure 5 depicts the ammonia, nitrogen, and nitrous oxide weight ratios as a function of SCWO reactor temperature.

The advantages and disadvantages of the SCWO process are as follows. The process can treat aqueous waste streams with a wide range of flows and composition. The streams may contain both inorganic and organic compounds. The reaction exotherm is sufficient to make the oxidation self-sustaining and to provide preheat for feed to about critical temperature. No catalysts are required for this oxidation process. Inorganic salts can be readily removed by precipitation. Finally, the necessary residence time in the reactor/oxidizer is from one-half to one minute, only. The disadvantages of the SCWO process are that it requires extremely high temperature and pressures. Large

TABLE 9

SCW - U.S. PATENT 4,113,446 (1978)

RESULTS AT CRITICAL
CONDITIONS (647K AND 218 ATM)

RUN	CARBON CLOSURE	% C AS VOLATILE GAS	GLUCOSE IN WATER*				
			H ₂	CH ₄	CO ₂	CO	C ₂ ⁺
9(c)	97	10	30	1.5	42	27	-
10	86	8	25.8	1.3	34.4	38.5	-
11(c)	86	20	45.1	3.2	38.5	12.5	0.7
12(c)	94.1	23.3	45.13	2.9	40.6	12.6	0.75

C DENOTES CATALYST RUN.

RUNS 9 AND 10 FOR ONE HOUR.

RUNS 11 AND 12 FOR 30 MINUTES.

* TABLE III

ORIGINAL PAGE IS
OF POOR QUALITY

TABLE 10
SCW - GLUCOSE AND WOOD

Reproducibility of Results; Glucose Feed and 60-Min. Residence Time

Run No.	Carbon in Feed (g)	Ave. Temp. (C)	Gas Composition					Carbon Gasified (%)
			H ₂	CO	CH ₄	CO ₂	C ₂ ⁺	
G-1	2	377	16.3	67.1	1.2	14.8	0.6	16.9
G-2	2	377	10.2	70.6	1.5	17.5	-	16.6
G-3	2	377	14.4	63.0	1.9	17.8	0.9	21.3
G-4	2	377	11.5	70.8	1.5	15.5	0.7	22.9
Ave.	2	377	13.1	68.4	1.5	16.4	0.3	19.5
G-5	2	371	19.9	53.5	2.3	23.3	1.1	25.9
G-6	2	371	8.5	54.6	9.8	34.8	1.2	25.0
Ave.	2	371	14.2	54.1	1.6	29.1	1.1	25.5
G-8	4	371	12.3	43.9	0.9	41.7	1.7	10.7
G-9	4	371	25.8	38.5	1.3	34.4	-	8.2
Ave.	4	371	19.1	41.2	1.1	38.1	0.9	9.5

MODELL, M. (1977)

TABLE 11

SCW - GLUCOSE AND WOOD

Product Distribution in the Critical Region

Feed (Run No.)	Reaction Time (min)	Carbon in Feed (g)	Ave. Temp. (C)	← Gas Composition →					← % Carbon as: →		Recovered Water (cm ³)
				H ₂	CO	CH ₄	CO ₂	C ₂ ⁺	Gas	Extracted Liquid	
Glucose											
G-1-4	60	2	377	13.1	68.4	1.5	16.4	0.3	19.5	1.2	266
G-5,6	60	2	371	14.2	54.1	1.6	29.1	1.1	25.5	2.5	280
G-7	150	2	371	12.3	42.8	1.2	41.4	2.3	28.9	-	271
G-8,9	60	4	371	19.1	41.2	1.1	38.1	0.9	9.5	-	265
Levulinic acid											
L-1	60	4.82	377	4.8	87.9	0.6	6.6	-	10.8	-	251
Maple sawdust											
M-1	5	.59	377	8.3	79.2	2.3	10.1	-	16.8	1.1	241
M-2	15	.96	377	17.9	69.4	3.7	9.1	-	18.1	1.5	258
M-3	30	.10	377	15.9	65.5	5.1	13.0	0.5	88.3	-	249
M-4	30	.67	377	5.0	82.4	2.9	9.6	0.1	33.1	0.6	252
M-5	60	.29	377	16.8	57.2	5.6	19.6	0.9	39.5	6.2	258

MODELL, M. (1977)

TABLE 12

SCW - U.S. PATENT 4.113 446 (1978)

RESULTS AT CRITICAL CONDITIONS
(647K AND 218 ATM)*

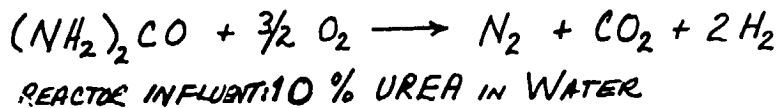
RUN #	CARBON CLOSE %	% CARBON VOLATILE	H ₂	GAS COMPOSITION (MOLE % DRY)			C ₂ +
				CH ₄	CO ₂	CO	
CELLULOSE 13	95.7	18.31	14.5	1.5	19.7	64.2	0.13
POLYETHYLENE 15	90.3	2.30	26.6	2.54	65.87	≤5.0	-
POLYETHYLENE 16	93.7	4.01	35.75	3.73	54.43	≤5.0	1.2
UREA 17	88.8	11.11	-	-	100	-	-

ALL RUNS WITH CATALYST.

* TABLE IV

ORIGINAL PAGE IS
OF POOR QUALITY

TABLE 13
SUPERCRITICAL WATER OXIDATION - UREA
DESTRUCTION: (O₂, 23 SEC, 25 CC/MIN)



	<u>RUN No.</u>				
	<u>81A</u>	<u>81B</u>	<u>81C</u>	<u>82</u>	<u>225</u>
Temperature (°C)	561	596	621	632	670
Nitrogen In (mg/l) (water + feed)	51422	50501	50825	50935	56679
<u>Effluent Liquid Composition (mg/l)</u>					
Nitrate N	100	85	29	57	.04
Nitrite N	-	-	-	-	0.005
Ammonia N	17537	15798	3447	2719	1.65
Effluent pH	9.21	8.95	7.92	7.52	7.24
<u>Effluent Gas Composition (mole %)</u>					
O ₂	95.59	90.18	37.61	20.46	8.09 (3.63)*
CO ₂	0.45	1.05	18.38	38.48	41.28 (18.53)
N ₂	3.60	7.92	41.72	39.04	50.63 (22.73)
H ₂ O	0.37	.85	2.33	0.51	0.00 (0.00)
<u>Nitrogen in Liquid Effluent (%)</u>					
	26.7	26.7	5.5	4.5	0.0
<u>Nitrogen in Gas Effluent (%)</u>					
	5.2	11.6	59.4	69.2	97.7
<u>Nitrogen Recovery (%)</u>					
	31.8	38.3	65.3	73.7	97.7

* Values in parentheses represent the actual measured quantities. For Run 225, with 40% helium present, values are normalized for comparison purposes.

TIMBERLAKE, S.H., ET AL. (MODAR), 1982.

TABLE 14

SCW-ORGANIC HALIDE DESTRUCTION

SUMMARY OF RESULTS: OXIDATION OF ORGANIC CHLORIDES

<u>Run No.</u>	11	12	13	14	15
<u>Residence Time (min)</u>	1.1	1.1	1.1	1.1	1.3
<u>Carbon Analysis</u>					
Organic Carbon In (ppm)	26,700.	25,700.	24,500.	38,500.	33,400.
Organic Carbon Out (ppm)	2.0	1.0	6.4	3.5	9.4
Destruction Efficiency (%)	99.993	99.996	99.975	99.991	99.97
Combustion Efficiency (%)	100.	100.	100.	100.	100.
<u>Gas Composition</u>					
O ₂	25.58	32.84	37.10	10.55	19.00
CO ₂	59.02	51.03	46.86	70.89	70.20
CH ₄	-	-	-	-	-
H ₂	-	-	-	-	-
CO	-	-	-	-	-
<u>Chloride Analysis</u>					
Organic Chloride In (ppm)	876.	1266.	748.	775.	481.
Organic Chloride Out (ppm)	.023	.037	<.028	.032	.036
Organic Chloride Conversion (%)	99.997	99.997	99.996	99.996	99.993
<u>GC/MS Effluent Analysis</u>					
Compound B (ppb Cl)	-	-	-	-	-
C	-	-	-	-	-
E	-	9	-	14	-
F	18	12	18.	-	-
H	-	-	<4.	-	-
K	5	16	<5.	6	-
M	-	-	0.2	-	-
N	-	-	0.3	-	36
O	-	-	-	12	-

MODELL, M., ET AL., 1983.

ORIGINAL PAGE IS
OF POOR QUALITY

TABLE 15
SCW - ORGANIC HALIDE DESTRUCTION

TABLE 2. COMPOSITION OF FEED MIXTURES FOR RUNS 11 - 15

		wt %	wt % Cl
<u>Run 11</u>			
DDT	$C_{14}H_9Cl_5$	4.32	2.133
MEK	C_4H_8O	$\frac{95.68}{100.0}$	$\frac{-}{2.133}$
<u>Run 12</u>			
1,1,1-trichloroethane	$C_2H_3Cl_3$	1.01	0.806
1,2-ethylene dichloride	$C_2H_2Cl_2$	1.01	0.729
1,1,2,2-tetrachloroethylene	C_2Cl_4	1.01	0.866
o-chlorotoluene	C_7H_7Cl	1.01	0.282
1,2,4-trichlorobenzene	$C_6H_3Cl_3$	1.01	0.591
biphenyl	$C_{12}H_{10}$	1.01	-
o-xylene	C_8H_{10}	5.44	-
MEK	C_4H_8O	$\frac{88.48}{100.0}$	$\frac{-}{3.284}$
<u>Run 13</u>			
hexachlorocyclohexane	$C_6H_6Cl_6$	0.69	0.497
DDT	$C_{14}H_9Cl_5$	1.00	0.493
4,4'-dichlorobiphenyl	$C_{12}H_8Cl_2$	1.57	0.495
hexachlorocyclopentadiene	C_5Cl_6	0.65	0.505
MEK	C_4H_8O	$\frac{96.09}{100.0}$	$\frac{-}{1.99}$
<u>Run 14</u>			
PCB 1242	$C_{12}H_xCl_{4-6}$	0.34	0.14
PCB 1254	$C_{12}H_xCl_{5-8}$	2.41	1.30
transformer oil	$C_{10}C_{14}$	29.26	-
MEK	C_4H_8O	$\frac{67.99}{100.0}$	$\frac{-}{1.44}$
<u>Run 15</u>			
4,4'-dichlorobiphenyl	$C_{12}H_8Cl_2$	3.02	.96
MEK	C_4H_8O	$\frac{96.98}{100.0}$	$\frac{-}{0.96}$

MODELL, M., ET AL., 1983.

temperature gradients apparently exist in the system which may make it difficult to duplicate measurements and to scale available data. The oxygen or air flow requires precise control along with the waste feed stream. The particle size in the waste stream, solids in water, must be reduced to less than a millimeter in diameter. The data available for the SCWO indicates that the gaseous effluents are not simply carbon dioxide and nitrogen but may contain significant amounts of carbon monoxide, methane, and hydrogen. The presence of these gases would require extensive post-treatment for Space Station application.

ZIMPRO PROCESS

The Zimpro process was invented about 50 years ago, in the mid-1930's. This process is also a wet air (oxygen) oxidation process but at temperatures and pressures well below water's critical conditions. Figure 6 is a schematic of a wet air oxidation (WAO) system. In WAO molecular oxygen reacts with suspended solid matter or dissolved organics almost complete (90 to 95%) reduction of the wastes to carbon dioxide and water. With a residence time of 90 minutes and temperatures/pressures below critical conditions the maximum amount of carbon monoxide is estimated to be 1000 ppm, average carbon monoxide concentrations are 200 ppm. The organic materials, if not converted to carbon dioxide, go to the water phase as alcohols, aldehydes, and ketones. The degree of oxidation can be controlled by WAO temperature, pressure, and residence time. For some applications catalysts have been used. The major advantage of WAO is that

contaminants tend to stay in the aqueous phase; effluent gas consists mainly of carbon dioxide and spent air (or excess oxygen).

As evident from Figure 6 the WAO system is similar to SCWO, Figure 2, except for the salt precipitation. In this report details of the WAO operating procedure are not described. However, the WAO operates at temperatures of 200 to 300 degrees C which are much less than SCWO. It is important to note that the WAO is commercially available with decades of operations in more than 200 units, world-wide. These units have been applied mostly to sewerage sludge treatment and manufacturing process wastewaters.

The wet air oxidation system can be used either on a batch or continuous basis.

CHEMICAL OXIDATION

Chemical agents such as potassium permanganate, potassium dichromate, and many other alkali metal salts can oxidize solid wastes. The advantage of a chemical oxidation process is that it would operate at about 1 atm pressure, or be a low pressure system in contrast to the SCWO and WAO processes. A chemical oxidation system would need heating to temperatures from a minimum of 100 degrees C to several hundred degrees Celsius. About one kilogram (kg) of oxygen is needed to oxidize an equal mass of solid wastes. If a chemical oxidizer was provided than the mass of oxidizer

would be no more than twice that of pure (liquid) oxygen; however, the volume of chemical oxidizer would be about the same since the salts have a density more than twice that of liquid oxygen. The salts might also provide nitrogen needed for atmospheric control. With chemical oxidation system reactor materials of construction would have to be carefully considered. More expensive materials such as titanium and Hastelloy-C would probably be required. But, Hastelloy-C is often used in the WAO process.

Chemical oxidations could operate in a batch or continuous mode. Due to the nature of the solid wastes on a Space Station a batch type treatment process is suggested. This would allow the collection of materials for say about one week, then their oxidation.

OTHER PROCESSES

A few other processes were considered, namely the IT Enviroscience homogenous catalyst system, Figure 7 and the plasma torch under development at the Royal Military College, Ontario, see Figure 8. With regard to dry combustion, a study of General American Transportation (1968) of fecal matter incineration indicates that it is feasible but that such a system requires precise control of oxygen flow rate, and continuous monitoring of

temperature and oxygen concentration. This experimental study determined that dry feces will ignite at about 200 degrees C, and will burn very rapidly - under certain conditions will detonate. Thus, the collection and storage of dried fecal matter on a Space Station should be considered a potential fire hazard.

The burning of polyethylene (wastes) is difficult and would probably not be practical on a Space Station.

Biodegradation processes would probably require too much astronaut attention and too much space in the Station.

SPACE STATION TREATMENT PROCESS

A proposed solid waste management treatment system for a Space Station is presented in Figure 9. This schematic diagram indicates that the transfer of solid wastes from the collection point to the treatment system should be minimized. Furthermore, the maceration shredding, grinding of plastic and cellulosic wastes, if attempted, will pose severe maintenance problems. The specific type of treatment process needs to be developed. Prior to any chemical reactions the system would dry and compact the solid wastes. The treatment reactor is envisioned to be about 5 gallon capacity, with no penetrations between the reactor cavity and the outside. This could be done by means of a magnetically controlled stirrer, with a chain drive. Equipment other than the

the reactor has been used in existing spacecraft or developed. The proposed system would exhibit zero-leakage except for spent filters and in-exchange resins. The amount of solid ash from the treatment process should be a few percent of the total feed mass.

Figures 10 to 13 summarize the principle reactions for oxidation of wastes, considered as a mixture of carbon, hydrogen and oxygen, and subsequent reduction of carbon dioxide to oxygen and either carbon or methane.

CONCLUSIONS

As a result of this study the following general conclusion is made; a solid waste(s) treatment process for a Space Station needs further study to achieve a reliable operational system. The solid waste rates determined in this study, especially those due to food wastes, paper and plastics, need to be better ascertained from at least Shuttle operational data. Processes for the conversion of solid wastes to carbon dioxide and other inert substances need additional experimental measurements.

There are a few feasible treatment processes, chemical or wet air oxidation; supercritical water oxidation does not appear suitable for a Space Station. In addition to the treatment system design needs, the problem of mechanical transfer of wastes from collection point(s) to the treatment vessel is critical. This

aspect along with total systems integration needs to be considered.

Finally, when design criteria for a Space Station are better established and better data are available on treatment performance, a trade study should be conducted to evaluate alternatives.

NAME LIST OF PERSONS CONTACTED REGARDING
TREATMENT OF SOLID WASTES OF A SPACE STATION

NASA Employees

non-NASA Personnel

Fullerton, G.
Grimaud, J.

Allen, L. (Excell)

Johnson, C. (Ames)
Kimzey, H.

Barton, T. (Royal Military College)

Langdoc, W.

Bourland, C. (Technology)

Martin, R.

Engmann, R. (Zimpro)

Rapp, R.

Howell, G. (U.S. EPA)

Samonski, F.

Lamparter, R. (Michigan Tech)

Sauer, R.

Modell, M. (Modar)

Winkler, E.

Murray, R. (GE)

Obert, J. (McDonnell-Douglas)

O'Connor, T. (Univ. Missouri-Columbia)

Schaefer, P. (Zimpro)

Weitzmann, A. (Lockheed)

REFERENCES

-Treatment Processes-

- Hurwitz, E., and Dundas, W.A., "Wet Oxidation of Sewage Sludge," *Water Pollution Control Federation Journal*, Vol. 32 (9), pp. 918-929, 1960.
- Pipes, W.O., "Waste-Recovery Processes for a Closed Ecological System," *National Academy of Sciences-National Research Council, Publication 898*, Washington, D.C., 1961.
- Zimmerman, F.J., "Wet Air Combustion," *Industrial Water and Wastes*, Vol. 5, pp. 102-106, 1961.
- Quon, J.E. and Pipes, W.O., "Thermal Decomposition of Human Wastes," *Proceedings American Society of Civil Engineers*, Vol. 89, No. SA1, January, 1963.
- Dodson, J., and Wallman, H., "Research on a Waste System for Aerospace Stations," *Technical Documentary Report No. AMRL-TDR-64-33*, 1964.
- Harding, J.C., and Griffin, G.E., "Sludge Disposal by Wet Air Oxidation at a Five MGD Plant," *Water Pollution Control Federation Journal*, Vol. 37, pp. 1134-1141, 1965.
- Rich, L.G., Ingram, W.M., and Berger, B.B., "Waste Disposal on Space Craft and Its Bearing on Terrestrial Problems," *U.S. Department Health, Education, and Welfare, Public Health Service, PB 168787*, 1965.
- Wheaton, R.B., Brown, J.R.C., Ramirez, R.V., and Roth, N.G., "Investigation of the Feasibility of Wet Oxidation for Spacecraft Waste Treatment," *NASA Contractor Report No. 66450*, 1966.
- Elms, R.V., "Design Study of Integrated Life Support System for Aerospace Application Utilizing Radioisotopes for Thermal Energy," *Final Report, LMSC 680 679*, 1968.
- Hurley, T.L., Rollo, E.J., and Remus, G.A., "Study for Evaluation of Incineration and Microwave Treatment of Human Fecal Matter for Spacecraft Operation," *NASA CR-73247*, 1968.
- Hamilton Standard, "Alternate Mission Studies (AILSS)," *NASA Contractor Report-66876*, 1969.
- Huggett, C., "Combustion Processes in the Aerospace Environment," *Aerospace Medicine* Vol. 40, pp. 1176-1180, 1969.
- Jagow, R.B., Jaffe, R.J., and Saunders, C.G., "The Processing of Human Wastes by Wet Oxidation for Manned Spacecraft," *American Society of Mechanical Engineers, Paper 70-Av/SpT-1*, Presented at Space Technology and Heat Transfer Conference, Los Angeles, CA, June 21-24, 1970; in *Space Systems and Thermal Technology for the 70's, Part 1, Proceedings* pp. 1-8, 1970.

REFERENCES

Zimpro Process

Hurwitz, E., Teletzke, G.H., Gitchel, W.B., "Wet Air Oxidation of Sewage Sludge," Water and Sewage Works, Vol. 112, pp. 298-305, 1965.

Pradt, L.A., "Developments in Wet Air Oxidation," Chemical Engineering Progress, Vol. 68 (12), pp. 72-77, 1972.

Randall, T.L., and Knopp, P.V., "Detoxification of Specific Organic Substances by Wet Oxidation," Reprint, Presented at 51st Annual Conference, Water Pollution Control Federation, Anaheim, CA, October, 1978.

Flynn, B.L., "Wet Air Oxidation of Waste Streams," Chemical Engineering Progress, Vol. 75 (4), pp. 66-69, 1979.

Wilhelmi, A.R., and Knopp, P.V., "Wet Air Oxidation-An Alternative to Incineration," Chemical Engineering Progress Vol. 75 (8), pp. 46-52, 1979.

Randall, T.R., "Wet Oxidation of Toxic and Hazardous Compounds," Reprint, Presented at 13th Mid-Atlantic Industrial Waste Conference, June, 1981.

Schaefer, P., "Consider Wet Oxidation," Hydrocarbon Processing, Reprint, October, 1981.

Canney, P.J., and Schaefer, P.T., "Detoxification of Hazardous Industrial Wastewaters by Wet Air Oxidation," Presented at Spring National AIChE Meeting, Houston, Texas, March, 1983.

REFERENCES

-Process Reviews-

Presti, J.B., "Life Support System for Space Flights of Extended Time Periods," NASA-Contractor Report-168467, 1963.

Rich, L.G., Ingram, W.M., and Berger, B.B., "Waste Disposal on Space Craft and Its Bearing on Terrestrial Problems," U.S. Department of Health Education, and Welfare, Public Health Service, PB 168787, 1965.

Parker, J.F., and West, V.R., Eds, Bioastronautics Data Book, NASA SP-3006, Second Edition pp. 922-930, 1973.

Whitaker, C.F., Murray, R.W., and Scheikopf, J.D., "Shuttle Era Waste Collection," Institute Environmental Sciences, Proceedings 22nd Annual Technical Meeting, Philadelphia, PA, pp. 257-260, 1976.

Bioenvironmental Systems Study Group of the Society of Automotive Engineers, "Review of Technology Developments Relevant to Closed Ecological Systems for Manned Space Missions," NASA - Contractor Report-153000, 1977.

Modell, M., "Sustaining Life in a Space Colony," Technology Review, pp. 36-43, July/August 1977.

Society of Automotive Engineers, "Space Technology Available for Transfer to Civil Environmental and Pollution Control," SAE Aerospace Information Report AIR 1246, 1977.

DeRenzo, D.J., Ed., Unit Operations for Treatment of Hazardous Industrial Wastes, (Noyes Data Corporation, New Jersey), 1978.

Spurlock, J.M., and Modell, M., "Technology Requirements and Planning Criteria for Closed Life Support Systems for Manned Space Missions," Final Report for NASA, Contract No. NASw-2981, 1978.

Meissner, H.P., and Modell, M., "Recycling plant, Human and Animal Wastes to Plant Nutrients in a Closed Ecological System," American Society of Mechanical Engineers, Publication 79-ENAs-29, 1979.

Spurlock, J., and Modell, M., "Systems Engineering Overview for Regenerative Life-Support Systems Applicable to Space Habitats," in Space Resources and Space Settlements, Billingham, J., Gilbreath, W., and O'Leary, B., Eds., NASA SP-428, pp. 1-11, 1979.

Basta, N., "Firms Avidly Seek New Hazardous-Waste Treatment Routes," Chemical Engineering, pp. 53-55, September 6, 1982.

REFERENCES

Supercritical Water Oxidation

Amin, S., Reid, R.C., and Modell, M., "Reforming and Decomposition of Glucose in an Aqueous Phase," American Society of Mechanical Engineers, Publication 75-ENAs-21, 1975.

Modell, M., "Reforming of Glucose and Wood at the Critical Conditions of Water," American Society of Mechanical Engineers, Publication 77-ENAs-2, 1977.

Modell, M., Gasification Process, United States Patent 4,113,446, Sept. 12, 1978.

Anon., "Using Supercritical Water to Destroy Tough Wastes," Chemical Week, Reprint, April 21, 1982.

Josephson, J., "Supercritical Fluids," Environmental Science and Technology, Vol. 16, pp. 548A-551A, 1982.

Modell, M., Processing Methods for the Oxidation of Organics in Supercritical Water, United States Patent 4,338,199, July 6, 1982.

Modell, M., Gaudet, G.G., Simson, M., Hong, G.T., and Biemann, K., "Destruction of Hazardous Waste Using Supercritical Water," United States EPA, Proceedings of Eighth Annual Research Symposium, pp. 202-212, March 8, 1982.

Modell, M., Gaudet, G.G., Simson, M., Hong, G.T., and Biemann, K., "Supercritical Water-Testing Reveals New Process Holds Promise," Solid Wastes Management, Reprint, August, 1982.

Timberlake, S.H., Hong G.T., Simson, M., and Modell, M., "Supercritical Water Oxidation for Wastewater Treatment: Preliminary Study of Urea Destruction," Society of Automotive Engineers. Technical Paper Series 820872, Presented at Twelfth Intersociety Conference on Environmental Systems, San Diego, CA. July, 1982.

REFERENCES (CONT'D)

- Cadotte, A.P., and Laughlin, R.G.W., "The Wetox (R) Process for Industrial Waste Treatment," in Waste Treatment and Utilization, Moo-Young, M. and Farquhar, G.J., Eds., Pergamon Press, Oxford, pp. 157-172, 1979.
- Farquhar, G.J., "Biological Treatment of Industrial Wastes: Review of Principles, Methods and Applications," in Wastewater Treatment and Utilization, Pergamon Press, Oxford, pp. 373-393, 1979.
- Othmer, D.F., "Earth + Water + Air = Fire," Mechanical Engineering, pp. 30-37, 1979.
- Chow, C.L., and Verhoff, F.H., "Process for Power Generation from Wet Air Oxidation with Application to Coal Gasification Waste Waters," Industrial Engineering and Chemistry Process Design and Development, Vol. 20, pp. 12-19, 1981.
- Onisko, B.L., and Wydeven, T., "Wet Oxidation as a Waste Treatment in Closed Systems," American Society of Mechanical Engineers, ASME-81-ENAs-22, 1981.
- Shuler, M.L., Nafis, D., and Sze, E., "The Potential Role of Aerobic Biological Waste Treatment in Regenerative Life Support Systems," ASME, Paper 81-ENAs-20, 11th Intersociety Conference on Environmental Systems, San Francisco, CA, 1981.
- Barton, T.G., "Plasma Destruction of Polychlorinated Biphenyls," Royal Military College, Kingston Ontario, Contract Report prepared for Ministry of Environment, Ontario, March 1982.
- Barton, T.G., "Mobile Plasma Pyrolysis System," Presented at United States EPA, Cincinnati, 18 May 1983.
- Excell, Inc., "Method for Destroying Toxic Organic Chemical Products," Personal Communication (Confidential Business Information) to T.R. Marrero, July 8, 1983.
- IT Corporation, "Catalyzed Wet Oxidation Process Description and Summary of State-of-the-Art," Personal Communication from R.W. Helsel to T.R. Marrero, June 20, 1983.
- Johnson, C.C., and Wydeven, T., "Wet Oxidation for Waste Treatment in a Controlled Ecological Life Support System (CELSS)," National Aeronautics and Space Administration, Preprint, Presented at Thirteenth Intersociety Conference on Environmental Systems, San Francisco, July 11-13, 1983.
- Miller, R.A., and Swientoniewski, M.D., "The Destruction of Various Organic Substances by a Catalyzed Wet Oxidation Process," Proceedings of Eighth Annual Research Symposium, March 8-10, 1982, Incineration and Treatment of Hazardous Waste, United States EPA, pp. 213-221, 1983.

REFERENCES (CONT'D)

Schelkopf, J.D., Witt, F.J., and Murray, R.W., "Integrated Waste Management - Water System Using Radioisotopes for Thermal Energy," Summary Report. United States Atomic Energy Commission, Contract Number AT (30-1)-4104, 1970.

Jagow, R.B., "Design and Development of a Prototype Wet Oxidation System for the Reclamation of Water and the Disposition of Waste Residues Onboard Space Vehicles," NASA Contractor Report 112151, 1972.

Labak, L.J., and Remus, G.A., "Integrated, Zero "G" Waste Incineration System," General American Research Division, General American Transportation, Research Report (Phase B), NASA Contract No. NAS 2-6386, 1972.

Schelkopf, J.D., Witt, F.J., and Murray, R.W., "Integrated Waste Management-Water System Using Radioisotopes for Thermal Energy," United States Atomic Energy Commission, Document No. 74SD4201, 1974.

Bioenvironmental Systems Study Group of the Society of Automotive Engineers, "Evaluation and Comparison of Alternative Designs for Water/Solid-Waste Processing Systems for Spacecraft," NASA-Contractor Report-162492, 1975.

Chowdhury, A.K., and Ross, L.W., "Catalytic Wet Oxidation of Strong Waste Waters," American Institute of Chemical Engineers, Symposium Series, No. 151, Vol. 71, pp. 46-58, 1975.

Budininkas, P., "Study of Removal of Ammonia from Urine Vapor by Dual Catalyst," NASA Contractor Report 151930, 1976.

Jagow, R.B., "Design, Fabrication and Testing of a Spacecraft Wet Oxidation System Including Trash Pulverization Studies," American Society of Mechanical Engineers, ASME-76-ENAs-15, 1976.

Katzer, J.R., Ficke, H.H., and Sadana, A., "An Evaluation of Aqueous Phase Catalytic Oxidation," Water Pollution Control Federation Journal, Vol. 48 (5), pp. 920-933, 1976.

Budininkas, P., "Removal of Ammonia from Vapor by a Dual-Catalyst System," American Society of Mechanical Engineers, Publication 77-ENAs-48, 1977.

Heidemann, R.A., and Prausnitz, J.M., "Equilibrium Data for Wet-Air Oxidation. Water Content and Thermodynamic Properties of Saturated Combustion Gases," Industrial Engineering Chemistry, Process Design and Development, Vol. 16 (3), pp. 375-381, 1977.

Modell, M., "Sustaining Life in a Space Colony," Technology Review, July/August, pp. 36-43, 1977.

Weitzmann, A.L., "Development and Testing of a Wet Oxidation Waste Processing System," National Aeronautics and Space Administration, NASA-CR-151324, 1977.

ORIGINAL PAGE IS
OF POOR QUALITY

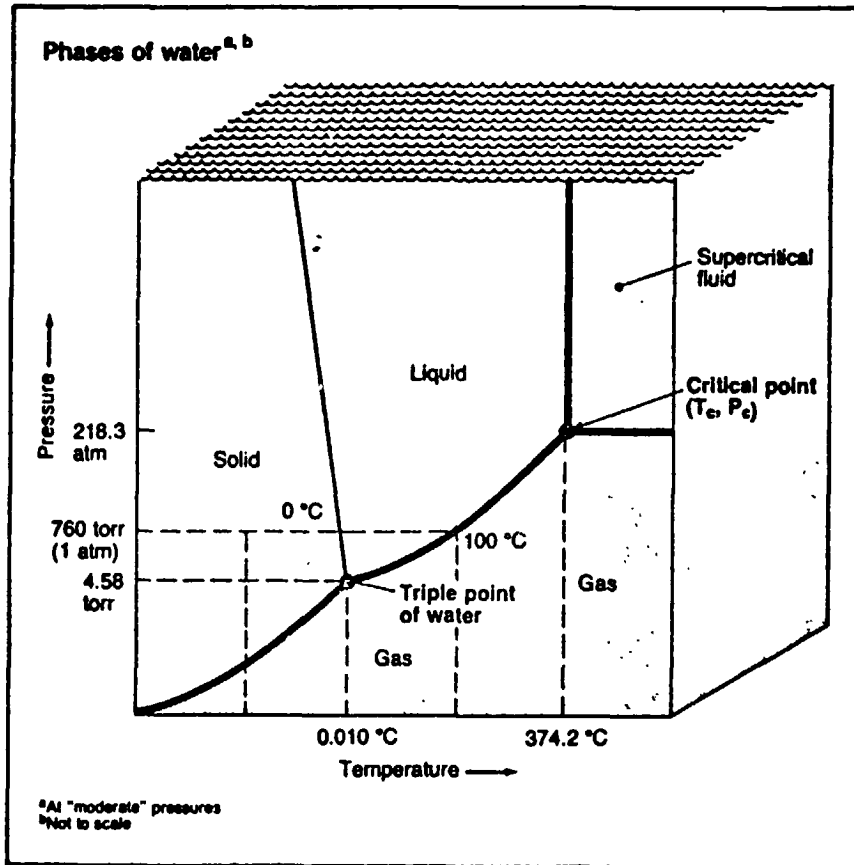


Figure 1.

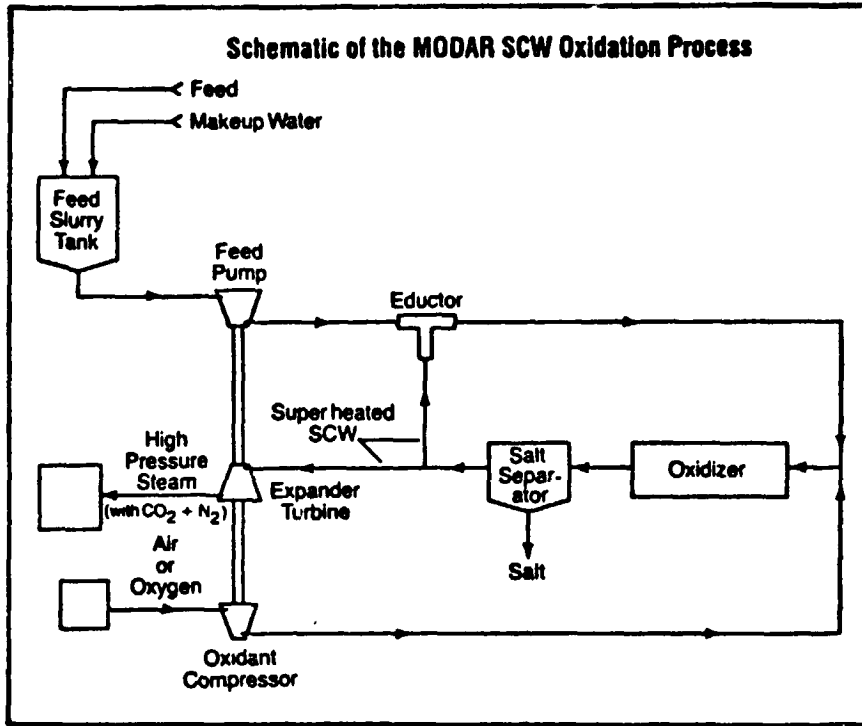


Figure 2.

ORIGINAL PAGE IS
OF POOR QUALITY

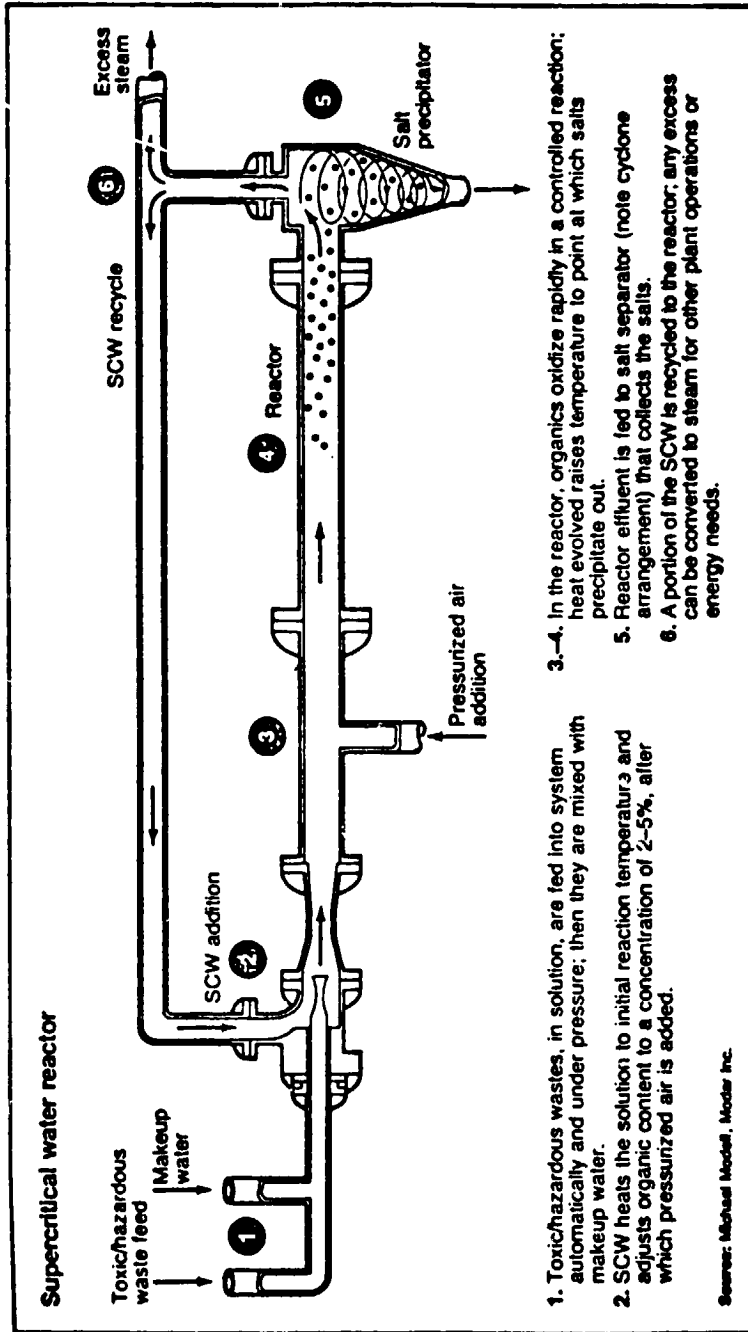
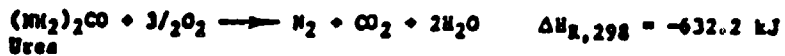


Figure 3.

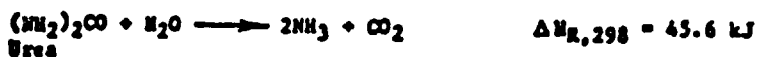
ORIGINAL PAGE IS
OF POOR QUALITY

UREA REACTIONS IN SUPERCRITICAL REGION

Overall Reaction at High Temperature



Step 1: Hydrolysis of urea to ammonia and carbon dioxide



INITIAL

Step 2A: Oxidation of ammonia to nitrogen



≈ 561 °C

Step 2B: Oxidation of ammonia to nitrous oxide



≈ 621 °C

Step 3: Decomposition of nitrous oxide to nitrogen and oxygen



≈ 670 °C

Figure 4.

SCW - UREA DESTRUCTION

DISTRIBUTION OF NITROGEN SPECIES IN THE LIQUID
AND GASEOUS EFFLUENTS (TIMBERLAKE, S.H., ET AL., 1982)

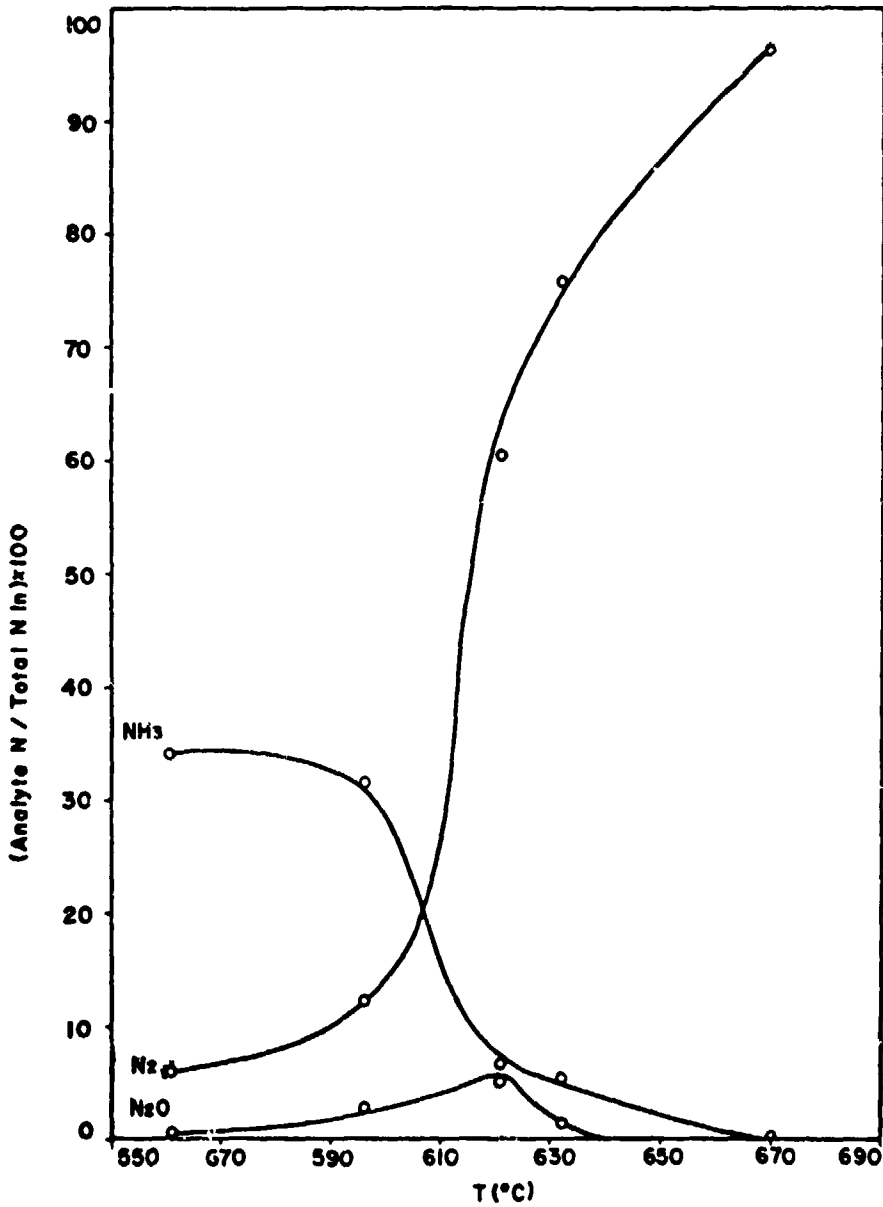
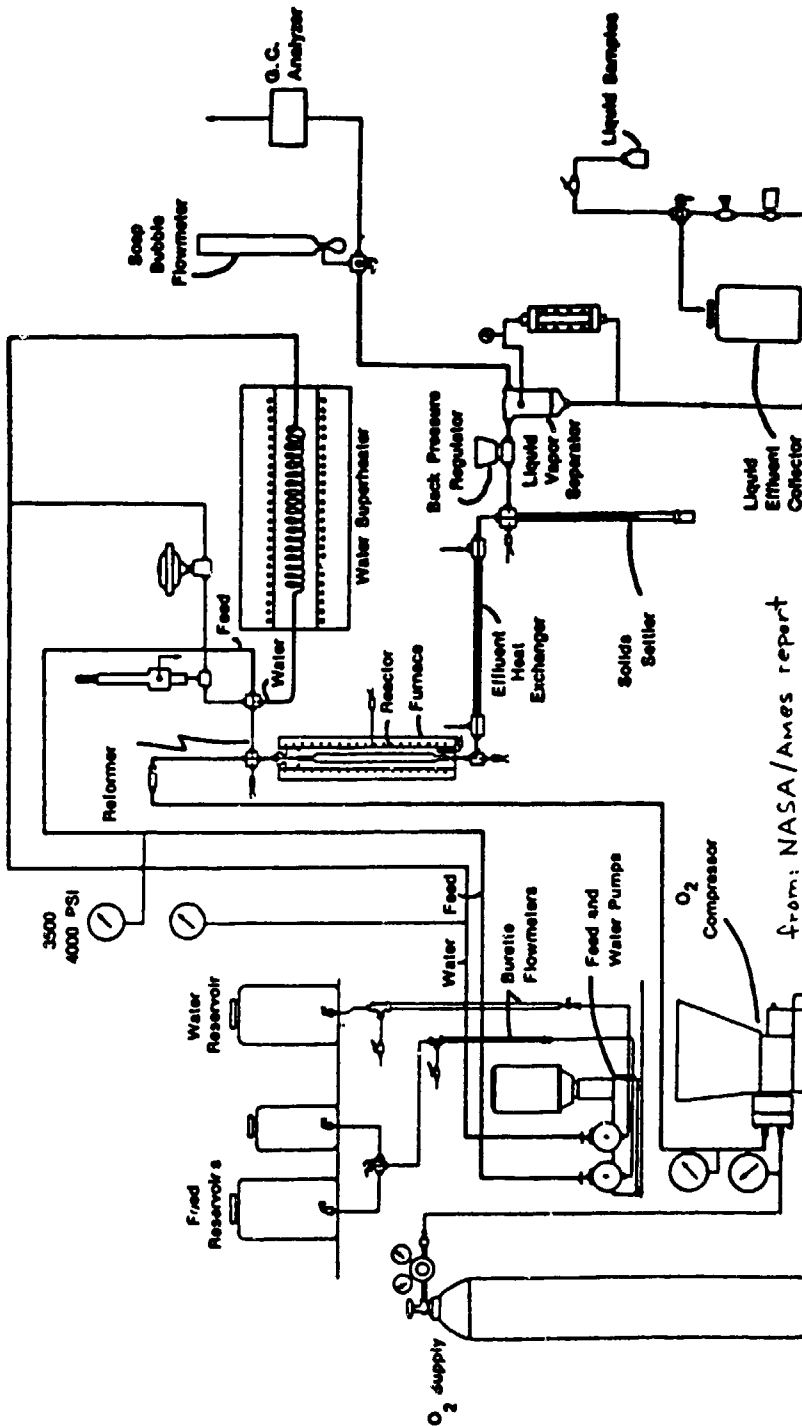


Figure 5.

Wet Oxidation System



from: NASA/Ames report

Figure 6.

I T ENVIROSCIENCE PROCESS CONCEPT
FOR
HOMOGENEOUS CATALYST

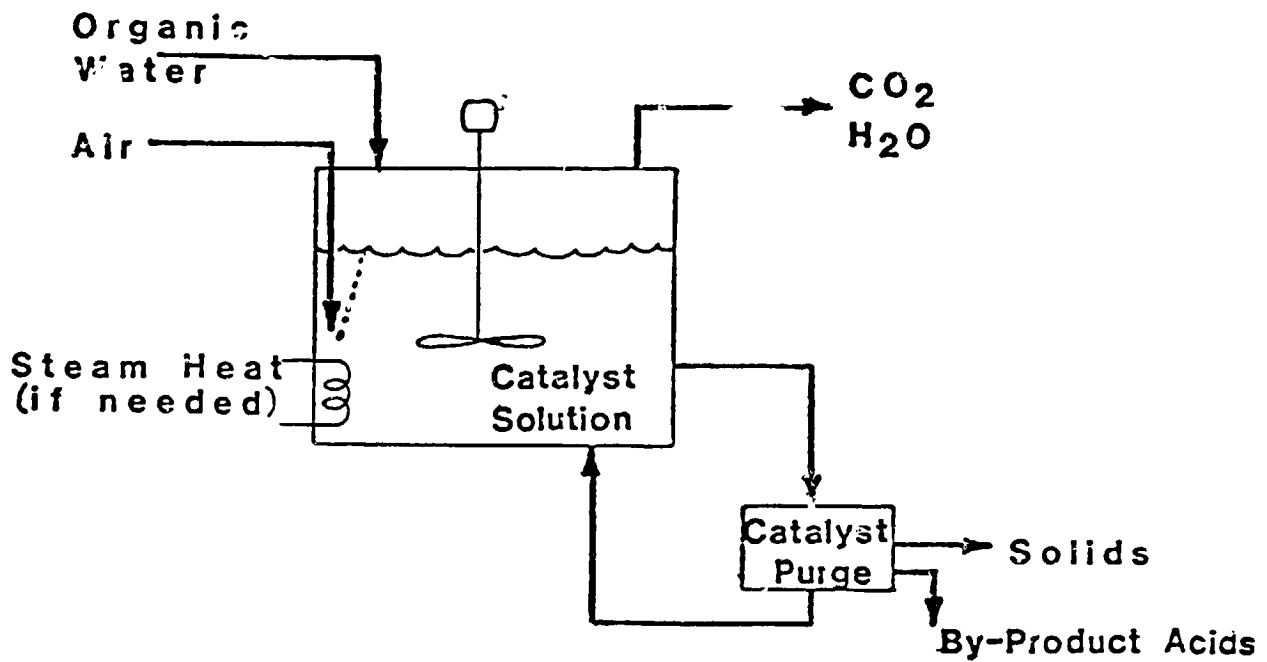


Figure 7.

REACTION VESSEL SCHEMATIC

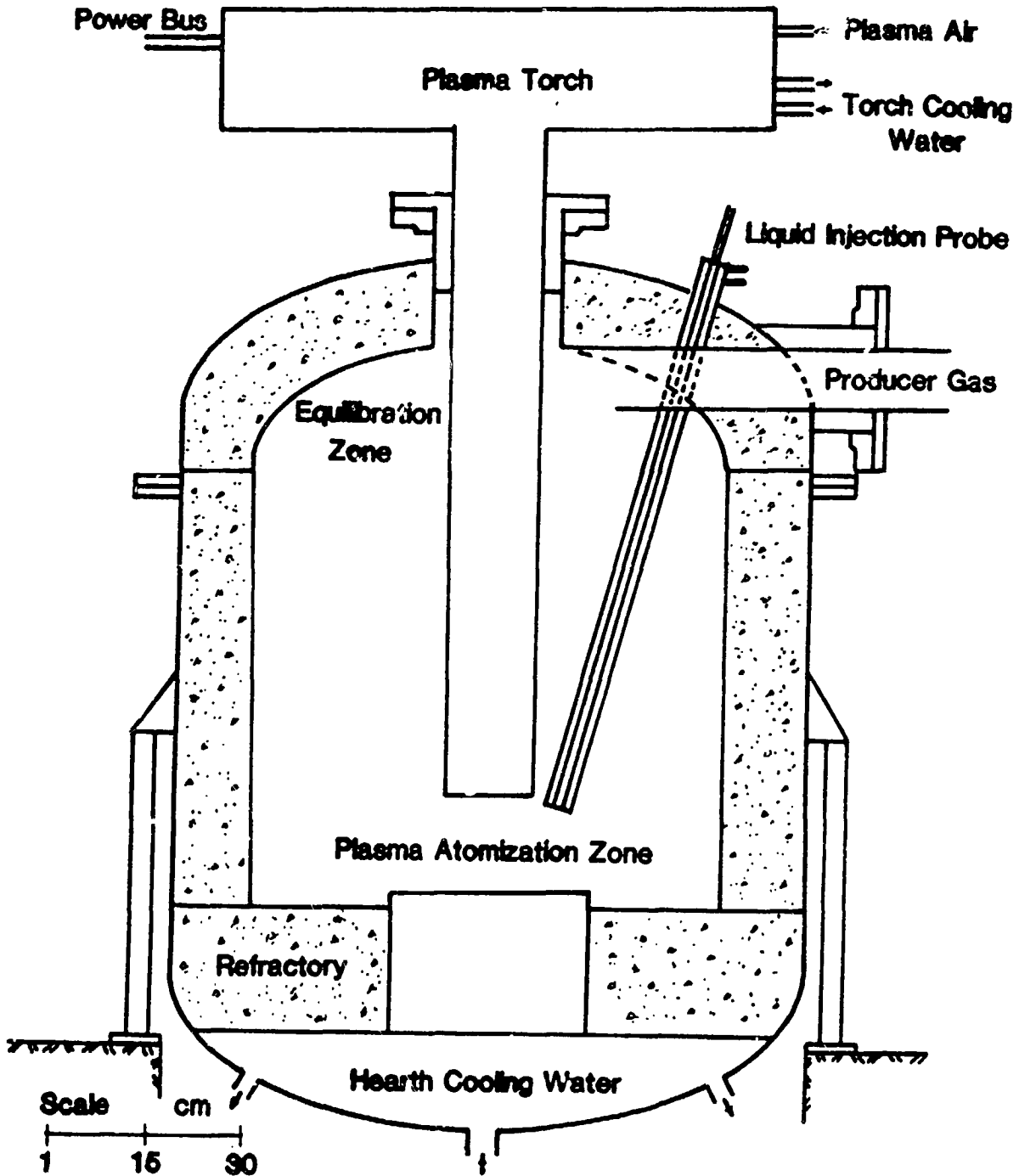
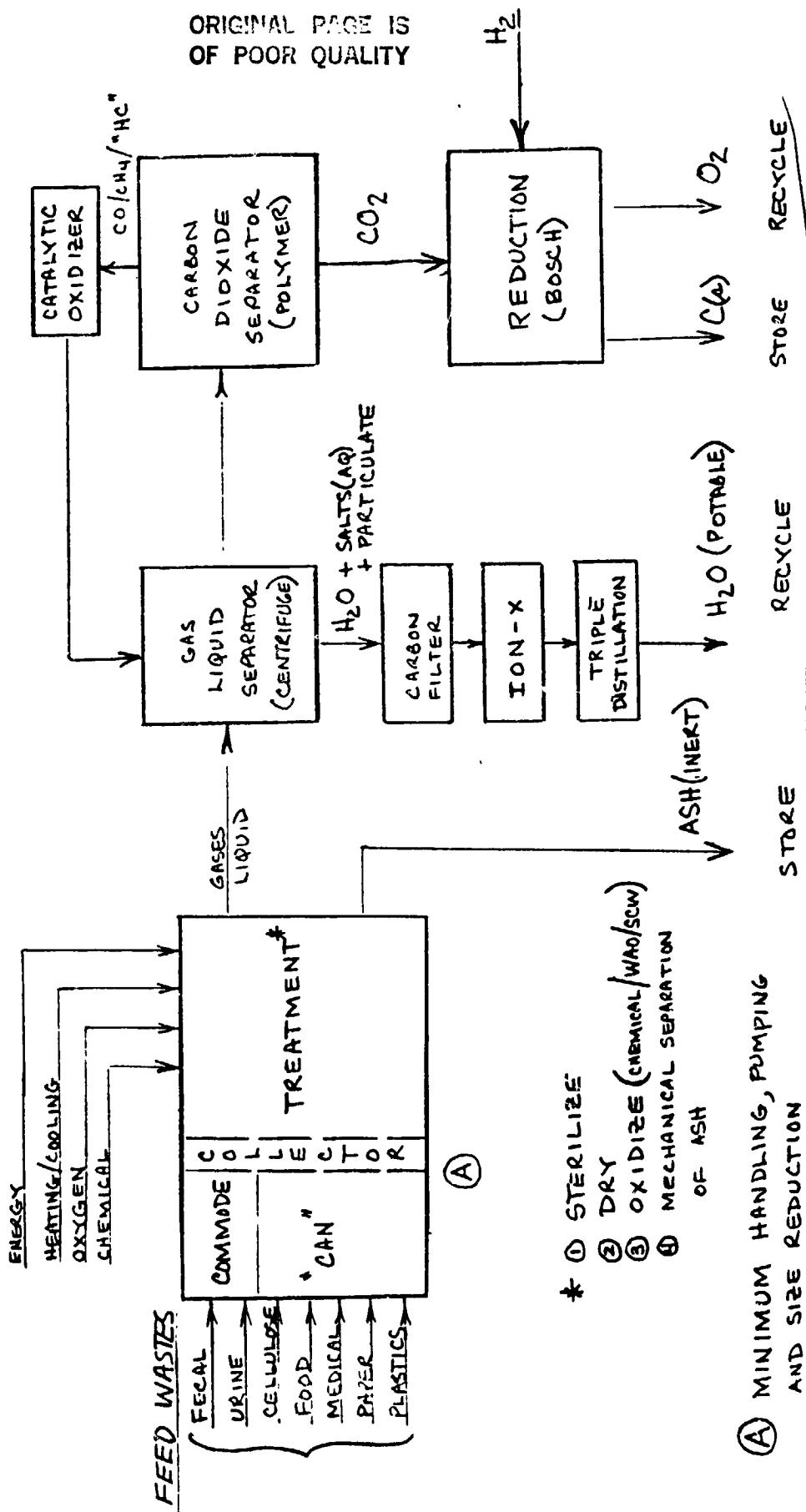


Figure 8.

SOLID WASTES TREATMENT SYSTEM FOR SPACE STATION

ZERO-GRAVITY & ZERO-LEAKAGE

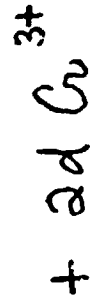
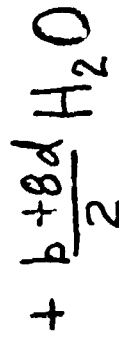
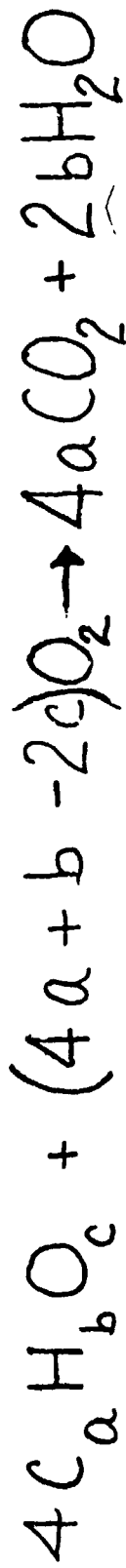


- * ① STERILIZE
- ② DRY
- ③ OXIDIZE (CHEMICAL/WAO/SCW)
- ④ MECHANICAL SEPARATION OF ASH

① MINIMUM HANDLING, PUMPING AND SIZE REDUCTION

Figure 9.

OXIDATION REACTION(S)



where $d = \frac{2}{3}a + \frac{b}{6} - \frac{c}{3}$

Figure 10.

Carbon dioxide reduction by hydrogen

general



$$y = 2x$$

$a, b, c, d = f(\text{time, temperature, pressure, initial concentration of reactants})$

conversion efficiency = 5 to 8 % (carbon & water)

recycle ratio = 20 to 12

Figure 11.

CARBON DIOXIDE REDUCTION



iron catalyst

530°C to 730°C

Bosch process

Figure 12

CARBON DIOXIDE REDUCTION



Sabatier reactor

Figure 13.

JOHN W. MEASEL

PAPER UNAVAILABLE

LUNAR LUMINESCENCE MEASUREMENTS
Thomas H. Morgan
Assistant Professor of Physics
Southwestern University
Georgetown, Texas

N86-14092

ABSTRACT

Spectra of lunar sites obtained in June 1983 have been analyzed for residual luminescence using the spectral line depth technique. The results for three sites each at three wavelengths indicate:

SITE	Na D	Ha	K I
Mare Crisium	9.4(\pm 1.1)	8.7(\pm 1.4)	6.8(\pm 1.5)
Kepler	8.1(\pm 1.3)	8.1(\pm 1.1)	9.5(\pm 1.9)
Aristarchus	8.5(\pm 1.7)	8.3(\pm 1.1)	8.0(\pm 1.4)

In each case, the value quoted was based not only on the strong Fraunhofer line in the spectral range covered but also on from 11 to 21 weaker lines within 80 A of the strongest feature.

These data do not support previous observations. The values here given do not indicate a greatly reddened spectrum, and the luminescence spectrum of the mare site is not significantly different from the two young crater sites. These observations cannot be adequately explained by thermal luminescence, theories of direct excitation are also unable to explain the strength of the flux.

Center Research Advisor: Dr. A. E. Potter

INTRODUCTION

Reports of lunar luminescence extend back almost 50 years, yet instrumental limitations have, until recently, made accurate values for the luminescent flux(as a percent of reflected light) difficult or impossible to obtain. Nevertheless, these early measurements did demonstrate the existence of the phenomenon. The early measurements showed variability both from site to site and with phase angle at a given site. Both direct excitation and thermal luminescence have been proposed.

APPROACH

Recently, the application of multi-element arrays to observational astronomy has made accurate determinations of luminescence possible. Accordingly, the coude spectrograph of the 2.7 m telescope at McDonald Observatory was recently used to obtain observations of selected sites at a number of strong Fraunhofer lines. These measurements require a solar spectrum obtained with the same spectrograph for interpretation. If there is a non-reflective component in the observed light from a lunar site then the apparent depths of the Fraunhofer lines in the lunar spectrum plotted against the Fraunhofer line-depths for the corresponding line in the solar spectrum should have a positive intercept. Figure 1 shows the raw data, and figure 2 shows a plot of the relative line depths as described above. Attachments 1 and 2 are computer programs which take the measured relative line depths (stored on disk), determine a least-squares fit, do some elementary

statistics, and calculate the residuals in form suitable for plotting. Figure 3 illustrates the quality of the fit.

RESULTS

On the three sites whose data have been measured, the luminous fluxes fall in the range 6-10 percent of reflected light. the most significant results are that (1) the luminescence of Aristarchus is not stronger than the other two sites and (2) that the luminescence is not increasing as a percent of reflected light in the red as reported previously in the literature.

TABLE 1

SITE	Na D	Ha	K I
Mare Crisium	9.4 (± 1.1)	8.7 (± 1.4)	6.8 (± 1.5)
Kepler	8.1 (± 1.3)	8.1 (± 1.1)	9.5 (± 1.9)
Aristarchus	8.5 (± 1.7)	8.3 (± 1.1)	8.0 (± 1.4)

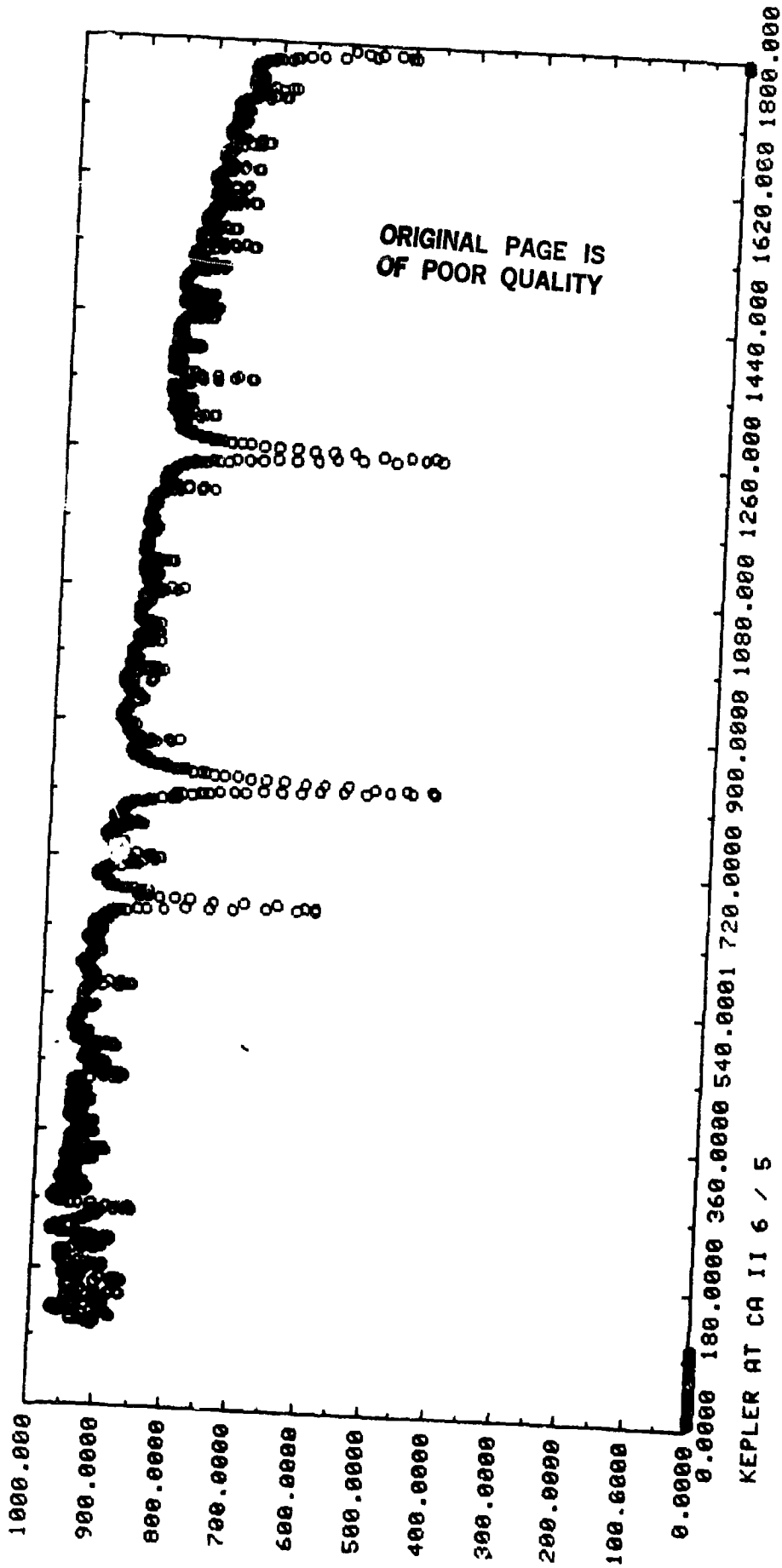
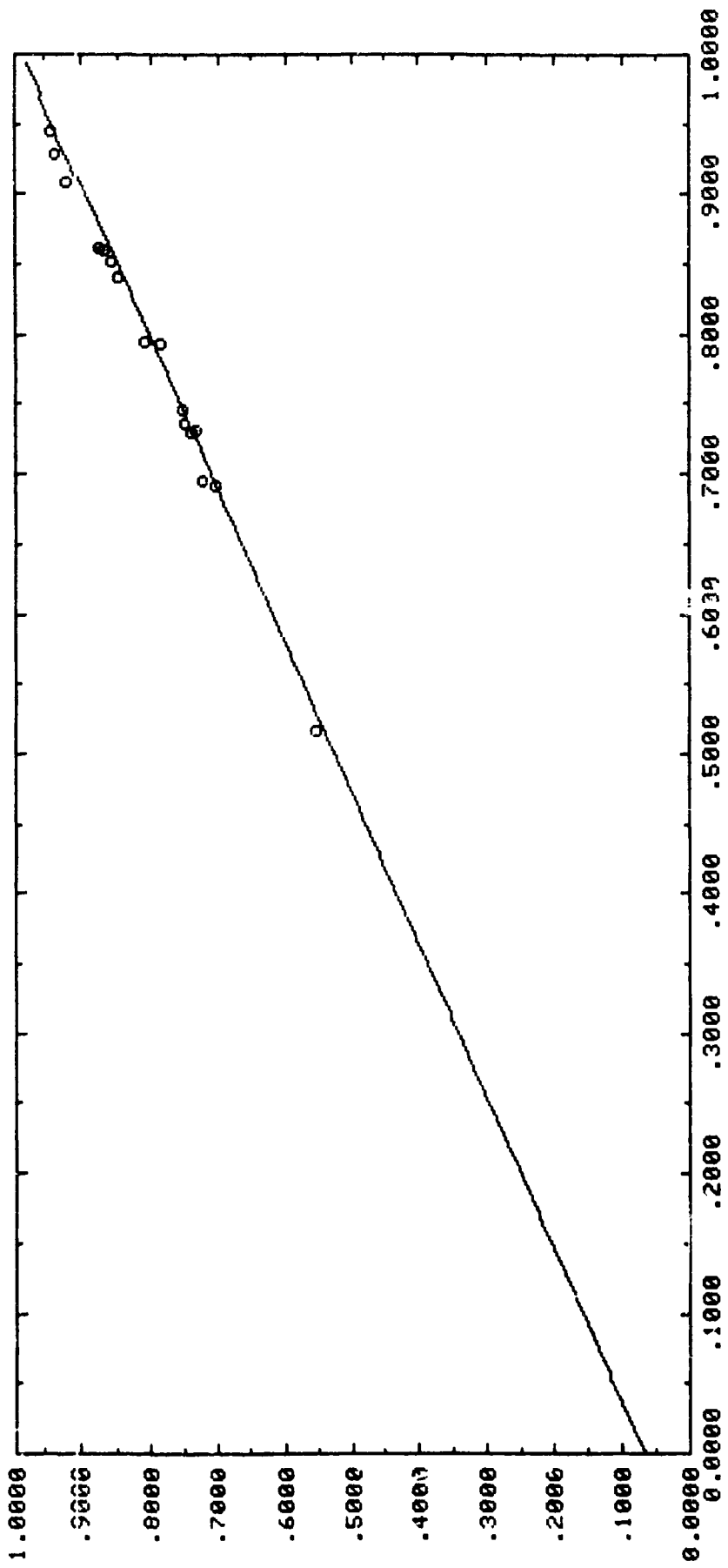


FIGURE 1



ARISTARCHUS AT K I

FIGURE 2

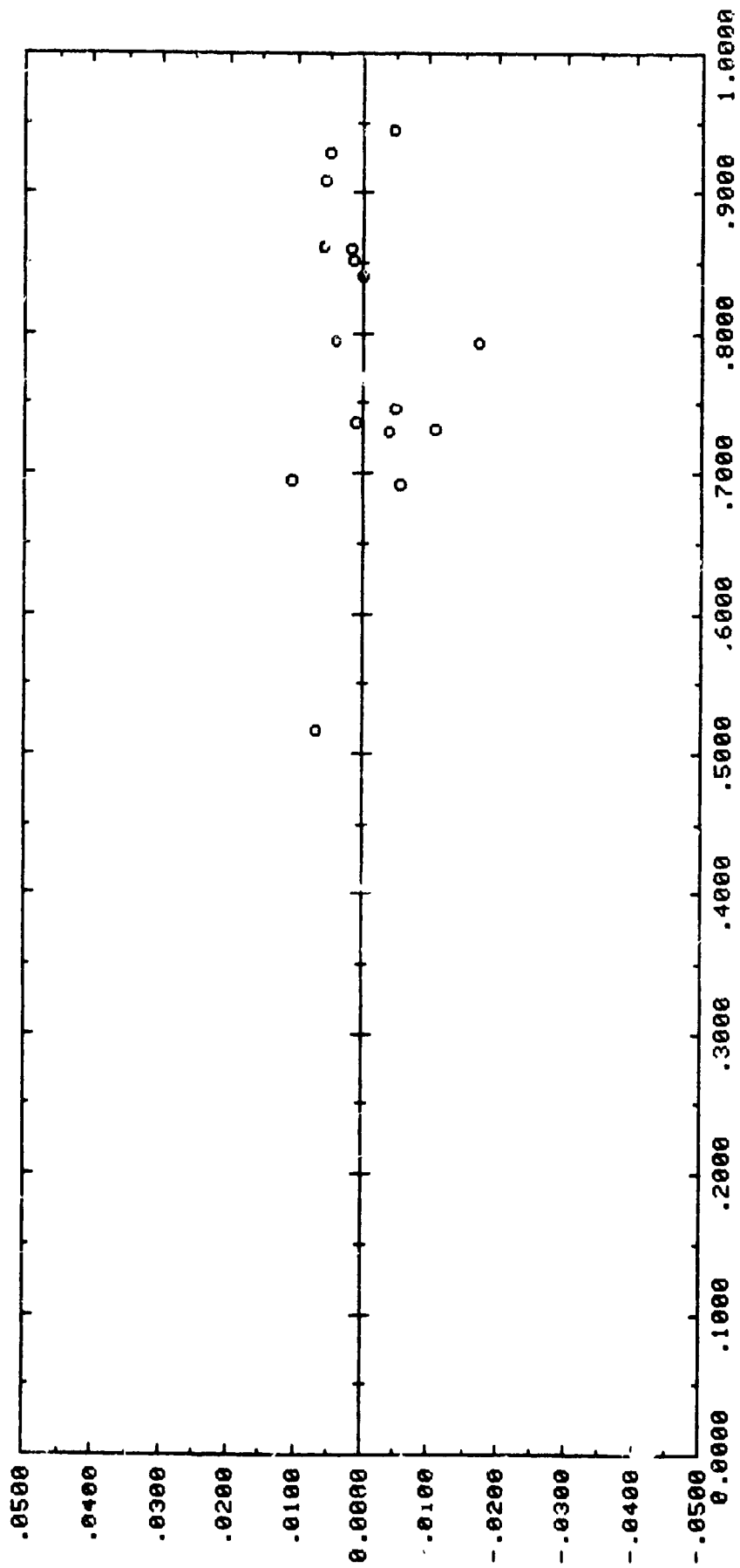


FIGURE 3

PROGRAM LUMF11.FOR

THIS PROGRAM WILL READ DIGITIZER FILES SPECIALLY CREATED FOR IT.
IN PARTICULAR, THESE FILES ARE:

1. EACH FOR A NUMBER OF FRAUNHOFER LINES IN A GIVEN WINDOW.
2. DATA IN GROUPS OF 3S--CON,LINE CTR,CUN.
3. FILES READ ARE CREATED BY DIGITIZER.

IN ADDITION, THE PROGRAM WILL CREATE A DATA FILE WITH THE RESULTING
RATIOS IN IT. IT WILL CALCULATE THE LEAST SQUARES
FIT SLOPE AND INTERCEPT FOR THE DATA SET AND CREATE A DATA FILE.

--BUT--

WRITE DOWN THE FITTING TERMS.

DONE 15/JUL/83 THM

MODIFIED 20/JUL/83//MODIFIED 21/JUL/83

SECTION I
INITIALIZATION

CHARACTER*64 LINEM,LINES
CHARACTER*30 MFILE,SFILE,RFILE
DIMENSION YMN(200),YSN(200),RATM(100),RATS(100)
INTEGER NMAXM,NMAXS

SECTION II
READ TWO DIGITIZER FILES

WRITE(6,*) ' ENTER MOON FILE NAME AS XXX.N;M ' !LIKE DIR LIST
FORMAT(A64) !DIGITIZER MOONFILE
10 READ(5,10)MFILE
OPEN(UNIT=4,FILE=MFILE,STATUS='OLD',READONLY)
DO 50 I=1,200 !READS Y'S OUT OF LINE
READ(4,10,END=50) LINEM
DECODE(7,20,LINEM(51:58)) YMN(I)
20 FORMAT(F10.1)
NMAXM=I
50 CONTINUE
WRITE(6,*) ' ENTER SUNFILE AS XXX.N;M ' !DIGITIZER SUNFILE
READ(5,10) SFILE
OPEN(UNIT=4,FILE=SFILE,STATUS='OLD',READONLY)
DO 100 J=1,200 !Y'S FOR SUN
READ(4,10,END=100) LINES
DECODE(7,20,LINES(51:58)) YSN(J)
100 NMAXS=J
CONTINUE
IF(NMAXM.EQ.NMAXS) GO TO 150
WRITE(6,*) ' FILES DO NOT HAVE SAME NO. OF LINES '
GO TO 999
150 IF((MOD(NMAXM,3)).EQ.0) GO TO 200
WRITE(6,*) ' NO OF LINES NOT MULTIPLE OF THREE '
GO TO 999

SECTION III
HERE THE DEPTH TO CONTINUUM RATIOS ARE CALCULATED

200 LIMMS=NMAXM-1
INES=1
DO 250 K=1,LIMMS,3
RATM(INES)=((YMN(K+1))/(((YMN(K))+YMN(K+2)))/2.0)) ! M DEPTH
RATS(INES)=((YSN(K+1))/(((YSN(K))+YSN(K+2)))/2.0)) ! S DEPTH

```

250      IRES =IRES+1
        CONTINUE
C
C      SECTION IIII
C      WRITES A DATA FILE WITH THE LUNAR AND SOLAR RATIOS PAIRED
C
WRITE(6,*) ' LUNAR AND SOLAR RATIOS '
IRES=IRES-1
300     WRITE(5,300)(RATM(N),RATS(N),N=1,IRES)
        FORMAT(2X,2F15.5)
        WRITE(6,*) ' MAKE NAME OF RATIO FILE AS XXXX.DAT '
        READ(5,10) RFILE
        OPEN(UNIT=10,FILE=RFILE,STATUS='NEW')
        WRITE(10,300)(RATM(N),RATS(N),N=1,IRES)
C
C      SECTION V
C      LEAST SQUARES CALCULATION
C
        SMXS=0 !SUM OF RATM SQUARED TERMS      ZEROED
        SMX=0  !SUM OF RATS VALUES            ZEROED
        SMY=0  !SUM OF RATM VALUES           ZEROED
        SMXYS=0 !SUM OF CROSS TERMS           ZEROED
        DO 350 ICNT=1,IRES
          SMX=RATS(ICNT)+SMX      !DOING THE SUMS
          SMXYS=((RATM(ICNT))*(RATS(ICNT)))+SMXYS
          SMXS=((RATS(ICNT)**2)+SMXS
          SMY=(RATM(ICNT))+SMY
350     CONTINUE
          DELLS=((IRES*(SMXS))-((SMX**2)
          AFIT=((SMXS*SMY)-(SMX*SMXYS))/DELLS ! SLOPE
          BFIT=((IRES*SMXYS)-(SMX*SMY))/DELLS ! INTERCEPT
          WRITE(6,*) ' INTERCEPT AND SLOPE ARE '
          WRITE(5,425) AFIT,BFIT
425     FORMAT(2X,F15.5,2X,F15.5)
          XLUMB=(AFIT+100)/(1-AFIT)
          WRITE(6,*) ' PERCENT LUMINENCE IS '
          WRITE(5,450) XLUMB
450     FORMAT(5X,F15.5)
999     CONTINUE
        STOP
        END

```

ORIGINAL PAGE IS
OF POOR QUALITY

ATTACHMENT 2

PROGRAM LUMSTAT.FOR

THIS PROGRAM WILL READ DIGITIZER FILES SPECIALLY CREATED FOR LUMFIT
AND DO AN EXTENDED STATISTICAL ANALYSIS OF THEM. IT DOES, IN ADDITION
THE A AND B COEFFICIENTS FOR THE LEAST SQUARES FIT, THE FOLLOWING:

1. A GOODNESS OF FIT ESTIMATOR FOR A AND B
 2. THE SUM OF THE SUM OF THE SQUARES TYPE CALCULATION.
 3. THE DIFFERENCE DELTA SUM I FOR ALL THE DATA POINTS.
- IN ADDITION, THE PROGRAM WILL CREATE A DATA FILE WHICH CONTAINS THE
DIFFERENCES AND THEIR SQUARES FOR FURTHER CONSIDERATION.
THE SOURCE FOR THE EQUATIONS CONTAINED HEREIN IS

DATA REDUCTION AND ERROR ANALYSIS FOR THE
PHYSICAL SCIENCES

BY

P. H. NEVINGTON

(SEE CHAPTER SIX IN PARTICULAR)

ONLY THE DIFFERENCES ARE SAVED AS A DATA FILE.

DONE BY TOM MORGAN

CREATED 25/JULY/83/

MODIFIED 26/JUL/83//27JULY/83//28/JUL/83//

SECTION I
INITIALIZATION

CHARACTER*1 XAFF
CHARACTER*64 LINEM,LINES
CHARACTER*30 MFILE,SFILE,RFILE
DIMENSION YMN(200),YSN(200),RATM(100),RATS(100)
DIMENSION DFLAM(100),DFLAMS(100)
INTEGER NMAXM,NMAXS

SECTION II
READ TWO DIGITIZER FILES

```
10 WRITE(6,*) ' ENTER MOON FILE NAME AS XXX.N;M ' !LIKE DIR LIST
   FORMAT(A64) IDIGITIZER MOONFILE
   READ(5,10)MFILE
   OPEN(UNIT=4,FILE=MFILE,STATUS='OLD',READONLY)
   DO 50 I=1,200 IREADS Y'S OUT OF LINE
     READ(4,10,END=50) LINEM
     DECODE(7,20,LINEM(51:58)) YMN(I)
   FORMAT(F10.1)
   NMAXM=I
50 CONTINUE
   WRITE(6,*) ' ENTER SUNFILE AS XXX.N;M ' !DIGITIZER SUNFILE
   READ(5,10) SFILE
   OPEN(UNIT=4,FILE=SFILE,STATUS='OLD',READONLY)
   DO 100 J=1,200 IY'S FOR SUN
     READ(4,10,END=100) LINES
     DECODE(7,20,LINES(51:58)) YSN(J)
   NMAXS=J
100 CONTINUE
   IF(NMAXM.EQ.NMAXS) GO TO 150
   WRITE(6,*) ' FILES DO NOT HAVE SAME NO. OF LINES '
   GO TO 999
150 IF((MOD(NMAXM,3)).EQ.0) GO TO 200
   WRITE(6,*) ' NO OF LINES NOT MULTIPLE OF THREE '
```

GO TO 999

C
C
C
C
200

SECTION III
HERE THE DEPTH TO CONTINUUM RATIOS ARE CALCULATED

LIMMS=NMAXN-1
IRES=1
DO 250 K=1,LIMMS,
RATH(IRES)=((YMN(K+1))/(((YMN(K))+YMN(K+2))/2.0)) : M DEPTH
RATS(IRES)=((YSN(K+1))/(((YSN(K))+YSN(K+2))/2.0)) : S DEPTH
IRES =IRES+1
CONTINUE

250
C
C
C
C

SECTION IIII
LEAST SQUARES CALCULATION OF LUMINANCE

IRES=IRES-1
SMXS=0 !SUM OF RATH SQUARED TERMS ZEROED
SMX=0 !SUM OF RATS VALUES ZEROED
SMY=0 !SUM OF RATH VALUES ZEROED
SMXYS=0 !SUM OF CROSS TERMS ZEROED

DO 350 ICNT=1,IRES
SMX=RATH(ICNT)+SMX !DOING THE SUMS
SMXYS=((RATH(ICNT))*RATS(ICNT))+SMXYS
SMXS=((RATS(ICNT))*2)+SMXS
SMY=(RATH(ICNT))+SMY

350

CONTINUE
DELLS=(IRES*(SMXS))-SMX**2
AFIT=((SMXS*SMY)-(SMX*SMXYS))/DELLS ! INTERCEPT
BFIT=((IRES*SMXYS)-(SMX*SMY))/DELLS ! SLOPE

WRITE(6,*) ' INTERCEPT AND SLOPE ARE '

425

WRITE(5,425) AFIT,BFIT

FORMAT(2X,F15.5,2X,F15.5)

XLUMA=(AFIT*100)/(1-AFIT)

XLUMB=((1-BFIT)/BFIT)*100

WRITE(6,*) ' PERCENT LUMINANCE FROM A AND B IS RESPECTIVELY '

WRITE(5,450) XLUMA,XLUMB

FORMAT(2(5X,F15.5))

450

C
C
C
C

SECTION V
CALCULATING THE DIFFERENCES THEIR SQUARES AND SIGMAS

VAR5=0 ! ZEROES VARIANCE
SLAM=0 ! ZEROES RUNNING SUM
DO 500 IS=1,IRES ! DOES LUM AND VAR CAL
DFLAM(IS)=RATH(IS)-(AFIT+BFIT*(RATS(IS)))
DFLAM5(IS)=(DFLAM(IS))**2
VAR5=DFLAM5(IS)+VAR5

500

CONTINUE
VAR5=VAR5/(IRES-2)
SIGA=(VAR5*SMXS)/DELLS
SIGB=(IRES*VAR5)/DELLS
SSIGA=SQRT(SIGA)
SSIGB=SQRT(SIGB)
SVARS=SQRT(VAR5)

WRITE(6,*) ' SIGMA A SIGMA B SIGMA Y IRES '

WRITE(5,525)SSIGA,SSIGB,SVARS,IRES

525

FORMAT(2X,F10.5,2X,F10.5,2X,F10.5,2X,13)

WRITE(6,*) ' PAUSE HIT ANY KEY WHEN YOUR READY '

READ(5,750)XAFF

WRITE(6,*) ' TABLE OF DEVIATIONS '

ORIGINAL PAGE IS
OF POOR QUALITY

```
725      WRITE(5,725)(IPT,DFLAM(IPT),DELAYS(IPT),IPT=1,INES)
750      FORMAT(2X,I3,2X,F10.5,2X,F10.5)
      FORMAT(A1)
      WRITE(6,*) ' NAME THE DELTA 1 FILE AS ZZZZ.CAT '
      READ(5,10)MFILE
      OPEN(UNIT=10,FILE=MFILE,STATUS='NEW')
      WRITE(10,775)(DFLAM(LDIF),NATS(LDIF),LDIF=1,INES)
775      FORMAT(2X,2F15.10)
999      CONTINUE
      STOP
      END
```

N 86 - 14093

Development of a Mass Spectrometer System for the
Measurement of Inert Gases in Meteorites

Russell L. Palma
Assistant Professor
Physics Department
Sam Houston State University
Huntsville, Texas

ABSTRACT

The study of the inert gases in meteorites has provided many clues as to the origin and evolution of the solar system. Particularly crucial and complex have been the gases krypton and xenon. To accurately measure the isotopic compositions of these gases requires a mass spectrometer of high sensitivity and resolution.

In this project a previously unused and largely untested mass spectrometer system was brought to the point where it was ready for routine sample analyses. This involved, among other things, focusing the ion beam for optimal peak shape and sensitivity, documenting the instrument's response to a series of characteristic tests such as multiplier gain checks, and interfacing the instrument to a computer to run the sample analyses.

Following this testing and setting up, three iron meteorite samples were to be analyzed for argon, krypton, and xenon. The three samples have been shown in prior work by the author to possibly contain primordial heavy inert gases. Although these analyses have not yet been carried out, it is anticipated that they will be completed in the near future.

Center Research Advisor: Don Bogard

INTRODUCTION

There were two primary objectives which I hoped to carry out during my 1983 summer research fellowship. The first was to help bring the new mass spectrometer in the gas analysis laboratory to the point where it was set up for routine analyses of meteorite samples. Following this, I wished to analyze the inert gases argon, krypton, and xenon in three iron meteorite samples to confirm, with reduced error bars, prior work which indicated possible primordial heavy inert gases. In the theory section, I will discuss the impetus for the iron meteorite sample analyses, while in the results section I will discuss the progress toward achieving the original two objectives.

THEORY

Meteorites are classified into three macroscopic groups: irons, stony-irons, and stones. These three broad classifications are further broken into many finer divisions based on mineralogical and structural differences. Many investigators of stony meteorites have found unusual elemental isotopic ratios relative to those seen in the earth's atmosphere, the sun, and bulk meteorite compositions. These data have provided clues to the solar system's origin and evolution. In seeking explanations for the anomalies seen, studies of stony meteorites have burgeoned, with increasingly more precise techniques and data. Meanwhile, the iron meteorites have been more-or-less ignored in the search for primordial inert gas anomalies. This treatment is not totally without justification, since iron meteorites clearly represent samples which have undergone a significant amount of metamorphism.

Thus they might well be expected to have lost, or at least appreciably altered, original inert gas compositions. Nevertheless, this is a conclusion reached more by assumption than by experimental confirmation.

Those studies of the inert gases in iron meteorites which have been carried out were generally done with a different objective in mind than the detection of possible primordial anomalies. Because of this, the samples selected for study and the procedures used were inappropriate for the objective I hoped to achieve. First of all, measurements of inert gases in iron meteorites have been almost exclusively restricted to the light gases helium, neon, and argon. This was done because the light gases are expected to have much greater concentrations than the heavy gases, krypton and xenon. The reason for this is due to the elemental composition of iron meteorites being approximately 90% iron and 10% nickel. Assuming that all the gas in these meteorites is the result of spallation induced by galactic cosmic rays, the target elements iron and nickel can yield the gases lighter in weight than themselves, helium, neon, and argon, but not the gases heavier than themselves, krypton and xenon. Thus spallogenic krypton and xenon will only be produced from heavy trace elements.

On one hand that is favorable for my objective, since it means that spallation produced krypton and xenon may not overwhelm a small primordial gas component. On the other hand, it means the concentration of the gases is probably going to be extremely low. This expected low concentration requires an extremely sensitive mass spectrometer with sufficient resolution to clearly separate the isotopes of xenon. The new mass spectrometer at Johnson Space Center was well suited for this investigation.

RESULTS

For the following discussion of adjustments made in the mass spectrometer system, I will first very briefly outline its overall operation. Neutral gas atoms are released from a heated sample, enter the mass spectrometer and are ionized in the source region by bombardment with electrons from a filament. The ions are now collimated and accelerated through a series of slits in parallel plates with a voltage drop. The resulting ion beam enters the field of an electromagnet where it is split due to the varying charge to mass ratios in the beam. Those ions whose charge to mass ratio is such that they will enter the analyzer slit impinge on an ion collector. The signal thus received is then amplified and recorded on a strip chart.

At the beginning of the summer, the ion beam was obviously not well focused since the shape of the peaks made when scanning over a mass was poor and the sensitivity low. The desired peak shape is one which has a flat top and steep sides. The flat top ensures that when one measures the height of the peak, the exact place on the peak selected will not be critical; this is especially important for peak jumping where a computer is running the sample analysis. The steep sides make it possible to clearly resolve adjacent mass peaks. The focus of the instrument is affected by a number of variables, and the adjustment of one parameter will usually have an effect on the others. Thus the proper focus was only reached after a long series of trial and error adjustments. Among the coarse adjustments are a magnet in the source region, the main electromagnet, rotation of the collector slit, and the collector slit width. The source slit width is not adjustable on this machine. Finer adjustments included the level and

difference of the source divider; the deflection plate voltage, repeller, and dynode #1 of the electron multiplier; and the repeller of the emission regulator.

The best focus for one mass may not be optimal for another. The original focusing was done with ^{40}Ar since that is always in the background of the system. However, after it became evident that the sensitivity of the instrument was such that measuring argon would not be a problem in typical lunar or meteorite samples, the focusing was readjusted for xenon, which is generally of much lower concentrations. Part of this readjustment involved an analysis of the five inert gas peak heights as a function of the electron accelerating voltage. This voltage is the potential difference between the filament and the ionization chamber walls. The peak sensitivity for krypton and xenon came with the electron voltage at 43.5 V, and this value was adopted for all gases for convenience and because double ionization of ^{40}Ar (which would then contribute to the ^{20}Ne peak) would be small.

Constant sweep rate scans of the krypton and xenon mass regions after the final focusing adjustments are presented in Figures 1 and 2. As the magnetic field increases, the charge to mass ratios differ by less and less, so the excellent resolution at xenon is one of the instruments clear strengths. Thus the machine is set up in such a way that the sensitivity in measuring the isotopes of krypton and xenon is optimized (while still retaining a good peak shape) at the slight expense of the generally far more abundant inert gases helium, neon, and argon.

Since the concentrations of the heavy inert gases are so low (^{132}Xe on the order of 10^{-11} cm^3/g STP), it is naturally vital to maintain as low a pressure and clean a system as possible. This is accom-

plished by enclosing the all metal mass spectrometer in a hood and baking it with resistance heaters when necessary. It is always possible that during these bakeouts the metal flanges and copper seals may expand and contract in such a way as to produce a leak. The leaks are detected by blowing ^4He over the various flanges while monitoring the ^4He peak on the recorder. One large copper seal and a gold valve ring had to be replaced (the gold ring by one of paladium) this summer, and the machine subsequently baked out at approximately 150°C for several days. Another small leak was plugged by applying leak sealant to the affected region. The background gases (in particular benzene, which interferes with ^{78}Kr) were monitored and found to be steadily, albeit slowly, decreasing, so that by the end of the summer there was a much cleaner machine with an ionization gauge pressure of about 2.5×10^{-9} torr.

Other tests run on the machine were multiplier gain tests and sensitivity tests. The results of these were used primarily to compare the new mass spectrometer in the lab to the old one. In the multiplier gain test, a peak is first measured by having the beam strike a Faraday cup, rather than the electron multiplier. The gain of the multiplier is then computed by comparing the multiplier signal at various multiplier voltages to that of the Faraday cup. In the sensitivity tests, inert gases of known amounts and isotopic compositions are admitted to the mass spectrometer to determine the instrument's response.

After the focusing problems were largely overcome, the next major phase of bringing the new mass spectrometer into routine operation was the interface with the computer. Under the computer's control, scans of the peaks can be made much more swiftly and accurately. However, because the vibrating reed electrometer and the magnet regulator

on the new instrument differed from that of the old, the software had to be modified. In the interfacing process many problems arose from the different characteristics of the hardware. The magnet regulator in particular had to be modified to damp out oscillations which were keeping it from coming to rest on a peak by the time the computer was integrating the peak's height. The nonlinearity of the electrometer presented difficulties in measuring the signal from widely different peak heights (for example, ^{38}Ar relative to ^{40}Ar in atmospheric composition) while on a volt range setting sufficiently high to keep the larger peak on scale.

CONCLUSIONS

At the time of this report, the mass spectrometer and the computer interfacing are very close to being ready for sample analyses. Already sensitivity checks and blank background measurements have been completed in anticipation of the melting of the first of the iron meteorite samples, Babb's Mill. I expect that in the following weeks the other two, Braunau and Sierra Gorda, will also be run. Although the results of these measurements cannot be reported here, it is hoped that they will soon be included in a paper with due credit to the NASA/ASEE summer faculty program for their support.

ORIGINAL PAGE IS
OF POOR QUALITY

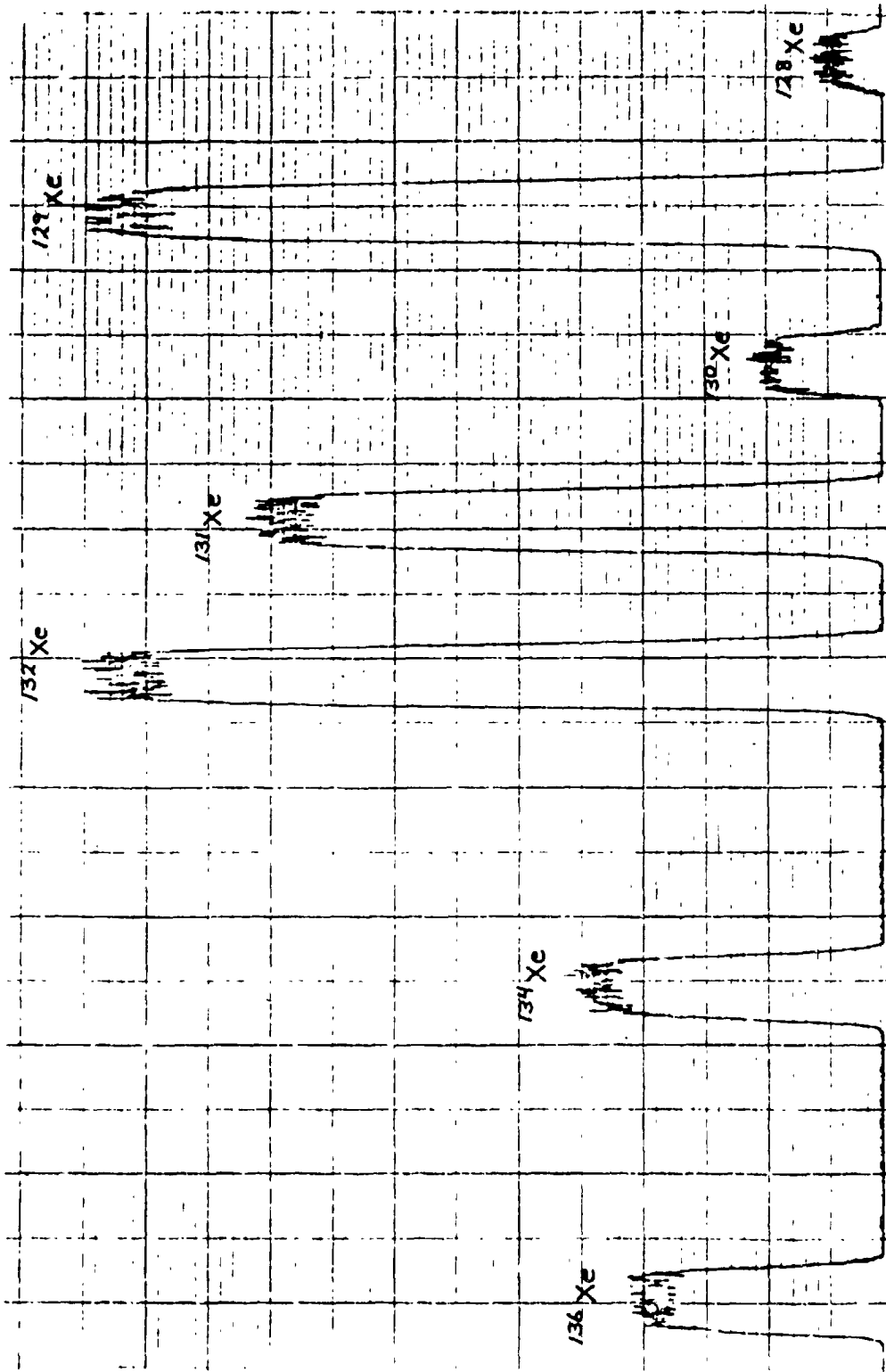


Figure 1. Constant sweep rate scan of xenon with atmospheric composition.

ORIGINAL PAGE IS
OF POOR QUALITY

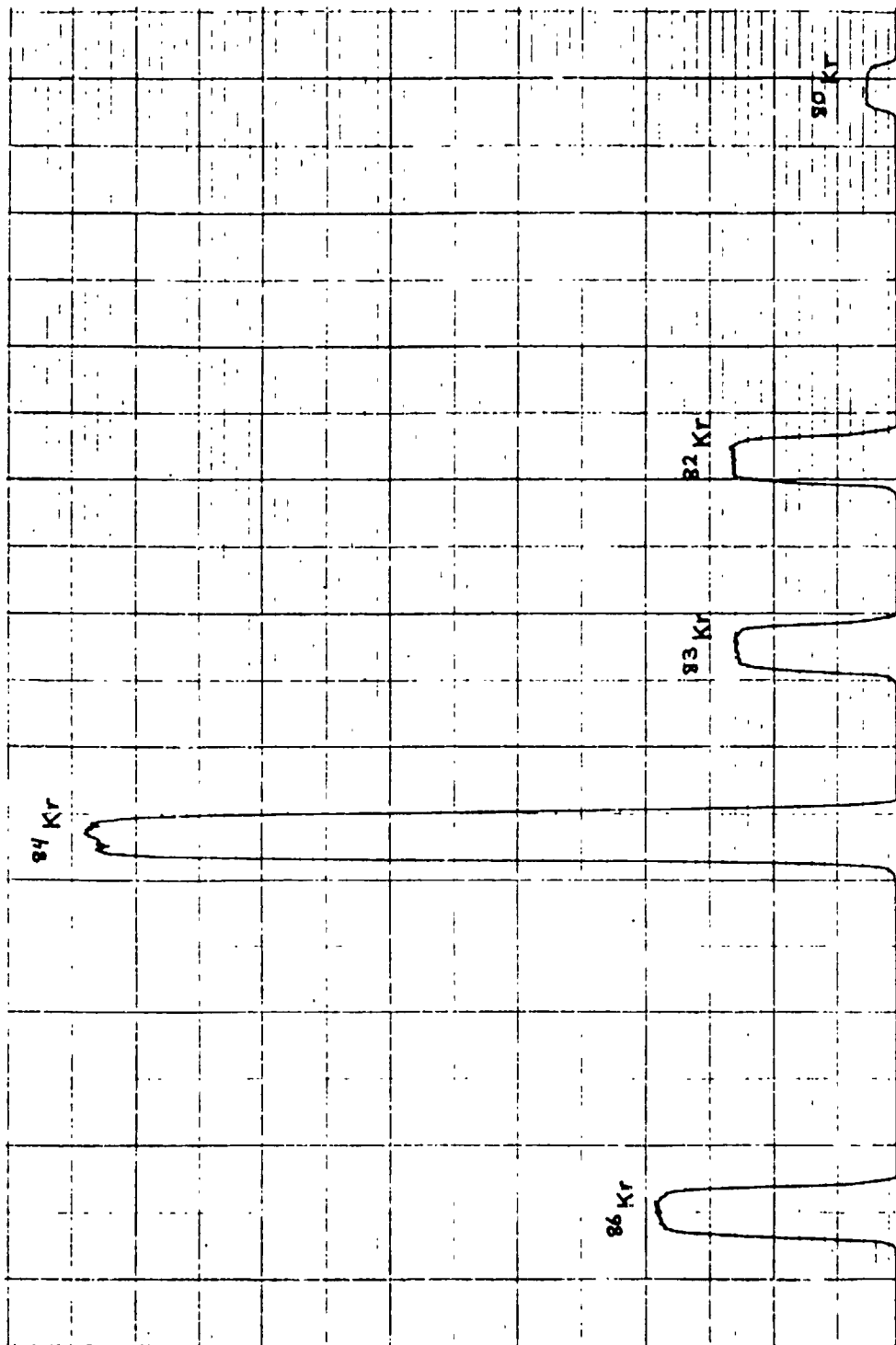


Figure 2. Constant sweep rate scan of krypton with atmospheric composition.

BOBBY JOE PRESLEY

PAPER UNAVAILABLE

N86-14094

An Analysis of Cryotrap Heat Exchanger Performance
Test Data (400 Area) and Recommendations for a
System to Handle Apollo RCS Engines

By: Allen Rakow

Contents

- A. Introduction
- B. Characterization of Existing System
- C. Design of a Higher Capacity System
- D. Recommendations

A. INTRODUCTION

The attached photograph shows the current arrangement of a Platecoil heat exchanger which uses LN₂ on the inside of parallel tubes, in counter flow to the test cell engine exhaust gases which are drawn through a box surrounding the plates by the existing vacuum blowers. As a result of inadequate performance and special test data it was decided to redesign the system to accommodate an Apollo RCS engine.

B. CHARACTERIZATION OF EXISTING SYSTEM

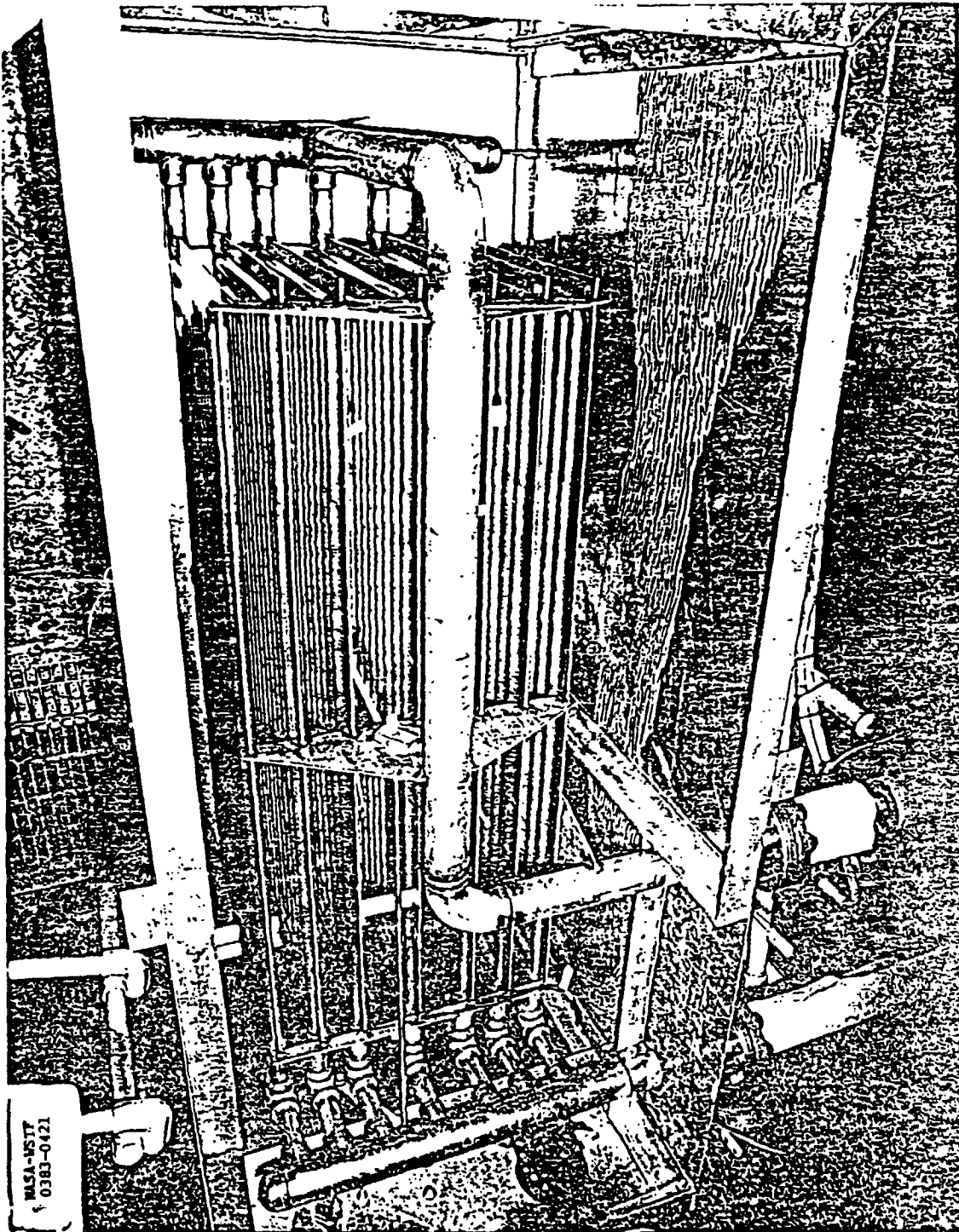
Test LN₂ - 3 (TR-329-002) was used to determine tube and shell side heat transfer coefficients for the system (Table I). At the 68 second mark it should be noted that only sensible heat is transferred, i.e., at an exit temperature of 350F no ice formation would be occurring since the H₂O vapor pressure in the bulk gas phase is higher than in the inlet vapor stream. During this test the LN₂ rate was 2.5 gpm on the average. The Platecoil catalogue 5-63 indicates that each tube is about 1" in I.D. with a wall thickness of .083." There are 84 tubes, each 47" in length.

At a cell pressure of .2079 psia (68 second mark) Altitude Prediction methods (TR-329-001) yield a rate of 91.5 scfm through the exchanger. Since there are 84 tubes this would be about 1 scfm per tube.

The composition of the gases at the heat exchanger inlet was taken to be:

	<u>Volume %</u>
H ₂	- 8.3
N ₂	- 33.3
CO ₂	- 6.8
CO	- 9.2
H ₂ O	- 40.1
CH ₄	- <u>2.1</u>
	99.8

ORIGINAL PAGE IS
OF POOR QUALITY



ORIGINAL PAGE 13
OF POOR QUALITY

TABLE 1.

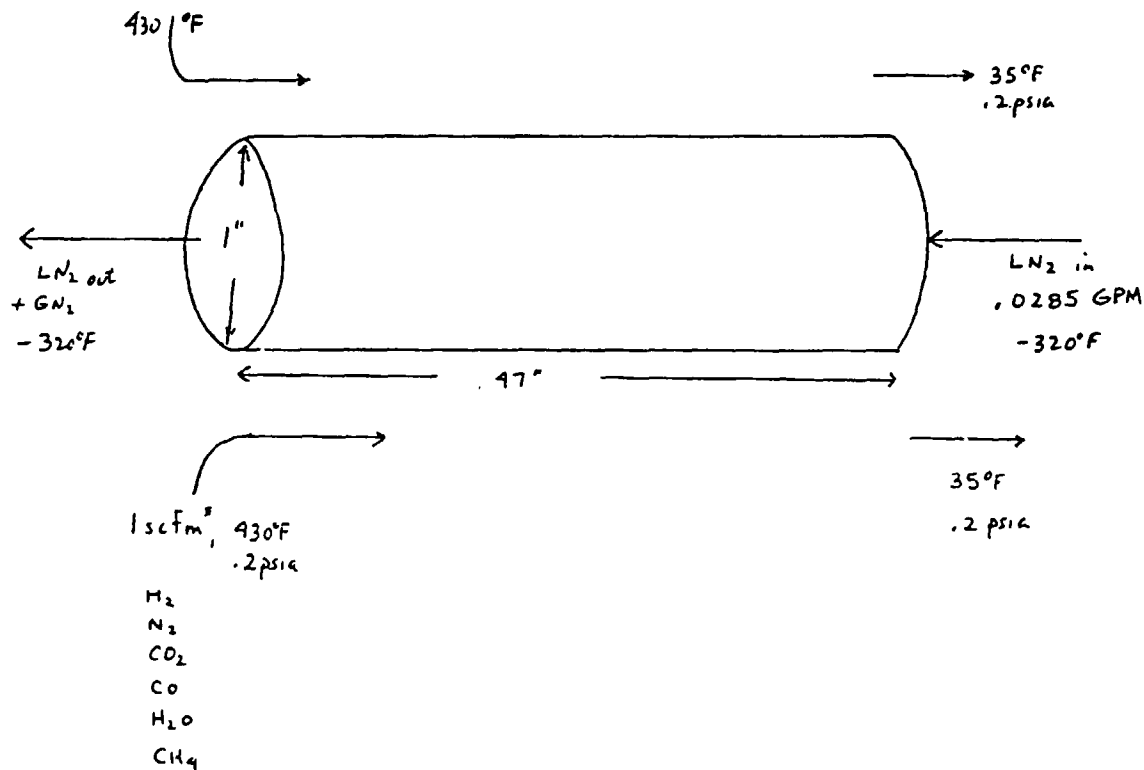
TEST NO.: LM₂ - 3 DATE: 4-1-83
 FIRING PROFILE: Steady State (68 sec) (0.37 lbs mass/sec)
 BLOWERS IN OPERATION: 4 Sets (West and South)

	TIME (SECONDS)			
	-10	20	40	60
Heat Exchanger Inlet Flowrate (gpm)				
Heat Exchanger Inlet Temp (°F)	-316	-317	-314	-312
Heat Exchanger Outlet Temp (°F)	-313	-316	-314	-312
Cold Plate A - Inlet Skin Temp (°F)	-286	-261	-213	-166
Cold Plate A - Middle Skin Temp (°F)	-230	-209	-179	-150
Cold Plate A - Outlet Skin Temp (°F)	-273	-251	-225	-198
Cold Plate C - Inlet Skin Temp (°F)	-293	-268	-223	-182
Cold Plate C - Middle Skin Temp (°F)	-255	-242	-213	-183
Cold Plate C - Outlet Skin Temp (°F)	-295	-272	-243	-214
Heat Exchanger Gas Inlet Temp (°F)	97	357	433	430
Heat Exchanger Gas Inlet Temp (°F)	91	362	438	433
Heat Exchanger Gas Outlet Temp (°F)	-92	-11	9	30
Heat Exchanger Gas Outlet Temp (°F)	-141	-8	6	23
Heat Exchanger Outlet Pressure (Baratron) (psia)	.0037	.083	.142	.169
Chamber (Heat Exchanger Inlet) Pressure (Baratron) (psia)	.0043	.086	.146	.192
Cell Altitude (ft x 1000)	192.5	114.5	101.8	95.6
North Chamber Outlet Temp (°F)	108	135	169	178
Right North Blower Inlet Temp (°F)				
Left North Blower Inlet Temp (°F)				
South Chamber Outlet Temp (°F)	73	130	162	181
Right South Blower Inlet Temp (°F)	79	110	128	138
Left South Blower Inlet Temp (°F)	80	110	129	141
West Chamber Outlet Temp (°F)	-51	3	33	61
Right West Blower Inlet Temp (°F)	67	69	75	80
Left West Blower Inlet Temp (°F)	59	65	73	80
Predicted Cell Pressure (psia)		.0662	.1187	.1675
Predicted Cell Altitude (ft x 1000)		120.9	106.7	98.7
				.1888
				96.0

ORIGINAL PAGE IS
OF POOR QUALITY

It should be noted that at 1 scfm per tube, with 40% H₂O by volume in the inlet gas, the heat load to freeze all the water would be 22.4 BTU/min. At an LN₂ rate of 2.5 gpm (.0285 gpm/tube) there is only 17 BTU/min available on the N₂ side if a constant T of -320°F is to be maintained, i.e., there is inadequate LN₂ to do the job of removing water and sensible heat.

The conditions for characterizing the system are summarized in the following sketch:



* unreacted N₂O₄ + MMH
not considered in analysis

The rate of heat transfer Q (BTU/hr) for this case, neglecting wall and ice resistances, is given by:

$$Q = \frac{2 L (T_i - T_o)}{\frac{1}{Rh_i} + \frac{1}{Rh_o}}$$

Where

- L = length of tube
- T_i = inside bulk temperature
- T_o = outside bulk temperature
- R = Radius of tube
- h_i = inside coefficient of heat transfer
- h_o = outside coefficient of heat transfer

The rate of heat transfer is also given by:

$$Q = \dot{m} C_p \Delta T = (\text{gas flowrate}) (\text{heat capacity}) (430-35^\circ\text{F})$$

since only sensible heat is transferred from the gas side.

$$\text{So } Q = 1 \frac{\text{scfm}}{\text{min}} \times \frac{1 \text{ lb mole}}{359 \text{ ft}^3} \times 7.5 \frac{\text{BTU}}{\text{lb mole } ^\circ\text{F}} \quad (395^\circ\text{F})$$

$$Q = 8.25 \frac{\text{BTU}}{\text{min}} = 495 \frac{\text{BTU}}{\text{hr}}$$

On the outside we have forced convection heat transfer, therefore, as an approximation, we can employ a correlation for flow normal to a cylinder (see attached Figure from McAdams). There are eight channels in the heat exchanger, therefore, dividing the flow by eight gives us a velocity of 1820 ft/min past the cylinders. Correcting for temperature and pressure (we're at .2 psi and 230°F on the average as opposed to 14.7 psi and 32°F for standard conditions) gives a value of .00054 lb/ft³ for the gas density resulting in a Reynold's number of approx. 100. This gives a Nusselt number, Nu, of 5 and an outside heat transfer coefficient of 1.2 BTU/hr ft² °F.

Using a mean outside temperature of 230°F we get:

$$h_i = 3.36 \text{ BTU/hr ft}^2 \text{ } ^\circ\text{F}$$

As a check we can compute the inside coefficient from a forced convection correlation for flow inside a tube:

$$h_i = \frac{k}{D} (.023) (\text{Re})^{.8} (\text{Pr})^{.4}$$

At a Reynold's number of 1317 we get:

$$h_i = 11.5 \text{ BTU/hr ft}^2 \text{ } ^\circ\text{F}$$

Remember, however, that this correlation is for turbulent flow, therefore, it's not unusual to get a higher number for h_i since our Reynold's number is only 1317. Therefore, an inside coefficient of 3.36 is realistic.

Before we use this information to redesign the system it is worth mentioning that in forced convection boiling (see attached notes) the heat transfer coefficient will rise significantly and then fall off again as one goes down the tube. This might explain the fact (see LN₂ -3 test data) that the skin T on the outside of the tube is highest at the middle for most of the run.

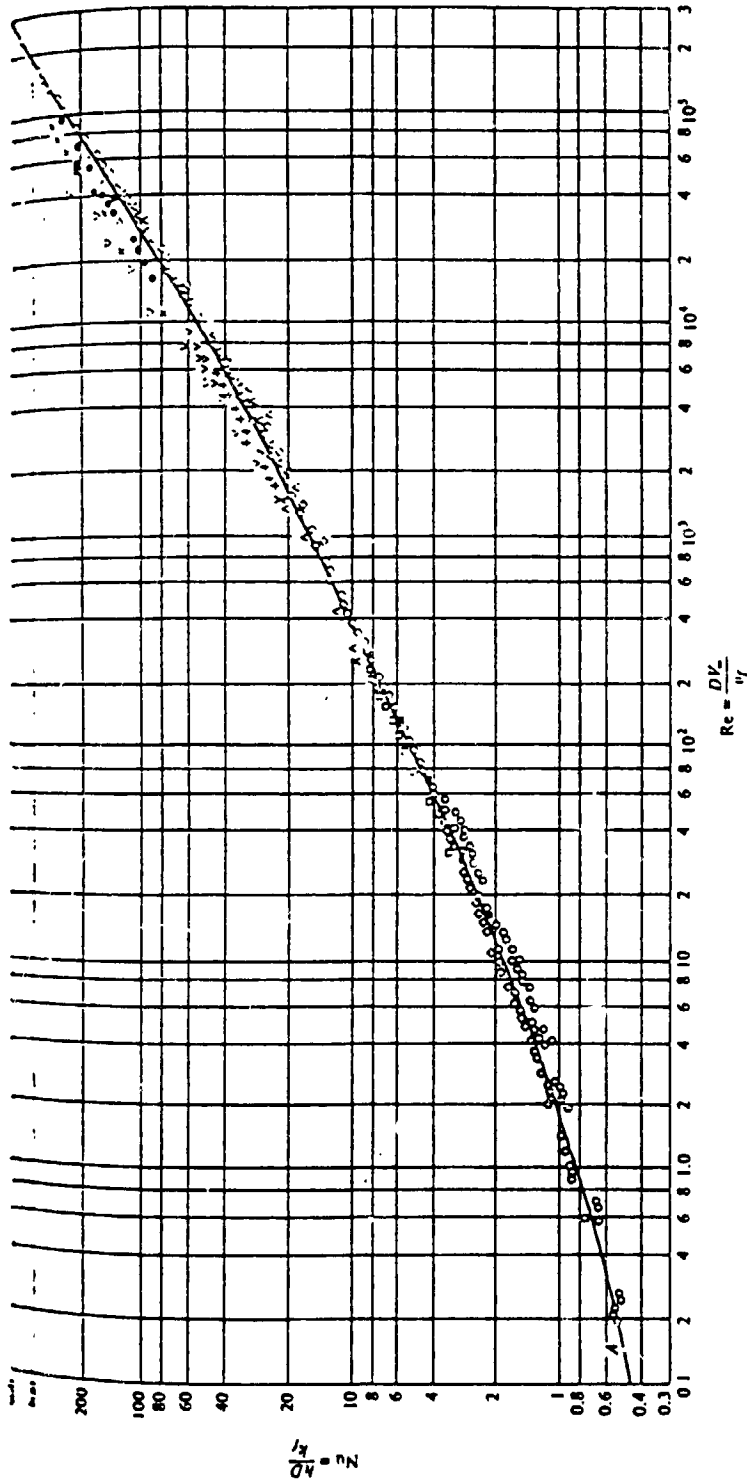


Figure 4-11 Average Nusselt number versus Reynolds number for a circular cylinder in air, placed normal to the flow. (SOURCE: W. H. McAdams, *Heat Transmission*, 3rd ed. McGraw-Hill, New York, 1954) D = diameter of cylinder, V_∞ = fluid full stream velocity, ν_f = fluid kinematic viscosity, h = heat transfer film coefficient, k_f = fluid thermal conductivity, Re = Reynolds number, Nu = Nusselt number

Notes

ORIGINAL PAGE IS
OF POOR QUALITY

10.2.4 Forced-Convection Boiling

Forced-convection boiling is usually associated with boiling from the inner surface of a heated tube through which a liquid is flowing. Bubble growth and separation are strongly influenced by the flow velocity, and hydrodynamic effects are significantly different than those corresponding to pool boiling. The process is complicated by the existence of different two-phase flow patterns that preclude the development of generalized theories.

Consider flow development in the heated tube of Figure 10.5. Heat transfer to the subcooled liquid which enters the tube is initially by forced convection and may be predicted from the correlations of Chapter 8. However, boiling is soon initiated, with bubbles appearing at the surface growing and being carried into the mainstream of the liquid. There is a sharp increase in the convection heat transfer coefficient associated with this *bubbly flow regime*. As the volume fraction of the vapor increases, individual bubbles coalesce to form plugs or slugs of vapor. This *slug-flow regime* is followed by an *annular-flow* regime in which the liquid forms a film. This film moves along the inner surface, while vapor moves at a faster velocity through the core of the tube. The heat transfer coefficient continues to increase through the *bubbly flow* and much of the *annular-flow* regimes. However, dry spots eventually appear on the inner surface,

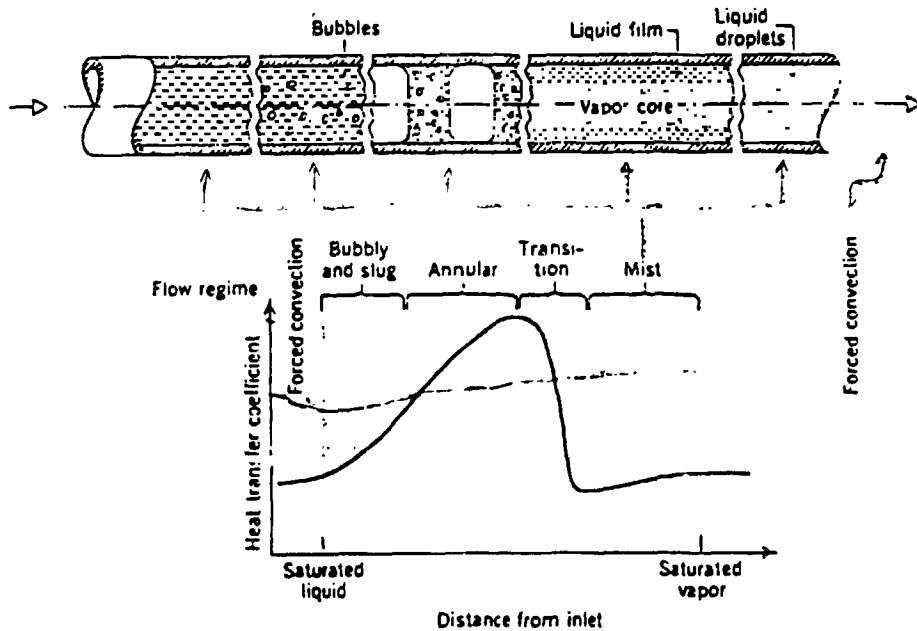


Figure 10.5 Flow regimes for forced-convection boiling inside a tube.

*Cryo Panels 47" x 22"
7 Panels in Array*

*LENS 3/4" DIA
3/4" DIA
3/4" DIA*

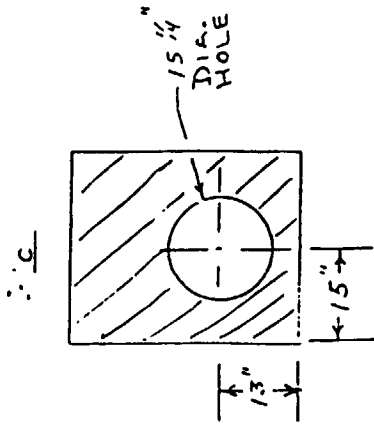
GOLD TRAP BOX

- FRAME: 2 ALUM L, WELDED
- SIDES: SHEET ALUM/SS POP RIVETED TO FRAME
- A - 30 X 13 APPROX.
- B - 69 X 36 WITH 2 5/4 X 8 1/4 CORNER CUTOUT
- C - 30 X 36 WITH 1 5/4 DIA HOLE (DETAIL →)
- D - 69 X 36 APPROX.

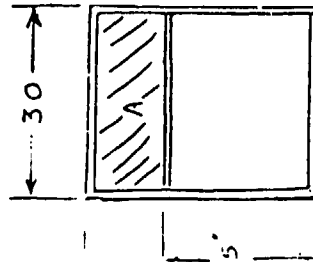
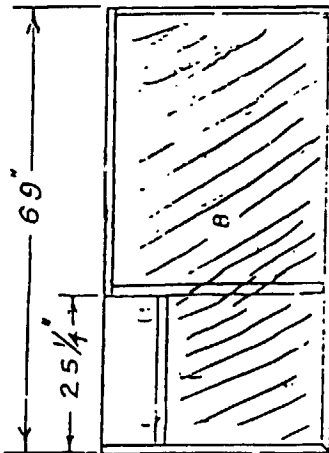
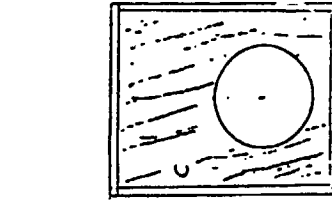
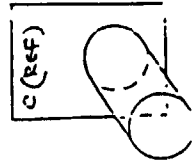
TOP: PLEXIGLASS SMT. (34 X 73)

BOTTOM: S.S. DRIP PAN
WITH AM+24-16
WELDED IN CTR
ON OUTSIDE
SURFACE

NOTE: Do Not USE
ANY GALVANIZED COMPONENTS!



FMB A 23 x 15 1/4
O.D. SHEET ALUMDUCT
STICK THRU "C"
AND SECURE TO PAN!



ORIGINAL PAGE IS
OF POOR QUALITY

C. DESIGN OF A HIGHER CAPACITY SYSTEM

The configuration chosen for the future modified system according to I. D. Smith will be three heat exchangers per test cell each in line with two blowers. At any time two heat exchangers will be utilized while the third is being regenerated due to ice buildup. Therefore, half the total gas flow from an Apollo RCS will go through each exchanger. As a result, we now have to design for 2 scfm per tube. Also we'll set the outlet gas temperature at 32°F and provide enough LN₂ to theoretically freeze out 1/2 the H₂O entering the exchanger.

The amount of H₂O to be theoretically removed is:

$$\frac{1}{2} (.4) (2 \text{ scfm}) \left(\frac{1 \text{ lb mole}}{359} \right) = .00111 \frac{\text{lb moles}}{\text{min}}$$

$$.00111 \frac{\text{lb mole}}{\text{min}} \text{ H}_2\text{O} \times 1117 \frac{\text{BTU}}{\text{lb}} \times \frac{18 \text{ lb}}{1 \text{ lb mole}} = 22.3 \frac{\text{BTU}}{\text{min}}$$

The sensible heat load is ~ 9.4 BTU/min. With a total heat load of 32 BTU/min we need about twice the previous LN₂ rate, i.e., we now need .0570 gpm of LN₂ per tube or 5 gpm for the entire exchanger.

Based on the previous discussion of forced convection boiling and a higher LN₂ rate it's probable that we'll have a higher h_1 this time, however, we'll design conservatively and use the same h_1 and h_0 .

With a load of 32 BTU/min (4 times as great as the previous case) we need 4 times the original length.

In summary, our conservative estimate yields, for the same configuration:

- a) 4 x the existing length
- b) 5 gpm LN₂

Lastly, it is worth looking at whether a finned tube arrangement will provide any advantages. According to Ludwig (Applied Process Design for the Chemical Industries, Vol. 3) "Economically, the outside coefficient should be about 1/5 or less than the inside to make a finned unit look attractive." They have a general chart which gives the reduction in number of tubes on the ordinate and the following expression on the abscissa:

$$\frac{1}{\frac{1}{h_i} + r_i} \quad / \quad \frac{1}{\frac{1}{h_o} + r_o}$$

An abscissa value of 2.38 shows a 20% reduction in the number of tubes required with fins employed. Therefore, it is recommended that the current non-fin configuration be utilized.

D. RECOMMENDATIONS

- 1) Relocate exchanger outside test stand with a stronger box.
- 2) Provide 5 gpm of LN₂ per exchanger
- 3) Use the identical units now in use only add more units to the system in series if necessary. In this regard it would be best to start with one exchanger at the higher LN₂ flow and observe the performance of the system. If insufficient keep adding modules in series until the required performance is met.
- 4) As previously indicated, one exchanger will be regenerated due to ice buildup while the other two are in operation. Data taken by A. Rakow on 5-27-83 at Test Stand 400 indicates a linear buildup of ice at the inlet section of the exchanger. In fact, toward the end of the run (Vernier RCS) the off center left and right side plate buildup was close to occluding the flow, i.e., regeneration is important.

ADDENDUM

In addition to determining the heat exchanger configuration required for testing an Apollo RCS it was decided to determine the necessary design for a Vernier RCS as well as a procedure for regenerating the exchangers through ice melt off.

Vernier

Test VRCS 2-118 (5-27-83) was used to analyze the vernier case. In this test the burn rate was .093 lbs/sec and at a cell pressure of .07 psia the inlet and outlet gas temperatures were 250°F and 320°F, respectively.

Use of the same analytical approach as the Apollo yields the data given in Table I. Most notable is the fact that in the vernier case only 1 gpm of LN₂ is needed and only 1/2 to 1 module is necessary. Therefore, if one set of two blowers can maintain altitude only one series of heat exchangers will do the job. The recommended scheme for an Apollo vs. a vernier is summarized in Figure 1.

Regeneration

A melting procedure could be the use of hot air or GN₂ on the inside of the tubes with gravity collection of a maximum of 2.0 gallons of liquid.

TABLE I. APOLLO -VS- VERNIER RCS

	<u>APOLLO</u>	<u>VERNIER</u>
Test Data		
Gas Rate/Tube, scfm	1 scfm	.43
Cell Pressure, psia	.2	.07
Anticipated Rate Based on Stiochiometry per Tube	2 scfm	.48
Inlet Gas Temperature	430°F	250°F
Outlet Gas Temperature	35°F	32°F
Heat Load per Tube if 1/2 Incoming H ₂ O is Removed	32 BTU/min	7 BTU/min
Area Required	3-4 Modules	1/2 - 1
LN ₂ Required	5 gpm	1 gpm
LN ₂ Actually Used in Test	2.5 gpm (average)	1 gpm (not reliable)

N86-14095

FLUORINE DISPOSAL

By: Allen Rakow

A preliminary design of an F_2 disposal system for HELSTF is presented here along with recommendations on operational policy and identification of potential operational problems. The analysis is based on sizing a system to handle two different modes of the HELSTF Fluorine Flow System (one operational and one catastrophic). This information should serve both as a guide to a final detailed design for HELSTF as well as a reference for subsequent monitoring and/or modification of the system which consists of a charcoal reactor followed by a dry soda lime scrubber.

Contents

- A. HELSTF F_2 Flow System - Disposal Design Criteria
- B. Literature Review
- C. Analysis
- D. Proposed System Design
- E. Recommendations

A. HELSTF F₂ FLOW SYSTEM - DISPOSAL DESIGN CRITERIA

Two cases were considered in the design of the waste disposal system:

1. TRW Pallet - consists of an 8.2 ft³ sphere filled with F₂ at 450 psi with a 1" burst disk and approximately 80 feet of 1" tubing leading up to the disposal system. Treating F₂ as an ideal gas gives 25 lbs of F₂ stored in the vessel which could be dumped through the disposal system. The following equation was used to compute the emptying time (p. 482 of Transport Phenomena by Bird, Stewart, and Lightfoot):

$$t = \frac{V/S_2}{\sqrt{\gamma \left(\frac{P_0}{P_0}\right) \left(\frac{2}{\gamma+1}\right)^{\frac{\gamma+1}{\gamma-1}}}} \left(\frac{2\gamma}{\gamma-1}\right) \left(1 - \left(\frac{\rho_1}{\rho_0}\right)^{\frac{\gamma-1}{2\gamma}}\right)$$

Where

- t = emptying time
- V = volume of tank
- S₂ = area of outlet
- γ = Cp / Cv
- P₀, ρ₀ = initial pressure and density in tank
- ρ₁ = final density

This gives an emptying time of about 8.4 seconds which is an average of 1697 scfm or approximately 3 lb/sec. Neglected here is the resistance in the line from the tank to the disposal system, therefore, these numbers represent an extreme worst case.

2. Aspirator - Composition of the F_2-N_2 mixture through the aspirator will vary; however, a 50-50 mixture by volume at 36 scfm will be taken as a typical starting condition. At $.03 \text{ lb}_m F_2/\text{sec}$ this would be 1/100 of the F_2 rate in the catastrophic case above.

B. LITERATURE REVIEW

For the purpose of summarizing several reports on F_2 disposal consider the following three step process to remove F_2 from gas streams:

Process Flow Scheme

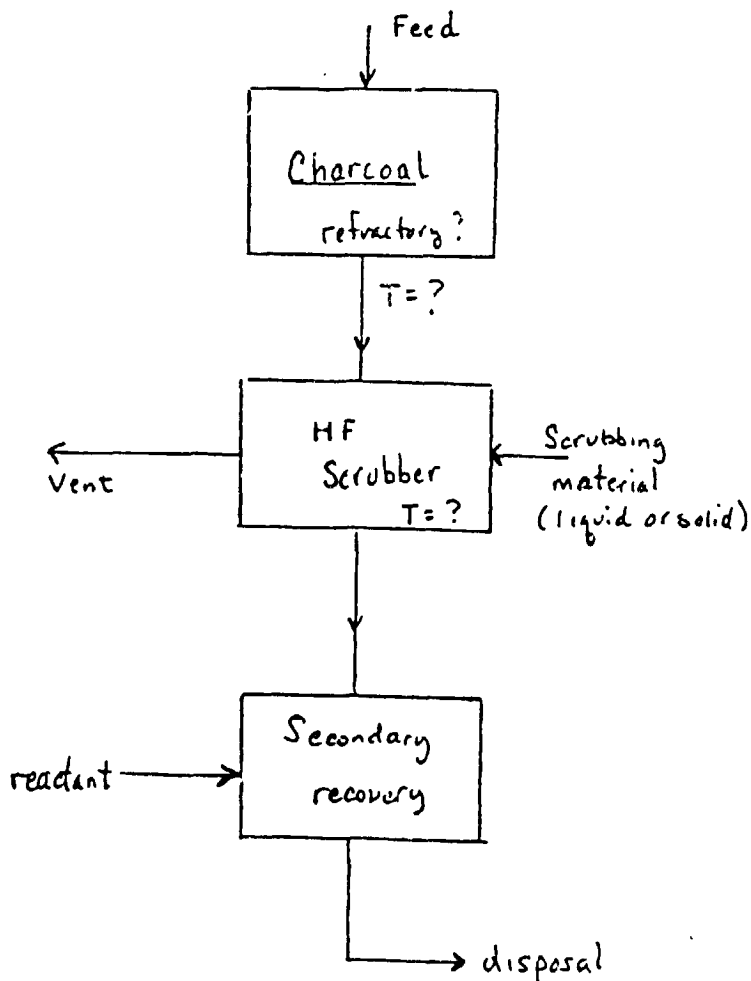


Table I is a summary of various designs and operating conditions. Note that KOH is a popular scrubbing fluid for HF. This is probably due to its greater solubility in H₂O than NaOH as well as a marked difference in solubility of KF vs. NaF in H₂O as shown in Table II. KOH would have a definite advantage over NaOH since a scrubber could run longer

Table II. Solubility* g/100 ml H₂O

NaOH	42 ⁰
KOH	97 ⁰
NaF	4.22 ¹⁸
KF	92.3 ¹⁸

*Handbook of Chemistry & Physics

on recycled liquid before an insoluble salt would form. There are several disadvantages of a KOH scrubber; however, which would make a solid system more desirable. First, the scrubbing liquid would have to be treated in a secondary step to remove KF. Secondly, the freezing point of KOH would probably be in the 20-30⁰F range which could cause problems since the system will be outdoors. Third, a packing material would be desirable to effect mass transfer, and lastly liquid handling equipment would be necessary. If a liquid system could be avoided this would be a great advantage.

TABLE I.

SOURCE	F ₂ FEED CONC.	FEED RATE	CHARCOAL TYPE	SIZE OF REACTOR	RETRACTORY	EXIT T. + COMPOSITION	SCRUBBING LIQ. + RATE	W-V-T COND.	SECONDARY PROCESS	COMMENTS + PROBLEMS
Air Products 1963	High They make OF 4 Insulator, Refrigerant	Industrial	Granulated Carbon	?	?	2000°F Some F ₂ Cryo Trap HF, for Economics	KOH (45%) Steel Tellerettes	2ppm HF?	for HF	Industrial
Air Products 1963	?	Small	Briquettes	Portable - Design Available	?	Dump to Secluded Area	Scrubber Attached Solid Na ₂ CO ₃	?	---	Portable for remote venting
Union Carbide 1975	≤ 10% (mole)	≤ 2000 $\frac{cc}{min}$	Wood, purified recommended different types tested	Lab Scale 2" x 14"	No	< 200°F < 650°F (heated)	---	< 50 ppm	---	Pure chier- coal needed to prevent non OF 4 fluorocarbon products. A /lot of F ₂ trapped in unreacted charcoal.
MESA Lewis 1968	≤ 100%	≤ 61 $\frac{lbs}{hr}$?	6.7 ft ²	Yes	?	---	5-82. ppm	---	Inufficient Data
WADD Handbook 1960	?	?	---	---	---	---	NaOH Motel, egg size fluorspar packing	Good ?	---	Inufficient Data

ORIGINAL PAGE IS
OF POOR QUALITY

TABLE I. (Continued)

SOURCE	F ₂ FEED CONC.	FEED RATE	CHARCOAL TYPE	SIZE OF REACTOR	REFRACTORY COMPOSITION	EXIT T + COMPOSITION	SCRUBBING LIQ + RATE	VENT COND.	SECONDARY PROCESS	COMMENTS + PROBLEMS
Air Force Kirtland 1978	?	?	?	1-1/3' x 2-1/3' ash removal port	Ceramic (3 inches) or Al ₂ O ₃	?	Unknown Scrubber	---	---	No info.
L. Livermore 1972	?	?	?	1-1/3' x 2-1/3' ash removal port	Ceramic (3 inches) or Al ₂ O ₃	?	KOH with KI to speed reaction	---	Recycle Liq.	
General Dynamics I 1971	Small-100%	3-600 lb/hr max	?	---	---	---	KOH-10% 200 gpm 7 ft dia tank	< 1000 ppm ?	Neutralize KF with lime to make CaF ₂	Claim Allied Chem has several yrs. success with system
General Dynamics - II 1971	?	9000 lb / hr combur 'ion rate	Graded Oak Min. ash and hydro-carbon	Twice stoichio-metric	Firebrick vapor barrier over charcoal	? 25200R max	F ₂ + H ₂ O HF + O ₂	Gas Velocity < 1 fpm	HF + CaCO ₃ CaF ₂ + H ₂ O + CO ₂	---

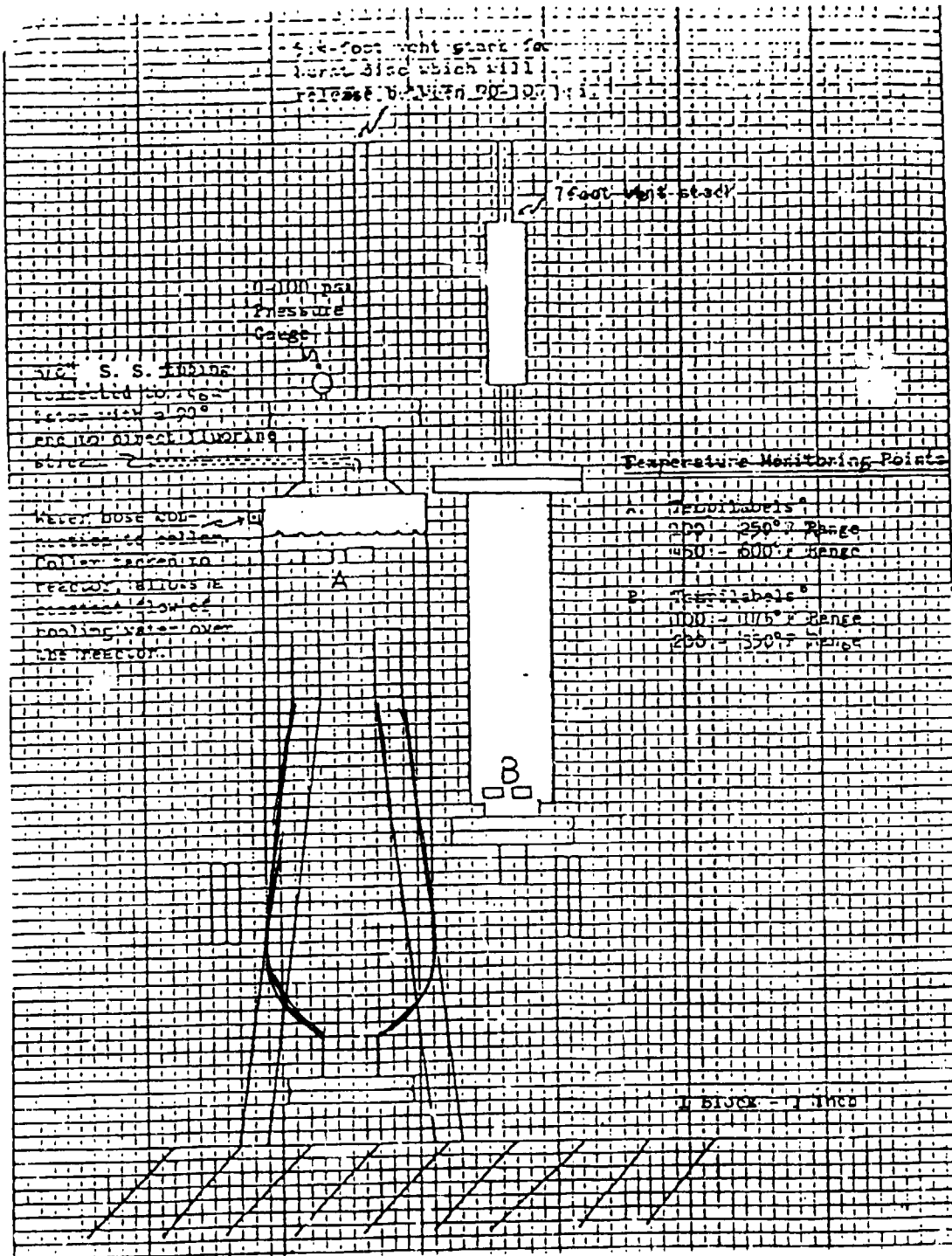
NASA Lewis strongly recommends a charcoal reactor for a first step and Air Products has developed a portable system (Figures 1 and 2) to handle small quantities of F_2 (dumping a single cylinder in a remote location). The Air Products system is an all solid system, i.e., Na_2CO_3 is used in the second stage to remove HF. Note also that the charcoal system has water cooling available since the heat of reaction is very high for $C+2F_2 \rightarrow CF_4$.

It should be noted that Union Carbide, as a result of a lab scale study ($< 10\% F_2$ in N_2 , < 2000 cc/min), recommended the purification of wood charcoal by heating to $850^\circ C$ to eliminate the formation of precipitates from non- CF_4 fluoro carbons formed. In the same study they found that for dry charcoal and $1\% F_2$ in N_2 with no heat source other than heat of reaction conversion of F_2 to CF_4 was poor (5800 ppm F_2 in effluent). Whether these problems will appear at higher rates and concentrations is doubtful. Nevertheless, this information should be kept in mind should any problems arise in the charcoal reactor (they resorted to sintered metal filtering and heating the reactor to alleviate these problems).

H. Schmidt of NASA Lewis (Feb. 1959) concluded that "for engineering design approximations, the stoichiometric charcoal requirement is 17.5 pounds charcoal per 100 pounds of fluorine gas to be burned, plus minimum charcoal for maintaining reaction efficiency toward the end of the burning period." Also mentioned is "low F_2 flowrate through high capacity

ORIGINAL PAGE IS
OF POOR QUALITY

19 March 1979



Fluorine Disposal Unit

Figure 1

ORIGINAL PAGE IS
OF POOR QUALITY

Portable F₂ Disposal Unit

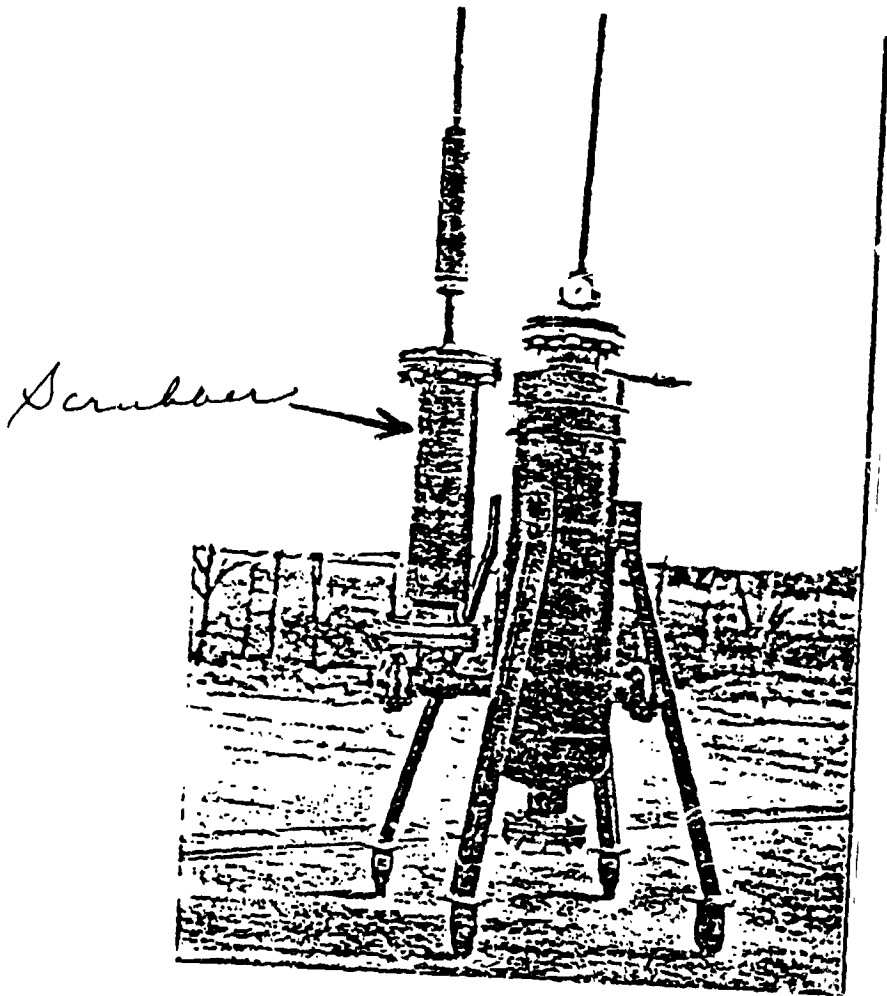


Figure 2

reactors has on two occasions allowed excessive heating of the F_2 inlet nozzles in uncooled reactors, causing F_2 attack on the nozzles and refractory lining in the lid. Higher flowrates through the nozzles provided sufficient cooling to prevent this attack. in one test the equipment was operated at over 600 pounds per hour for approximately three minutes (equivalent to 30 lb F_2) without damage to the reactor." One can conclude from this report that careful attention must be paid to the use of cooling to prevent damage to the system. In fact, it is also mentioned that "with a furnace grating support with bottom inlet feed, the reaction process tends to consume the grating."

NASA Lewis concluded that only the external surfaces of the charcoal particles are active in the reaction and that the controlling factor in the reaction is probably "mass transfer by counter diffusion of the reactants and products into and away from the solid surface through the gas layer." They then recommend the following as a design equation:

$$R = \frac{65V}{D} \text{ lb } F_2/\text{hr}$$

where R = F_2 rate in lb/hr - max allowable

V = charcoal volume, ft^3

D = particle diameter, in.

Lastly, it should be mentioned that no attempt has been made here to review KOH liquid scrubbing since a solid bed system is recommended. An extensive literature exists in this area, however, should interest arise. Also, there are several industrial processes and patents by the Japanese, Russians, and Germans on F₂ removal which could be studied.

C. ANALYSIS

For the two cases described in Section A the following calculations are made:

1. Amount of charcoal required
2. Amount of soda lime required
3. Exit gas temperature from charcoal
4. Exit gas temperature from soda lime
5. Pressure drop thru charcoal and soda lime

1. Amount of Charcoal Required

a) TRW Pallet - From a stoichiometric point of view we have 25 lbs of F₂, therefore, we need":

$$25 \times \frac{17.5}{100} \quad 4.4 \text{ lbs charcoal}$$

If we were to use the NASA design equation $R = \frac{65V}{D}$ for

3/8" charcoal and a rate of 1697 scfm (10,780 lb/hr) we'd need 62 ft³ of charcoal. Considering a void volume of .4 and a charcoal density of 12 lb/ft³ this would be 446 lbs of charcoal.

We can also use the following equation to compute the volume of charcoal required to achieve a particular exit concentration of F₂ from the bed:

$$V = \frac{G}{akg\bar{c}} \ln \left(\frac{Y_{A_1}}{Y_{A_2}} \right)$$

- where V = volume of bed, ft³
- G = molar rate of gas, $\frac{\text{lb moles}}{\text{min}}$
- a = effective surface area/vol of bed, $\frac{\text{ft}^2}{\text{ft}^3}$
- kg = mass transfer coefficient, ft/min
- \bar{c} = molar density of gas = $\frac{P}{RT} = \frac{\text{lb moles}}{\text{ft}^3}$
- Y_{A₁} = mole fxn of F₂ into reactor
- Y_{A₂} = mole` fxn of F₂ out of reactor

This equation is based on steady isothermal flow and diffusion control, i.e., as soon as the F_2 reaches the charcoal surface it reacts instantaneously with the carbon on the surface only.

For the TRW pallet case, $Y_{A_1} = 1$, $G = 4.73 \frac{\text{lb mole}}{\text{min}}$, $C = \frac{P}{RT} =$

$$\frac{14.7 \text{ psi} \times 144}{1544 (2000^\circ\text{R})} = .0007 \frac{\text{lb moles}}{\text{ft}^3} \text{ assuming a max T of } 2000^\circ\text{R in}$$

the reactor, $a = 115 \frac{\text{ft}^2}{\text{ft}^3}$ for 3/8" particles

and set $Y_{A_2} = 1 \text{ ppm} = 10^{-6}$

From Figure 3 we can take kg to be 10 cm/sec or 19.7 ft/min.

$$\text{so } V = \frac{4.73}{(115)(19.7)(.0007)} \ln 10^6$$

or $V = 41.2 \text{ ft}^3$ (not drastically different from the NASA design equation)

This would be 297 lbs of charcoal.

b) Aspirator

1) NASA Design:

$$18 \text{ scfm} \times \frac{1 \text{ lb mole}}{359 \text{ ft}^3} \times \frac{60 \text{ min}}{\text{hr}} \times \frac{38 \text{ lb}}{\text{lb mole}} = 114 \frac{\text{lb}}{\text{hr}}$$

$$V = \frac{114}{65} \times \frac{3}{8} = .65 \text{ ft}^3 \text{ (4.7 lb charcoal)}$$

2) Diffusion Control Equation:

$$Y_{A_1} = .5, G = .1 \frac{\text{lb mole}}{\text{min}}$$

$$k_g = 2 \text{ cm/sec} = 3.94 \text{ ft/min}$$

$$V = \frac{.1}{115 (3.54) (.0007)} \ln \frac{.5}{10^{-6}}$$

$$V = 4.13 \text{ ft}^3 \text{ (30 lb charcoal)}$$

ORIGINAL PAGE IS
OF POOR QUALITY

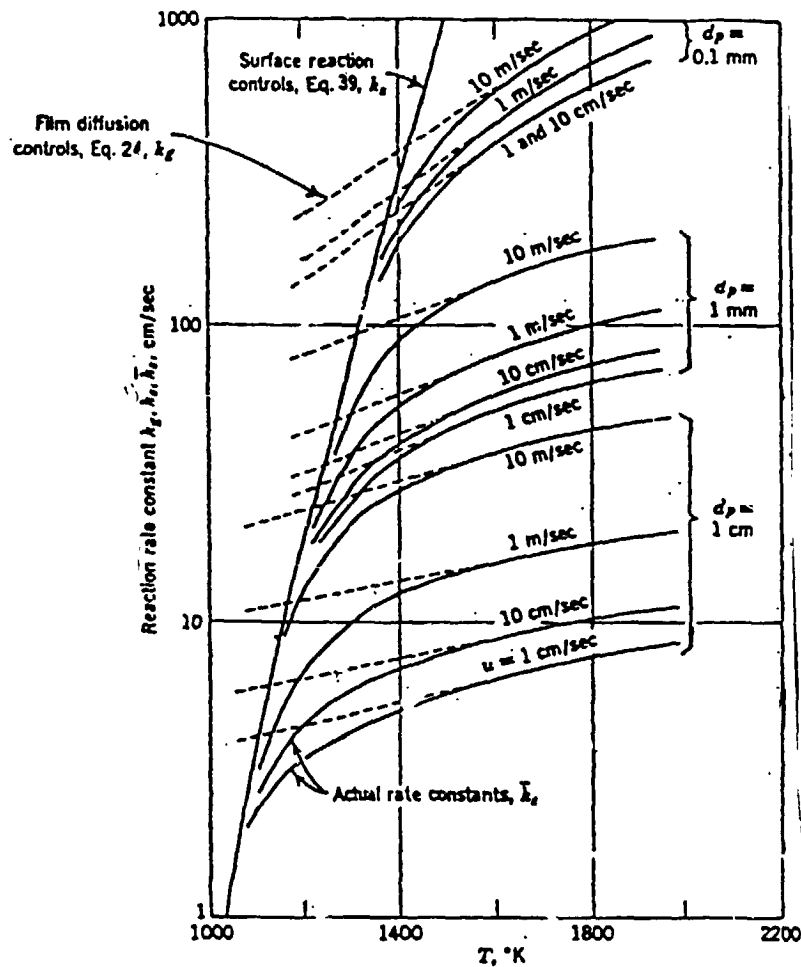


FIGURE 12. Rate of combustion of pure carbon particles, adapted from Yagi and Kunii (1955)

which the reaction kinetics, flow characteristics, and size distribution of solids are known.

Referring to Fig. 13, let us discuss briefly the various types of contacting in gas-solid operations.

Solids and Gas Both in Plug Flow. When solids and gas pass through the reactor in plug flow, their compositions will change during passage. In addition, such operations are usually nonisothermal.

Figure 3

2. Amount of Soda Lime Required

a) TRW Pallett - Assuming 10% HF out of the charcoal due to the residual H_2O in the charcoal and the same model (diffusion control) as the charcoal then:

$$Y_{A_1} = .1$$

$$a = 445 \frac{ft^2}{ft^3} \text{ for } 1/8" \text{ soda lime particles}$$

$$G = 2.36$$

Since there are half as many moles of gas ($C+2F_2 \rightarrow CF_4$) then:

$$V = \frac{2.36}{445 (19.7) (.0007)} \ln \frac{.1}{10^{-6}}$$

$$V = 4.42 \text{ ft}^3 \text{ (at a density of } 125 \frac{lbs}{ft^3} \text{ and a void}$$

fraction of .4 this would be 331 lbs of soda lime

b) Aspirator

$$\frac{4.42}{41.2} \times 4.13 = .44 \text{ ft}^3 \rightarrow 33 \text{ lbs of soda lime}$$

3. Exit Gas T From Charcoal

a) TRW Pallet - We'll assume that an equilibrium is established whereby the charcoal temperature rises to that of the exit gas and the system is adiabatic (no transfer through walls).

The heat of reaction of $C+2F_2 \rightarrow CF_4$ is 222 kcal/g mole.

$$\frac{25 \text{ lbs } F_2}{38 \text{ lbs/lb mole}} \times \frac{454 \text{ g mole}}{\text{lb mole}} \times \frac{222 \text{ kcal}}{\text{g mole}} = 66,308 \text{ kcal}$$

$$C_p \text{ carbon} = \frac{.387 \text{ cal}}{\text{g}^\circ\text{C}}$$

$$C_{p\text{gas}} = .25 \frac{\text{cal}}{\text{g}^\circ\text{C}}$$

$$66,308,000 = (446 \text{ lbs charcoal}) \left(\frac{454 \text{ g}}{\text{lb}} \right) (.387) (\Delta T) + 25(454) (.25) (\Delta T)$$

$$\Delta T = 816^\circ\text{C} = 1469^\circ\text{F}$$

$$\text{If the } F_2 \text{ comes in at } 70^\circ\text{F} \rightarrow \text{exit } T = \begin{matrix} 1530^\circ\text{F} \\ \text{or} \\ \sim 2000^\circ\text{R} \end{matrix}$$

b) Aspirator

Basis: 10 minutes of operation

$$\frac{18 \text{ scfm} \times 10 \text{ min}}{359} = .5 \text{ lb moles}$$

$$.5 \times 454 \times 222 = 50,394 \text{ kcal}$$

With the small quantity of charcoal required for this system it is clear that extremely high temperatures would be reached (of course, it is really necessary to know exactly the inlet F_2 concentration during aspiration to pin this number down).

Therefore, it is apparent that the system required for the TRW pallet case should be used for the aspirator as well to prevent excessive temperatures!

4. EXIST GAS TEMPERATURE FROM SODA LIME

a) TRW Pallett - Treating .1 lb mole HF with 331 lbs of soda lime would give a $\Delta T = 407^{\circ}F$. This would result in a temperature of about $2000^{\circ}F$ out of the soda lime (if there were no cooling between the charcoal reactor and soda lime system).

b) Aspirator - not considered.

5. PRESSURE DROP THRU CHARCOAL

a) TRW Case

Ergun equation:

$$\frac{\Delta P}{z} \frac{g_c \epsilon^3 d_p \rho_g}{(1-\epsilon) G'^2} = \frac{150 (1-\epsilon)}{Re} + 1.75$$

where $\frac{\Delta P}{z}$ = pressure drop per unit length of packed bed

ϵ = void volume

d_p = diameter of particles

ρ_g = gas density

G' = superficial mass velocity - mass/(area x time)

Re = $d_p G' / \mu$

μ = viscosity of gas

For the TRW case with a reactor 4' x 4' x 4':

$$G' = \frac{25 \text{ lbm}}{8.4 \text{ sec}} \times \frac{1}{16 \text{ ft}^2} = .186 \frac{\text{lbm}}{\text{sec ft}^2}$$

$$dp = 3/8''/12 = \frac{1}{32 \text{ ft}} \quad \epsilon = 0.4$$

$$\rho_G = \frac{(14.7)(144)(38)}{(1544)(2000)} = .026 \frac{\text{lbm}}{\text{ft}^3}$$

$$\mu \approx 7 \text{ lbf} \frac{\text{sec}}{\text{ft}^2} \times 10^{-9}$$

$$R_e = \frac{1}{\frac{(32)(.186)}{(7 \times 10^{-9})(32)}} \approx 26,000 \quad [\text{1st term negligible}]$$

$$\therefore \frac{\Delta P}{2} \frac{g_c \epsilon^3 dp}{(1-\epsilon) G'^2} \rho_g = 1.75$$

$$\frac{\Delta P}{2} = \frac{(1.75)(.6)(.186)^2}{(32.2)(.4)^3(1/32)(.026)} = 21.7 \frac{\text{lbf/ft}^2}{\text{ft}}$$

$$\frac{\Delta P}{2} = .15 \text{ psi/ft}$$

$$\Delta P = .6 \text{ psi (add a bit more [1 psi total] for soda lime)}$$

b) Aspirator - Not considered.

D. PROPOSED SYSTEM DESIGN

1. Charcoal Reactor - A volume of 62 ft³ (446 lbs of wood charcoal, 3/8" diameter) is required. The General Dynamics Sycamore Canyon Reactor (GDSCR) would be a suitable design. It is basically a cylindrical furnace with a firebrick floor, firebrick walls of 4-1/2 in. x 9 in. straights and wedges, and a conical sheet metal hood. Since the GDSCR was designed for 528 cu ft with 2 ft of ullage above the charcoal the GDSCR could be scaled down by 1/3 in cross-sectional area and 1/3 in height to give the required HELSTF volume. The inlet and outlet lines will of course be smaller but the inlet should be equipped with cooling water and the polyethylene isn't needed since the HELSTF system will be used for normal operation. Attached is a description of the GDSCR system.

2. Soda Lime Scrubber - A volume of 4.42 ft³ (331 lbs) is required. Fischer Chemical (Wendy 800/527-5920) can supply 14 kg containers (6-12 mesh) at \$135 per container. This amount should be sufficient for each aspiration. The design for this system could be the same as the GDSCR only scaled down to the smaller volume.

GDSCR SYSTEM DESCRIPTION

Distribution of fluorine flow in a charcoal charge cannot assure stoichiometric combustion. The reactor is therefore designed to hold twice the theoretically required charge of charcoal, giving sufficient bed depth to prevent channelling and blow-through, take care of ash content, and provide a safety margin. Nominally designed for disposal of 20,000 pounds of fluorine boiled off from the vehicle tank in an emergency, the reactor is also capable of handling the 30,000 pounds of fluorine in the storage tank, if necessary.

Density of graded oak charcoal, with a minimum ash and hydrocarbon content, is approximately 12 lb/cu ft. Theoretical volume of charcoal required for the reactor unit, Eq. 3-1, is therefore:

$$3160 \text{ lb} + 12 = 264 \text{ cu ft}$$

or 528 cubic feet with the double volume for allowances. A 9-ft. dia. cylindrical chamber 17 feet in height is adequate for the volume required, including a 28-in. ullage above charcoal level.

The reactor unit is shown in cross-section in Figure 3-15. It is basically a cylindrical furnace with a firebrick floor, firebrick walls of 4 1/2-in. x 9-in. straights and wedges, and a conical sheet metal hood. Gaseous fluorine is introduced through a 6-in. inlet, water-jacketed and protected from furnace heat by a firebrick injector tunnel, or igloo. Diffusion of fluorine into the charcoal is through a three-course diffuser as shown in Section A-A, Figure 3-15. The top and bottom courses are mortared. The intermediate course is recessed, with the vertical joints unmortared for fluorine egress. This is the final configuration of the fluorine injection system of the General Dynamics Sycamore Canyon reactor, successfully used for disposal of gaseous FLOX from Atlas vehicle tank tests.

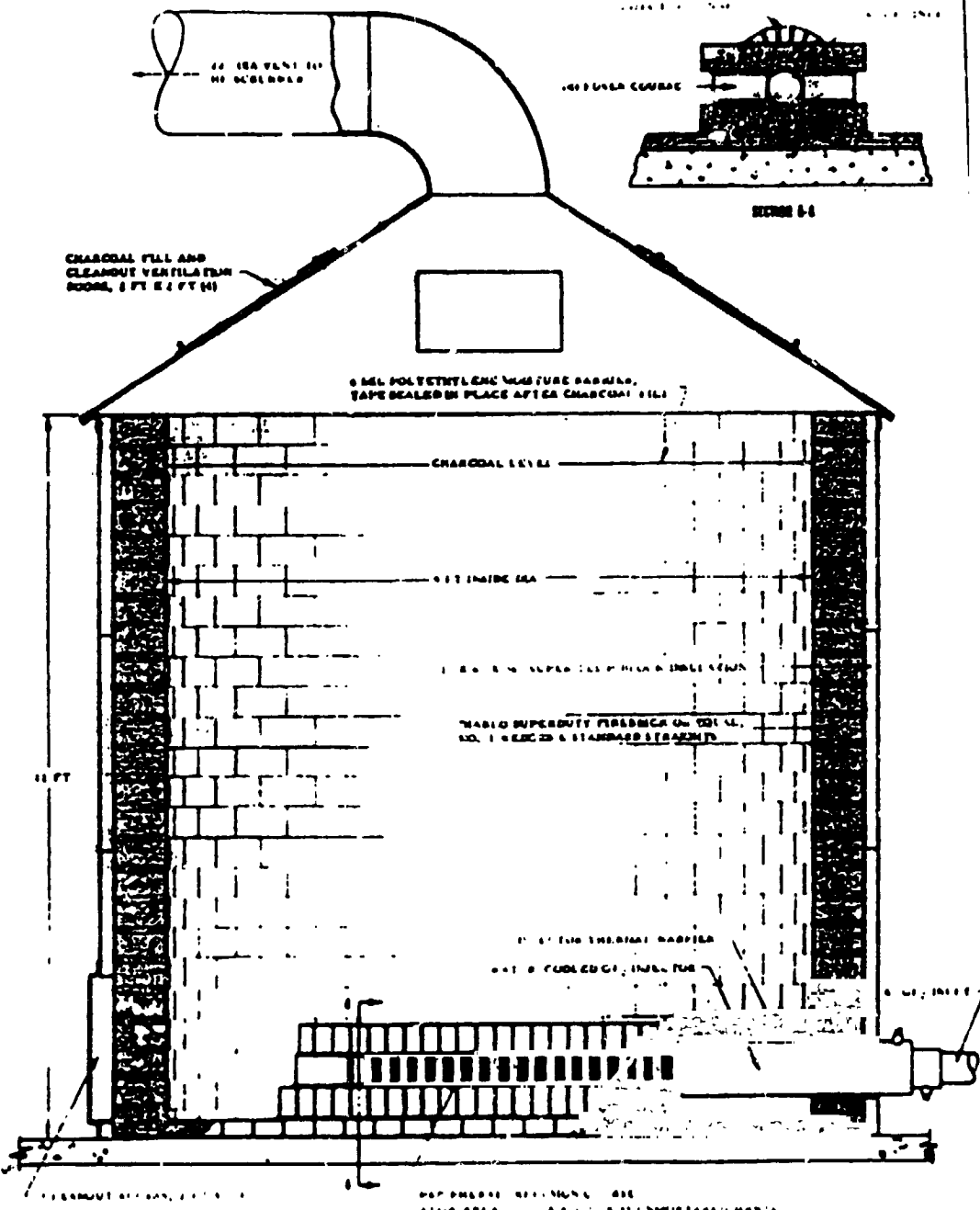
The hood of the reactor is fitted with four 2-ft x 2-ft swing-doors for charcoal loading and ventilation during cleanout. If the reactor is ever used, it is refurbished by first opening the ground-level cleanout access door and knocking out a firebrick soft patch. With the upper doors open for ventilation, ash and excess charcoal can be removed through the lower door. After cleaning and inspection, the access opening is firebricked, the door closed, and the furnace charged with charcoal through the upper loading doors. After charging, the charcoal is leveled and a 4-mil polyethylene vapor-barrier sheet laid in place and taped, to exclude atmospheric humidity and retain the charcoal in a dry state.

The burner vent line is sized for a maximum combustion rate of 9000 pounds of fluorine per hour, producing 2.9 pounds of CF_4 per second. The 20-in. dia. line delivers combustion products at a maximum velocity of 30 fps to the scrubber.

Estimated cost of the reactor unit is \$7,500, including fabrication of the water-cooled injector, sheet-metal work, and labor.

ORIGINAL PAGE IS
OF POOR QUALITY

GDCSR SYSTEM DESIGN



E. RECOMMENDATIONS

1. Measure F_2 and HF concentrations in effluent during test run to confirm efficiency of system (temperature would also be useful).
2. Use extreme caution in cleaning and replenishing system (after 10 aspirations) since fluorine could be present.
3. Should cooling water be unavailable make sure that F_2 metal inlet tube is replaced with refractory.
4. Same approach should be taken with soda lime scrubber.
5. System requires 3/8" wood charcoal, should particle entrainment become a problem consider adding a filter between the charcoal and soda lime reactors.

N86-14096

SPARGER SYSTEM FOR MMH-HELIUM VENTS

Based on a calculated vent flow rate and MMH concentration, a Tl-59 program was run to determine total sparger hole area for a given sparger inlet pressure. Hole diameter is determined from a mass transfer analysis in the holding tank to achieve complete capture of MMH. In addition, based on oxidation kinetics and vapor pressure data, MMH atmospheric concentrations are determined 2 ft above the holding tank.

By: A. Rakow

CONTENTS

- A. MMH Vent Rates
- B. Sparger Program
- C. Mass Transfer Analysis in Tank
- D. Mass Transfer Analysis from Tank to Atmosphere
- E. Recommendations

A. MMH Vent Rates

A typical venting profile is given on the attached TPS. With 800 gallons of ullage and the assumption of ideal behavior (in this pressure range helium exhibits heating rather than cooling upon expansion, but only about 0.06°C per atm; therefore, isothermal expansion is reasonable) the volumetric rate would be 1459 scfm during the first 10 seconds. With a vapor pressure of 0.957 psia the MMH concentration would be about 3400 ppm. At the completion of the vent the rate would be about 162 scfm and the concentration (assuming rapid vapor equilibrium during venting) 16,780 ppm.

For the purpose of designing a sparger, let's take 1500 scfm as the max flow and 100 psi as the sparger inlet pressure (either an analysis of ΔP in the vent system or pressure measurement during a vent is necessary to determine this parameter).

For the purpose of analysing dispersion of MMH to the atmosphere above the holding tank, we need to estimate the total amount of MMH vented. The average flow rate is 800 scfm for 3 minutes, i.e., we're venting 2400 scf which is 6.7 lb moles. At an average concentration of about 10,000 ppm MMH, we would be venting 0.067 lb moles of MMH.

B. Sparger Program

The attached sparger program will determine the total hole area and area distribution required for a liquid sparger.

Since our case is a gas dispersed into a liquid phase, we have to employ the gas orifice equation instead of equation (9) in the attached article by Mink.

The gas orifice equation:

$$W = 1891 \gamma d_o^2 C \left(\frac{\Delta P}{V_1} \right)^{\frac{1}{2}}$$

Where

$$\begin{aligned} W &= \text{lb/hr} \\ \Delta P &= \text{psi} \\ V_1 &= \text{ft}^3/\text{lb} \\ d_o &= \text{orifice diameter, in.} \end{aligned}$$

converts to

$$a = \frac{.26}{1830} \frac{Q}{[\Delta P/\rho]^{\frac{1}{2}}} \quad \text{using a value of 0.6 for both } \gamma \text{ and } C.$$

Therefore, equation (9) in the article by Mink probably overpredicts the area by a factor of 4. Keeping this in mind, the conditions of 1500 scfm and 100 psi were run, giving the following results:

For A = 11,220 GPM
 B = 100 psi
 C = 20 psi (includes 9-ft head in tank)
 D = 2 inches (Sparger I.D.)
 A' = 0.011
 B' = 0.011
 C' = 7 ft

$$a = 0.72 \text{ in}^2$$

Since this is an overprediction, we probably only need 0.18 in² total hole area (of course, it is extremely important to know the actual sparger inlet pressure; our value of 100 psi is used for illustrative purposes).

C. Mass Transfer Analysis in Holding Tank

1. Rate

The mass transfer rate to the tank can be approximated by:

$$N_A = \sqrt{\frac{4 D_{AB} V_t}{\pi d_p}} C_{A_0}$$

Where $N_A = \frac{\text{g moles}}{\text{CM}^2 \text{ sec}}$ MMH transferred to water

D_{AB} = diffusivity of MMH in H₂O
 V_t = terminal velocity of rise of drop
 C_{A_0} = solubility of MMH in H₂O in moles/volume
 d_p = drop diameter

In order to use this equation we need to determine the drop diameter, d_p , and the terminal velocity.

The terminal velocity is given by:

$$V_t = \sqrt{\frac{2 \Delta g_c}{d_p \rho_L} + \frac{g d_p}{2}}$$

Where Δ is the surface tension of water and ρ_L is liquid density.

The particle (drop) diameter in inches is given by:

$$d_p = 0.279 (Re_0)^{-0.05}$$

based on a jet correlation (p. 141, Treybal).

Using an upper limit of 50,000 on Re_0 , we get 0.16 inches for the bubble diameter. This gives a value of 0.77 ft/sec for V_t .

Plugging these values into the equation for N_A gives a very high rate of mass transfer indicating that most, if not all of the MMH, should be absorbed.

2. Orifice Diameter and Number of Holes

$$\text{The orifice Reynolds's number } Re_o = \frac{d_o v_o \rho}{\mu}$$

Where V_o is the velocity in the orifice and ρ and μ are density and viscosity, respectively.

Using the criterion of $Re_o = 50,000$, we get the following two equations:

For 1500 scfm

$$1. \quad n d_o = 11.36$$

$$2. \quad \pi \left(\frac{d_o}{2} \right)^2 n = a = 0.18 \text{ in}^2$$

where n = no. of holes

$$\text{Therefore } \frac{\pi d_o (11.36)}{4} = 0.18$$

$$\text{or } d_o = 0.020 \text{ inches}$$

$$\therefore n = 568$$

So 568 holes at 0.02 inches per hole (1/50") should do the job in this case.

D. Mass Transfer Analysis from Tank to Atmosphere

This analysis is based on the following assumptions:

1. 0.067 lb moles of MMH are completely absorbed from the sparger during a vent in a well mixed tank of water 10' X 5' X 9' filled to the 6-foot level.
2. MMH is depleted by two mechanisms
 - a. diffusion from the gas liquid interface through 3 ft of air to the top of the tank where it is swept away (zero concentration at top)
 - b. in the tank MMH disappears by oxidation at a rate of 100 ppm/day (This number is an average of open pan tests done by Eric Miller and data in the Florida Tech handbook.)

3. the Henry's law relationship for MMH is $y = mx$, where $m = 0.05$, and y and x are the mole fractions of MMH in air and H_2O , respectively

4. equilibrium exists at the gas liquid interface

5. diffusion in the gas phase is quasi-steady and unidirectional

First, let's compute the initial mole fraction of MMH in the tank, X_{l0} , in ppm:

$$300 \text{ ft}^3 \text{ H}_2\text{O} \times 62.4 \frac{\text{lb}}{\text{ft}^3} \times 1 \frac{\text{lb mole}}{18 \text{ lb}} = 1040 \text{ lb moles H}_2\text{O}$$

$$\frac{.067}{1040} = 64 \text{ ppm} = X_{l0}$$

The diffusion rate in the gas phase is given by

$$N_A = \frac{D_{\text{MMH-Air}} A C (0.05)(X_l)}{l}$$

Where N_A - flux in moles/area time
 $D_{\text{MMH-Air}}$ - diffusivity of MMH in air
 A - cross sectional area of tank
 C - gas molar density
 X_l - mole fxn of MMH in tank at any time, t
 l - distance between the gas-liquid interface and the top of the tank

Using a value of $0.2 \text{ cm}^2/\text{sec} = 0.775 \frac{\text{ft}^2}{\text{hr}}$

for $D_{\text{MMH-Air}}$ we get

$$N_A = 0.00177 X_l(t) \frac{\text{moles}}{\text{hr}}$$

Now we can write a mass balance for MMH in the tank to compute X_l as a function of time, t .

rate of accumulation = - rate of depletion - rate at which MMH leaves
of MMH in tank by oxidation thru interface

or

$$1040 \frac{dX_l}{dt} = -10^{-4} (1040) \frac{.1 \text{ day}}{24 \text{ hours}} - 0.00177 X_l$$

where t is in hours

The solution to this equation is:

$$X_{\ell} = 2.35(e^{-1.7 \times 10^{-6}t} - 1) + X_{\ell 0} e^{-1.7 \times 10^{-6}t}$$

or $X_{\ell} = (X_{\ell 0} + 2.35) (e^{-1.7 \times 10^{-6}t}) - 2.35$

for complete depletion $X_{\ell} = 0$ and $X_{\ell 0} = 64 \times 10^{-6}$

so
$$e^{-1.7 \times 10^{-6}t} = \frac{2.35}{2.35 + 64 \times 10^{-6}} = 0.99997$$

$$-1.7 \times 10^{-6}t = -0.0000272337$$

$$t = 16 \text{ hours}$$

Lastly, let's look at the concentration two feet above the gas-liquid interface initially (this will drop off to zero at 16 hours).

The concentration profile above the liquid is:

$$- \frac{dy_A}{dx} = 1.06 \times 10^{-6}$$

initially at the gas liquid interface we have $Y_A = 0.05 (64 \times 10^{-6})$
(where $X = 0$)

$$Y_A = 3.2 \times 10^{-6} = 3.2 \text{ ppm}$$

so
$$\frac{3.2 - Y_{2ft}}{2ft} = 1.06$$

$$Y_{2ft} = 1.08 \text{ ppm}$$

Any effort to speed up the oxidation process such as low ph should enable the maintenance of low concentration above the tank. Forced convection would also do the job.

E. Recommendations

1. Determine the holding tank inlet pressure during a vent
2. Measure MMH in the tank and in the vapor space above the tank during a vent with current system
3. Do 1 and 2 after sparger is installed
4. Consider agitation if bubble coalescence occurs
5. Determine treatment schedule and/or second stage process to meet EPA standards for atmospheric MMH

ORIGINAL PAGE IS
OF POOR QUALITY

NASA JSC WSTF
TEST PREPARATION SHEET
CONTINUATION SHEET

Page 2 of 2
2/5/83

TRN NO. 4-OTM-763
MOD NO.

ITEM NO.	DESCRIPTION CONTINUED						WORKED	INSPECTED
							SHOP	WADA
4	Announce Fuel Vapor Tube Vented to Pond							
5	Cycle DF32 rpm for 10 seconds. Record Pressures below. Repeat cycles until ACU is approx 40 PSIG							
	SEC	PSIA FADFHP	PSIG DF60	Sec	62P	60		
	Start	298	297	150	68	59		
	10	262	260	160	62	54		
	20	231	227	170	57	49		
	30	207	202	180	53	44		
	40	187	182					
	50	167	162					
	60	152	145					
	70	140	135					
	80	129	120					
	90	118	112					
	100	106	100					
	110	98	85					
	120	89	80					
	130	81	75					
	140	75	67					
6	Fully decrease DF110, close DF111, and open DF02							
<p><i>[Signature]</i></p>				<p>CF [Signature] 2-28-83</p> <p>[Signature] 2-28-83</p>				

1200 Gal. ON BOARD

Hole-area distribution for liquid spargers

This TI-59 program does the tedious calculations involved in designing spargers, and prints (or displays) the results.

William H. Mink, Battelle Columbus Laboratories **

□ In many operations, it is necessary to sparge a liquid or gas into another fluid; frequently, a uniform distribution is desired. Since, owing to frictional losses, the pressure decreases as the fluid flows down the sparger pipe, the hole area must increase along the length of the sparger to maintain uniform flow from it.

H. W. Cooper† has developed a series of relationships that are useful in calculating sparger hole area for uniform distribution. It has been pointed out that these equations are in error because the originator neglected to include the effect of velocity head. This velocity-head effect can be significant. Only when the pipe L/D ratio is high or when flowrates are low do the Cooper equations provide an approximation. The author has developed a new program, based on a stepwise calculation, which yields correct hole sizes regardless of L/D ratio or flowrates.

Calculational approach

The pressure causing flow through any orifice is the difference between the static pressure at the point of the orifice and the ambient pressure. The static pressure is the total pressure less the velocity head and any frictional loss:

$$P_t = P_s - P_{va} - P_f \quad (1)$$

For the sparger, the total inlet pressure is:

$$P_{t, in} = P_{s, in} + P_{va, in} \quad (2)$$

In Eq. (1) and (2),

$$P_{va} = \frac{V^2 \rho}{2g(144)} = \frac{V^2 \rho}{9,274} \quad (3)$$

$$V = \frac{0.4085Q}{d^2} \quad (4)$$

and

$$P_f = \frac{FV^2 \rho L / 10}{d(193)} \quad (5)$$

** For information about the author see p. 228

† Cooper, Herbert W., Area Allocation for Distributor Pipes, Chem. Eng. Oct.

The friction factor, F , depends on the Reynolds number, N_{Re} :

$$F = 16/N_{Re}, \text{ if } N_{Re} < 2,100 \quad (6)$$

$$F = 0.0035 + 0.264(N_{Re})^{-0.42}, \text{ if } N_{Re} \geq 2,100 \quad (7)$$

where

$$N_{Re} = \frac{124 \bar{v} d \rho}{\mu} \quad (8)$$

The orifice area can be calculated by the orifice equation, which can be simplified to:

$$a = Q / 1830[(P_s - P_a)/\rho]^{1/2} \quad (9)$$

A program has been developed for the TI-59/PC-100A, using the above procedure. The program calculates the hole area for each 10% of sparger length (using Eq. (9)).

The program is shown in Table I. Certain constants for the calculations and for the alphanumeric operations must be stored in the data registers. These are shown in Table II. Once the calculator has been programmed and the constants stored, both the program and data register contents may be recorded on magnetic cards for future use.

User instructions for calculation of the sparger hole areas that will achieve uniform flow distribution are given in Table III.

When running this program, the printer first prints out the entered data. Next, it prints the hole area for each 10% of sparger length, and finally it prints the total sparger hole area.

Procedure

For the calculation of the hole area in the first section (first 10% of length), the flowrate down the pipe is set at the entered value. For each subsequent hole-area calcu-

ORIGINAL PAGE IS
OF POOR QUALITY

Program for use in calculating hole area of liquid spargers

Table 1

Location	Code	Key															
000	76	LBL	060	69	DP	120	69	DP	180	04	4	240	03	3	300	73	RC*
001	11	A	061	05	05	121	00	00	181	95	=	241	00	0	301	09	09
002	42	STD	062	98	ADV	122	98	ADV	182	42	STD	242	95	=	302	69	DP
003	01	01	063	98	ADV	123	98	ADV	183	14	14	243	42	STD	303	04	04
004	25	CLR	064	43	RCL	124	43	RCL	184	02	2	244	17	17	304	43	RCL
005	91	R/S	065	21	21	125	19	19	185	01	1	245	87	IFF	305	10	10
006	76	LBL	066	69	DP	126	69	DP	186	00	0	246	01	01	306	44	SUM
007	12	B	067	04	04	127	01	01	187	00	0	247	89	*	307	08	08
008	42	STD	068	43	RCL	128	43	RCL	188	32	XIT	248	76	LBL	308	58	FIX
009	02	02	069	01	01	129	20	20	189	43	RCL	249	77	GE	309	03	03
010	25	CLR	070	69	DP	130	69	DP	190	13	13	250	29	CP	310	69	DP
011	91	R/S	071	06	06	131	02	02	191	65	x	251	43	RCL	311	06	06
012	76	LBL	072	43	RCL	132	06	6	192	01	1	252	18	18	312	58	FIX
013	13	C	073	22	22	133	01	1	193	02	2	253	75	-	313	09	09
014	42	STD	074	69	DP	134	69	DP	194	04	4	254	43	RCL	314	01	1
015	03	03	075	04	04	135	04	04	195	65	x	255	17	17	315	44	SUM
016	25	CLR	076	43	RCL	136	69	DP	196	43	RCL	256	95	=	316	09	09
017	91	R/S	077	02	02	137	05	05	197	04	04	257	42	STD	317	61	CTD
018	76	LBL	078	69	DP	138	03	3	198	65	x	258	18	18	318	69	DP
019	14	D	079	06	06	139	04	4	199	43	RCL	259	75	-	319	76	LBL
020	42	STD	080	43	RCL	140	42	STD	200	06	06	260	43	RCL	320	68	NOP
021	04	04	081	23	23	141	09	09	201	55	+	261	14	14	321	98	ADV
022	25	CLR	082	69	DP	142	86	STF	202	43	RCL	262	75	-	322	43	RCL
023	91	R/S	083	04	04	143	01	01	203	05	05	263	43	RCL	323	30	30
024	76	LBL	084	43	RCL	144	98	ADV	204	85	+	264	03	03	324	69	DP
025	16	R'	085	03	03	145	43	RCL	205	01	1	265	95	=	325	01	01
026	42	STD	086	69	DP	146	01	01	206	95	=	266	22	INV	326	43	RCL
027	05	05	087	06	06	147	42	STD	207	42	STD	267	77	GE	327	31	31
028	25	CLR	088	43	RCL	148	11	11	208	15	15	268	38	SIN	328	69	DP
029	91	R/S	089	24	24	149	01	1	209	77	GE	269	34	FX	329	02	02
030	76	LBL	090	69	DP	150	42	STD	210	87	IFF	270	35	1/X	330	43	RCL
031	17	B'	091	04	04	151	12	12	211	01	1	271	65	x	331	32	32
032	42	STD	092	43	RCL	152	00	0	212	06	6	272	40	RCL	332	69	DP
033	06	06	093	04	04	153	42	STD	213	55	+	273	01	01	333	03	03
034	25	CLF	094	69	DP	154	08	08	214	43	RCL	274	60		334	43	RCL
035	91	R/S	095	06	06	155	76	LBL	215	15	15	275	43	RCL	335	33	33
036	76	LBL	096	43	RCL	156	69	DP	216	95	=	276	06	06	336	69	DP
037	18	C'	097	25	25	157	43	RCL	217	42	STD	277	34	FX	337	04	04
038	42	STD	098	69	DP	158	11	11	218	16	16	278	55	-	338	69	DP
039	07	07	099	04	04	159	55	+	219	25	CLR	279	01	1	339	05	05
040	25	CLR	100	43	RCL	160	43	RCL	220	76	LBL	280	08	8	340	98	ADV
041	91	R/S	101	05	05	161	04	04	221	88	DMS	281	03	3	341	25	CLR
042	76	LBL	102	69	DP	162	33	X*	222	43	RCL	282	00	0	342	43	RCL
043	15	E	103	06	06	163	65	x	223	16	16	283	95	=	343	08	08
044	98	ADV	104	43	RCL	164	93	.	224	65	x	284	42	STD	344	58	FIX
045	29	CP	105	26	26	165	04	4	225	43	RCL	285	10	10	345	03	03
046	69	DP	106	69	DP	166	00	0	226	13	13	286	43	RCL	346	99	PRT
047	00	00	107	04	04	167	08	8	227	33	X*	287	11	11	347	58	FIX
048	43	RCL	108	43	RCL	168	05	5	228	65	x	288	75	-	348	09	09
049	27	27	109	06	06	169	95	=	229	43	RCL	289	43	RCL	349	76	LBL
050	69	DP	110	69	DP	170	42	STD	230	06	06	290	01	01	350	30	TAN
051	02	02	111	06	06	171	13	13	231	65	x	291	55	-	351	98	ADV
052	43	RCL	112	02	2	172	33	X*	232	43	RCL	292	01	1	352	98	ADV
053	28	28	113	07	7	173	65	x	233	07	07	293	00	0	353	98	ADV
054	69	DP	114	69	DP	174	43	RCL	234	55	-	294	95	=	354	98	ADV
055	03	03	115	04	04	175	06	06	235	43	RCL	295	22	INV	355	91	R/S
056	43	RCL	116	43	RCL	176	55	-	236	04	04	296	77	GE	356	76	LBL
057	29	29	117	07	07	177	09	9	237	55	-	297	68	NOP	357	38	SIN
058	69	DP	118	69	DP	178	02	2	238	01	1	298	42	STD	358	98	ADV
059	04	04	119	06	06	179	07	7	239	09	9	299	11	11	359	69	DP

Location	Code	Key												
360	00	00	375	69	DP	390	76	LBL	405	22	INV	420	93	.
361	43	RCL	376	00	00	391	89	*	406	86	STF	421	02	2
362	44	44	377	43	RCL	392	43	RCL	407	01	01	422	06	6
363	69	DP	378	47	47	393	02	02	408	61	GTD	423	04	4
364	01	01	379	69	DP	394	85	+	409	77	GE	424	85	+
365	43	RCL	380	03	03	395	43	RCL	410	76	LBL	425	93	.
366	45	45	381	43	RCL	396	14	14	411	87	IFF	426	00	0
367	69	DP	382	48	48	397	85	+	412	43	RCL	427	00	0
368	02	02	383	69	DP	398	43	RCL	413	15	15	428	03	3
369	43	RCL	384	04	04	399	17	17	414	45	Y*	429	05	5
370	46	46	385	69	DP	400	55	-	415	93	.	430	95	=
371	69	DP	386	05	05	401	02	2	416	04	4	431	42	STD
372	03	03	387	25	CLR	402	95	=	417	02	2	432	16	16
373	69	DP	388	61	GTD	403	42	STD	418	94	+/-	433	61	CTD
374	05	05	389	30	TAN	404	18	18	419	65	x	434	88	DMS

ORIGINAL PAGE IS
OF POOR QUALITY

Data register contents		Table II	
Register 200-110	Register	Register 200-110	Register
0.	00 Not used	1301327.	30
0.	01 <i>gr</i>	1222717.	31
0.	02 <i>A₁</i>	3351713.	32
0.	03 <i>A₂</i>	60243170.	33
0.	04 <i>d</i>	1630201.	34
0.	05 <i>s</i>	630301.	35
0.	06 <i>p</i>	630401.	36
0.	07 <i>L</i>	630501.	37
0.	08 <i>X₀</i>	630601.	38
0.	09 <i>M₀</i>	630701.	39
0.	10 <i>o</i>	631001.	40
0.	11 <i>r</i>	631101.	41
0.	12 <i>W</i>	631201.	42
0.	13 <i>N₀</i>	63020101.	43
0.	14 <i>P₀</i>	361727.	44
0.	15 <i>a</i>	1715370027.	45
0.	16 Not used	1335221735.	46
0.	17 Index	3375243100.	47
0.	18 <i>n</i>	3235002416.	48
243170.	19		
6302016127.	20		
223330.	21		
33752431.	22		
33751330.	23		
2416.	24		
42243615.	25		
161731.	26		
2724344124.	27		
1600363313.	28		
3522173500.	29		

Data entered by
user-defined keys

Calculated by
program

Alphanumeric code

Alphanumeric code

ORIGINAL PAGE IS
OF POOR QUALITY

User instructions for running program		Table III		
Step	Procedure	Enter	Press	Display/print
1	Enter program (use standard partitioning)			
2	Enter data	Flow to sparger, gpm Pressure to sparger, psia Ambient pressure, psia Sparger I.D., in. Sparger fluid viscosity, cP Sparger fluid density, lb/ft ³ Sparger length, ft	A B C D A' E' C'	GPM PAIN PAAM ID VISC DEN L
3	Calculate		E R/S*	Hole area per 10% of sparger length, and total hole area, in. ² Hole area per 10% of sparger length, and total hole area, in. ²

* Required only if program is altered for use without printer (see text).

lation, the flowrate down the pipe is reduced by 10% of the entered value.

The velocity is calculated by Eq. (4) (Step 157 in the program shown in Table I), the velocity head by Eq. (3) (Step 172), and the Reynolds number by Eq. (8) (Step 189).^a The appropriate equation for friction factor is selected [Eq. (6) or (7)]. The frictional loss is calculated by Eq. (5) (Step 222).

The pressure difference, $P_s - P_r$, is calculated using Eq. (1) and the entered ambient pressure. This difference is then used to calculate the area, using Eq. (9). This series of calculations starts at Step 251.

It should be noted that, since the entered P_{i0} is a static pressure, P_{i0} must be calculated using Eq. (2). (Since holes are assumed to be located at the center of each section, the frictional loss for the first section takes place over only 5% of the pipe length rather than 10% as for the subsequent sections. To adjust for the program, which subtracts the frictional loss for 10% of the pipe length for each hole calculation, the initial total pressure used in the calculation is increased by one-half of the initial frictional loss.)

Sample problem

Cooper demonstrated the calculation of hole area with the following example:

Consider 2,000 gal/min of water at 25 psia and 95°F, which is to be sprayed onto a distributor plate via holes in an internal pipe that is 10 ft long. Determine the area allocation for a 6-in. pipe. Tower pressure is 24.5 psia. In this case, $\rho = 62.4$ lb/cu ft, $\mu = 0.76$ cP.

Table IV shows the printout for this example. The areas calculated differ substantially from those calculated by Cooper; in this example, velocity head is an important factor.

^aThe Reynolds number is increased by 1 in the program so that Eq. (3) does not give an infinite result (causing the calculator to indicate an error condition at the end of the calculation) when $1' = 0$. The addition of 1 has negligible effect on the calculation results.

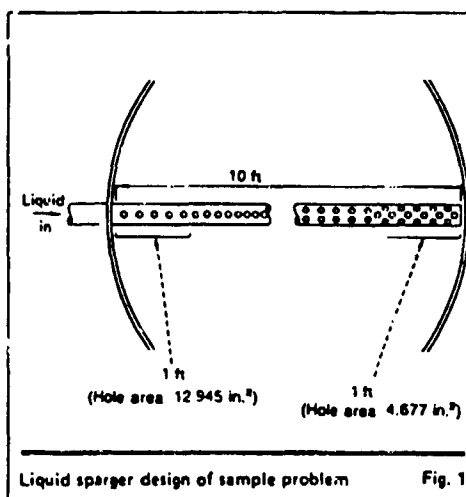


Fig. 1 shows, diagrammatically, the application of the calculated results. (The hole size and spacing shown are for illustrative purposes and do not relate to the sample problem.) In this example, the hole area could be obtained by several combinations of hole sizes and numbers of holes. One possible arrangement would be to have 16 1-in. holes over the first 10% of length, 11 1-in. holes over the next 10% of length, and finally 6 1-in. holes over the last 10% of length.

If the TI-59 is to be used without the printer, it will be necessary to make one change in the program, as follows:

1. Enter the program as shown in Table I

ORIGINAL PAGE IS
OF POOR QUALITY

HOLE-AREA DISTRIBUTION FOR LIQUID SPARGERS

Sample calculation		Table IV
LIQUID SPARGER		
2000.	GPM	
25.	P _A IN	
24.5	P _A AH	
6.0648	ID	
0.76	VISC	
32.4	DEN	
10.	L	
IN ² /10%L	%	
12.945	0/10	
9.697	/20	
7.101	/30	
6.230	/40	
5.680	/50	
5.307	/60	
5.047	/70	
4.866	/80	
4.746	/90	
4.677	/100	
TOTAL HOLE AREA, IN ²		
65.296		

Nomenclature

- a Orifice area, in.²
- d Sparger pipe I.D., in.
- D Sparger pipe I.D., ft
- L Pipe length, ft
- P_a Ambient pressure (pressure sparger is discharging into), psia
- P₀ Initial (entered) static pressure, psia
- P_f Frictional loss, psi
- P_s Static pressure, psia
- P_t Total pressure, psia
- P_{vh} Velocity head, psi
- Q Flowrate entering sparger pipe, gpm
- V Velocity in sparger pipe, ft/s
- ρ Fluid density, lb/ft³
- μ Fluid viscosity, cP

mode while the total hole area is displayed in Fix 9 mode.

Should the data entered result in an impossible solution (such as might occur if the sparger diameter were too small to permit the required flow at the specified pressures), the calculator will print out "SELECT LARGER P_A IN OR ID."

2. Make a program addition by pressing the following key sequence: GTO; 344; LRN; 2nd Del; 2nd Del; LRN; GTO; 312; LRN; 2nd Ins; R/S; LRN.

With this change, the calculator will display the hole area for the first 10% of sparger length after E is pressed. Repeatedly pressing R/S will cause the calculator to display the hole area for each of the next sparger segments in turn and, finally, the total hole area. As an aid to the operator, for identification purposes, the hole areas for the sparger segments are displayed in Fix 3

For HP-67/97 users

The HP version of the program closely follows the TI version. Table V provides a listing of the HP program, user instructions for the HP version are identical to those provided in Table III, with A', B', and C', replaced by a, b, and c, respectively.

ORIGINAL
OF POOR QUALITY

Program listing for HP version

Table V

Step	Key	Code	Step	Key	Code	Step	Key	Code	Step	Key	Code	Step	Key	Code
001	ALBL	11 11	021	K S	51	041	PRTA	-14	061	X	-35	081	3	03
002	STO1	31 01	022	ALBL	21 14	042	RCL6	36 06	062	YX	54	082	5	05
003	STO2	31 02	023	STO4	35 04	043	PRTA	-14	063	+	-	083	-	-35
004	CF1	16 22 00	024	K S	51	044	SFC	16-11	064	STO5	-	084	STO6	35 12
005	K S	51	025	ALBL	21 14 13	045	CF1	16 23 01	065	PCL7	36 07	085	RCL5	36 05
006	ALBL	21 14 11	026	STO6	35 05	046	CSB1	25 01	066	RCL5	36 05	086	34	53
007	STO1	31 01	027	K S	51	047	F02	16 23 00	067	+	-24	087	3	02
008	SF1	16 23 01	028	ALBL	21 14 14	048	CSB2	25 02	068	RCL6	36 06	088	-	-35
009	K S	51	029	STO6	35 06	049	RCL0	36 06	069	+	-24	089	RCL	36 11
010	ALBL	21 14 12	030	K S	51	050	-	-42	070	STO6	35 12	090	X	53
011	STO2	35 02	031	ALBL	21 15	051	3	03	071	-	-62	091	-	-45
012	STO6	35 06	032	RCL1	36 01	052	2	02	072	4	04	092	RCL6	36 12
013	CF0	16 22 00	033	PRT1	-14	053	5	05	073	1	01	093	X	53
014	P/S	51	034	PCL2	36 02	054	5	05	074	-	-35	094	3	03
015	ALBL	21 14 12	035	PRTA	-14	055	+	-24	075	CHS	-22	095	X	-35
016	STO2	35 02	036	RCL3	36 03	056	RCL5	36 03	076	1	01	096	+	-24
017	SF0	16 23 00	037	PRTA	-14	057	X	53	077	+	-35	097	STO6	35 12
018	K S	51	038	RCL4	36 04	058	+	-24	078	STO6	35 12	098	RCL4	36 11
019	ALBL	21 15	039	PRT2	-14	059	RCL4	36 04	079	RCL5	36 12	099	3	03
020	STO2	35 02	040	RCL5	36 05	060	RCL7	36 07	080	CF1	-62	100	17	31

Step	Key	Code	Step	Key	Code	Step	Key	Code	Step	Key	Code	Step	Key	Code
101	2	02	122	2	02	143	YX	54	164	2	02	185	6	06
102		-35	123	7	07	144	STO6	35 12	165	+	-35	186	0	00
103	RCL4	36 11	124	A	-35	145	+	-55	166	RCL6	36 12	187	6	06
104	1	01	125	+	-24	146	1	01	167	3	03	188	-	-35
105	6	06	126	CHS	-22	147	ENT1	-21	168	A	-35	189	STO7	35 07
106	X	-35	127	STO0	35 14	148	3	03	169	+	-24	190	RTK	24
107	RCL5	36 05	128	RCL0	36 14	149	+	-24	170	-	-45	191	ALBL2	21 02
108	X	53	129	2	02	150	1	01	171	YX	54	192	RCL2	36 02
109	+	-35	130	+	-24	151	RCL0	36 14	172	YX	54	193	RCL4	36 04
110	+	-55	131	CHS	-22	152	2	02	173	RCL3	36 03	194	X	-35
111	RCL6	36 12	132	RCL0	36 14	153	+	-24	174	A	-35	195	6	06
112	RCL9	36 09	133	X	53	154	CHS	-22	175	PRTA	-14	196	0	00
113	X	53	134	4	04	155	RCL6	36 12	176	SFC	16-11	197	+	-24
114	X	-35	135	+	-24	156	-	-45	177	CF0	16 22 00	198	STO6	35 05
115	2	02	136	RCL6	36 12	157	1	01	178	CF1	16 22 01	199	RTK	24
116	7	07	137	3	03	158	ENT1	-21	179	R/S	51	200	R/S	51
117	+	-35	138	Y	31	159	3	03	180	ALBL1	21 01			
118	+	-55	139	2	02	160	+	-24	181	RCL1	36 01			
119	RCL6	36 12	140	7	07	161	Y	31	182	-	-62			
120	-	03	141	+	-24	162	+	-55	183	0	00			
121	Y	31	142	+	-55	163	RCLA	36 11	184	3	03			

ADDENDUM

SPARGER SYSTEM FOR MMH-HELIUM VENTS

On page 4 the Sparger program for an example vent condition was run giving a result of $a = 0.72 \text{ in}^2$ (total Sparger area). It was decided to run the same program for the same conditions, except for the Sparger inlet pressure which was 100 psi previously and is now taken to be 21 psi (instead of a ΔP of 80 psi as in the previous case we now have a ΔP of 1 psi through the Sparger).

The results are the following:

<u>Hole Area, $\text{in}^2/10\%$ of Sparger length, L</u>	<u>%L</u>
.664	10
.605	20
.562	30
.529	40
.503	50
.484	60
.468	70
.457	80
.449	90
.444	100

$$\text{Total Area} = 5.166 \text{ in}^2 = a$$

Again, since the program is for liquids we need to multiply these numbers by $\frac{1}{4}$ to get the areas needed for a gas vent. Also, in this case the area required continuously decreases as we go down the Sparger to compensate for velocity head loss.

Using this result, if we now refer to page 5 we have the following two equations for the first 10% of Sparger:

1. $n d_o = 1.136$ (10% of flow for each 10% of Sparger length)

2. $\frac{\pi (d_o)^2 n}{2} = a = \frac{.664}{4} = .166 \text{ in}^2$

Therefore $\frac{\pi d_o}{4} (1.136) = .166$

and $d_o = .184 \text{ inches}$

$n = 6.17 \text{ holes}$

Table I shows the results for 10% increments in length down the Sparger.

TABLE I. HOLE SIZE AND NUMBER REQUIRED

<u>Percent</u>	<u>n (no. of holes)</u>	<u>do, in</u>
10	6.17	.184
20	6.80	.167
30	7.29	.156
40	7.75	.147
50	8.15	.139
60	8.47	.134
70	8.76	.130
80	8.97	.127
90	9.13	.124
100	9.23	.123

Note, that we need far fewer holes of a larger diameter than in the previous case.

N86-14097

COMPARATIVE EFFECT OF LUNAR FINES AND TERRESTRIAL ASH ON THE GROWTH OF A
BLUE-GREEN ALGA AND GERMINATING RADISH SEEDS

Esther J. Ridley
Professor of Biological Science
Morgan State University
Baltimore, Maryland

ABSTRACT

Although it is understood that photosynthetic organisms will be required as components of a closed ecological life support system (CELSS) for a manned lunar base, a basic problem is to identify organisms "best" capable of utilizing lunar regolith materials. Also, there is need to determine what nutrient supplements have to be added to lunar soils, and at what levels in order to promote high bio-mass production.

This research compares the growth of Anabaena flos-aqua, UTEX1444, when cultured in a water leachate prepared from Apollo 14 sample number 14148-6 to the alga's growth when cultured in a water leachate of terrestrial ash. The measure of chlorophyll absorption at 650 nm was used as the index of growth. Additionally, mean average root length is reported for radish seedlings at 24, 36, and 48 hours after seeds were allowed to germinate on leachate moistened filter paper or on lunar or terrestrial soil particulates.

Results showed that during the first 9 days, the growth of Anabaena flos-aqua in both lunar and terrestrial leachates was much less than that of alga growing on enriched culture medium. The addition of enriched medium to all cultures on day 9 resulted in dramatic increase in growth in all, and by day 15 the level of growth in lunar leachates surpassed that of control and terrestrial leachate cultures. Radish seedlings showed the greatest mean average root length at 24, 36, and 48 hours for those plants treated with terrestrial leachates or terrestrial soil particulates. After 24 hours, root growth of control plants exceeded that of plants treated with lunar leachate or lunar fines. However, the plants treated with lunar materials showed greater root growth at 36 and 48 hours than did the controls.

The findings indicate that the lunar material has an initial inhibitory effect followed by one that is stimulatory on the growth of both the alga and the radish seedlings. The stimulatory effect coupled with the addition of deficient nutrients to the algal cultures appeared to promote increased bio-mass production. More controlled experiments are required before definitive conclusions can be made.

Center Research Advisor: Wendell W. Mendell

INTRODUCTION

Among the major problems in the development of a closed ecological life support system (CELSS) for human habitation of the moon is that of a choice of biological components capable of utilizing lunar materials and man's metabolic waste products to regenerate into the system those materials required to support human life. Materials absolutely essential for human life are oxygen, water, and food. To repeatedly transport these materials from earth to a lunar base is generally recognized as infeasible. Photosynthesizing organisms produce the food required to support life on planet earth by utilizing solar energy, soil minerals, water, and carbon dioxide with concomitant evolution of oxygen and replacement of water into the biosphere. How efficient can these organisms be on the moon? Although at the present time the availability of water on the moon has not been determined, there is abundant solar energy, and the lunar regolith though lacking organic compounds contains all of the minerals required for plant growth with the exception of nitrogen, zinc, boron, and molybdenum (NASA 44-005-114, 1972). Supplies of nitrogen and carbon will become available from human waste products in the lunar base, while the last three of the foregoing nutrients are required in trace amounts only.

Early experiments with Apollo 11, 12, and 14 materials have shown that several species of higher plants demonstrated increased growth after treatment with lunar fines (Walkinshaw et al., 1970, and Walkinshaw and Johnson, 1971). Also, higher plants subjected to simulated lunar photoperiods were shown to develop high quality crops (Terskov et al., 1978). In a number of experiments directed toward the development of a CELSS, representative forms of green algae

have been used. Outstanding among these experiments is the work of Gitelson et al. (1975), and Fong and Funkhouser (1982). However, there is an apparent absence of data on blue-green algae as a component of CELSS.

The tenacious ability of blue-green algae to exist in the harshest as well as the milder of earth's environments for well over three billion years (Young, 1981) would suggest that this group of plants may include some species worthy of choice as components of a CELSS for a manned lunar base. Blue-green algae, known scientifically as cyanophyceae, are photosynthesizing plants widely distributed in and on soils and in both marine and freshwater habitats. Additionally, they are successfully maintained in the laboratory by agar and hydroponic techniques. Recently, blue-green algae were discovered growing 82 feet below the surface in ice-covered lakes in the Dry Valleys of Antarctica. Also, these algae were found growing inside of rocks collected in the Dry Valleys (Young, 1981).

The blue-greens exist as unicellular, colonial, and filamentous forms. All forms have been described as pro-karyotic because they lack a formed nucleus and other cellular organelles. Research on a number of species of blue-green algae has shown that these plants have remarkable adaptive capability, and as photosynthesizers they have a significant role in the regeneration of oxygen and the utilization of carbon dioxide as well as the recycling of mineral nutrients in the biosphere.

Outstanding examples of the adaptive capability of the blue-green algae are the unique physiological and ecological behavior of some species in response to environmental stresses. These behavioral responses include: (1) the ability to fix molecular nitrogen when inorganic nitrogen supplies are low; (2) the ability

to withstand pH values as low as 2 or as high as 10 (Lewin, 1962); (3) the ability to develop specialized cells for surviving phosphorus deficiency; and (4) the ability to grow in both aerobic and anaerobic conditions (Trainor, 1978). More unusual than the foregoing is the behavior of the blue-green algae in the lakes of the Dry Valleys of Antarctica referred to earlier. There the plants grow 82 feet below the surface, receiving only 0.1 of 1.0 percent of the surface light, and for one-third of the year they receive no light. Researchers theorize that during photosynthesis, the algae produce glycollate along with other short-chain carbon compounds that remain in the water and are used as an energy source when there is no light (Young, 1981). If indeed this explanation is correct, it is interesting to compare this mechanism of adaptation to that in earlier reports of uptake of phosphates by blue-green algae in excess of requirements and the storage of this nutrient for utilization when the external supply is depleted (Lewin, 1962).

Both algae and higher plants have specific requirements for light, moisture, hydrogen ion concentration, a carbon source, and macro- and micronutrients for continued growth and reproduction. The required macronutrients have been identified as Na, Ca, Mg, Cl, SO_4 , PO_4 , and N, and the micronutrients as Mn, Zn, Fe, Co, and Mo. Each species has optimum, minimum, and maximum levels for each factor or substance required. Deficiency or toxic levels of these requirements result in a broad spectrum of manifestations of morphological and/or physiological anomalies too numerous to be outlined here. Extreme deficiencies may result in the death of plants.

The ultimate source of light for all life forms is solar energy, while the earth's abundant water bodies supply the needed moisture. Temperature variations and fluctuations in hydrogen ion concentration are influenced in large part by geographical location and metabolic activity of all life forms in a given area. Terrestrial photosynthesizers depend for the most part on carbon from the atmosphere in the form of CO_2 , while soil and aquatic forms utilize carbonates from the growth medium. Terrestrial and soil, as well as aquatic forms, depend upon the soil as the ultimate source of the micro- and macronutrients.

Algal plant bodies absorb the required nutrients directly from the growth media, while the seeds of higher plants contain sufficient amounts of nutrients to permit seed germination and growth of the primary root and shoot systems under proper conditions of light, moisture, temperature, and available oxygen. As the seed stores are depleted, root hairs on the epidermal cells absorb nutrients from the growth medium to accommodate the further nutrient requirements of the seedling. Numerous culture studies have been done to establish the absolute nutrient requirements for a variety of species, and these are available in the literature.

THEORY

The purpose of the study reported here was to test the hypothesis that variations in inorganic content of lunar and terrestrial soil leachates will result in corresponding variations in the support of blue-green algal growth. Additionally, variations comparable to lunar and terrestrial soil nutrient variations will be demonstrated in the root growth of germinating radish seedlings exposed to lunar and terrestrial leachates, and to particulates of lunar fines and terrestrial ash.

Lunar mare surface material is described as unweathered basalt rock fragments similar to silts in particle size (2-60 μ), and it has a permeability similar to silt. The minerals of the lunar soils contain all of the elements found in terrestrial soils with the exception of Mo, Zn, Co, and N (NASA 44-005-114, 1972).

For this experiment, trench surface sample number 14148-5 from the Apollo 14 collection was used. The relative amounts of major and trace elements in this sample were determined by Philpotts et al. (1972) and Lindstrom et al. (1972). The sample of terrestrial soil used was collected on the JSC site just outside of Building 31. The terrestrial soil was ashed at 800°C for four hours in order to degrade the organic matter.

Leachate Preparation

Lunar and terrestrial leachates were each prepared in two separate batches. Lunar 1 (L1) and Terrestrial 1 (T1) were prepared by adding 49.59 mg and 50 mg respectively to two separate 50 ml Erlenmeyer flasks containing 50 ml of glass

distilled H₂O. Both samples were covered and magnetically stirred for four hours per day for three days at room temperature. The second batch, Lunar 2 (L2) and Terrestrial 2 (T2) was prepared by adding 41.40 mg and 50 mg respectively to two separate Erlenmeyer flasks, each containing 10 ml of glass distilled H₂O. The flasks were covered and stirred magnetically for six hours per day for five days. All samples were vacuum pumped through a membrane filter. The undissolved particles were stored for future reference. Determination of pH values were made on the supernatants and each was adjusted to pH 7.4.

Alga Culture Preparation

An agar culture of the blue-green alga, Anabaena flos-aqua UTEX 1444 was obtained from the University of Texas algae collection. To 50 ml of an aqueous culture medium for bacteria free axenic culture of blue-green algae (Aaronson, 1970), five 1-mm-square slices of agar were added. The flask was stoppered with a cotton plug containing a glass tube cotton filter. This flask was maintained under continuous light as a stock culture, and the pH was adjusted periodically by addition of culture medium.

Experimental Procedures

The design of the experiment is shown in figure 1, Scheme for Testing the Viability of Lunar Soil.

The algal bio-assay was done with L1 and T1 leachates only because of the small volume of L2 and T2 leachates.

Nine ml of an undiluted, a 1:2 dilution, and a 1:10 dilution of L1 and T1 leachates were added to six separate 50-ml flasks. In a seventh flask, 9 ml of

SCHEME FOR TESTING VIABILITY OF LUNAR SOIL

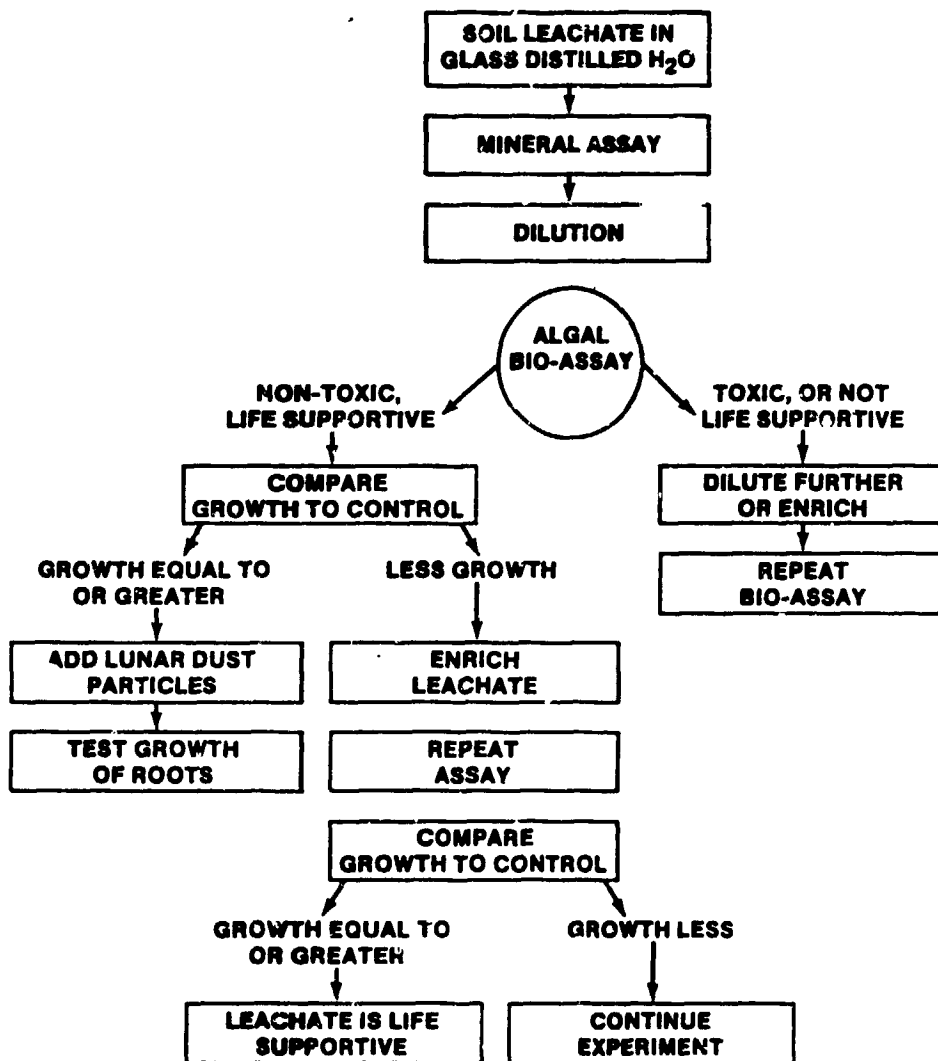


Figure 1.

algal culture medium was placed. This flask served as the control culture. All flasks were inoculated with a 1-cm-square slice of the agar culture of the alga. The flasks were stoppered with cotton plugs containing glass tube cotton filters, and maintained under continuous light at room temperature.

The cultures were allowed to stabilize for three days. Absorption at 650 mμ on the spectrophotometer was recorded for the control and each experimental culture on day 4, 7, 8, and 9. After the reading on day 9, each flask was inoculated with 1 ml of the algal culture medium. Thereafter, readings were made on day 10, 11, 14, 16, and 18.

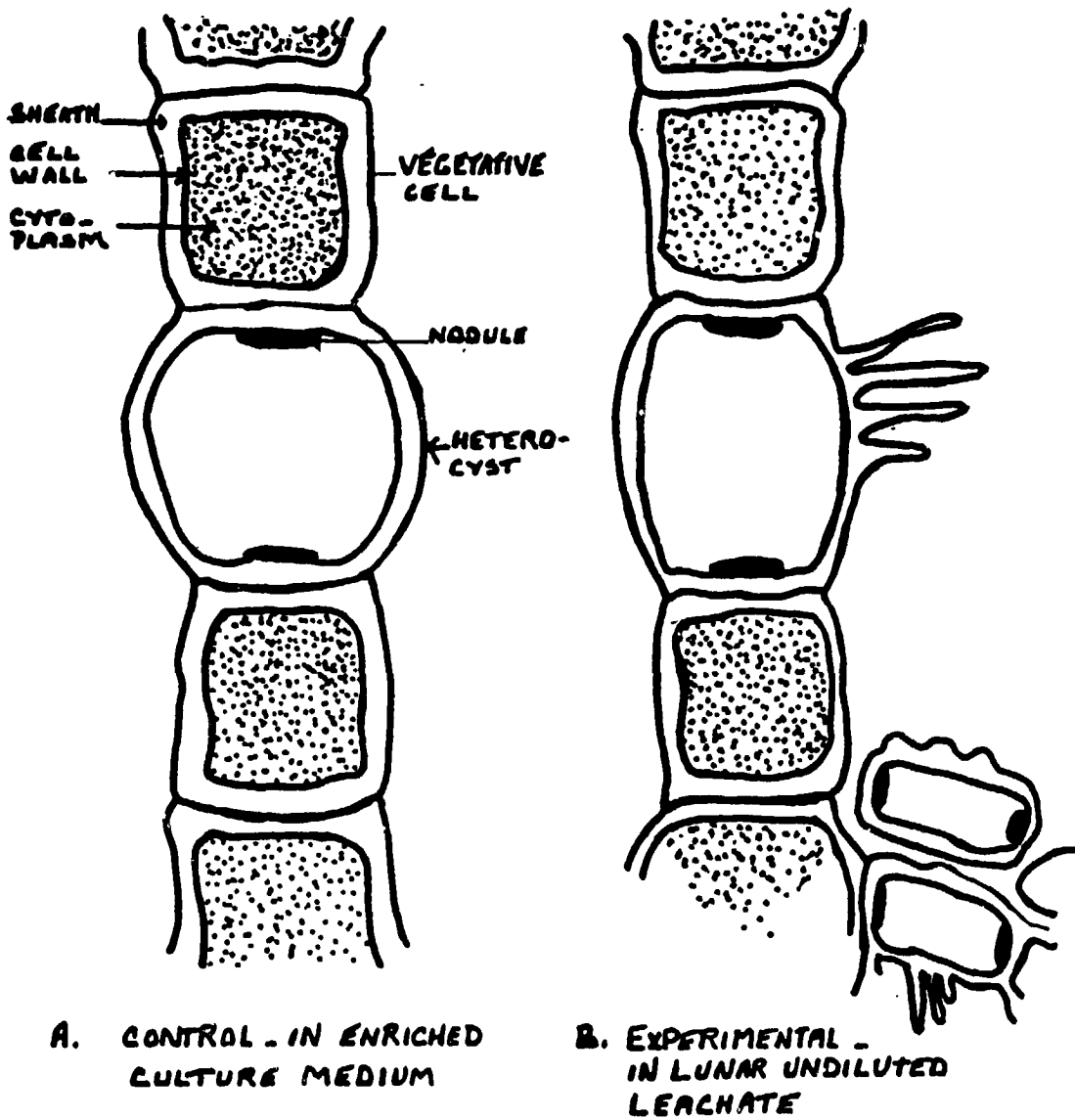
Radish seed germination tests were run with L1, T1, L2, and T2 leachates. Germination tests were also run with lunar fines particulates and terrestrial ash. To six separate filter paper-lined petri dishes, 1 ml of an undiluted, a 1:2 dilution, and a 1:10 dilution of L1 and T1 leachates was added. Glass distilled H₂O was added to a seventh petri dish which served as a control. Five radish seeds were placed in each dish approximately 2.5-3.0 cm apart. The dishes were covered and maintained in the dark. Measurements of root length were made at 24, 36, and 48 hours. During the 3-day period, the filter paper was kept moist with the respective diluents. The experiment was repeated with a parallel run of L2 and T2 leachates.

Additionally, to each of two filter-lined petri dishes 1 ml of distilled H₂O was added. Five radish seeds were placed approximately 2.5-3.0 cm apart in each dish. The seeds in one dish were sprinkled with 5 mg of lunar fines. Those in the other dish were sprinkled with 5 mg of terrestrial ash. The dishes were covered and maintained in the dark. Measurements of root length were made at 24,

ORIGINAL FIGURE
OF POOR QUALITY

36, and 48 hours. During the three-day period, the dishes were kept moist with glass-distilled H_2O .

HETEROCYST STRUCTURE IN ANABAENA



RESULTS

Anabaena flos-aqua cultured in a medium specific for blue-green algae and maintained under continuous fluorescent light demonstrated a four-day lag phase followed by exponential growth over a four-day period. Inoculation with additional culture medium after a slight decline in growth on the ninth day resulted in exponential increase to the 14th day.

Alga cells cultured in leachates from lunar fines or terrestrial ash did not demonstrate growth comparable to that of the control. Comparison of growth in the algal cultures is shown in figure 2. At all concentrations of the lunar leachates, the algal cultures were essentially still in lag phase at day 4 and there was decline of growth to day 9. Inoculation with culture medium at that time resulted in exponential growth but at a much slower rate than the control culture. The undiluted terrestrial leachate culture demonstrated a growth pattern approximating that of the control. However, the rate of growth was much less. At day 14, undiluted leachate cultures of both lunar and terrestrial samples showed comparable levels of growth. On day 15, the level of growth in the three lunar leachate samples was greater than that in the control culture as well as that of the terrestrial leachate samples.

The mean average root length of control radish seedlings exceeded that of all experimental samples at 24 hours of growth, with the exception of T1 and T2 undiluted, and the T1 1:10 dilution samples. At 36 hours, T1 and T2 undiluted, T2 1:2 dilution, and the terrestrial fines samples surpassed the control by 1-3 mm while at 48 hours the mean average root length of all experimental samples was greater than that of controls (figure 3). Root growth in undiluted terrestrial

leachate and the terrestrial ash samples was much greater than all other samples at 48 hours.

CHLOROPHYLL CONTENT AS INDEX OF ALGAL GROWTH

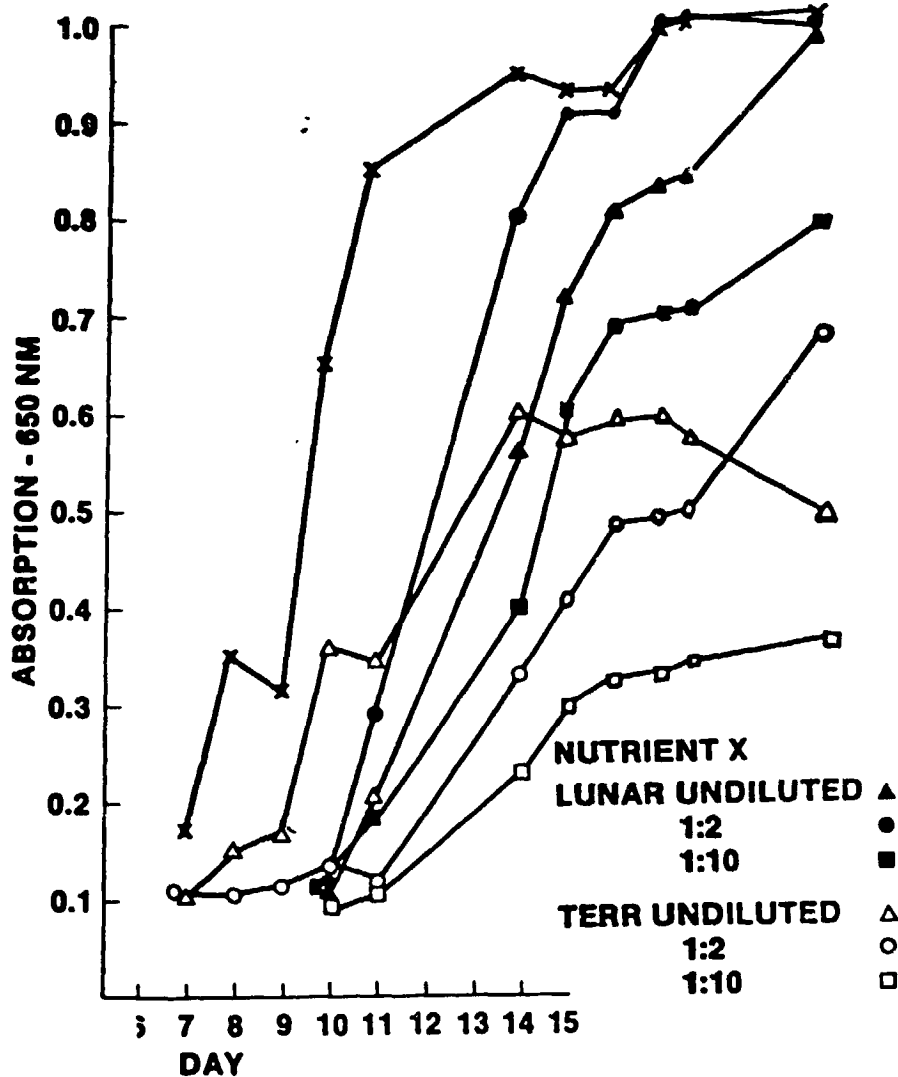


Figure 2.

MEAN AVERAGE ROOT LENGTH AT 48 HOURS

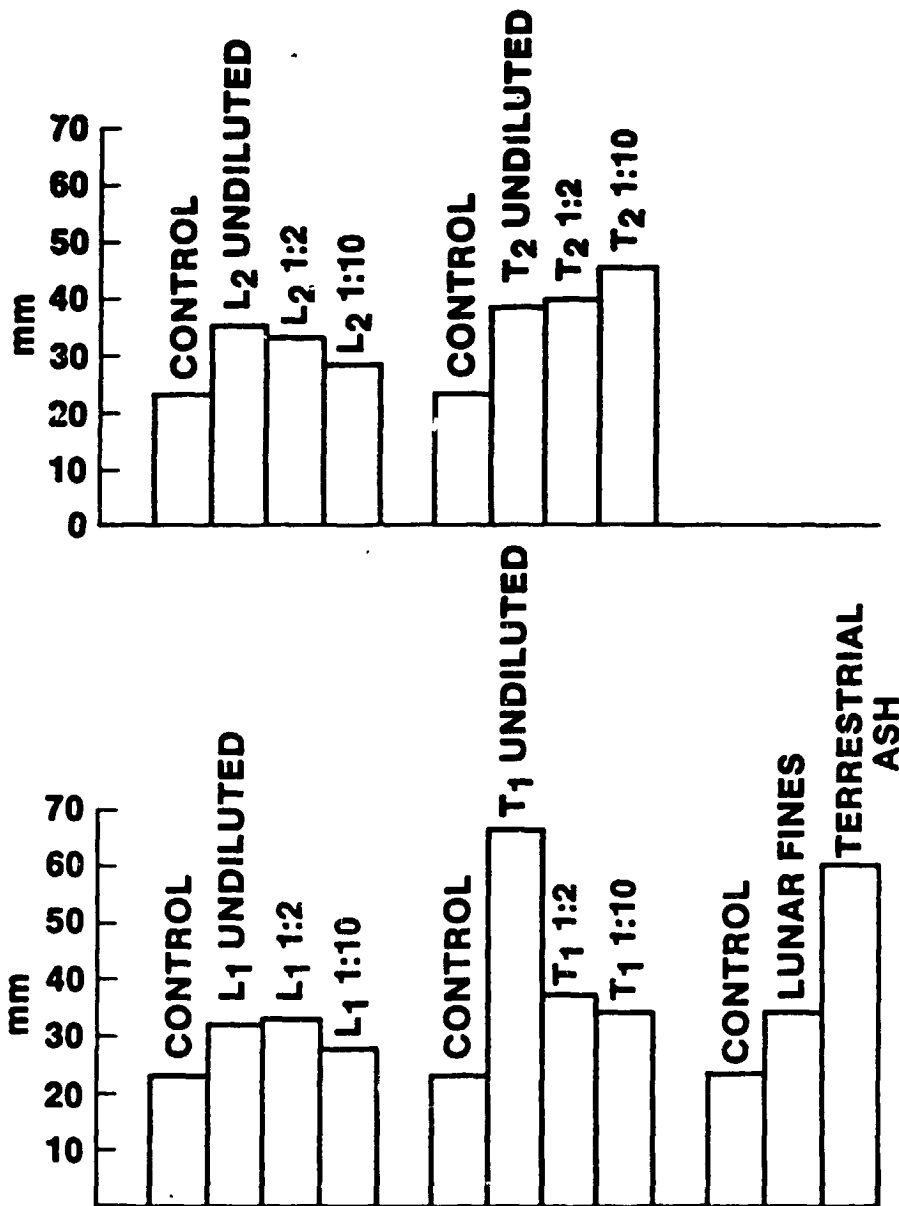


Figure 3.

CONCLUSIONS

Preliminary findings presented here suggest that amounts of nutrients sufficient to interact with the growth of plants are H_2O soluble from Apollo 14 sample number 14148-6. There is indication that the lunar material has an initial inhibitory effect followed by a stimulatory effect. However, there is evidence that addition of some nutrients may be required to permit optimal growth. These nutrients may be Bo, Mo, and Zn. In the case of nitrogen fixing blue-green algae such as Anabaena flos-aqua, additions of nitrogen may not be required since these organisms can utilize molecular nitrogen when Bo, Mo, and Zn are available. It is not possible to arrive at definitive conclusions based on the data obtained here. It is recommended that more controlled follow-up experiments be run. These controls should include:

- (1) bubbling of a measured amount of CO_2 through the algal cultures;
- (2) a measure of the incident light;
- (3) constant shaking of the algal cultures to dispel the build-up of oxygen gas;
- (4) microscopic study of algal cells for detection of morphological changes;
- (5) measurement of bio-mass quantity in each culture;
- (6) tests to determine whether the algal cells produce in the environment volatile substances that are toxic to higher plants;
- (7) radish seedlings should be grown to maturity in hydroponic lunar leachate medium with additions of measured amounts of specific nutrients. Growth of root and shoot systems should be monitored during the growth period and measurement of final bio-mass production should be made.

REFERENCES

1. Aaronson, S., Experimental Microbial Ecology, Acad. Press, N.Y., p. 188, 1970.
2. Fong, F. and Funkhouser, E. A., "Air Pollutant Production by Algal Cell Cultures," NASA Conference Publication No. 2247, pp. 57-59, 1982.
3. Gitelson et al., Experimental Ecological Systems Including Man, Problems of space Biology, Vol. 28, NASA Technical Translation, 1976.
4. Lewin, R. A., Physiology and Biochemistry of Algae, Acad. Press, N.Y. and London, Chapter 50, 1962.
5. Lindstrom, M. M. et al., "Compositional Characteristics of Some Apollo 14 Clastic Materials," Proceedings of the Third Lunar Science Conference, Vol. 11, pp. 1201-1215, 1972.
6. NASA Grant, University of Houston, MSC, and Rice University, Design of a Lunar Colony, NGT 44-005-114, p. 282, 1972.
7. Peavy, W. S., Southern Gardeners Soil Handbook, Pacesetter Press, Houston, Texas, pp. 25-26, 1975.
8. Philpotts, J. A. et al., "Apollo 14: Some Geochemical Aspects," Proceedings of the Third Lunar Science Conference, Vol. 11, pp. 1293-1307, 1972.
9. Terskov, I. A. et al., "Possibility of Using Higher Plants in Lunar Life-Support Systems," UD.C: 58.057:523.3, pp. 82-86, 1978.
10. Trainor, F. R., Introductory Phycology, John Wiley & Sons, N.Y., p. 525, 1978.
11. Walkinshaw, C.H. et al., "Results of Apollo 11 and 12 Quarantine Studies on Plants," Bio. Science, Vol. 20, pp. 1297-1302, 1970.
12. Walkinshaw, C. H. and Johnson, P. H., "Analysis of Vegetable Seedlings Grown in Contact with Apollo 14 Lunar Surface Fines," Hort. Sci. Vol. 6, No. 6, pp. 532-535, Dec., 1971.
13. Young, P., "In the Dry Valleys of Antarctica, Scientists Find Algae-Filled Lakes and Lichens Hidden in Rocks," Smithsonian, Vol. 12, No. 8, pp. 53-61, Nov., 1981.

VARIABILITY OF RAINFALL OVER SMALL AREAS

N86-14098

Robert C. Runnels
Assistant Professor
Department of Meteorology
Texas A&M University
College Station, Texas

ABSTRACT

A preliminary investigation was made to determine estimates of the number of raingauges needed in order to measure the variability of rainfall in time and space over small areas (approximately 40 mi²). The literature on rainfall variability was examined and the types of empirical relationships used to relate rainfall variations to meteorological and catchment-area characteristics were considered. Relations between the coefficient of variation and areal-mean rainfall and area have been used by several investigators. These parameters seemed reasonable ones to use in any future study of rainfall variations. From a knowledge of an appropriate coefficient of variation (determined by the above-mentioned relations) the number of rain gauges needed for the precise determination of areal-mean rainfall may be calculated by statistical estimation theory. The number of gauges needed to measure the coefficient of variation over a 40 mi² area, with varying degrees of error, was found to range from 264 (10% error, mean precipitation = 0.1 in) to about 2 (100% error, mean precipitation = 0.1 in).

Center Research Advisor: Dr. David E. Pitts

INTRODUCTION

This paper discusses some preliminary considerations necessary for planning a more-extensive study on the determination of the spatial and temporal variability of rainfall over small areas. These variations may be important in affecting the variability of soil moisture that, in turn, may affect crop yield.

The forecasting of crop yield by the remote sensing of the status of crops can provide routine assessments over larger geographical areas than measurements made at a few sample plots on the ground. Relations are sought between the amount and frequency of energy reflected, scattered, and emitted (the signature) back to the sensor from the crop at a particular stage of crop growth. The factors that can cause variations in signatures are numerous and the reduction of these factors to measureable proportions is an essential aim of remote-sensing research. Some of these factors are planting date, row direction, row width, leaf area index, spectral properties of individual leaves, the geometry of the canopy, soil background, crop stage, and crop condition (Pitts et al., 1983).

Weather-sensitive factors may produce significant correlations between yield and particular meteorological elements but these factors may not act in a direct cause-effect relation (Munn, 1970). Insect infestations and crop diseases are usually related to weather conditions but their impact may not be immediate. Many investigators feel that soil moisture is the best environmental predictor of crop yield (Munn, ibid.). However, once adequate rainfall has occurred, variation in rainfall amount seems to have a small effect on crop yield. Pitts et al. (1983) compared rainfall amounts with the prediction of the date when spring wheat would be ripe. These dates were obtained from a spring-wheat phenology model developed by Doraiswamy and Thompson (1982). Across small areal segments (5X6 nautical miles) the influence of rainfall on the phenology of spring wheat did not vary appreciably when rainfall amounts accumulated for periods of a day or longer were used. Variations, of the elapsed days to the ripe stage were only 1 to 2 days out of approximately 225 days necessary to attain the ripe stage. However, some slight variability, found within a few segments, did appear to be related to variations in rainfall. Changnon and Neill (1968) compared the association of corn yields from 60 farms with 10 weather and 4 agricultural variables. Nine years of data were used and the authors found that, among the meteorological variables, monthly rainfall amounts did not seem to be too

important. For a growing season extending from May until August, the best rainfall-related correlation coefficient was between August rainfall and yield. The value of this coefficient was 0.29. Rainfall amounts during July, June, and the pre-season months correlated more poorly.

The increasing use of sensors that can resolve spectral signatures of ever smaller areas suggests the desirability of understanding variations of rainfall within areas smaller than 40 square miles. A preliminary understanding of these variations is the object of this study.

Previous studies of rainfall variability were examined and the empirical relationships, from these studies, were chosen that showed the association among rainfall variability and mean precipitation, size of sampling area, season, type of precipitation, and synoptic weather type. When these relationships were combined with statistical estimation theory, a simple expression was obtained that indicates the number of rain gauges needed in order to measure rainfall variability, within certain error bounds, at a predetermined level of confidence.

THEORY

In order to find approximate empirical relationships between rainfall variability and meteorological quantities, the extensive studies performed by the Illinois State Water Survey (Huff and Neill, 1957, Huff and Shipp, 1968, and Huff, 1970) were chosen as being representative ones of rainfall during the growing season over relatively flat terrain. Catchment areas ranged from 10 to 550 square miles and they have been studied by this organization since 1955. Gauge densities ranged from 0.12 to 0.50 gauges per square mile. Uniform spacing between gauges was used. Such spacing is preferable when rain is produced by convective motions (Rodda, 1972). Convective rainfall is the type most likely to occur during growing seasons.

The coefficient of variation (V) is a useful statistic for showing both variation about the mean and variability relative to the mean.

$$V = \frac{s}{P}$$

where s is the sample standard deviation and P is the sample mean rainfall amount.

Huff and Neill (1957) have shown the following relations involving V:

$$V \propto 1/P,$$

$$V \propto A,$$

where A is area,

$$V \propto \text{rainfall gradient},$$

and

$$V \propto 1/D,$$

where D is the duration of the rain event.

Rainfall gradient and duration are strongly proportional to mean rainfall. Thus, to a first approximation, the natural variation of rainfall, expressed by V, is

$$\log V = \log k + a \log P + b \log A, \quad (1)$$

where k, a, and b are constants obtained by regression analysis. Logarithms of P and A were used since they range over several orders of magnitude. Typical values, for shower-type precipitation, are $k = 9$, $a = -0.44$, and $b = 0.15$ when V is in per cent, P is in inches, and A is in square miles. The correlation coefficient of Eq. (1) is about 0.7.

To relate the coefficient of variation, obtained by Eq. (1), with the minimum number of gauges needed for adequate measurements, the following expression for confidence intervals, for V, is used, viz.,

$$V \pm Z_{\alpha/2} \frac{V}{\sqrt{2N}} \sqrt{1 + 2V^2}, \quad (2)$$

where Z is the standardized value of V and N is the number of observations (rain gauges) (Spiegel, 1961). This expression gives the interval for $(1 - \alpha)100\%$ confidence.

Solution of Eq. (2) for N gives

$$N = \frac{1}{2} \left[\frac{Z_{\alpha/2}}{d} \right]^2 \sqrt{1 + 2V^2}, \quad (3)$$

where d is the percentage uncertainty in the measurement of V that is acceptable. To be 95% confident, $1 - \alpha = 0.95$, and $Z_{0.025} = 1.96$.

RESULTS

An illustration of the results anticipated by the method explained above is shown in Table 1. An area of 40 square miles was chosen to correspond to the sizes of areas recently observed by the Landsat Multi-Spectral Scanner (Pitts et al., 1983).

Table 1. Required number of gauges (N) and gauge density (G) to measure the variation of rainfall over an area of 40 square miles with a confidence of 95%.

P	V	N	G	
inches	-	-	$\frac{\text{Miles}^2}{\text{Gauge}}$	
0.1	0.43	264	0.15	d = 0.1V
0.5	0.21	209	0.19	
1.0	0.15	202	0.20	
2.0	0.11	198	0.20	
0.1	0.43	66	0.61	d = 0.2V
0.5	0.21	53	0.75	
1.0	0.15	51	0.78	
2.0	0.11	49	0.82	
0.1	0.43	11	3.6	d = 0.5V
0.5	0.21	9	4.4	
1.0	0.15	8	5.0	
2.0	0.11	8	5.0	
0.1	0.43	3	13.3	d = 1.0V
0.5	0.21	2	20.0	
1.0	0.15	2	20.0	
2.0	0.11	2	20.0	

CONCLUSIONS

The relationship between V and P and A, from the Illinois State Water Survey, is consistent with results of other studies of the characteristics of shower-type rainfall. The effect of mean rainfall is greater than the effect of area in the empirical determination of V. However, area of rainfall is not independent of rainfall mean. Eq. (1) with a correlation coefficient of 0.7 and a coefficient of determination of 0.49 means that only 49% of the variation is explained by a linear relation of logarithms. It remains to be seen whether or not non-linear relations and/or the incorporation of other variables will produce higher correlations.

Huff(1970) indicates that Eq. (1) may have an uncertainty of 2 orders of magnitude. This range of uncertainty is not unusual for many geophysical measurements but it may be large enough to affect the estimate of the minimum number of gauges determined by Eq. (1).

The regression coefficients for Eq. (1) vary, to some extent, with locality. This variation, in the coefficients, suggests a survey of rainfall characteristics in a variety of crop-growing regions during the growing season.

Continuation of this research will consist of an investigation of rainfall data collected during concomitant surveys of crops by remote sensing from Landsat. Sites from several climatic zones were surveyed with each site having dimensions of 5 x 6 n mi. Terrain is relatively smooth and the number of rain gauges varies from 1 to 23 per site. The rainfall data can be stratified in several ways and regression relationships other than linear will be investigated. Since the rainfall-producing processes are complex, an initial investigation, as suggested here, is needed to detect some of the predominant relations between these processes and the resulting rainfall characteristics.

REFERENCES

1. Changnon, Jr., S.A., and J.C. Neill, "Corn-Weather Response on Cash-Grain Farms," Journal of Applied Meteorology, Vol. 7, pp 94-104, February, 1968.
2. Doraiswamy, P.C., and D.R. Thompson, "A Crop Moisture Stress Index for Large Areas and Its Application in the Prediction of Spring Wheat Phenology," Agricultural Meteorology, Vol. 27, pp 1-15, 1982.
3. Huff, F.A., "Sampling Errors in Measurement of Mean Precipitation," Journal of Applied Meteorology, Vol. 9, pp 35-44, February, 1970.
4. _____, and J.C. Neill, Rainfall Relations on Small Areas in Illinois, Illinois State Water Survey, Urbana, 1957, 61 p.
5. _____, and W.L. Shipp, "Mesoscale Spatial Variability in Mid-western Precipitation," Journal of Applied Meteorology, Vol. 7, pp 886-891, October, 1968.
6. Munn, R.E., Biometeorological Methods, Academic Press, N.Y., Chapter 11, 1970.
7. Pitts, D.E., D.R. Thompson, K.E. Henderson, and M. Wise, "The Effect of Rainfall Variability on Spring Wheat Growth Stages," Preprint Volume of Extended Abstracts, 16th Conference on Agricultural and Forest Meteorology, American Meteorological Society, Boston, pp 159-162, April, 1983.
8. Rodda, J.C., "Precipitation," Casebook on Hydrological Network Design Practice, World Meteorological Organization, Geneva, pp 1-1.2-1 - 1-1.2-15, 1972.
9. Spiegel, M.R., Theory and Problems of Statistics, Schaum Publishing Co., N.Y., Chapter 8, 1961.

N86-14099

Transformation Matrices
Between
Non-Linear and Linear
Differential Equations

Robert L. Sartain

Associate Professor

Department of Mathematics and Physics

Houston Baptist University

Houston, Texas

ABSTRACT

In the linearization of systems of non-linear differential equations, we consider those systems which can be exactly transformed into the second order linear differential equation $Y'' - AY' - BY = 0$ where Y , Y' , and Y'' are $n \times 1$ vectors and A and B are constant $n \times n$ matrices of real numbers. We use the $2n \times 2n$ matrix $M = \begin{bmatrix} 0 & I \\ B & A \end{bmatrix}$ to transform the above matrix equation into the first order matrix equation $X' = MX$. We study specifically the matrix M and the conditions which will diagonalize or triangularize M . We indicate transformation matrices P and P^{-1} to accomplish this diagonalization or triangularization and how to use these to return to the solution of the second order matrix differential equation system from the first order system.

We conclude with a study of the relationship between the diagonalization of M to that of the submatrices A and B .

Center Research Advisor: Victor R. Bond

Introduction

(Szebehely, 1976), (Bond and Horn, 1978), and (Bond, 1982) have studied the linearization of systems of non-linear differential equations. In each of these cases the transformation of one system to the other involves square matrices A and B of order n.

In the present paper we consider only those non-linear differential equation systems which can be exactly transformed into the second order linear differential equation system $Y'' - AY' - BY = 0$ where the matrices A and B are constant matrices of real numbers and where Y, Y', and Y'' are n x 1 vectors.

We form the matrix $M = \begin{bmatrix} 0 & I \\ B & A \end{bmatrix}$ which is a matrix of order 2n which arises in the standard transformation of the second-order linear equation to a first-order linear equation by the transformation

$$\left. \begin{array}{l} Z_1 = Y \\ Z_2 = Y' \end{array} \right\} \text{where } Y \text{ is the vector } (Y_1, Y_2, \dots, Y_n)^T \text{ and } Y' = (Y'_1, Y'_2, \dots, Y'_n)^T$$

Observe that this transformation yields $Z'_1 = Y' = Z_2$ and $Z'_2 = Y'' = AZ_2 + BZ_1$.

Written in matrix form we have

$$\begin{bmatrix} Z'_1 \\ Z'_2 \end{bmatrix} = \begin{bmatrix} 0 & I \\ B & A \end{bmatrix} \cdot \begin{bmatrix} Z_1 \\ Z_2 \end{bmatrix}$$

Letting $X = \begin{bmatrix} Z_1 \\ Z_2 \end{bmatrix}$ and $M = \begin{bmatrix} 0 & I \\ B & A \end{bmatrix}$ the equation $Y'' = AY' + BY$ can be reduced to the linear first-order matrix equation $X' = MX$.

This research is concerned with the following questions:

- (1.) What are the conditions on the matrix M which will allow us to solve the matrix differential equation system $X' = MX$.

(2.) Under the assumption that this system can be solved, how does one actually recover the matrices to return to the original second order differential equation system $Y'' - AY' - BY = 0$.

This paper shall try to answer these questions as completely as possible.

Theory

The solution of the first-order linear differential equation system $X' = MX$ depends heavily on the matrix M given. We consider two cases. The most satisfactory solution occurs when the matrix M is similar to a diagonal matrix and much of our research has centered upon what must be known about the submatrices A and B of $M = \begin{bmatrix} 0 & I \\ B & A \end{bmatrix}$ in order to assure that M can be diagonalized. We give some elementary linear algebra theory to familiarize everyone with the ideas.

For a linear homogeneous transformation such as M above, there exist scalars λ_i and vectors X_i which satisfy the equation $MX_i = \lambda_i X_i$. The values of λ_i for which this equation is satisfied are called the eigenvalues of M and the vectors X_i which are fixed under the transformation M for each λ_i are called the eigenvectors. There are many other names associated with these values and vectors, some of which are characteristic values and vectors, latent values and vectors, and proper values and vectors.

Clearly, the zero vector will always satisfy the equation $MX = \lambda X$ for any λ chosen. However, we desire to find nontrivial solutions to the problem. Rewriting the equation as $(M - \lambda I)X = 0$ we see that any nontrivial vector X will satisfy the equation if and only if $\det(M - \lambda I) = 0$ where \det stands for the determinant of the matrix $M - \lambda I$.

The determinant of this is a polynomial equation in λ . Since, in our case, M is of order $2n$, the polynomial equation $f(\lambda) = 0$ will be of degree $2n$, and hence there will be $2n$ eigenvalues associated with M . These values may or may not be distinct, and we shall discuss the consequences later in the paper.

For each distinct eigenvalue, λ , satisfying $f(\lambda) = \det(M - \lambda I) = 0$ there will exist at least one non-trivial eigenvector X satisfying $(M - \lambda I)X = 0$. (Stein, 1967).

The eigenvalues and eigenvectors play a central role in the solution of the differential equation $X' = MX$ and this is our purpose in discussing them here.

A matrix M is said to be similar to the matrix C if there exist a nonsingular matrix P such that $M = P C P^{-1}$.

The matrix M is diagonalizable if it is similar to a diagonal matrix

$$D = \begin{bmatrix} d_1 & & 0 \\ & d_2 & \\ 0 & & \ddots \\ & & & d_n \end{bmatrix}$$

where the large zeros indicate that all elements off the main diagonal are zeros.

Suppose now that the matrix M of our system $X' = MX$ is known to be diagonalizable, then there exists a nonsingular matrix P such that $P^{-1}MP = D(\lambda_1, \dots, \lambda_{2n})$ where the notation $D(\lambda_1, \dots, \lambda_{2n})$ will always mean a diagonal matrix where the $\lambda_1, \lambda_2, \dots, \lambda_{2n}$ are the eigenvalues of M and they lie on the main diagonal of D . See Theorems 6.7.1 and 6.8.1 of (Stein, 1967) for a proof of the above statement.

If we now set $X = PZ$ where P is the matrix which diagonalizes M , then $X' = PZ'$ and $Z = P^{-1}X$. So $PZ' = X' = MX$ or $Z' = P^{-1}MX = (P^{-1}MP)Z$. Thus $Z' = DZ$ where D is our diagonal matrix. Using elementary differential equation theory, it is known that a solution of $Z' = DZ$ is

$$Z = \begin{bmatrix} c_{11} e^{\lambda_1 t} \\ \vdots \\ c_{2n,2n} e^{\lambda_{2n} t} \end{bmatrix}$$

So $X = PZ$ will then solve the original system simply by multiplying the matrix P by the vector Z . Thus it is of paramount importance first to determine whether or not the original matrix M can be diagonalized and if it can, then how does one obtain the matrix P which both diagonalizes M and gives the final solution for the X once we have Z as shown above.

Now consider the second case where the matrix M is not diagonalizable. Every square matrix M is similar to a triangular matrix T with the eigenvalues of M as the diagonal elements of T . A constructive proof of this fact is given in (Stein, 1967) as Theorem 6.8.5. The process again generates a nonsingular matrix P such that $P^{-1}MP = T$. Using the same construction of $X = PZ$ given above, by elementary differential equation theory (Murdoch, 1957), one can solve the system for the original vector $X = (X_1, X_2, \dots, X_n)^T$. If we assume the matrix T is upper triangular then after computing PZ , we will have $X_{2n} = C_{2n,2n} e^{\lambda_{2n}t}$ as in the preceding case, and in general depending on the multiplicity of the eigenvalues, if λ is an eigenvalue of multiplicity r , then the solution for this case will be of the form $e^{\lambda t} p(t)$ where $p(t)$ is a polynomial of degree $r-1$. Thus a solution is possible even in this case although not as easy to obtain or use. If the λ 's are distinct then, for example, if $X_{2n} = C_{2n,2n} e^{\lambda_{2n}t}$, then the solution for

$$X_{2n-1} = C_{2n-1,2n-1} e^{\lambda_{2n-1}t} + C_{2n-1,2n} e^{\lambda_{2n}t}$$

where the C_{ij} 's are the nonzero elements in the upper triangular matrix which correspond to each row i and column j position. One can use these solutions then to substitute in and solve for the next X_i , and so on, until a complete solution is obtained.

Results

We next describe the process of actually obtaining P which will diagonalize or triangularize the matrix to give us the solutions indicated above. We consider each of the cases separately.

Suppose first that M is diagonalizable, then there exists a set of $2n$ linearly independent eigenvectors, say U_1, U_2, \dots, U_{2n} and this is true regardless of whether or not any eigenvalue has multiplicity greater than one or not. See (Edelen, 1976) for a discussion of this property. If we suppose that U_1 corresponds to λ_1, U_2 to λ_2, \dots, U_{2n} to λ_{2n} even if some of the λ 's are equal, then the matrix $P = (U_1, U_2, \dots, U_{2n})$ where each column of P is a vector of length $2n$ will be nonsingular since these $2n$ vectors are linearly independent. We observe that if $\lambda_i = \lambda_j$ for instance, there will still be distinct eigenvectors U_i and U_j which are linearly independent when M is diagonalizable. P nonsingular implies that it has an inverse and the product $P^{-1}MP$ will actually be a diagonal matrix with the eigenvalues down the main diagonal.

We will address the process of determining the eigenvectors for a given λ later in the paper.

We now consider the problem of finding the nonsingular matrix P when the matrix M is not diagonalizable.

The process is given as follows. Process:

- (1.) Find an arbitrary eigenvector, X_1 , for the first eigenvalue λ_1 of your matrix. (We shall assume $\lambda_1, \lambda_2, \dots, \lambda_{2n}$ are successively on the diagonal from top left to lower right.)

(2.) Form $P_1 = (x_1, e_2, \dots, e_{2n})$ provided that P so formed is nonsingular.

(3.) Compute P_1^{-1} and calculate the product $P_1^{-1} M P_1$ where M is our original matrix.

(4.) Using $P_1^{-1} M P_1$ we now have λ_1 in upper left corner. Call the submatrix formed by crossing out the row and column which contains λ_1 , M_1 . If M_1 is a 2×2 matrix skip to step 10. Otherwise compute an eigenvector for λ_2 using M_1 (not M , but it will be the same eigenvalue, λ_2 , as for M).

(5.) Form $P_2 = (x_2, e_3, \dots, e_{2n})$ where x_2 is the $2n-1$ eigenvector found in step 4.

(6.) Compute P_2^{-1} and calculate the product $P_2^{-1} M_1 P_2$. This matrix is of order $2n-1$.

(7.) $P_2^{-1} M_1 P_2$ will now have λ_2 in the upper left hand corner and zeros in the column below it.

(8.) Form the submatrix M_2 by crossing out the row and column containing λ_2 .

(9.) If M_2 is 2×2 goto step 10. If not continue the process as illustrated in steps 5-8 until a submatrix which is 2×2 is finally obtained.

(10.) When M_j is reached which is 2×2 the process will be changed as follows:

Process (Continued)

- (a) Compute an eigenvector using M_j for λ_{2n-1} .
- (b) Compute an eigenvector using M_j for λ_{2n} .
- (c) Let $P_{j+1} = (X_{2n-1}, X_{2n})$. Note it does not contain standard basis vectors as in previous cases.

(11.) Finally form the matrix P as follows:

$$P = P_1 \cdot \begin{bmatrix} I_1 & 0 \\ 0 & P_2 \end{bmatrix} \cdot \begin{bmatrix} I_2 & 0 \\ 0 & P_3 \end{bmatrix} \cdots \begin{bmatrix} I_{n-2} & 0 \\ 0 & P_{2n-1} \end{bmatrix} \text{ where } I_1 = I, I_2 = \begin{bmatrix} 1 & 0 \\ 0 & 1 \end{bmatrix}, \text{ etc.}$$

(12.) Compute P^{-1} . Then the final product $P^{-1}MP$ will triangularize M and leave the eigenvalues on the diagonal of $P^{-1}MP$. Note that this form will create an upper triangular matrix.

Note: Each successive eigenvector is found by reducing $M_j - \lambda I$ to canonical form for $j = 0, \dots, 2n-1$. Then multiplying the reduced matrix by the appropriately sized vector made up of the X_j 's to be in the eigenvector. Solve this system of linear equations by choosing appropriate values for the arbitrary X 's. You can choose $X_j = 1$ for arbitrary X 's if so desired. This then will make up the necessary eigenvector for that λ .

In determining eigenvectors for an M which is diagonalizable, there are two cases to consider. The first case is that for which all eigenvalues are distinct. In this case use Gaussian elimination to reduce the matrix $M - \lambda I$ to canonical form (we use this name to imply that the matrix has ones on the main diagonal and zeros off the main diagonal in so far as possible and always zeros below the main diagonal). Other authors use the phrase "row echelon" form to describe this.

If C is the row echelon form of $M - \lambda I$, then setting $CX = 0$, where X is the $2n \times 1$ vector $X = (X_1, X_2, \dots, X_{2n})^T$, will allow us to obtain the elements X_1, X_2, \dots, X_{2n} of the eigenvector for λ by solving the homogeneous system $CX = 0$. Any convenient choice of the arbitrary X 's will give us an eigenvector for λ . Since all λ 's are distinct in this case, then each of the eigenvectors will be linearly independent so the matrix P formed from the eigenvectors will be nonsingular.

The second case is that where some of the eigenvalues have multiplicity greater than one. In this case, if λ_i is an eigenvalue of multiplicity k_i , then there will be k_i -linearly independent eigenvectors associated with each such λ_i . Recall that we are assuming the diagonalizability of M at this point, otherwise we would not know that this is possible. For each i , one can obtain distinct eigenvectors by choosing different values for the arbitrary variables in the equation $CX = 0$ when solved. Each of these eigenvectors will not only be linearly independent of each other but also linearly independent of eigenvectors obtained from distinct eigenvalues. See the proof of Theorem 6.8.4 of (Stein, 1967) for a proof of this fact.

Thus all $2n$ of the eigenvectors so obtained will be linearly independent and thus the matrix P formed from the eigenvectors as previously indicated will be nonsingular.

We have made the assumption in the above work that M is diagonalizable. Consider now the question of what conditions on M will guarantee that M is diagonalizable.

The most well-known theorem says that every real symmetric matrix is diagonalizable (Stein, 1967). See Theorem 6.8.6. However, our matrix $M = \begin{bmatrix} 0 & I \\ B & A \end{bmatrix}$ is in general not symmetric so we seek other criterion.

A second theorem (6.8.2) indicates that M is diagonalizable if and only if M has $2n$ linearly independent eigenvectors.

The difficulty with using this theorem is that we would like to determine whether or not M is diagonalizable before we compute the eigenvectors so we will know whether to use the diagonalization or triangularization process which we have described above in finding the matrix P and its inverse.

One further theorem (6.8.4.) tells us M is diagonalizable if and only if for each λ_i , the multiplicity of λ_i is equal to $k=2n-r$ where r is the rank of $M-\lambda_i I$. (Stein, 1967).

Although this theorem is better than those above and works on all matrices, it still requires checking the multiplicity of every λ_i against the rank of $M-\lambda_i I$ which could be a rather formidable task.

Thus we look specifically at the form of our matrix $M = \begin{bmatrix} 0 & I \\ B & A \end{bmatrix}$ to determine, if possible, conditions on B and A which will help us decide the diagonalizability of M . To this end, consider the following little known theorem from (Hohn, 1964).

If P is $m \times n$, Q is $m \times n$, R is $n \times m$ and S is $n \times n$ and nonsingular, then

$$\det \begin{bmatrix} P & Q \\ R & S \end{bmatrix} = \det S \cdot \det (P - QS^{-1}R).$$

We now assume that P , Q , R , and S above are all square of size $n \times n$ and also that $SQ = QS$. We can then prove the following theorem.

$$\det \begin{bmatrix} P & Q \\ R & S \end{bmatrix} = \det (PS - QR)$$

Proof: By the first theorem above $\det \begin{bmatrix} P & Q \\ R & S \end{bmatrix} = \det S \cdot \det (P - QS^{-1}R)$. Then using the well-known theorem that $\det AB = \det A \cdot \det B$ when A and B are square $n \times n$ matrices we apply this to the right member above to have $\det S \cdot \det (P - QS^{-1}R) = \det (S(P - QS^{-1}R)) = \det (SP - SQS^{-1}R)$. Since we are assuming $SQ = QS$ we have

$$\det (SP - SQS^{-1}R) = \det (SP - QSS^{-1}R) = \det (SP - QR) \text{ since } S \cdot S^{-1} = I.$$

We now apply this theorem to our matrix $M = \begin{bmatrix} 0 & I \\ B & A \end{bmatrix}$. Since I , the identity matrix, commutes with every matrix of the same size, we have $IA = AI$ so $\det M = |0 \cdot A - B \cdot I| = \det (-B) = (-1)^n \cdot \det (B)$.

Considering the eigenmatrix $M - \lambda I$ we have $\det (M - \lambda I) = \det \begin{bmatrix} -\lambda I & I \\ B & A - \lambda I \end{bmatrix} = \det ((-\lambda I)(A - \lambda I) - B) = \det (-\lambda A + \lambda^2 I - B) = \det (\lambda^2 I - \lambda A - B)$.

Our purpose in looking at $\det (M - \lambda I)$ is to observe that $\det (M - \lambda I) = 0$ is the characteristic equation of the matrix M , but since $\det (M - \lambda I) = \det (\lambda^2 I - \lambda A - B)$, then $\det (\lambda^2 I - \lambda A - B) = 0$ is also the characteristic equation for M , and it is a polynomial equation in terms of the matrices A and B which are submatrices of the original matrix M . Assume first $A=0$, then $M = \begin{bmatrix} 0 & I \\ B & 0 \end{bmatrix}$ and even though we cannot use the theorem just proved ($S = 0$ is not nonsingular) we can still see that $\det M = (-1)^n \cdot \det B$

by Laplace's expansion. To compute the determinant of $M - \lambda I$ in this case we have $\det(M - \lambda I) = \det \begin{bmatrix} -\lambda I & I \\ B & -\lambda I \end{bmatrix}$ and since $-\lambda I$ is nonsingular, the theorem does apply in this case to give us

$\det(M - \lambda I) = \det(\lambda^2 I - B) = (-1)^n \det(B - \lambda^2 I)$. Since for a fixed n , $(-1)^n$ is a constant, it will not affect the eigenvalues in the polynomial characteristic equation. Thus if μ_i , $i = 1, \dots, n$ are the eigenvalues of B , then $\lambda_i = \pm \sqrt{\mu_i}$ will be the eigenvalues of M . (Note: $\det(B - \mu_i I) = 0$ implies $\det(M - \lambda_i I) = 0$.)

Assume now that B is diagonalizable. Then for each μ_i , $i = 1, 2, \dots, n$ there exists an eigenvector U_i , $i = 1, 2, \dots, n$ such that the set (U_1, U_2, \dots, U_n) of eigenvectors is linearly independent. Thus let $T = (U_1, U_2, \dots, U_n)$ be the matrix of eigenvectors as columns in the matrix. Then $T^{-1}BT = D(\mu_1, \mu_2, \dots, \mu_n)$ will be the diagonal matrix of eigenvalues.

Let $S = \begin{bmatrix} \lambda_1 & & 0 \\ & \lambda_2 & \\ 0 & & \lambda_n \end{bmatrix}$ be the matrix where the

λ_i 's here are the positive square roots of the μ_i 's and thus are half of the eigenvalues of M . Consider first the case where $\mu_i \neq 0$ for all $i = 1, 2, \dots, n$. Then S^{-1} exists and

is given by $S^{-1} = \begin{bmatrix} 1/\lambda_1 & & 0 \\ & 1/\lambda_2 & \\ 0 & & 1/\lambda_n \end{bmatrix}$. In this case let $P = \begin{bmatrix} TS^{-1} & TS^{-1} \\ T & -T \end{bmatrix}$ and $P^{-1} = \frac{1}{2} \begin{bmatrix} ST^{-1} & T^{-1} \\ ST^{-1} & -T^{-1} \end{bmatrix}$

or $P^{-1}MP = \frac{1}{2} \begin{bmatrix} ST^{-1} & T^{-1} \\ ST^{-1} & -T^{-1} \end{bmatrix} \begin{bmatrix} 0 & I \\ B & 0 \end{bmatrix} \begin{bmatrix} TS^{-1} & TS^{-1} \\ T & -T \end{bmatrix} = \frac{1}{2} \begin{bmatrix} T^{-1}BT S^{-1} + S & T^{-1}BT^{-1}S^{-1} - S \\ -T^{-1}BT S^{-1} + S & -T^{-1}BT S^{-1} - S \end{bmatrix}$

Computing $T^{-1}BT S^{-1}$ we obtain: $\begin{bmatrix} \mu_1 & & 0 \\ & \mu_2 & \\ 0 & & \mu_n \end{bmatrix} \begin{bmatrix} 1/\lambda_1 & & 0 \\ & 1/\lambda_2 & \\ 0 & & 1/\lambda_n \end{bmatrix} = \begin{bmatrix} \lambda_1^2 & & 0 \\ & \lambda_2^2 & \\ 0 & & \lambda_n^2 \end{bmatrix} \begin{bmatrix} 1/\lambda_1 & & 0 \\ & 1/\lambda_2 & \\ 0 & & 1/\lambda_n \end{bmatrix}$

$= \begin{bmatrix} \lambda_1 & & 0 \\ & \ddots & \\ 0 & & \lambda_n \end{bmatrix} = S$. Since $T^{-1}BT$ diagonalizes B to its eigenvalue matrix.

$$\text{Thus } P^{-1}MP = \frac{1}{2} \begin{bmatrix} S+S & S-S \\ -S+S & -S-S \end{bmatrix} = \begin{bmatrix} S & 0 \\ 0 & -S \end{bmatrix}.$$

Hence this choice for P will diagonalize M where the positive square roots of λ_i are down the diagonal of the upper-left $n \times n$ matrix and the negative square roots of λ_i are the diagonal elements of the lower right $n \times n$ matrix. Thus we have shown how to diagonalize M given any diagonalizable B provided the eigenvalues of B are nonzero. Thus M is diagonalizable when B is diagonalizable provided none of B 's eigenvalues are zero, and provided that $A = 0$.

Now suppose $A = \beta I$, where β is any nonzero scalar. We then obtain

$$\begin{aligned} \det(M - \lambda I) &= \det(\lambda^2 I - \lambda(\beta I) - B) \\ &= \det((\lambda^2 - \lambda\beta)I - B) \\ &= (-1)^n \det(B - (\lambda^2 - \lambda\beta)I). \end{aligned}$$

Again let μ_i , $i = 1, 2, \dots, n$ be the eigenvalues of B . We then have $\lambda_i^2 - \lambda_i\beta = \mu_i$ or $\lambda_i^2 - \lambda_i\beta - \mu_i = 0$, for $i = 1, 2, \dots, n$. By solving these quadratic equations we again obtain the eigenvalues for M from the eigenvalues for B .

If we assume $\mu_i \neq 0$ for all i and that all of the eigenvalues for B are distinct, then the eigenvalues for M will be distinct, and thus M is diagonalizable.

References

1. Bond, V. R., "Error Propagation in the Numerical Solutions of the Differential Equations of Orbital Mechanics", *Celestial Mechanics*, Vol. 27, No. 1 pp. 65-77, May 1982.
2. Bond, V. R. and Horn, M. K., "An Explicit Solution of the Linear Variational Equations of the Two-Body Problem", NASA 78-FM-47, JSC-14440, September 1978.
3. Edelen, D. G. B. and Kydoniefs, A. D. An Introduction to Linear Algebra for Science and Engineering, Elsevier, Lectures 12, 13 and 17, 1976.
4. Hohn, F. E., Elementary Matrix Algebra, Macmillan, Chapters 2, 4 and 8, 1964.
5. Murdoch, D. C, Linear Algebra for Undergraduates, John Wiley & Sons, Chapter 7, 1957.
6. Stein, F. M., Introduction to Matrices and Determinants, Wadsworth, Chapters 6 and 7, 1969.
7. Szebehely, V., "Three Theorems on Relative Motion", *Celestial Mechanics*, Vol. 14, pp. 113-119, 1976.

ION BOMBARDMENT AND ADSORPTION STUDIES
ON ILMENITE (FeTiO₃) BY
X-RAY PHOTOELECTRON SPECTROSCOPY

by

Paul D. Schulze, Ph.D.
Professor of Physics
Abilene Christian University
Abilene, Texas 79699

ABSTRACT

The effects of 5 KeV argon and oxygen ion bombardment on FeTiO₃ (ilmenite) at low temperatures have been studied using X-ray photoelectron spectroscopy (XPS). Also, using this same technique, the adsorption of O₂, NO, N₂O, and CO at 300 K and the adsorption of O₂ and D₂O at 150 K have been studied.

Argon and oxygen ion bombardment of ilmenite have confirmed earlier studies on metal oxides that argon ions generally reduce the anion species while oxygen ions generally oxidize the anion species. The two iron states involved were Fe⁺² and Fe⁰. The reduction of Ti⁺⁴ was not verified although a significant shift in the Ti(2p_{1,3}) binding energies toward the metallic state was observed after oxygen ion bombardment at low temperatures.

At temperatures above 150 K, O₂ adsorbs dissociatively on ilmenite while D₂O adsorbs molecularly below 170 K. Above 300 K NO, N₂O, and CO do not appear to adsorb dissociatively. Low temperature adsorption of D₂O was found to be inhibited by predosing the ilmenite with O₂.

Center Research Advisor: Dave S. McKay

INTRODUCTION

X-ray photoelectron spectroscopy (XPS) has been used extensively to study solar-wind reduction mechanisms on lunar samples¹⁻⁶ and more recently, to study ion-bombardment damaged metal surfaces.⁷⁻⁹ The earlier experiments showed that under ion bombardment, the surface Fe^{+2} in the iron rich lunar samples could be reduced to metallic Fe or Fe^0 . In general, studies have shown that under ion bombardment the reduction to the metallic state is (1) accompanied by the loss of the anion species, e.g., O^- in the case of FeO , and (2) is nearly independent of the incident ion mass.^{4,7} In contrast to the reduction of the cation species under argon ion bombardment, the dominant process during oxygen ion bombardment has been found to be cation oxidation.⁸

Recently this laboratory has been using the technique of XPS to study the adsorption properties of gases on transition metal surfaces.¹⁰⁻¹¹ In the present work we have begun a sequence of experiments designed to investigate the adsorption of small molecules on FeTeO_3 (ilmenite) as a function of ion-bombardment parameters and temperature. Specifically we have considered thus far the adsorption of D_2O , O_2 , NO , N_2O , and CO on polycrystalline terrestrial samples of ilmenite under varying conditions of radiation damage.

EXPERIMENTAL

The present experiments were performed in an ultra-high vacuum chamber having a base pressure on the order of 10^{-9} torr which was equipped with a quadrupole mass spectrometer, a 0-5 keV ion gun, an electron gun for Auger spectroscopy, a magnesium X-ray source (1253.6 eV), and a high-resolution double-pass cylindrical mirror electron energy analyzer.

The XPS data were obtained by coupling the energy analyzer to a 1024 channel analyzer and microcomputer. The ilmenite sample was cut from a larger rock sample with a slow speed diamond saw. The unpolished sample was attached to tantalum foil by bending tabs over the edges of the ilmenite. The foil was then spotwelded to tantalum posts which were in turn attached to a liquid nitrogen-cooled cold stage. The sample could be heated well above 1000 K by passing a current through the tantalum foil. The temperature was monitored by a thermocouple spotwelded to the tantalum foil. The ilmenite was ion bombarded in situ by raising the chamber background pressure of the desired gas to around 10^{-5} torr with the ion gun in the rastering mode. All adsorbates except D_2O , were admitted to the sample chamber through a leak valve after being passed through an appropriate cold trap in order to remove any water.

ION BOMBARDMENT RESULTS AND DISCUSSION

In order to characterize the ilmenite sample and in order to establish a baseline for the present studies, the effects of 5 KeV argon, hydrogen, and oxygen ion bombardment on the sample at 300 K and 150 K were considered. Typical XPS spectra in the $Fe(2p_{1,3})$ region taken after oxygen and argon ion bombardment at 150 K are shown in figure 1. Also seen is the $O(KVV)$ Auger peak near 742 eV. Ion bombardment was found to have little effect on the position of the $O(KVV)$ or $O(1s)$, not shown, binding energies but does alter the peak intensities (peak areas). The $Fe(2p_{1,3})$ peaks were found to be very sensitive to ion bombardment. Argon and hydrogen ions reduced the Fe^{+2} to Fe^0 with approximately the same efficiency. The Fe binding energies from computer deconvolved spectra are given in table 1. The $Fe^0(2p_{1,3})$ states are clearly seen in figure 1 near 710 eV and 722 eV respectively.

TABLE 1. Fe Binding Energies (B.E.) in Electron Volts.

State	Fe ⁰		Fe ⁺²	
	2p ₁	2p ₃	2p ₁	2p ₃
B.E.	711.7	707.8	724.3	720.7

As was expected, very little difference was found between the spectra after argon and hydrogen ion bombardment. Both ions were found to reduce Fe⁺² to Fe⁰ but neither ion would produce any reduction of the Ti⁺⁴ state of ilmenite. Kim, *et. al.*,¹² using XPS, found that Ti⁺³ in Ti₂O₃ was not reduced during argon ion bombardment. In contrast to argon and hydrogen ion bombardment, oxygen ion bombardment would not reduce Fe⁺² but would oxidize any Fe⁰ present near the surface. The O(KVV) intensity during oxygen ion bombardment increased as expected. Figure 2 shows the XPS spectra in the Ti(2p_{1,3}) region for oxygen ion-bombarded FeTiO₃ at 150 K and 300 K. Somewhat surprising was the nearly 1 eV shift to lower binding energies at 150 K. This shift was observed only after oxygen ion bombardment at low temperatures. Work is continuing to determine the origin of this shift and the states that are involved. Oxygen ion bombardment did produce much sharper spectra at 150 K than at 300 K. The spectra after argon ion bombardment gave no indication of any temperature dependence.

ADSORPTION RESULTS AND DISCUSSION

The adsorption of O₂, NO, N₂O, and CO on ilmenite between 300 K and 800 K, and D₂O and O₂ at 150 K has been studied. One difficulty in studying these molecules on ilmenite is the presence of a strong O(1s) XPS signal from the FeO and TiO₂ complexes. Additional O(1s)

contributions are thus hard to observe unless the adsorbate contributions are either very large or several eV's removed from the substrate O(1s) binding energy.

The present study showed that the oxygen-containing molecules NO, N₂O, and CO do not adsorb dissociatively on ilmenite between 300 K and 800 K. This was indicated by the lack of oxidation of Fe⁰ on an argon ion-bombarded surface. Oxygen was found to adsorb dissociatively above 150 K. The oxygen would oxidize the Fe⁰ but not as well as oxygen ions during ion bombardment. This suggests that the radiation damage extends many atomic layers beneath the surface whereas the oxidation that was observed occurs only at the top few atomic layers. Future studies using angle-resolved XPS would be useful in examining this problem.

Figure 3 shows XPS spectra taken in the O(1s) region for argon ion-bombarded ilmenite followed by exposures of 50 L and 250 L (1 L = 1 Langmuir = 10⁻⁶ torr-sec) D₂O at 150 K. Also shown is the spectrum for 200 L D₂O adsorbed on ilmenite predosed with 10 L O₂. The D₂O adsorbed molecularly at 150 K with an O(1s) binding energy of 534.4 eV as opposed to 530.8 eV for the O(1s) of FeTiO₃. Mass spectrometer data yielded a D₂O desorption temperature of 170 K. At 215 K, XPS spectra verified the absence of D₂O from the O(1s) region and also verified the absence of any Fe⁰ oxidation which would have occurred if the D₂O had dissociated upon warming. Curve (d) in figure 3 indicates that the presence of preadsorbed oxygen atoms tends to inhibit the adsorption of D₂O. Similar results were found after oxygen ion bombardment.

CONCLUSIONS

Hydrogen and argon ion bombardment reduced the surface Fe^{+2} to metallic Fe of FeTiO_3 with approximately the same efficiency. Neither ion reduced Ti^{+4} . Oxygen ion bombardment oxidized a previously reduced surface much more efficiently at 150 K than at 300 K. At 150 K, oxygen ion bombardment produced 1 eV shift in the $\text{Ti}(2p_{1,3})$ spectra that was not observed after argon and oxygen ion bombardment.

At 300 K NO , N_2O , and CO would not adsorb dissociatively on an argon ion-bombarded surface of ilmenite. Oxygen was found to adsorb dissociatively above 150 K while D_2O was found to adsorb molecularly below 170 K. Finally, an argon ion-bombarded surface having a preadsorbed oxygen layer or an oxygen ion-bombarded surface inhibits the formation of D_2O ice layers.

REFERENCES

1. R. M. Housley and R. W. Grant, Proc. Lunar Sci. Conf. 6th (1975) 5269.
2. T. Gold, E. Bilson, and R. L. Baron, Proc. Lunar Sci. Conf. 6th (1975) 3285.
3. L. Yin, T. Tsang, and I. Adler, Proc. Lunar Sci. Conf. 6th (1975) 3277.
4. R. M. Housley and R. W. Grant, Proc. Lunar Sci. Conf. 7th (1976) 881.
5. L. Yin, T. Tsang, and I. Adler, Proc. Lunar Sci. Conf. 7th (1976) 891.
6. Yu. P. Dikov, O. A. Bogatikov, V. L. Barsukov, K. P. Florensky, A. V. Ivanov, V. V. Nemoshkalenko, V. G. Alyoshin, and M. G. Chudinov, Proc. Lunar Sci. Conf. 9th (1978) 2111.
7. T. Tsang, G. J. Coyle, I. Adler, and L. Yin, J. Electron Spectrosc. Relat. Phenom. 16 (1979) 389.
8. G. J. Coyle, T. Tsang, and I. Adler, J. Electron Spectrosc. Relat. Phenom. 20 (1980) 169.
9. G. J. Coyle, T. Tsang, I. Adler, and N. Ben-Zvi, J. Electron Spectrosc. Relat. Phenom. 24 (1981) 221.
10. P. D. Schulze, D. L. Utley, and R. L. Hance, Surf. Sci. 102 (1981) L9.
11. P. D. Schulze, S. L. Schaffer, R. L. Hance, D. L. Utley, J. Vac. Sci. Technol. 1 (1983) 97.
12. K. S. Kim, W. E. Baitinger, J. W. Amy, and N. Winograd, J. Electron. Spectrosc. Relat. Phenom. 5 (1974) 351.

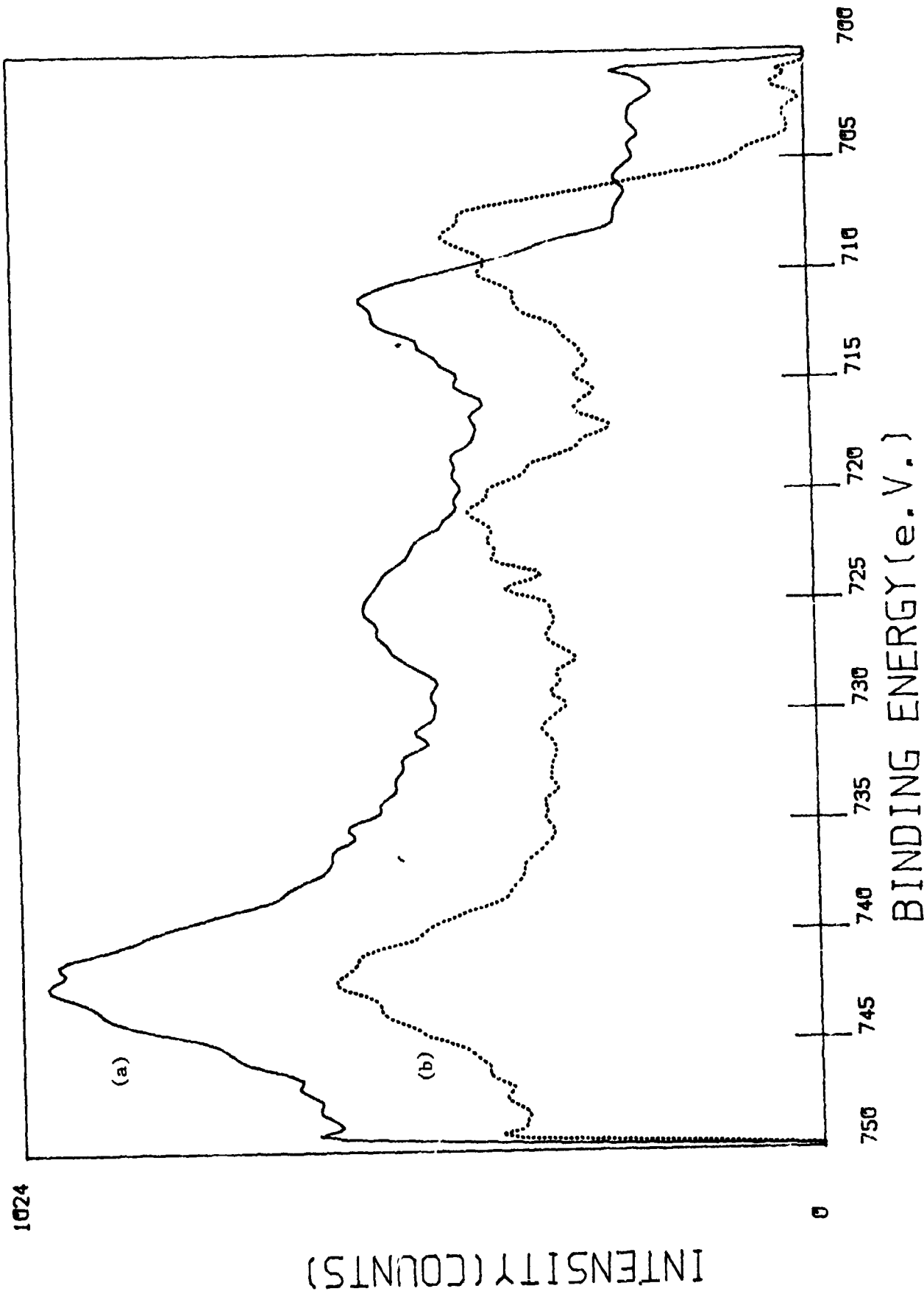


Figure 1. XPS Fe(2p) region at 150 k for (a) oxygen and (b) argon ion-bombarded ilmenite. The curves have been shifted vertically for clarity.

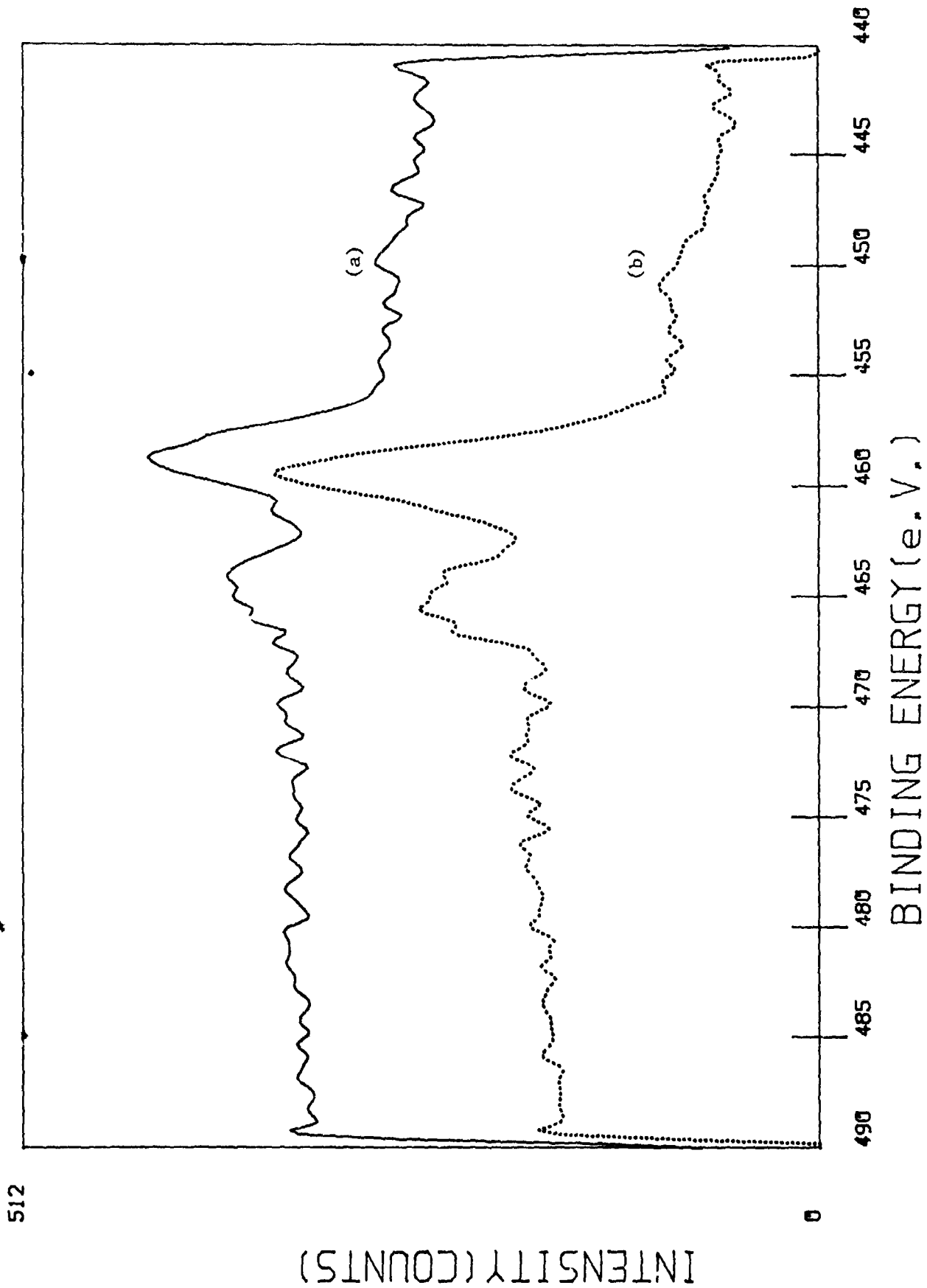


Figure 2. XPS Ti(2p) region for an oxygen ion-bombarded ilmenite surface at (a) 150 K and (b) 300 K. The curves have been shifted vertically for clarity.

INTENSITY (COUNTS)

INTENSITY (COUNTS)

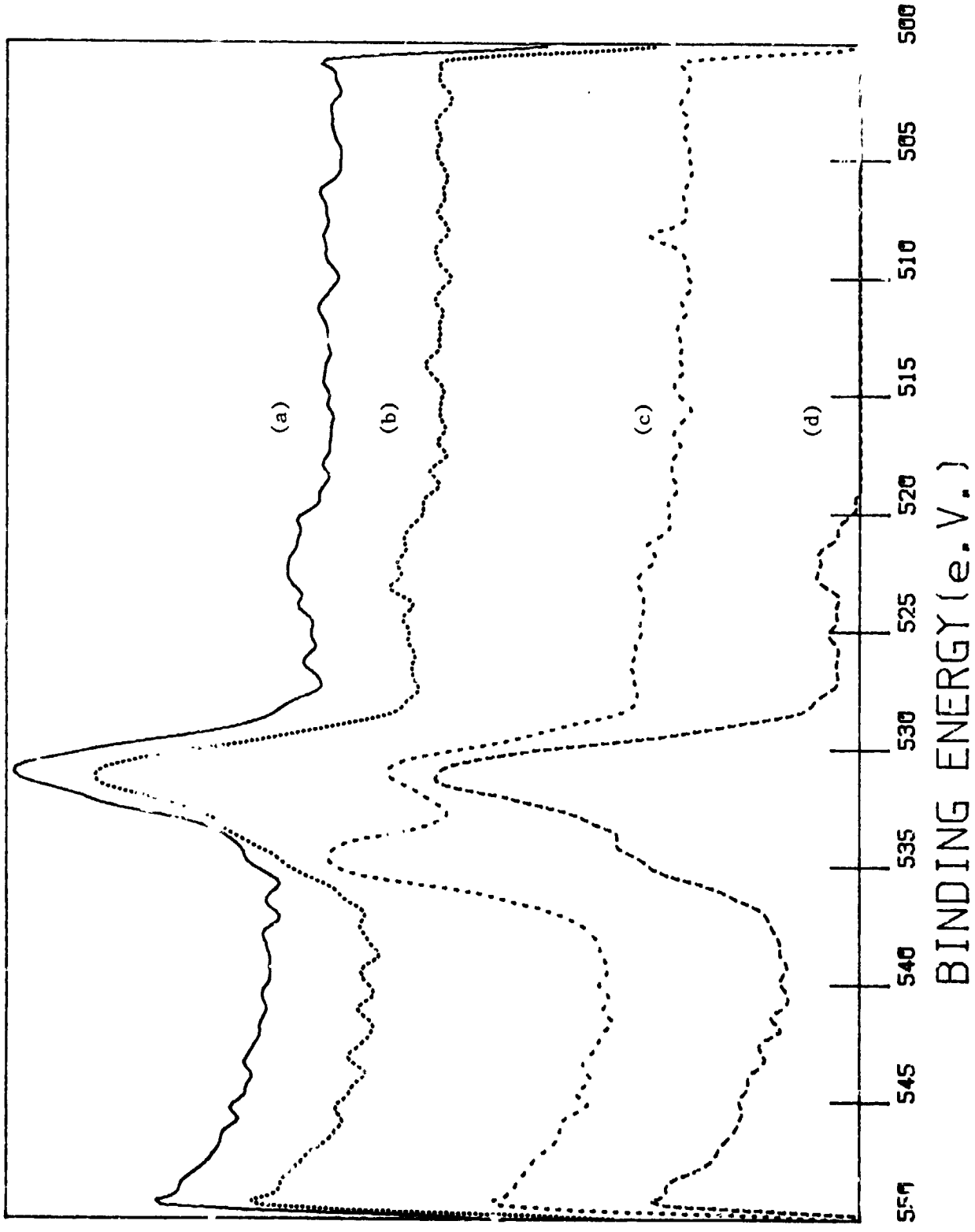


Figure 3. XPS O(1s) region at 150 K for an (a) argon ion-bombarded ilmenite surface and for the same surface exposed to (b) 50 L D₂O; (c) 250 L D₂O; and (d) 10 L O₂ + 200 L D₂O. The curves have been shifted vertically for clarity.

N86-14101

ADVANCED ALGORITHM FOR ORBIT COMPUTATION

By

Victor Szebehely
L.B. Meaders Professor
Department of Aerospace Engineering
University of Texas
Austin, Texas

ABSTRACT

This paper is a report on the continuation of the author's work with V. Bond of NASA-JSC performed in 1981-82. The subject is the formulation of computational and analytical techniques which simplify the solution of complex problems in orbit mechanics, Astrodynamics and Celestial Mechanics.

The major tool of the simplification is the substitution of transformations in place of numerical or analytical integrations. In this way the rather complicated equations of orbit mechanics might sometimes be reduced to linear equations representing harmonic oscillators with constant coefficients.

The first part of this work was reported in several papers and reports by V. Bond and V. Szebehely, which are listed and discussed in the body of this paper. One outcome of the previous work was the derivation of an equation from which the transformations may be computed for a given problem. This equation is known today in the literature as the "Szebehely-Bond-Equation."

The recently performed work reported here, generalizes the previous results to multi-dimensional problems, investigates the role of integrals in conjunction with the transformations and discusses some of the, as yet unsolved problems.

Center Research Advisor: Victor R. Bond,

INTRODUCTION

The method of transforming non-linear differential equations of orbit mechanics into linear differential equations is one of the major problems in celestial mechanics. Hamiltonian canonical transformations in the extended phase-space attack this problem and the relation of this approach to regularization is discussed in detail in several reference books, see for instance Szebehely, 1967. Regularization is the technique to eliminate the singularities of the differential equations of motion and the associated transformations often lead to linearization, see for instance Levi-Civita, 1903 or Stiefel and Scheirele, 1971.

One of the first general investigation of regularization was performed by Sundman, 1912 who introduced a new independent variable and regularized binary collisions in the general problem of three bodies. The purpose of Sundman's work was not to linearize the equations of motion but to show the existence of solutions of the non-linear but regular differential equations of motion. For this reason Sundman's work was not generally accepted and was seldom used by workers in orbital mechanics until close-approach trajectories had to be computed in connection with lunar and planetary missions. Regularization and linearization were rediscovered and were described usually as "transformations" since, as it will be shown, new independent and dependent variables are to be introduced to linearize.

THEORY

The basic idea of this project is deceptively simple. The execution is, on the other hand, extremely complicated and difficult.

The equations of motion in Astrodynamics are second order differential equations with non-linear terms and with singularities. All three difficulties (second order, non-linear, singular) were already known to Sir Isaac Newton; they are due to Newton's second law of motion (according to which the acceleration, \ddot{x} is related to the force), and are connected with Newton's law of gravity (according to which the force is inversely proportional to the square of the distance). The simplest demonstration of the problem uses a one-dimensional example which is represented by the equation

$$\ddot{x} = -\frac{\mu}{x^2}, \quad (1)$$

where dots denote derivatives with respect to time, x is the distance between the participating bodies and μ is a constant depending on the masses of the participating bodies and on the constant of gravity. Equation (1) is a second order, non-linear differential equation with a singularity at $x=0$. In this, simplest of all cases, linearization is easily accomplished by introducing a new independent variable and consequently measuring time (t) with a new clock. The two times (s and t) are connected (Sundman, 1912) by:

$$ds = \frac{dt}{x} \quad (2)$$

It might be seen that this equation introduces a new time s . As x becomes small and the usual time step Δt is reduced during numerical integration, the new time step Δs remains approximately constant. This might be looked upon as a built-in time step control, popular in numerical integration techniques. If we rewrite Equation (1) in terms of s instead of t we obtain another non-linear equation, which, however, with the use of the integral of the energy, might be written in a linear form. The analysis is simple, nonetheless, it reveals some fundamental aspects of the problem and, therefore, it will be reproduced here. The two "time derivatives", i.e. the two velocities

$$\dot{x} = \frac{dx}{dt} \quad \text{and} \quad x' = \frac{dx}{ds}$$

are related by $\dot{x} = \frac{x'}{x}$ (3)

and the two accelerations by

$$\ddot{x} = \frac{x''}{x^2} - (x')^2/x^3 \quad (4)$$

So the new equation of motion becomes

$$x'' = -\mu + \frac{(x')^2}{x} \quad (5)$$

which is just as unpleasant as the original equation was, see Equation (1). So the famous Sundman transformation (Equation 2) neither regularizes nor linearizes the equation of motion. Nevertheless, it might be shown that

the term

$$(x')^2/x$$

becomes linear when the principle of energy conservation is used.

Equation (1) has an energy integral which might be written as

$$\dot{x}^2 = \frac{2\mu}{x} + 2h \quad (6)$$

or as

$$\left(\frac{x'}{x}\right)^2 = 2\mu + 2hx \quad (7)$$

Consequently, Equation (5) becomes

$$x'' - 2hx = \mu \quad (8)$$

This simple example reveals several difficulties of fundamental importance in the theory of linearization, some of which have still not been overcome in the case of the n-dimensional perturbed motion.

As we have seen, the use of Sundman's transformation was not sufficient to linearize the equation of motion and an integral of the system had to be used to accomplish linearization. Furthermore, the dependent variable x was not transformed. The fact is that with a proper $x=f(y)$ transformation, Equation (1) may be linearized without the use of the energy integral.

Consequently, in principle, non-linear equations without energy conservation might be linearized when the proper dependent variable is selected. This is discussed in considerable detail in Szebehely (1976a,b); Schrapel (1978); Szebehely and Bond (1982 and 1983); Bond and Szebehely (1982); Mittleman and Jezewski (1982); Belen'kii (1981), etc.

Now that the basic approach and some fundamental problems have been presented, we are ready to increase the dimensionality from one to two. One of the recent papers on this problem is by Szebehely and Bond (1983) in which the Szebehely-Bond equation is derived in the form:

$$A\rho + B = \frac{1}{2} \frac{d}{d\rho} \left[\left(\frac{g}{F^*} \right)^2 G \right], \quad (9)$$

where $r=F(\rho)$ is the transformation of the old radial coordinate r to the new one ρ , $g(r)$ is the function controlling the time transformation which now becomes

$$ds = \frac{dt}{g(r)}, \quad (10)$$

the function

$$G = 2h + \frac{2\mu}{r} - \frac{c^2}{r^2} \quad (11)$$

represents the energy integral and

$$F^* = \frac{dF}{d\rho}. \quad (12)$$

Those functions (F and g) which satisfy Equation (9) will linearize the two-dimensional equations of motion. Various combinations of these functions were and are discussed in the literature (beginning with Kepler).

The most recent is by Ferrer, to be published in Celestial Mechanics, [Ferrer, 1983].

Similar techniques are available and applicable to accurate orbit calculations for relative motion of satellites, for docking of space probes. etc. [Nacozy and Szebehely, 1976; Szebehely, 1975 and 1976c; etc.]

Transformations leading from unsolved non-linear differential equations to solved non-linear equations are also popular in the mathematical literature. These transformations do not transform the independent variable and, consequently, might not be ideal for problems pertinent to celestial mechanics, nevertheless, they are mentioned here since they may open up new avenues of research [Dasarathy and Srinivasan, 1968; de Spautz and Lerman, 1967 and 1969].

RESULTS

The generalization to n-dimensional motion was performed during the period of May 9 - July 15, 1983. The results will be summarized in this section using analytical description. The verbal evaluation of these results is in the section entitled CONCLUSIONS.

The two-pronged attack may be described as using the direct and the inverse approaches.

The analytical formulation may be represented by matrix notation or by subscript notation.

Consequently, four basic equations represent the results.

The direct approach starts with given non-linear differential equations and attempts to find the transformations which result in linear differential equations. The transformations of the independent and dependent variables are

$$ds = \frac{dt}{g} \quad (13)$$

and

$$y_i = F_i(x_j) ; x_i = F_i(y_j) \quad (14)$$

Using matrix notation these become

$$P = F(R) ; R = \Phi(P) . \quad (15)$$

Here $g=g(x_i)$ or $g=g(R)$ is the function which controls the transformation of the independent variable t . Furthermore x_i is the i -th component of the position vector appearing in the original, nonlinear differential equation. The corresponding vector in matrix notation is R . The dependent variable of the transformed linear equation is y_i or in matrix notation P . Consequently, Equations(14) represent the coordinate transformations in subscript notation and Equations (15) in matrix notation. All symbols represent vectors (R, F, R, Φ) or components of vectors (y_i, F_i, x_i, f_i) excepting the function g which is a scalar depending on the original dependent variable. The function g in the literature is often called a scalar - vector function.

The original nonlinear equation to be transformed is

$$\ddot{x}_i + H_i(x_j, \dot{x}_j, t) = 0 \quad (16)$$

or
$$\ddot{R} + H(R, \dot{R}, t) = 0 \quad (17)$$

where dots represent derivatives with respect to time.

The desired result of the transformation is

$$y_i'' + a_{ij} y_j' + b_{ij} y_j = 0 \quad (18)$$

or

$$P'' + AP' + BP = 0, \quad (19)$$

where primes are derivatives with respect to the transformed time s and $A(a_{ij}), B(b_{ij})$ are matrices with constant or s -dependent elements.

Equations (16) and (17) are the equations to be transformed and are represented here in their most general forms. After the transformations, Equations (16) and (17) become

$$y_1'' + g F_{1,i} (f_{i,j} g^{-1})_{,k} y_k' y_j' - g^2 F_{1,i} H_i = 0 \quad (20)$$

and

$$p'' + (\phi^*)^{-1} \left[(\phi^{**} - \frac{\phi^*}{g} I \frac{dg}{d\phi} \phi^*) P' \right] P' - g^2 (\phi^*)^{-1} H = 0 \quad (21)$$

Here

$$y_1' = \frac{dy_1}{ds}, \quad p' = \frac{dp}{ds},$$

$$F_{1,i} = \frac{\partial F_1}{\partial x_i} \quad \text{and} \quad \phi^* = \frac{d\phi}{dP}$$

Consider Equations (19) and (21). In order to accomplish linearity the two last terms of Equation (19) must be equal to the two last terms of Equation (21). Similarly for Equations (18) and (20). These are the conditions to be satisfied by the transformation functions, g and F in order to obtain linearization.

The problems associated with these requirements will be discussed in the section entitled CONCLUSIONS. Several examples were investigated and interesting and unexpected results were obtained.

The inverse approach starts with the linear Equations (18) and (19), then the transformations, given by Equations (14) and (15), are applied and the following results are obtained:

$$\ddot{x}_l + \alpha_{ljk} \dot{x}_j \dot{x}_k + \beta_{lk} x_k + \gamma_l = 0 \quad (22)$$

and

$$\ddot{R} + [A \dot{R}] \dot{R} + B\dot{R} + \Gamma = 0 \quad (23)$$

where

$$\alpha_{ljk}, \beta_{lk}, \gamma_l, A, B \text{ and } \Gamma \text{ depend on } x_j, R, F, g, a_{ij}, A, b_{ij}, B.$$

Equations (22) and (23) describe the type of non-linear equations which might be linearized by properly selected transformations. Once again, the requirements placed on the transformations will be discussed in the next section. It is noted here that Equations (22) and (23) (or in other words $\alpha, \beta, \gamma, A, B, \Gamma$) are available in forms similar to the details given in Equations (20) and (21).

CONCLUSIONS

(1) The two major approaches, using two different notations were formulated and a thorough study of the comparison revealed complete agreement. From this it may be concluded that the main results, i.e. Equations (20) - (23) are reliable.

(2) Specific examples pertinent to orbit mechanics have shown that integrals of the motion play an important role in addition to the transformations selected.

(3) Transformations given in the literature were substituted and the requirements mentioned in the previous section were satisfied.

(4) It was found that the linearized systems did not necessarily represent the final solutions of the problems and presently diagonalization and triangularization requirements of the matrices A and B are investigated.

(5) The literature concerning transformations of nonlinear differential equations is impressive, to say the least, and the number of references given here could be easily tripled.

(6) The transformations described in this report are restricted and their generalizations might be of considerable interest.

(7) Linear differential equations do not necessarily have Lyapunov-stable solutions. This should influence the selection of the transformation functions.

(8) There are several dynamical systems of considerable importance in orbit mechanics which represent so-called non-integrable systems. If

these systems are investigated in the light of the present report we arrive at one of the following conclusions:

- (i) Non-integrable dynamical systems cannot be transformed to linear systems since linear systems are integrable and their integrals, transformed back into the system of the original variables, would produce integrals of the system. The contradiction might be resolved by claiming that the transformations do not exist.
- (ii) Another resolution is that non-integrable systems are in reality not-integrated systems, meaning that the non-integrability condition exists only under certain conditions, see Poincaré's and Bruns' assumptions concerning the non-integrability of the restricted and of the general problems of three bodies. Accordingly, transcendental transformation functions might result in linearization and consequently in showing integrability of these famous "non-integrable" dynamical systems since some of the above-quoted conditions claim non-integrability in terms of algebraic functions.
- (iii) Furthermore, it is known that certain non-integrable systems have locally valid integrals. These should correspond to locally valid transformations which should satisfy the requirements mentioned in the previous section.

(9) The two, seemingly most significant conclusions are left to items (9) and (10). From a practical point of view, transformations which reduce or eliminate numerical integrations are of the utmost importance. Numerical accuracy is increased and the time requirement for computations is reduced. Autonomous operations require such improvements and their executions are associated closely with the success of establishing the proper transformations.

(10) Establishing transformations either to linear systems or to integrated non-linear systems might be considered one of the greatest accomplishments of modern celestial mechanics. Accurate long-time predictions would be possible for any length of time. This is intimately associated with the study of the stability of the solar system and of the origin and evolution of the Universe. To integrate "non-integrable" systems would show that these systems should have been called "not-integrated" systems to begin with and would challenge the foundation and the famous and classical results of celestial mechanics.

Acknowledgements

This work could not have been performed without the cooperation of two eminent NASA-JSC scientists, Victor R. Bond and Donald J. Jezewski of the Mission Planning and Analysis Division.

Considerable amount of technical support was received from two visiting faculty members, Dr. A. Jackson and Dr. R. Sartain whose cooperation proved to be most beneficial.

Part of this Report was typed by Judi Gilbreath of the Summer Faculty Program of the Johnson Space Center, NASA and part by Mariou Barr of the Department of Aerospace Engineering of the University of Texas at Austin. Their wonderful and most valuable cooperation is gratefully acknowledged.

REFERENCES

1. Belen'kii, I.M., "A Method of Regularizing the Equations of Motion in the Central Force-Field," *Celestial Mechanics*, Vol. 23, pp 9-23, 1981.
2. Bond V. and Szebehely V., "Transformations of the Two-Body Problem to Harmonic Oscillators," NASA-JSC-17933, March 1982.
3. Dasarathy, B.V. and Srinivasan, P., "On the Use of Certain Transformation Techniques in the Study of Non-linear Systems," *International Journal of Control*, Vol. 7, No. 4, pp 361-364, 1968.
4. de Spautz, J.F. and Lerman, R.A., "Equations Equivalent to Nonlinear Differential Equations," *Proceedings of the American Mathematical Society*, Vol. 18, pp 441-444, 1967.
5. de Spautz, J.F. and Lerman, R.A., "Nonlinear Differential Equations and the Terrestrial Brachistochrone," *American Institute of Aeronautics and Astronautics, Journal*, Vol. 7, No. 6, pp 1173-1174, June 1969.
6. Ferrer, S. and Sein-Echaluce, M.L., "On the Szebehely-Bond Equation," to be published in *Celestial Mechanics*, July, 1983.
7. Levi-Civita, T., "Traiettorie Singolari ed Urti nel Problema Ristretto dei Tre Corpi," *Ann. Math.*, [3], Vol. 9., p. 1., 1903.
8. Mittleman, D. and Jezewski, D.J. "A Class of Problems in Celestial Mechanics Reducible to Perturbed Harmonic Oscillator," NASA-JSC-18344, September 1982.
9. Nacozy, P. and Szebehely, V., "The Computation of Relative Motion with Increased Precision," *Celestial Mechanics*, Vol. 13, pp 449-453, 1976.
10. Schrapel, H.D., "Lineare und nichtlineare Hauptschwingungen," *Zeitschrift fur Angewandte Mathematik und Mechanik*, Vol. 58, pp.T. 172-173, June 1978.
11. Stiefel, E. and Scheifele, G., "Linear and Regular Celestial Mechanics," Springer Verlag, Berlin and N.Y., 1971.
12. Sundman, K. "Memoire sur de Probleme des Trois Corps," *Acta Math.*, Vol. 36, p. 105, 1912.
13. Szebehely, V., "Accurate Computation of Relative Motion by Orbit Smoothing," NASA-JSC-09834, August, 1975.
14. Szebehely, V. and Bond, V., "Equations for Autonomous Orbit Calculations," NASA-JSC-18280, June 1982.

15. Szebehely, V. and Bond, V., "Transformations of the Perturbed Two-Body Problem to Unperturbed Harmonic Oscillators, CELESTIAL MECHANICS Vol. 30, pp. 59-69, 1983
16. Szebehely, V., "Lectures on Linearizing Transformations of Dynamical Systems" in Long-Time Predictions in Dynamics (V. Szebehely and B. Tapley editors), pp 17-42. D. Reidel Publishing Company, Dordrecht-Holland, 1976a.
17. Szebehely, V. "Linearization of Dynamical Systems Using Integrals of the Motion," Celestial Mechanics, Vol. 14, pp 499-508, 1976b.
18. Szebehely, V. "Theory of Orbits," Academic Press, N.Y. Chapters 2,3, and 10, 1967.
19. Szebehely, V., "Time Transformations for Relative Motion," Celestial Mechanics, Vol 13, pp 465-470, 1976c.

N86-14102

SOLAR CONCENTRATOR DEGRADATION
IN
LOW EARTH ORBIT (LEO)

Richard G. Thomas, Ph.D.
Professor of Physics
Prairie View A&M University
Prairie View, Texas

ABSTRACT

The use of parabolically or spherically-shaped mirrors is being considered in order to increase the solar energy intensity on solar cells. Their use will significantly decrease the size and number of the cells needed for a particular application, hence the total array cost. Questions arise, however, regarding the long-term (five to ten years) efficiency of these devices. Performance degradation of the mirror surfaces might result from known hostile elements in the low earth orbit (LEO) environment (150-350 nautical miles). This study addresses the degradation issue in light of present knowledge of this environment.

The following characteristics of the LEO environment are identified for study: (1) the vacuum of space; (2) sputtering by the residual atoms and particles in space; (3) solar electromagnetic radiation; (4) contamination of the mirror surface; (5) atomic oxygen interactions with the surface; (6) bombardment of the surface by meteoroids; and (7) irradiation of the surface by ionizing particles (protons). Using the best available information for the magnitudes of the necessary quantities, we carry-out a mathematical analysis, where possible, to determine the degradation in reflectance or other loss caused by each characteristic. Otherwise, reasonable estimates are made of corresponding losses, based on already published data.

It is concluded that vacuum effects on a reflecting surface are negligible for the temperatures expected in space. Also, negligible is the effect of bombardment of the surface by meteoroids. Solar electromagnetic radiation is found to cause a slight (two percent to six percent) degradation in reflectance within the first year or two of exposure, after which no further change is expected. Atomic oxygen interactions pose great danger to a reflecting surface, because large effects have already been observed on relatively short Space Shuttle missions.

Based on the results and studies of solar radiation and atomic oxygen interactions, both of which are fairly well defined at LEO, it seems likely that these two will combine to produce a degradation in reflectance of at least 10 percent over a five to ten-year period. The low energy (<20 kev) protons could play a major role in the degradation in the reflectance. If the flux is as high as 10^{10} /cm²/sec, the degradation is likely to be much higher than 10 percent. This will also be the case if atomic oxygen interactions turn out to be considerably higher than assumed here. On the other hand, if the flux is less than 10^8 /cm²/sec, proton effects will probably be negligible.

Center Research Advisor: William A. Chandler

INTRODUCTION

As the space program expands and the Space Station becomes a reality, there will be more, and no doubt, larger devices needing electrical power. At least part of this need is likely to be satisfied by the use of solar cells, continuously changed in position to track the sun. In order to minimize the number needed (and hence cost) of these rather expensive devices, consideration is now being given to the use of concentrators that will increase the intensity of energy falling on each cell. The concentrators are likely to be of some parabolic or spherical design, with a reflective coating of aluminum, nickel, silver, or some other suitable material. The mirror coatings may or may not be protected by a thin, transparent outer oxide layer of silicon, depending on circumstances. For both kinds (coated and uncoated), but particularly the bare unprotected surfaces, there is some concern that their initially high reflectivities might decrease significantly before the period of planned use (five to ten years) has expired, as a result of their exposure to the LEO environment. The purpose of this study is to investigate the long-term (five to ten years) effect that the near-earth (150-350 nm) environment is likely to have on the specular reflectance of these mirrors.

THEORY AND RESULTS

At LEO, we will consider the following known characteristics of space as being potentially damaging to optical surfaces: (a) the vacuum of space; (b) sputtering phenomena; (c) solar electromagnetic radiation; (d) contamination by thin films; (e) atomic oxygen interactions; (f) bombardment by meteoroids; and (g) irradiation by ionizing particles.

The Vacuum of Space

At a distance of 125 miles from the surface of the earth, atmospheric pressure is about 10^{-6} mm of Hg. At this low value, there is the possibility that molecules of the solid reflective surface will evaporate into the surrounding vacuum much faster than they return to it. The Langmuir equation (1) describes this process and is written:

$$(1) W = P/17.14 (M_s/T)^{1/2} \quad \text{where}$$

W = rate of evaporation (gm/cm²/sec)

P = vapor pressure of the material (mm Hg)

T = temperature (⁰K)

M_s = molecular weight of the surface material in the gas phase

The vapor pressure of Al is 10^{-10} atm at 744⁰C. Using these figures in equation (1), one finds an evaporation rate of 0.084 mm/year. This is a rather large rate but poses no serious problem, because the temperature is much higher than will be encountered at LEO. At LEO temperatures (-70⁰C to +50⁰C), the vapor pressures of all commonly used reflecting metals are considerably smaller than 10^{-10} atm. It is believed, therefore, that this effect will at most cause a very slow decrease in optical reflectivity due to possible differences in evaporation rates in different grains of the metal.

Sputtering Phenomena

The removal of atoms from the reflecting surface as a result of its bombardment by low energy (<1 mev) atoms and ions in the environment is called "sputtering". A threshold energy exists for doing this that depends on the nature of the impinging atom or ion and of the surface. For protons hitting an aluminum surface, this threshold is found to be about 0.5 kev, while it is about 0.1 kev for nitrogen or oxygen atoms. For atoms and ions with energies above their threshold values, it can readily be shown that

$$(2) \Delta t_s = \phi \epsilon M_s / \rho A_v \text{ where}$$

Δt_s = rate of decrease in thickness of the film (cm/sec)

ϕ = incident flux of atoms or ions (no/cm²/sec)

ϵ = yield, the number of surface atoms liberated/incident atom

ρ = density of the reflective material (gm/cm³)

A_v = Avogadro's Number

The greatest uncertainties in the use of equation (2) for LEO are in the yield factor and the incident flux of protons. Using the best available estimates of these, we find the sputtering loss due to residual air (oxygen and nitrogen) will be about 0.15 \AA^0 /year. This is considered a negligible amount. On the other hand, the low energy protons at LEO will potentially sputter off about 100 \AA^0 /year, which is a relatively large amount.

Solar Electromagnetic Radiation

The effect of ultraviolet radiation on a bare aluminum surface has been studied (2), and a reproduction of one of the graphs resulting from this study is shown in figure 1. In this study, a mercury-arc lamp was used as the source of U-V radiation. The most striking feature of these curves is the saturation effect that appears after about 2,000 Equivalent Space Sun Hours (ESSH). After this time, there is essentially no further change in reflectance. If one assumes continuous sun exposure, 2,000 hours will be accumulated in about three months. At an exposure of 8 hours/day, one sees that maximum degradation of two percent to six percent will occur in about nine months.

Contamination by Thin Films

At every stage in the assembly and deployment of a mirror, great care must be taken to see that the surface is kept clean. Additionally, a thin film of carbon or other contaminant material can form from organics used in

surrounding parts of the structure, if they outgass significantly. Bremer (3) has calculated the maximum allowable contaminant film thickness that will lead to a degradation of 10 percent in reflectance. His conclusion is that a film about one nanometer thick will produce such a loss. In a study of this problem, Gillette (2) used a source of protons. It has been observed over the years in the laboratory that radiation, too, can cause the buildup of a contaminant film. He estimated that a film from 0.5 to about 1.5 nanometers accumulated in three to four hours exposure at 16 kev, $10^{13}/\text{cm}^2/\text{sec}$. If one assumes that the buildup time varies inversely with beam intensity, then at the assumed intensity of the protons in LEO ($\sim 10^{10}/\text{cm}^2/\text{sec}$) a 10 percent degradation in reflectance, due to this effect, might be expected to occur in about five or six months of exposure. On the other hand, if the flux is less than $10^8/\text{cm}^2/\text{sec}$, as has been estimated in another source (8), no film buildup will occur.

Atomic Oxygen Interactions

On the first three missions of the Space Shuttle, it was observed that physical changes occurred in some of the commonly used materials after exposure to the space environment. Following this observation, a series of specially selected materials was set up in an experiment designed to investigate this effect. A report of the results of this exposure has been made (4). In the series were a group of thin films ($100 \text{ \AA} - 2,000 \text{ \AA}$) of silver, carbon, and osmium. The osmium was completely lost through evaporation, while the silver was completely oxidized. In another test, aluminum was exposed, but the results were inconclusive. It is now thought that these changes are due to the chemical action of oxygen in the environment on the surface atoms. Because of its similarity to sputtering, this process is sometimes considered to be a form of it. (8) No loss rates have been

established for the metals likely to be used as reflector coatings. On the other hand, a large loss of 5.25 mils is predicted for kapton and mylar over a ten-year period. On the basis of the size of this effect, the behavior of silver in a very short time, and the uncertainty in the behavior of aluminum, one has to be concerned about this interaction.

Bombardment by Meteoroids

Meteoroids are very small solid particles moving in interplanetary space. A model of the flux-mass distribution has been constructed and is given in figure 2. (5) To simulate the behavior of these particles striking a mirror surface, Bjork designed a mathematical model. (6) This model, which has been verified experimentally, predicts that the bombardment will result in hemispherical craters being formed in the mirror surface. The radius of a crater is given by:

$$(3) \quad r = C (mv)^{1/3} \quad \text{where}$$

r = radius (cm)

m = mass of projectile (grams)

v = impact velocity (km/sec)

C = a constant that depends on the target

Bjork found C = 1.09 for Al on Al, and 0.606 for Fe on Fe. In this study, we set C = 1. The analysis of meteoroid damage consists of calculating the fraction of the total area of a reflector damaged by strikes. It is assumed that no two particles strike the same area, that all are moving with the average speed of 20 km/sec (5), that the damaged area has a lower constant average reflectance, and that meteoroids have the mass and flux distribution given in figure 2. The result of this analysis is that there will be no damage from this source, because of the smallness of the flux and masses of the meteoroids.

Irradiation by Protons

While the very low energy protons will be unable to penetrate the reflecting surface and will interact basically by sputtering, those at some slightly higher energies will penetrate to depths that depend on their energies. If the energy is too high, they will pass through the thin film with little or no damage. In the range of energies that result in their being stopped in the film, radiation damage may occur. This phenomenon was observed for a bare aluminum reflector by Gillette. (2) He found that severe blistering of the film resulted from an exposure of 10^{17} protons/cm² of 16 kev energy. He estimated their range in Al to be 3500 Å. Using these figures, one readily finds this to be a radiation dose of 2.7×10^{11} rads (1 rad = 100 ergs/gm). Fuller (7) estimates that radiation damage occurs for an exposure between 10^8 and 10^{12} rads. Another estimate (8) places this threshold at about 10^{14} rads for Al and other metals. Gillette's results tend to support the smaller estimate. We have previously assumed a flux of 10^{10} /cm²/sec of low energy solar protons. Their average energy, however, is lower than 16 kev. Assuming this value is say 2 kev, we find the dose rate to be 8.54×10^{11} rads/year. On the basis of the above results, one would certainly expect blistering of this material under these conditions.

CONCLUSIONS

Since all of the processes that have been considered are actually occurring simultaneously in LEO, the question naturally arises as to their combined effect on a reflecting surface. There does not appear to be a way, a priori, of combining these effects. Nevertheless, some reasonable conclusions can be drawn.

Vacuum effects on a reflecting surface are negligible for the temperatures expected in space. Also negligible is the bombardment of the surface by

meteoroids. Of the remaining five characteristics considered, protons are involved in three. The remaining two, solar electromagnetic radiation and atomic oxygen interactions, are both fairly definite processes that have already been observed, and to some extent studied. Based on these studies, it appears likely that they will combine to produce a degradation in reflectance of at least 10 percent over a five to ten-year period. Such a minimum degradation will be independent of the material used, its size, or how it is exposed (bare or protected) to the environment. The fact that protons are involved in three of the characteristics emphasizes the need to know this flux distribution more accurately. If the flux is as high as we generally assumed ($10^{10}/\text{cm}^2/\text{sec}$), the degradation in reflectance is likely to be much higher than 10 percent. This will also be the case if atomic oxygen interactions turn out to be considerably higher than assumed here. On the other hand, if the flux is less than $10^8/\text{cm}^2/\text{sec}$, proton effects will probably be negligible.

REFERENCES

1. Jaffe, L. D., and Rittenhouse, J. B., "Behavior of Materials in Space Environment," JPL Technical Report Number 32-150, November 1961.
2. Gillette, R. B., "Ultra-violet-Proton Radiation Effects on Solar Concentrator Reflective Surfaces," NASA CR-1024, May 1968.
3. Bremer, J. C., "General Contamination Criteria for Optical Surfaces," SPIE, Volume 287, Shuttle Optical Environment, 1981.
4. Leger, L. J., "Oxygen Atom Reaction with Shuttle Materials at Orbital Altitudes - Data and Experiment Status," AIAA - 83-0073, AIAA 1983, January 1983.
5. Meteoroid Environment Model - 1969 (Near Earth to Lunar Surface), NASA SP-8013, March 1969.
6. Bjork, R. L., "Effects of a Meteoroid Impact on Steel and Aluminum in Space," Rand Document P-1662, December 1958.
7. Fuller, F., "Mathematical Model of Factors Affecting Solar Energy Collector Efficiency," Wadd Technical Report 60-907, December 1960.
8. NASA Research Advisory Committee on Missile and Space Vehicle Structures, "Environmental Problems of Space Flight Structures: I. Ionizing Radiation in Space and Its Influence on Spacecraft Design", NASA TN-D-1474.

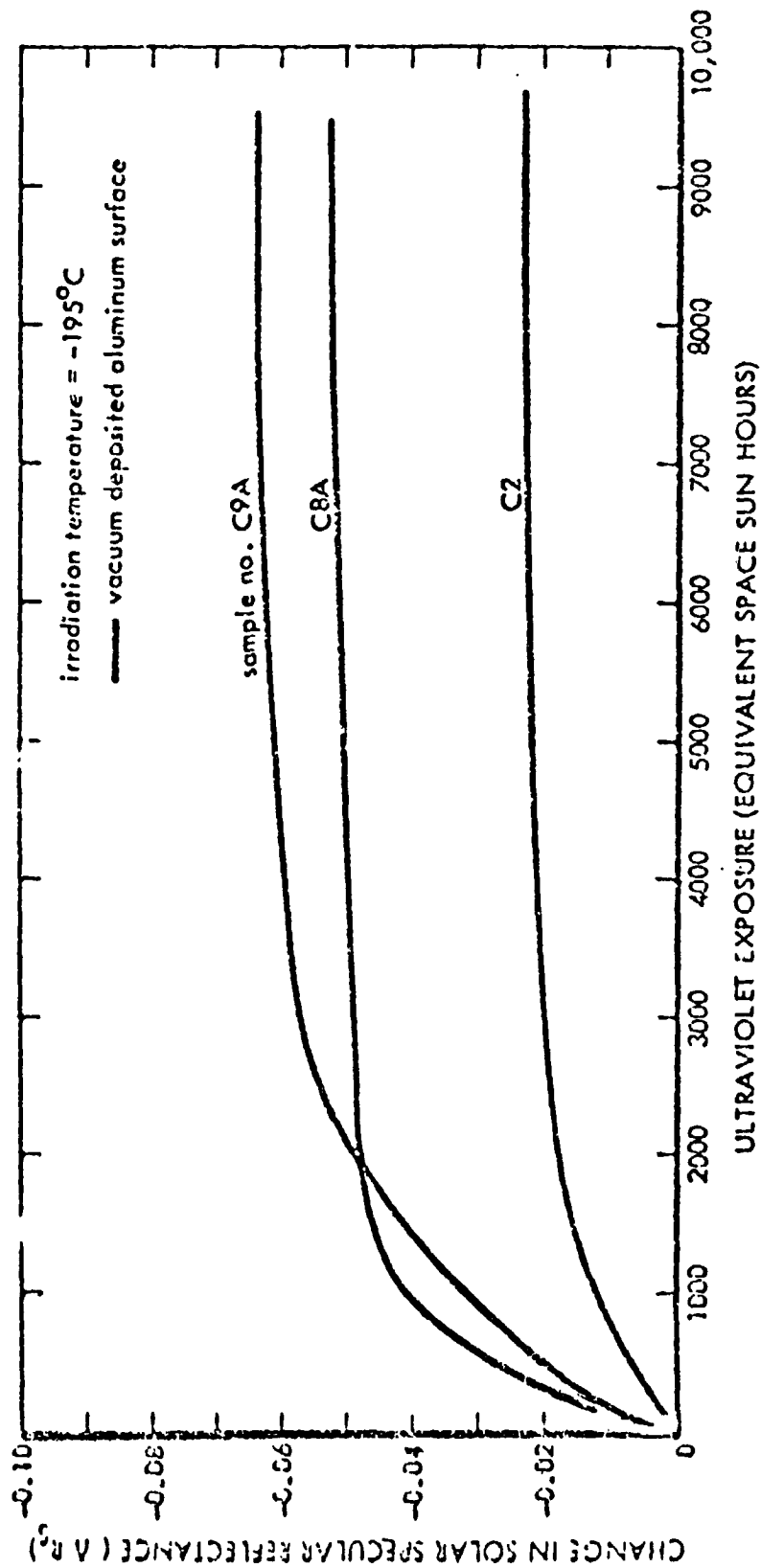


Figure 1. Effect of Ultraviolet Radiation on Solar Specular Reflectance of Nickel Substrate Mirrors (From Reference 2)

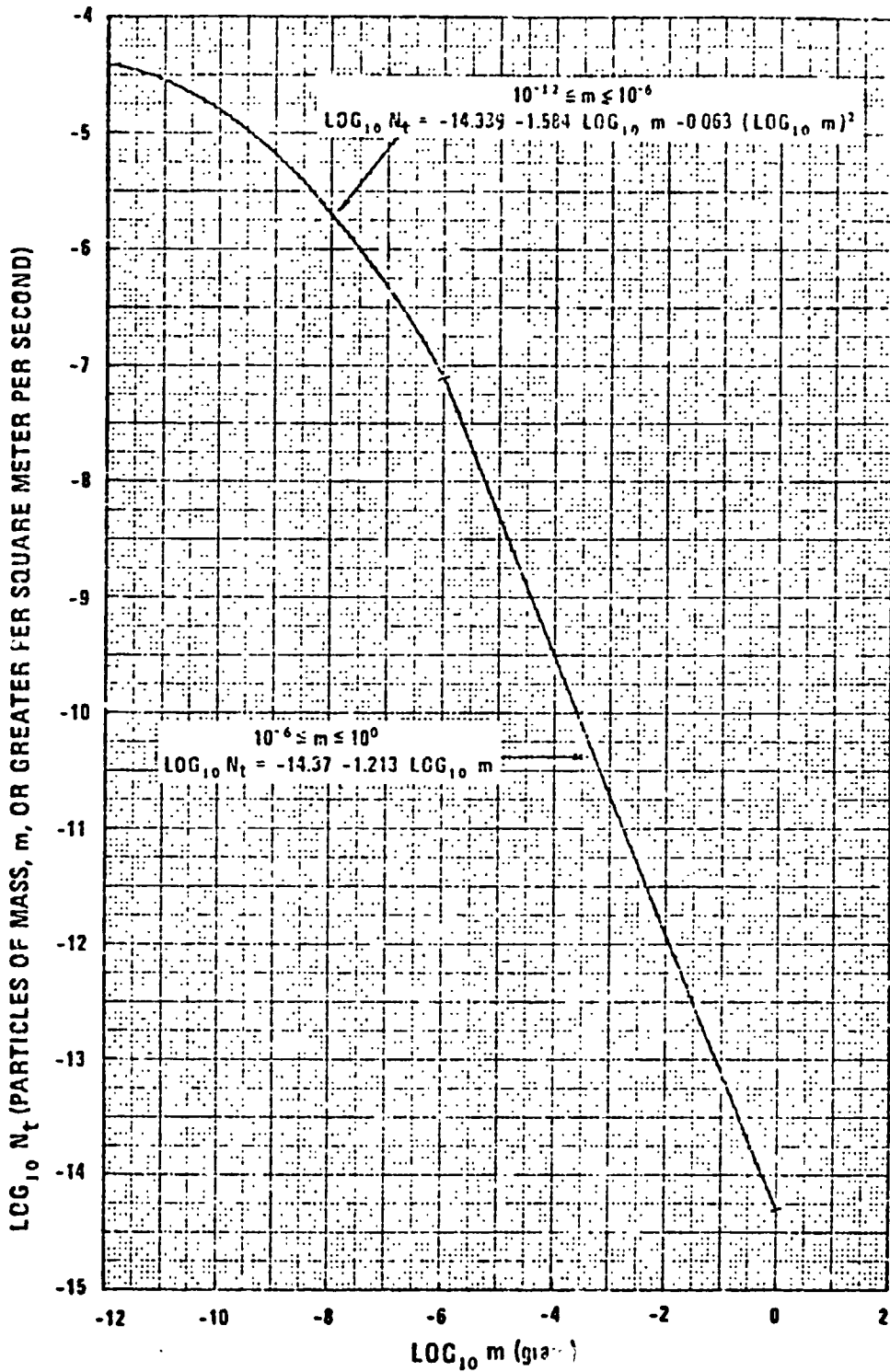


Figure 2. Average Cumulative Total Meteoroid Flux-mass Model for 1 A.U. (From Reference 5)

ORIGINAL PAGE IS
OF POOR QUALITY

N86-14103

FORTRAN PLOTTING SUBROUTINES FOR
THE SPACE PLASMA LABORATORY

BY

RAYMOND WILLIAMS
MISSISSIPPI VALLEY STATE UNIVERSITY

FORTRAN Plotting Subroutines for the Space Plasma Laboratory
Raymond Williams, Computer Science and Mathematics Department
Mississippi Valley State University

ABSTRACT

The computer program outlined in this paper referred to as PLOTRW was custom made to satisfy some of the graphics requirements for the data collected in the Space Plasma Laboratory at the Johnson Space Center (JSC).

The general requirements for the program were as follows:

- (1) All subroutines shall be callable through a FORTRAN source program.
- (2) All graphs shall fill one page and be properly labeled.
- (3) There shall be options for linear axes and logarithmic axes.
- (4) Each axis shall have tick marks equally spaced with numeric values printed at the beginning tick mark and at the last tick mark.
- (5) There shall be three options for plotting. These are 1) point plot, 2) line plot and 3) point-line plot.

The subroutines were written in FORTRAN IV for the LSI-11 Digital Equipment Corporation (DEC) Computer. The program is now operational and can be run on any TEKTRONIX graphics terminal that uses a DEC Real-Time-11 (RT-11) operating system.

INTRODUCTION

There are numerous plotting packages on the market today. Some of which are very general and comprehensive, while others are written for specific applications or tasks. Many of the comprehensive graphics packages require a great deal of computer memory for its operation and therefore operates more effectively in a main frame computer environment. But most small science

laboratories employ a microcomputer for their data reduction and data analysis. Thus, a comprehensive plotting package may not be very useful in a small laboratory environment.

Additionally, the specific application software packages very seldom if ever satisfy the many approaches a scientist might employ to study an experiment. For these reasons, among others, small laboratories strive to obtain custom made software that is compatible with their present computer system for their data reduction and data analysis.

THE RT-11 OPERATING SYSTEM

A computer system is the concerted efforts of the computer hardware and computer software working together to make it as easy as possible for a programmer to use the computer to solve problems and/or process data. The hardware elements are the mechanical devices in the system, the machinery and the electronics. While the software elements are the programs that are written to perform logical and mathematical operations and provides a means for you to control the system.

The LSI-11 computer employs an RT-11 operating system. the RT-11 is a disk based, single-user, real-time operating system designed for interactive program development. It offers optional support of a number of high-level language processors, including FORTRAN IV, BASIC, and APL.

A minimum RT-11 system must include the following: (1) a processor such as the LSI-11 processor, (2) at least 24K bytes of memory, (3) a console terminal, (4) a line frequency clock, (5) a system device (random access mass storage device, and (6) a system backup device.

SUMMARY - DOCUMENTATION PLOTRW

PLOTRW is written on a single side, single density flexible disk. The program consists of some three hundred and seventy two (372) lines of codes and twenty-one (21) subroutines. (See figure 1). Some of the subroutines are modifications from an existing plasma program at JSC, others are TEKTRONIX software and the remainder were developed by the writer.

PLOTRW is very easy to use. The hardware requirements include an RT-11 operating system, a DEC processor, a TEKTRONIX graphics terminal, and a TEKTRONIX printer. The program is started by typing on the terminal the string RUN PLOTRW followed by a carriage return. The following message will then be displayed (see figure 2):

```
IDATA = 1 INPUT DATA AT TERMINAL
IDATA = 2 INPUT DATA OTHER SOURCES
NDPTS = NO. OF DATA POINTS
IDATA? NDPTS?
```

The user should now enter a one or a two followed by a comma or blank, the number of data points and a carriage return. The string X? Y? is now written to the screen. The ordered pairs of real data points are now entered. Each ordered pair of points is followed by a carriage return. After all data points have been entered the screen will now display:

```
MODEP = 1 POINT PLOT
MODEP = 2 LINE PLOT
MODEP = 3 POINT-LINE PLOT
MODEP?
```

The number 1, 2 or 3 should now be entered followed by a carriage return to continue. The next message displayed on the screen gives options for plotting. The choices are linear-linear scales, log-linear, linear-log, and log-log.

It is not mandatory that all data in a data set be graphed. PLOTBW allows you to enter the number of data points you wish to be graphed. After entering this number and a carriage return another message is displayed on the screen. To continue enter any single digit integer and a carriage return.

The desired graph will now be displayed. A copy of the graph can be transferred to the printer. PLOTBW will make ten cycles with the same data set to allow the user options for changing graph requirements such as MODEP, MODE, etc. To initialize another cycle enter any single digit integer followed by a carriage return. To terminate the programs short of ten cycles, enter a control (CTRL) C.

SUBROUTINES FOR PLOTW

.MAIN.
SCALEP
MINMAX
SCALE
RANGE
AXSET
RNDTIC
ZINIT
AXES
AXTICS
AXLABL
TIC
NUMBER
PLOT
ZPLOT
XPLOT
TITLE
YULOGX
LOGYUX
LYULX
DATA
*

FIGURE 1

TERMINAL DISPLAY - PLOTW INITIALIZATION CONSTANTS

RUN PLOTW

IDATA=1 INPUT DATA AT TERMINAL

IDATA=2 DATA INPUT OTHER SOURCE(SEE SOURCE PROGRAM)

NOPTS= NO OF DATA POINTS

IDATA? NOPTS?

1,2

X? Y?

1.0,3.0

4.0,5.0

MODEP=1 POINT PLOT

MODEP=2 LINE PLOT

MODEP=3. POINT-LINE PLOT

MODEP?

2

MODE=1 Y VERSES X

MODE=2 LOG(Y) US X

MODE=3 Y US LOG(X)

MODE=4 LOG(Y) US LOG(X)

MODE?

4

XUMIN=MIN VALUE X-AXIS XUMAX=MAX VALUE X-AXIS

YIMIN,YIMAX=MIN AND MAX VALUES Y-AXIS

XUMIN?

XUMAX?

0.0,3.0

YIMIN?,

YIMAX?

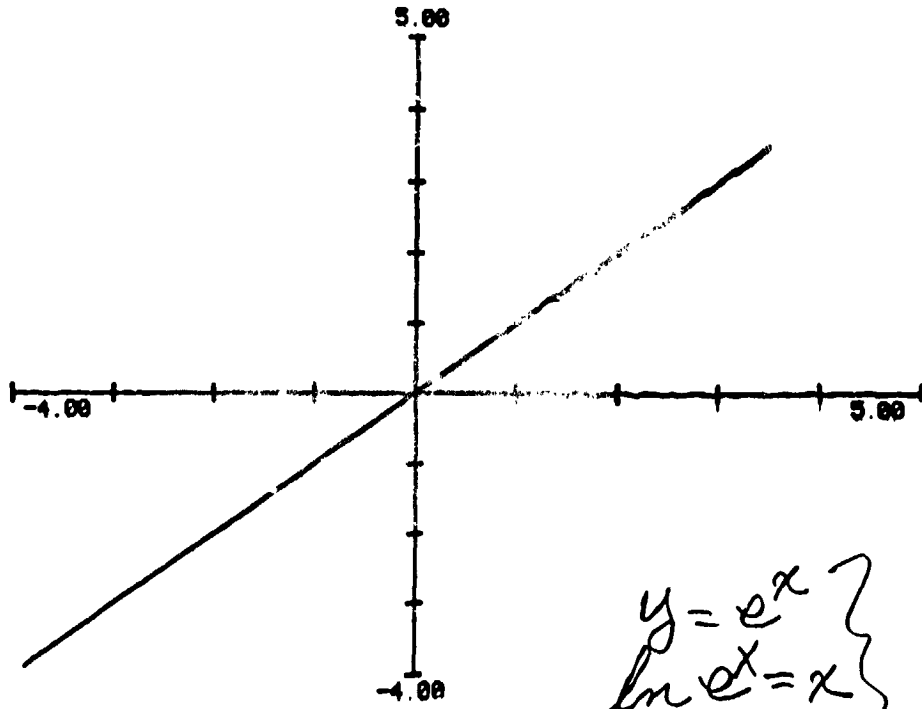
3.0,5.0

NPTS=NO. OF DATA POINTS TO BE PLOTTED. NPTS SHOULD BE LESS THAN OR EQUAL TO NO.DATA POINTS

NPTS?

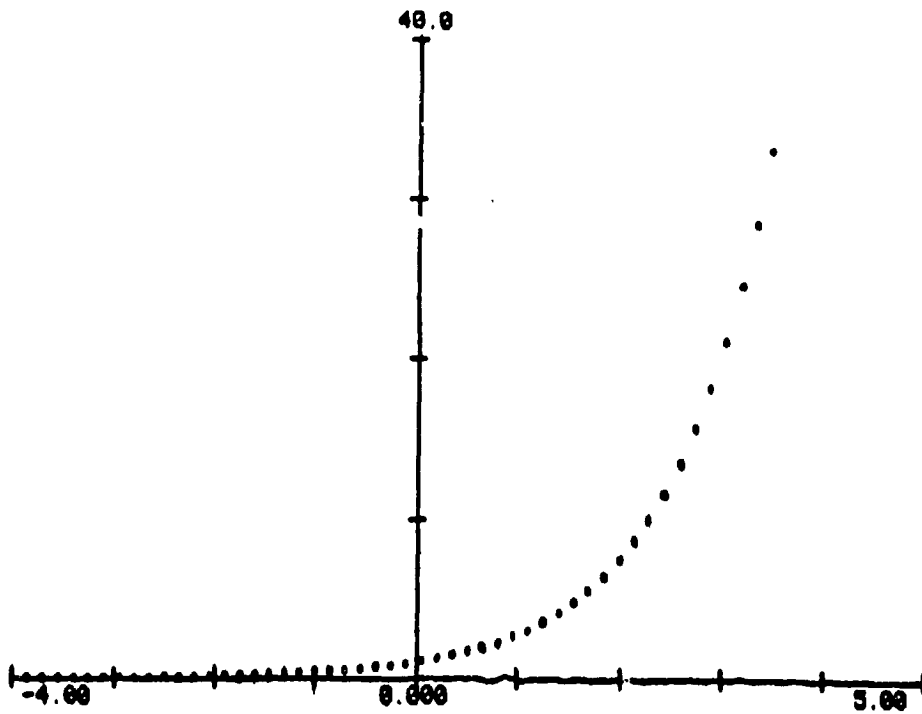
FIGURE 2

LOG Y VERSUS X



$$\left. \begin{array}{l} y = e^x \\ \ln e^x = x \end{array} \right\} y = x$$

Y VERSUS X



N86-14104

COMPUTER GRAPHICS APPLICATIONS
TO CREW DISPLAYS

Joan Wyzkoski
Assistant Professor
Department of Mathematics
Bradley University
Peoria, Illinois 61625

ABSTRACT

Astronauts are provided much data and information via the monochrome CRT displays on the orbiter. For this project two areas were investigated for the possible introduction of computer graphics to enhance and extend the utility of these displays. One involved reviewing the current orbiter displays and identifying those which could be improved via computer graphics. As an example, the tabular data on electrical power distribution and control was enhanced by the addition of color and bar charts. The other dealt with the development of an aid to berthing a payload with the Remote Manipulator System (RMS). This aid consists of a graphics display of the top, front and side views of the payload and cargo bay and point of resolution (POR) position and attitude data for the current location of the payload. The initial implementation was on an IBM PC clone. This program previews the demonstration software installed in the Johnson Space Center Manipulator Development Facility (MDF). Due to current hardware limitations, the MDF version is slow, i.e. about a 40+ second update rate and, hence, not "real-time." Despite this fact, the evaluation of this additional visual cue as an RMS operator aid indicates that this display, with modifications for speed, etc., can assist the crew. Further development is appropriate.

INTRODUCTION

Color and graphics, if carefully selected, enhance the display and understanding of data. Computer graphics, in particular color graphics, furnishes an excellent means to improve the presentation of information. This, in turn, encourages quicker interpretation and, hence, response to data. More efficient response to information facilitates man-machine interaction.

Orbiter computer CRT displays provide much data and information to the crew. Reviewing these displays and identifying those which can be enhanced via computer graphics was one facet of the project. The other area of investigation involved the development of an aid to facilitate payload berthing by the Remote Manipulator System (RMS) operator.

Displays

Numerous CRT displays are selectable by the crew during each flight of the shuttle. These show data and information in a variety of formats. Some are quite specific and apply to the ascent and reentry of the orbiter. Others indicate the status of the various shuttle systems and typically are in tabular form.

All the displays were reviewed. A display of the data on electrical power distribution and control was chosen to demonstrate a possible enhancement of displays. Color and bar charts replace tabular digital data. Most entries have a high(H), medium(M) or low(L) range. Red, green and yellow, respectively indicate each range. In order to respond to the

high range of a particular portion of the electrical system, spotting a "red" condition is easier than spotting an "H".

Payload Berthing Aid

To berth a payload the RMS operator, working in the aft flight deck, currently uses several visual cues. In most cases a portion of the payload can be viewed from the two aft payload bay viewing windows. Starboard and port TV cameras are positioned on the fore and aft bulkheads of the cargo bay. Two others are located at the elbow and wrist, respectively, of the manipulator arm. On monitors, located in the aft flight deck, the operator can select views from up to four of the cameras. Digital information about the position and attitude of the point of resolution (POR) of the payload (This is explained in the Theory section.) is also available.

An additional visual cue to aid in payload berthing was developed. This aid consists of a computer graphics display of the top, front and side views of the payload and cargo bay along with the POR position and attitude data. See figures 1 and 2.

THEORY

The choice of colors and the selection of an appropriate graphic played major roles in the implementation of an enhanced display for the orbiter.

Developing the software to display the updated views of the payload required some mathematical analysis and computation. As shown in figure 3, the orbiter coordinate system is a right-handed system. The positive x-axis is forward, the y-axis is starboard and z is down. The FOR is a preselected point within the payload. The position is indicated as x, y, z values in the orbiter coordinate system. The attitude of the payload, or the pitch, yaw and roll of the payload which would orient it into its present attitude, is a series of rotations about lines passing through the specified control point and parallel to the appropriate orbiter axis. Pitch is a rotation about the orbiter y-axis in a clockwise direction. A counterclockwise rotation about the orbiter's z-axis produces yaw. While a clockwise rotation about the x-axis of the orbiter causes the payload to roll.

Three dimensional data bases along with the appropriate move/draw specifications were defined for the cargo bay and payload, respectively. These data points are placed in n (# of data points for the cargo bay or payload) by 3 matrices. The updated position of the payload is a translation by the change in x, y and z, respectively. These changes are added to the respective coordinates of each data point for the payload. The rotations to accomplish pitch, yaw and roll are easily represented as 3 by 3 matrices (See Foley and Van Dam, 1982, pp. 255-258. Note, 4 by 4 matrices are not necessary for this application.). Composition of these matrices and then a matrix multiplication of the data set with the FOR centered at the

origin of the orbiter coordinate system, create new, transformed data points of the payload.

To show the top view, the x,y values, transformed to screen coordinates, are plotted. The front view is a plot of the y,z values and the x,z values are drawn for the side view.

IMPLEMENTATION

The sample orbiter display, the current and enhanced versions, and the RMS berthing aid were implemented in color on an IBM PC clone. These programs are basically for demonstrations, although much potential exists for application of computer graphics on the orbiter. Using the PDR data from an actual berthing procedure, the berthing display updated approximately every 12 seconds. See figures 1 and 2.

In order to evaluate the effectiveness of this payload berthing aid, the displays were implemented on a Z80 microprocessor equipped with a Microangelo card and displayed on a monochrome graphics monitor. This is interfaced with the SE1 computer which controls and monitors the Manipulator Development Facility (MDF). [The MDF is a JSC training facility for RMS operators.] During a payload berthing maneuver, current PDR data is sent to the Z80 microprocessor, which draws the appropriate display for the operator to view. Due to the limitations of the hardware, especially the 8 bit processor, the update rate is about 40 seconds for a full display.

RESULTS

The sample displays appear to have potential but have not been adequately evaluated. This is mainly due to the emphasis and time devoted to the MDF berthing aid.

The response by the MDF/RMS operators to the payload berthing aid has been very favorable. The present system was developed with the hardware which was on hand at JSC and costs less than \$4000. Viewed as an initial step in the development of a close to real-time berthing aid, the current system shows much potential. The slow update rate of the display, except as a demonstration, is not acceptable. This is easily remedied by a better, more powerful processor which is readily available.

FUTURE ENHANCEMENTS AND DIRECTIONS

An obvious direction of the orbiter display portion of the project is additional review of the displays in order to identify specific categories of the displays and the corresponding color computer graphics enhancements. This review will also benefit current definition of space station systems display requirements.

The utility of the payload berthing aid has been demonstrated. It is apparent that speeding up the refresh rate of the display is the first goal. Other enhancements could include graphical indications of the collision of the payload with the cargo bay and the ability to select, via keystrokes,

light pen or some other interactive device, a portion of the display on which to zoom. Zooming in on a particular segment of the display would allow the operator to see the fine detail that is helpful in the final stages of berthing. Further development of this computer graphics payload/cargo bay display will certainly indicate additional refinements and enhancements.

REFERENCES

1. Angell, Ian O., A PRACTICAL INTRODUCTION TO COMPUTER GRAPHICS, Halsted Press (John Wiley), NY, 1981.
2. Foley, James D. and Andries Van Dam, FUNDAMENTALS OF INTERACTIVE COMPUTER GRAPHICS, Addison-Wesley, Reading, MA, 1982.
3. Rogers, David F. and J. Alan Adams, MATHEMATICAL ELEMENTS FOR COMPUTER GRAPHICS, McGraw-Hill, NY, 1976.

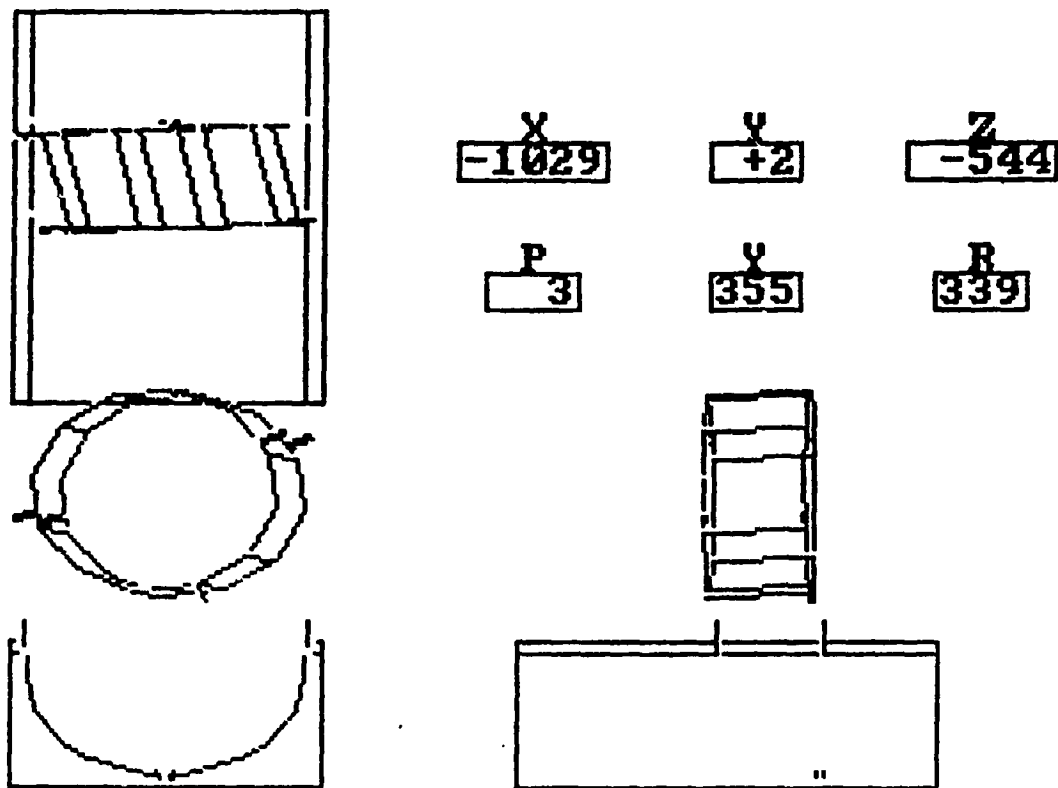
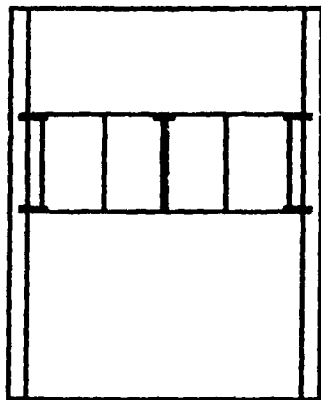


Figure 1. IBM PC demonstration of a typical payload berthing display. Beginning in the upper left-hand corner in a counterclockwise direction, the top, front and side views of the payload and cargo bay, and the point of resolution position and attitude data are displayed



X
-1050

Y
+0

Z
-400

P
0

Y
0

R
0

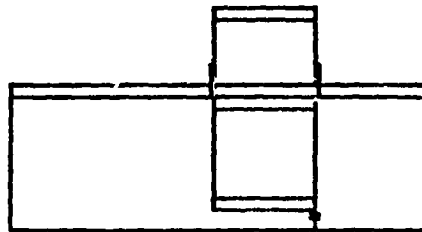
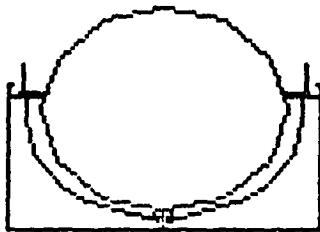


Figure 2. IBM PC demonstration of a berthed payload display. Beginning in the upper left-hand corner and moving in a counterclockwise direction, the top, front and side views of the payload and cargo bay, and the point of resolution position and attitude data are displayed.

ORIGINAL PAGE IS
OF POOR QUALITY

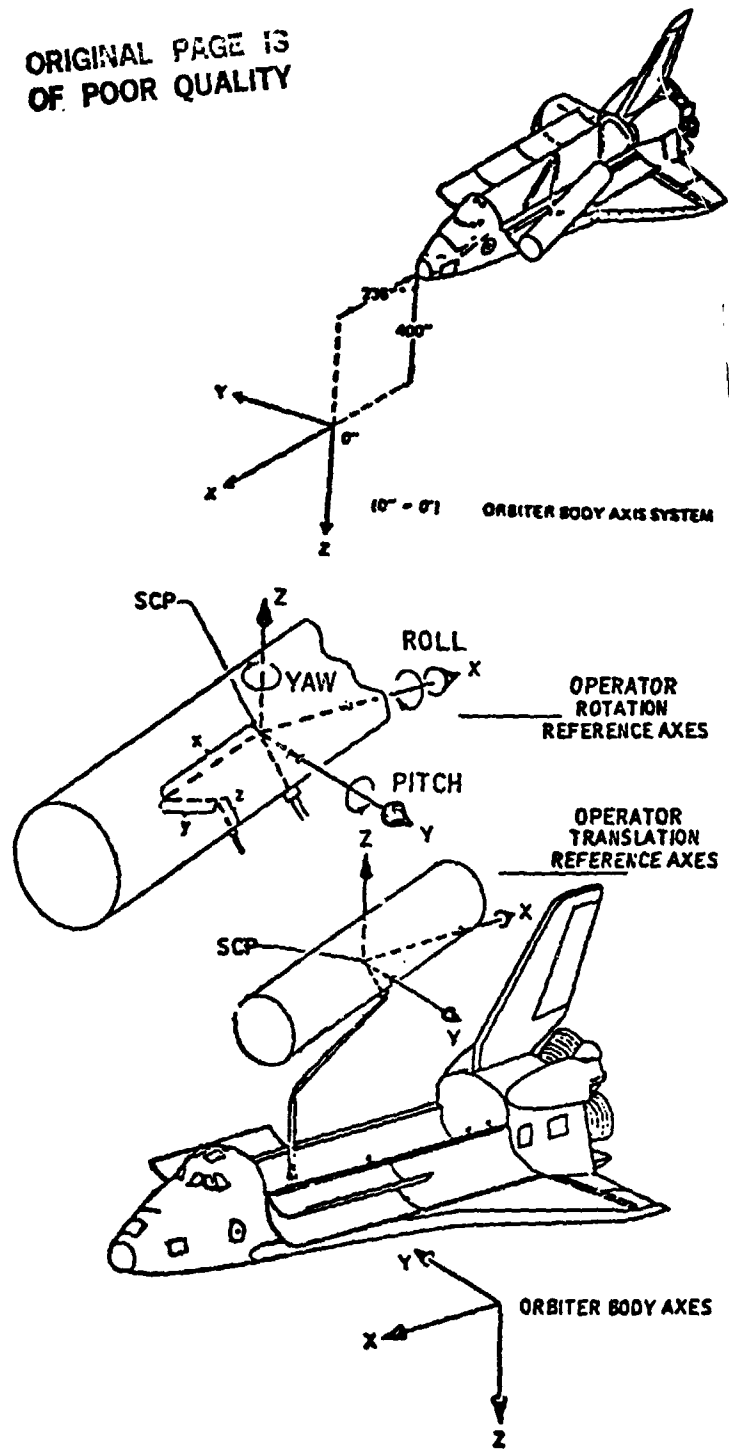


Figure 3. Orbiter Body and Payload Reference Axes

ORIGINAL PAGE IS
OF POOR QUALITY

N86-14105

REPORT. 1

18-AUG-1983 16:21

SIGNAL PROCESSING OF ANTHROPOMETRIC DATA

Wayne J. Zimmermann
Associate Professor
Department of Computer Science
East Texas State University
Commerce, Texas

ABSTRACT

The Anthropometric Measurements Laboratory has accumulated a large body of data from a number of previous experiments. The data is very noisy, therefore it requires the application of some signal processing schemes. Moreover, it was not regarded as time series measurements but as positional information; hence, the data is stored as coordinate points as defined by the motion of the human body.

The accumulated data defines two groups or classes. Some of the data was collected from an experiment designed to measure the flexibility of the limbs, referred to as radial movement. The remaining data was collected from experiments designed to determine the surface of the reach envelope.

The purpose of this project is to design and implement an interactive signal processing package. Since the data does not include time this package does not include a time series element. Presently the results is restricted to processing data obtained from those experiments designed to measure flexibility.

Center Research Advisor: Barbara Woolford

ORIGINAL PAGE IS
OF POOR QUALITY

INTRODUCTION

An accurate analysis of human motion is required if substantial improvements in suit and control panel design are to be obtained. In [1] it has been indicated that efficient well designed workstations must take into consideration the interactive role of the human operator. Garg and Kohli, [2], indicate that complex equipment produced during the second world war operating as high speed generally required unusual capabilities beyond the operator. They further indicate that the design of equipment must take into account human capacities and limitations. This requires the acquisition, processing, and interpretation of large amounts of data.

At NASA/JSC the acquisition is accomplished by the use of a modified SELSPOT system as illustrated in Figure 1. The system consist of four cameras used to measure position, a monitor to view the experiment and data transfer, a pair of 6502 microprocessors for handling the data and controlling the hardware, and a video tape recorder. This system can provide for the acquisition of three dimensional data with time and LED identification numbers. Thus each point can be defined by the five-tuple: (x,y,z,t,i) . The VRA (Video Recording Adapter) records not only visual image but data. Positional data from, up to thirty, LEDs which emit IR radiation are measured and digitized by the cameras. The acquired data which is stored on the video tape is then processed by the HP-21MX system. Eixon, [3], provides a functional description of the acquisition system.

The processing consist of several programs designed to format and plot the data. This project provided some statistical processing

ORIGINAL PAGE IS
OF POOR QUALITY

capability. The software system consist of the following program:

- &MPINI A package designed to transfer the data from the VCR to the HP disk on the HP-21MX system.
- &CHKFL A package to rearrange the packed bits thereby reconstructing the actual data.
- &FRID1 A package to determine the frequency, range, median and mean of the data associated with each LED.
- &SELVC A package which computes the coordinates of each LED.
- &CALPL A package which computes calibration points.
- &XYZTP A package used to generate a tape containing the XYZ coordinates for transferring to the VAX-780. At present the time is not transferred.
- PLAID A package used to generate some graphic displays. Is implemented on the VAX. An interactive package.
- PROJECT A package used to aid in filtering the data maintained on the VAX. The package is interactive.

The interpretation segment will involve two primary segments: formulation of mathematical models for various limbs and implementation of these models for simulation. There are numerous papers on the subject, see [4], [5] and [6]. The initial stage is to acquire a data bank of statistical information related to human motion. This data bank must include data related to the design of seats, control panels, control modules, and operational procedures. With such a data bank a system can then be devised which will permit the designer to use a graphics terminal for designing a particular interface, then test the design for general use by allowing a bubbleman, Refs. [7] and [8], to work through the various operations. Such a project will require many new techniques: pattern recognition, artificial intelligence, computer graphics, data base methodology, and the like. At present work is just beginning and the project consist primarily of data acquisition.

A SIGNAL PROCESS SYSTEM

It has been indicated that there are two problems. One related to radial movement, the other related to reach envelopes. This section considers only the first. Since the radial movement involves a limb moving through a fixed pattern the data will closely approximate a circle as seen in Figure 2. Hence this geometrical structure is implemented in the system.

In looking for existing technique some variations of a number of time series models were tried. See [9], [10], [11], and [12]. A design of one of these methods will be included later, but the process presently consist of employing manual selection, moving averages, and some statistical methods for removing the noise. These techniques are designed to use the best fitting circle.

In quickly reviewing the package, we note that the system begins by asking which file is to be processed. The data is read. Initially it contains the coordinates for all LEDs in a multiplexed form. If we select a single LED the data is demultiplexed and the corresponding data is retained. Then we may select to display or not to display this data on the terminal, a Digital VT125 or equivalent. This should be done since it provides us with the opportunity to judge which data is valid and which is noise. In addition, the plotting gives us a feeling for the particular motion involved. We then estimate the center and radius of the best circle. Next, the system applies a moving average for the purpose of removing isolated spikes. On completion of these smoothing processes we are asked if we wish to manually remove any data we view as noise. Again we are queried with regard to plotting. We may estimate the parameters for the best circle again, after which the system determines the parameters for the best circle and prompts for replacing the

ORIGINAL PAGE IS
OF POOR QUALITY

generated value or leaving them as calculated. Once the parameters are determined the circle is used to remove any data not lying within a specified band defined by the circle. The remaining data is then used to generate the parameters of the best circle. The center of this best circle is then used to partition the plane into a number of wedges. The data lying within a wedge is then used to define a new set of values, namely the distance from the center of the best circle to the data point. These distances are then ordered, smallest to largest. Next, a set of differences, $DIST(J+1)-DIST(J)$, are formed. This last set of values is used to define a cluster measure which is the standard deviation of these difference. This cluster measure is then used to cluster the set of distances. See Figure 3. The mean and the standard deviation of each cluster is then determined and retained. These averages and standard deviation are converted to plane coordinates using the angle which bisects the wedge. If there are too few data points the system assumes that the wedge does not contain any data. Using the wedges a set of expected values for the angles is determine along with the number of data points in the wedge, and the associated standard deviation. This information is made available for writing to a disk file. Clearly, small sample statistics must be employed. Finally, the user is queried on whether he desire to write the results to the file or simply quit.

FUTURE

In closing a number of future directions should be pointed out. Some are related to the area of signal processing, others are related to the use of the computer as a designing tool in the area of human factors. These include:

- Implement a time series approach, i.e., use an FFT.
- Modify the system to permit hardcopy of all graphics.

- Modify the read file subroutine to read new data files containing time and LED numbers.
- Develop and implement an algorithm for processing reach data and thereby determine a reach envelope.
- Increase the intelligence of the system by providing it with the ability to remove any data which is not within reach.
- Implement Ted Kell's subroutine to permit unsolicited input.
- Begin the task of designing a data base for the overall problem of computerized control panel design.
- Try to develop a statistical theory for convex combinations of normal distributions.

ORIGINAL PAGE IS
OF POOR QUALITY

REFERENCES

- [1] Junge, M.K., Giacomini, M.J., "Human Factors in Equipment Development for the Space Shuttle", Proceeding of the Human Factor Society, pp 218-222, 1981
- [2] Garg, A., Kohli, D., "Human Factors in Machine Design", Jour. of Mech. Design, Vol 101, PP 587-593, 1979
- [3] Nixon, J.H., Cater, J.P., "A Functional Video-Based Anthropometric Measuring System", Southwest Research Institute San Antonio, Texas, 1982
- [4] Hight, T.K., Piziali, R.L., Nagel, D.A., "A Dynamic Nonlinear Finite-Element Model of a Human Leg", Jour. of Biomech. Engr. Vol 101, pp 176-184, 1979
- [5] Dainis, A., "Whole Body and Segment Center of Mass Determination from Kinematic Data", Jour. Biomechanics, Vol 13, pp647-651, 1980
- [6] Kasvand, T., Milner, M., Ropley, L.F. "A Computer Based System for the Analysis of some Aspects of Human Locomotion", Human Locomotion Engineering, London, Institute of Mechanical Engr., pp 170-174, 1974
- [7] Badler, M.I., Smoliar, S.W., "Digital Representation of Human Movement", Computer Surveys, Vol 11, pp 19-38, 1979
- [8] Garrett, G., Reed, W.S., Widule, C., Garrett, R.E., "Human Motion: Simulation and Visualization", Medicine and Sport, Vol 6, Biomechanics II, pp 299-303, 1971
- [9] Dunsmuir, W., Robinson, P.M., "Estimation of Time Series Models in the Presence of Missing Data", Jour of the Amer. Stat. Assoc. Vol 76, No 375, pp 560-568, 1981
- [10] Pynsent, P.S., Hanka, R., "A Simple Program for A Phaseless Recursive Digital Filter", Jour. Biomed. Engr., Vol 4, pp 252-254, 1982
- [11] Engelken, E.J., Stevens, K.W., Wolfe, J.W., "Application of Digital Filters in the Processing of Eye Movement Data", Behavior Research Methods & Instrumentation, Vol 14, pp 314-319, 1982
- [12] Vincent, R., English, M.J., et al., "A Flexible Signal-Averaging System for Cardiac Waveforms", Jour. Biomed. Engr., Vol 2, pp 15-24, 1980
- [13] Andriacchi, T.P., et al., "Three-Dimensional Coordinate Data Processing in Human Motion Analysis", Journ. of Biomech. Engr., Vol 101, pp 229-233, 1979

ORIGINAL PAGE IS
OF POOR QUALITY

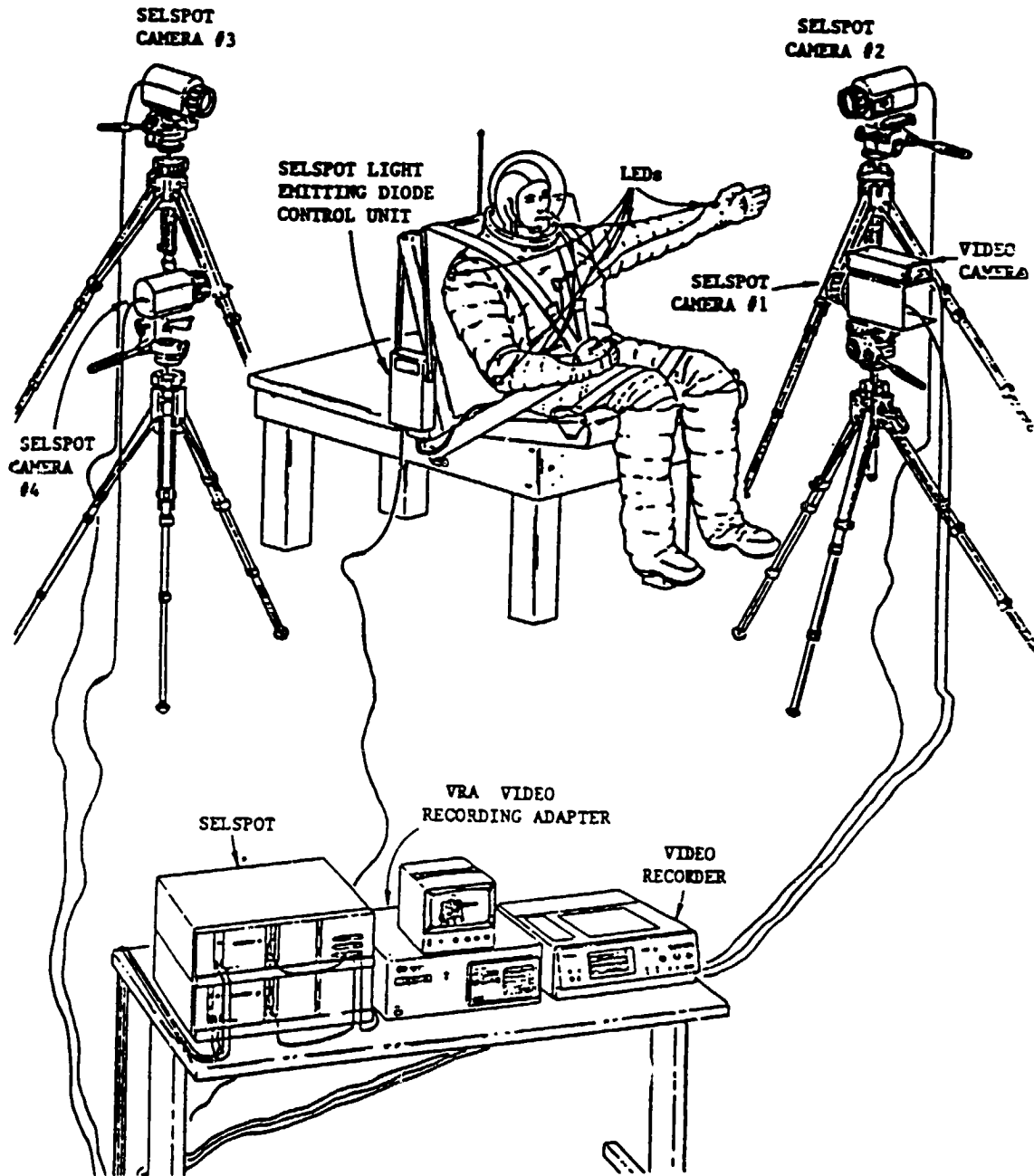


Figure 1. Anthropometric Measuring Setup

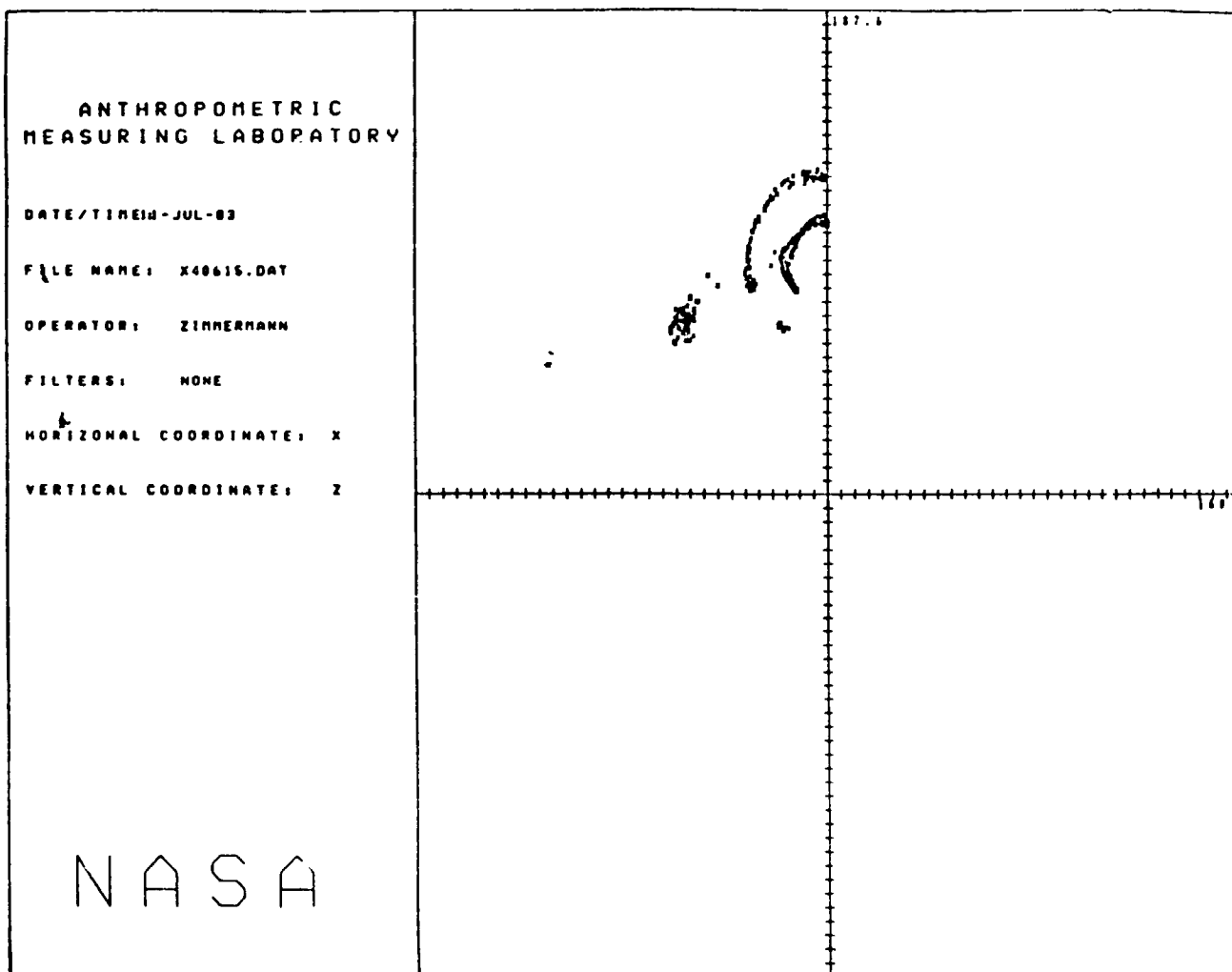


Figure 2. Radial Motion Data

Report No. NASA CR-171904	2. Government Accession No.	3. Recipient's Catalog No.	
Title and Subtitle 1983 NASA/ASEE Summer Faculty Fellowship Program Research Reports		5. Report Date SEPTEMBER 1983	
		6. Performing Organization Code	
Author(s) Editors: Dr. Walter J. Horn and Dr. Michael B. Duke		8. Performing Organization Report No.	
		10. Work Unit No.	
Performing Organization Name and Address Lyndon B. Johnson Space Center, Houston, Texas Texas A&M University, College Station, Texas The University of Houston - University Park, Houston, Texas		11. Contract or Grant No. NGT-44-001-800	
		13. Type of Report and Period Covered Contractor Report	
Sponsoring Agency Name and Address National Aeronautics and Space Administration Washington, D.C. 20546		14. Sponsoring Agency Code	
		Supplementary Notes	
Abstract			
<p>The 1983 NASA/ASEE Summer Faculty Fellowship Research Program was conducted by Texas A&M University and the Lyndon B. Johnson Space Center (JSC). The 10-week program was operated under the auspices of the American Society for Engineering Education (ASEE). The program at JSC, as well as those at other NASA Centers, was funded by the Office of University Affairs, NASA Headquarters, Washington, D.C. The basic objectives of the programs, which began in 1965 at JSC and in 1964 nationally, are (1) to further the professional knowledge of qualified engineering and science faculty members, (2) to stimulate an exchange of ideas between participants and NASA, (3) to enrich and refresh the research and teaching activities of participants' institutions, and (4) to contribute to the research objectives of the NASA Centers.</p> <p>The faculty fellows spent 10 weeks at JSC engaged in a research project commensurate with their interests and background. They worked in collaboration with a NASA/JSC colleague. This document is a compilation of the final reports on their research during the summer of 1983. Texas A&M Research Foundation Report No. 4194-83 is the Co-Directors' report on the administrative operations of the Summer Faculty Fellowship Program.</p>			
Key Words (Suggested by Author(s))		18. Distribution Statement Unclassified-Unlimited	
Security Classif. (of this report) Unclassified	20. Security Classif. (of this page) Unclassified	21. No. of Pages 410	22. Price* NTIS